

Pharmacological intervention for tumor-induced cachexia

Vignesh Karthikaisamy

Vollständiger Abdruck der von der TUM School of Life Sciences der Technischen Universität München zur Erlangung eines **Doktors der Naturwissenschaften (Dr. rer. nat.)** genehmigten Dissertation.

Vorsitz: Prof. Dr. Nina H. Uhlenhaut

Prüfer der Dissertation:

1. Prof. Dr. Martin Klingenspor
2. Prof. Dr. Richard Lehner
3. Prof. Dr. Stephan Herzig

Die Dissertation wurde am 03.01.2023 bei der Technischen Universität München eingereicht und durch die TUM School of Life Sciences am 08.05.2023 angenommen.

SUMMARY

Cancer cachexia is a multifactorial metabolic syndrome characterized by energy-wasting, increased systemic inflammation, and metabolic dysfunctions, leading to muscle and fat mass deterioration. Cachexia is observed in about 50-80% of advanced cancer patients and is currently poorly treated in clinics. Skeletal muscle atrophy driven by disrupted protein homeostasis and adipose tissue wasting through increased lipolysis represent the key indicators of cancer cachexia. The importance of adipose tissue in cancer cachexia is increasingly recognized, and reports suggest that, in some cases, adipose tissue loss precedes the onset of muscle loss. During cachexia, energy and lipid metabolism are altered and maintaining adipose tissue mass and homeostasis is hypothesized to improve the survival outcomes in these patients.

The present study screened for and identified antilipolytic compounds and investigated their effect against cancer cachexia-induced weight and tissue loss in a mouse model of cancer cachexia. Using 3T3-L1 adipocytes, mouse primary adipocytes, and differentiated human mesenchymal stem cells (hMSC-Tert), fifty-one compounds from a pre-screen were tested for their ability to inhibit lipolysis under basal and induced conditions upon treatment with tumor cell conditioned medium (TCCM) from cachexia-inducing colon 26 adenocarcinoma (C26) cells. Two out of the fifty-one compounds inhibited lipolysis in three adipocyte cell models tested. Four other compounds inhibited lipolysis significantly in 3T3-L1 and hMSC-Tert adipocytes. Thus, six compounds inhibited lipolysis consistently in at least two different cell models. Based on the literature review and additional *in vitro* experiments, three compounds (Diphenylethylidene diethylcarbazole (DEED), *N*-Oleoyldopamine (OLDA), and BioF) were selected for *in vivo* testing using the C26 cancer cachexia model.

In Balb/c mice, C26 tumor cell implantation induced cachexia development, as evidenced by weight loss and muscle and fat atrophy. Plasma metabolite levels were also significantly altered in response to the cachexia-inducing C26 tumor cell-mediated dysregulation. Treatment with the hit compounds from the screening (DEED, OLDA, and BioF) did not protect against the C26-induced cachexia. Interestingly, changes in the phosphorylation state of hormone-sensitive lipase (HSL) upon OLDA and BioF treatment suggested an inhibitory effect on adipose tissue lipolysis, accompanied by a modulated expression of critical genes and proteins involved in lipolysis and lipogenesis. However, the changes in the molecular levels of critical metabolic regulators were insufficient to prevent cachexia-induced fat loss. BioF treatment in the non-tumor-bearing mice increased the body weight significantly. *In vitro*, BioF also rescued the C26 TCCM-induced C2C12 myotube atrophy. Therefore, I further investigated the effect of BioF on the tumor-bearing mice held at a thermoneutral temperature and started the compound treatment earlier. BioF treatment altered specific plasma metabolite levels in the tumor-bearing mice; however, the modifications in treatment initiation and the housing temperature did not affect the cachexia outcome.

In summary, three compounds selected from the lipolysis assay-based compound screening at the used dosages affected specific cachexia-related molecular pathways *in vivo*. However, they did not ameliorate the weight and tissue loss in the C26 cachexia model. Targeting adipose tissue wasting and lipolysis is hypothesized to be an effective treatment strategy against cancer cachexia. Therefore, further studies to optimize the compound dosage, test different cachexia models and assess combinatorial treatment

approaches are required to finally clarify the potential of the selected antilipolytic compounds to counteract cancer cachexia.

ZUSAMMENFASSUNG

Kachexie ist ein multifaktorielles Syndrom, das durch Gewichtsverlust, systemische Entzündung und metabolische Fehlfunktionen gekennzeichnet ist, die zur Abnahme von Muskel- und Fettgewebe führen. Obwohl 50-80% der Krebspatienten von Kachexie betroffen sind, mangelt es an adäquaten Behandlungsmöglichkeiten. Die wichtigsten Kennzeichen von Kachexie sind durch fehlgeleiteten Proteinstoffwechsel hervorgerufene Skelettmuskelatrophie, sowie Fettabbau durch erhöhte Lipolyse. Letzterer wird vermehrt als elementarer Bestandteil des Krankheitsbildes betrachtet und in manchen Fällen sogar als initial für die Entstehung von Kachexie angesehen. Da veränderter Energie- und Fettstoffwechsel als kausale Bestandteile von Kachexie beschrieben werden, wird angenommen, dass eine Verbesserung derselben zu einer verbesserten Überleben bei diesen Patienten führen könnte.

Die vorliegende Arbeit hat eine Vielzahl von Wirkstoffen auf ihre anti-lipolytische Wirkung hin überprüft und eine Verwendung zur Behandlung von Kachexie in Mausmodellen krebsinduzierter Kachexie untersucht. Unter Verwendung von 3T3-L1 Adipozyten, murinen primären Adipozyten, sowie ausdifferenzierten humanen mesenchymalen Stammzellen (hMSC.Tert) wurden 51 Wirkstoffe auf ihre Fähigkeit Lipolyse zu inhibieren, getestet. Diese Tests wurden sowohl in unstimulierten Zellen, als auch in Zellen, die mit Tumor-Zell-konditioniertem Medium (tumor cell conditioned medium, TCCM) von Kachexie-induzierenden „Colon 26 adenocarcinoma“ (C26) behandelt wurden, durchgeführt. Sechs der getesteten Wirkstoffe inhibierten Lipolyse in mindestens zwei Adipozyten-Systemen. Auf Grundlage publizierter Literatur und zusätzlicher *in vitro* Experimente wurden drei Wirkstoffe (Diphenyleneiodonium chlorid (DPI), N Oleoyldopamin (OLDA) und BioF) zu weiteren *in vivo* Tests ausgewählt.

Implantation von C26 Tumor-Zellen in Balb/c Mäuse führte zur Entstehung von Kachexie in diesen Tieren, was sich in Gewichtsverlust, Muskel- und Fettatrophie und veränderten Blutparametern äußerte. Eine Behandlung mit den drei identifizierten Lipolyse-Inhibitoren (DPI, OLDA, BioF) hatte keine Auswirkung C26-Tumor-induzierte Kachexie. Interessanterweise führten die Behandlungen mit OLDA und BioF zu Veränderungen des Phosphorylierungs-Status von HSL (hormone-sensitive lipase) und damit verbundenen Veränderungen in der Gen- und Proteinexpression, was dennoch nicht ausreichend war, um Kachexie-induzierten Fettverlust zu unterbinden. In Mäusen, denen keine Tumore implantiert wurden, erhöhte BioF jedoch signifikant das Körpergewicht. *In vitro* führte die Behandlung von C2C12 Muskelzellen, in denen durch C26 TCCM Muskelatrophie hervorgerufen worden war, zu einer Umkehr derselben. Daher wurden die Auswirkung von BioF-Behandlung in Tumor-implantierten Mäusen bei Thermoneutralität und einem früheren Behandlungsbeginn weitergehend untersucht. Hier hat BioF-Behandlung zu Veränderung spezieller Blutparameter in Mäusen mit Tumor geführt, wobei jedoch die geänderte Haltungstemperatur und der frühere Behandlungsbeginn keinen Einfluss auf die Kachexie-Entstehung zeigten.

Zusammenfassend zeigt diese Arbeit, dass die Behandlung von kachektischen Mäusen mit drei in einem Wirkstoff-Auswahlverfahren identifizierten Wirkstoffen bestimmte Kachexie-bezogene molekulare Veränderungen hervorrufen konnten. Bei den verwendeten Dosierungen waren diese Veränderungen jedoch nicht in der Lage, dem Verlust in Körper- und Organgewicht entgegen zu wirken. Da die gezielte Beeinflussung von Fettgewebsverlust in Krebs-induzierter Kachexie weiterhin als potentielle Behandlungsmöglichkeit angesehen wird, sind weitere Untersuchungen mit angepassten Wirkstoff-

Dosierungen, anderen Kachexie-Mausmodellen, sowie kombinierende Behandlungsansätze nötig, um das Potential der ausgewählten Lipolyseinhibitoren zur Behandlung von Kachexie abschließend zu evaluieren.

ACKNOWLEDGEMENT

First of all, I would like to express my deepest gratitude to my supervisor Dr. Mauricio Berriel Diaz, for accepting me as a Ph.D. student in his laboratory and providing continuous mentoring and support in the diverse projects. I am also thankful to Prof. Dr. Stephan Herzig for having me at the Institute for Diabetes and Cancer and for his valuable comments and suggestions on developing this project.

I am incredibly grateful to my doctoral advisor Prof. Dr. Martin Klingenspor, and thesis advisory committee members, Dr. Siegfried Ussar, Prof. Dr. Richard Lehner, and Prof. Dr. Carla Prado for valuable discussions, feedback, and support for the smooth conduction of my thesis work.

I would like to extend my sincere thanks to Dr. Katarina Klepac, who co-supervised my early Ph.D. work, helped develop ideas, and provide guidance and feedback. Thanks should also go to everyone supporting me over the years: Dr. Maria Rohm, Dr. Juliano Machado, Dr. Pauline Morigny, Dr. Doris Kaltenecker, Dr. Julia Geppert, Dr. Honglei Ji, and Dr. Pia Benedikt-Kühnast. Besides the support from the researchers, I am very thankful for the technical support from the lab technicians. Special thanks are dedicated to Lisa Mehr and Daniela Haß, who have supported my projects with excellent technical experience. Many students have been working with me and supporting my projects during their internships and theses. Mainly, I would like to thank Lea and Sakthi for their dedicated experimental work. I very much enjoyed the teaching experience.

I am also thankful to the admins of the International Helmholtz Research School for Diabetes – Dr. Sofia Kappel, Dr. Kalina Draganova, and Susanne Drogin, for bringing in excellent workshops and valuable training programs that helped me immensely. This work would not have been possible without the 3-year fellowship from the graduate school.

Finally, I could not have accomplished this thesis without the support of my family and friends. I would like to thank all my friends, in particular Naga and Sashi, for being considerate when I called them untimed. Thanks to Senthil and Anbu for their motivation to pursue biological research. A big thanks to my partner, Priya, for her endless support, love, and encouragement to complete this research work. Lastly, I would be remiss in not mentioning my parents, Karthikaisamy and Mareeswari, for the love and support they have given me throughout my life.

INDEX

SUMMARY	i
ZUSAMMENFASSUNG	iii
ACKNOWLEDGEMENT	v
INDEX	vi
1. INTRODUCTION	1
1.1. Cancer Cachexia	1
1.1.1. Definition	1
1.1.2. Classification	1
1.1.3. Epidemiology of cachexia	2
1.1.4. Pathogenesis of cancer cachexia	2
1.1.5. Cachexia as a multiorgan syndrome	5
1.1.6. Animal models used for cancer cachexia research	6
1.1.7. Therapeutics developed against cancer cachexia	8
1.2. Adipose tissue and their function	9
1.2.1. Adipocyte physiology	9
1.2.2. Adipose tissue as an energy storage organ	9
1.2.3. Adipose tissue as an endocrine organ	10
1.2.4. Adipose tissue as thermoregulator	12
1.2.5. Dysfunction in metabolic syndrome	12
1.2.6. Therapeutics targeting adipose tissue metabolism	12
1.3. Aim of the study	13
2. RESULTS	14
2.1. 3T3-L1 adipocytes as a model to screen antilipolytic compounds <i>in vitro</i>	14
2.1.1. Establishment of <i>in vitro</i> adipocyte system for drug screening	14
2.1.2. Cachexia-inducing TCCM induces adipocytes lipolysis <i>in vitro</i>	14
2.2. Screening of compounds <i>in vitro</i>	15
2.2.1. Compounds used for the screening	16
2.2.2. Tumor-induced lipolysis assay-based compound screening on 3T3-L1 adipocytes	16
2.2.3. Tumor-induced lipolysis assay-based compound screening on hMSC-Tert adipocytes	17
2.2.4. Tumor-induced lipolysis assay-based compound screening on murine primary adipocytes	18
2.2.5. Selection of compound for validation	19
2.3. Validation of the hit compounds	20

2.3.1.	Validation of compounds using human TCCM	20
2.3.2.	Literature review of the selected compounds	21
2.3.3.	Dose-response curves for the selected compounds	22
2.3.4.	cAMP levels are not affected upon C26 TCCM treatment	23
2.3.5.	The fatty acid uptake of differentiated 3T3-L1 adipocytes	24
2.3.6.	The oxygen consumption rate of differentiated 3T3-L1 adipocytes	25
2.3.7.	Toxicity of compounds on 3T3-L1 adipocytes and C26 cells	26
2.4.	Effect of antilipolytic compounds <i>in vivo</i>	27
2.4.1.	Diphenyleiodonium chloride (DPI) is a potential compound to ameliorate cachexia.....	27
2.4.2.	Testing <i>N</i> -Oleoyldopamine (OLDA) for its antilipolytic effect <i>in vivo</i>	35
2.4.3.	Effects of BioF treatment in the Balb/c-C26 cachexia model.....	42
3.	DISCUSSION.....	54
3.1.	Targeting lipolysis as a treatment strategy against cancer cachexia.....	54
3.2.	Inhibition of NOX using DPI in cancer cachexia	57
3.3.	Testing endogenous fatty acid amide OLDA in cancer cachexia.....	59
3.4.	Effect of novel BioF compound against cancer cachexia.....	60
3.5.	Main conclusions and outlook	61
4.	METHODS.....	63
4.1.	Molecular Biology	63
4.1.1.	Preparation of Luria broth medium and agar plates.....	63
4.1.2.	Revival of <i>E. coli</i> glycerol stock	63
4.1.3.	Transformation of <i>E.coli</i>	63
4.1.4.	Bacterial liquid cultures.....	63
4.1.5.	Determination of DNA and RNA concentration	64
4.1.6.	DNA sequencing	64
4.1.7.	RNA extraction	64
4.1.8.	cDNA synthesis	65
4.1.9.	Quantitative PCR	65
4.2.	Cell Biology.....	65
4.2.1.	Cell culture conditions and media.....	65
4.2.2.	Freezing and thawing of cells	66
4.2.3.	Culturing of cells.....	66
4.2.4.	Isolation of preadipocytes from adipose tissue	67

4.2.5.	Differentiation of cells into adipocytes and myotubes	68
4.2.6.	Preparation of tumor cell conditioned medium (TCCM).....	68
4.2.7.	Treatment of adipocytes and myotubes	68
4.2.8.	Oil Red O staining and quantification.....	69
4.2.9.	Lipolysis assay.....	69
4.2.10.	cAMP assay.....	69
4.2.11.	Fatty acid uptake assay	70
4.2.12.	Seahorse Mito Stress assay	70
4.2.13.	Cytotoxicity assay	72
4.2.14.	Staining and analysis of myotube diameter	72
4.2.15.	Lentivirus production and concentration.....	73
4.2.16.	Transduction of 3T3-L1 adipocytes with lentiviruses.....	73
4.3.	Biochemistry	74
4.3.1.	Protein extraction.....	74
4.3.2.	Determination of protein concentration.....	74
4.3.3.	SDS-PAGE and immunoblotting.....	74
4.3.4.	NADPH Oxidase Activity Assay	75
4.4.	Animal experiments	75
4.4.1.	Mice for isolation of primary preadipocytes	76
4.4.2.	Testing the toxicity of the compounds.....	76
4.4.3.	C26 cachexia model.....	76
4.4.4.	Cachexia index.....	77
4.4.5.	Intraperitoneal glucose tolerance test	77
4.4.6.	Body composition analysis	77
4.4.7.	Blood plasma extraction.....	77
4.5.	Statistical Analysis.....	77
5.	MATERIALS.....	78
5.1.	Compounds used in the screen.....	78
5.2.	Animals.....	79
5.3.	Antibodies	79
5.4.	Chemicals and Reagents	80
5.5.	Kits.....	82
5.6.	Plasmids	82

5.7.	qPCR primers.....	82
5.8.	shRNAs	83
5.9.	Software.....	83
6.	APPENDIX.....	84
6.1.	Abbreviations.....	84
6.2.	List of Figures	88
6.3.	List of Tables	94
6.4.	Bibliography	95

1. INTRODUCTION

1.1. Cancer Cachexia

1.1.1. Definition

Cachexia derives from combining the Greek words *kakós* (bad) and *hexis* (condition). It describes disease resulting in the wasting of host tissue (Kern & Norton, 1988). Dating back to the ancient Greek period, physicians referred to cachexia as ‘*signum mali ominis*,’ which indicates end-stage disease and poor quality of life (Doehner & Anker, 2002). Cachexia is associated with different chronic diseases such as cancer, chronic heart failure (CHF), chronic kidney disease (CKD), chronic obstructive pulmonary disease (COPD), rheumatoid arthritis, and autoimmune deficiency syndrome (AIDS). In 2011, an international consensus defined cancer cachexia as “a multifactorial syndrome characterized by an ongoing loss of skeletal muscle mass (with or without loss of fat mass) that the conventional nutritional support could not protect against and leads to progressive functional impairment” (K. Fearon et al., 2011).

1.1.2. Classification

Stages of Cachexia

The international consensus classified cancer cachexia into three continuum stages with clinical relevance: precachexia, cachexia, and refractory cachexia (**Figure 1**). Patients demonstrate early clinical and metabolic signs such as anorexia, systemic inflammation, and impaired glucose tolerance with a substantial involuntary weight loss ($\leq 5\%$) in the precachexia stage. Patients with more than 5% weight loss over the past six months, or a body mass index (BMI) of less than 20 kg/m^2 , and ongoing weight loss of more than 2% but not have entered refractory cachexia are clinically classified into the cachexia stage. Refractory cachexia is the third and ultimate stage in which the patients have pre-terminal cancer or are not responsive to anticancer treatment. The life expectancy of patients in the refractory cachexia stage is less than three months (K. Fearon et al., 2011).

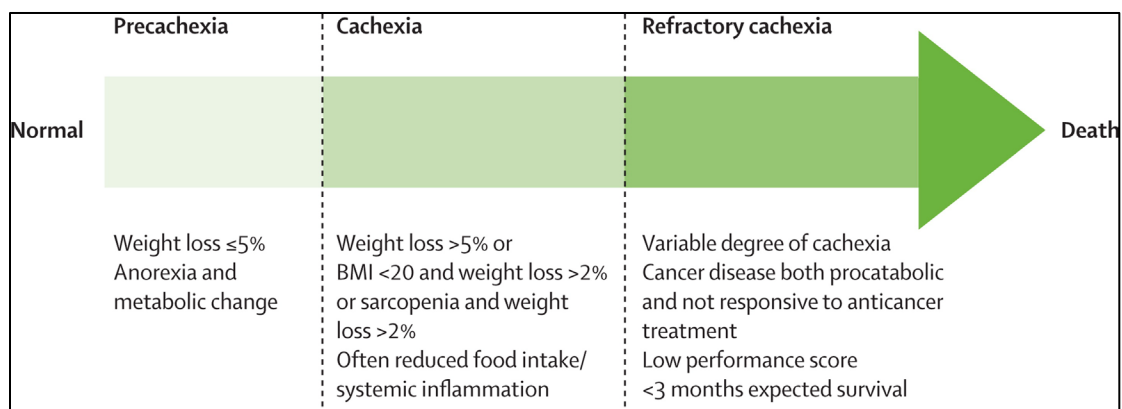


Figure 1: Stages of cancer cachexia. The cancer cachexia spectrum represents the different stages of the disease progression adapted from (K. Fearon et al., 2011). BMI – body mass index.

Severity of depletion

During cancer cachexia, skeletal muscle is depleted (in the presence or absence of fat mass loss). The depletion severity is classified based on the rate at which the body loses weight, energy stores, and protein

mass. According to the international consensus, “a fall of 5 kg/m² in BMI from an initial value of 22 has more severe implications than the same loss from an initial value of 35” (K. Fearon et al., 2011).

1.1.3. Epidemiology of cachexia

The overall incidence of cachexia due to any disease is growing, particularly in industrialized regions such as North America, Europe, and Japan. The prevalence rate stands around 1%, with about nine million patients (von Haehling & Anker, 2010). The occurrence of cachexia is astonishingly high in patients with chronic illness, between 5 and 15% in advanced CHF or COPD patients to 50-80% in end-stage cancer patients. Mortality rates of patients with cachexia also vary depending on the associated chronic illness. While the mortality rate is around 15% per year in COPD patients, it is estimated to be about 80% per year in cancer patients (von Haehling & Anker, 2014). The prevalence of cachexia and its associated weight loss is also highly variable among different cancer types (**Figure 2**). Cachexia is exceptionally high in pancreatic and gastrointestinal cancer patients, followed by other cancer patients. The degree of weight loss observed in cancer patients is also dictated by the cancer site, with prostate and breast cancer being less severe (Baracos et al., 2018).

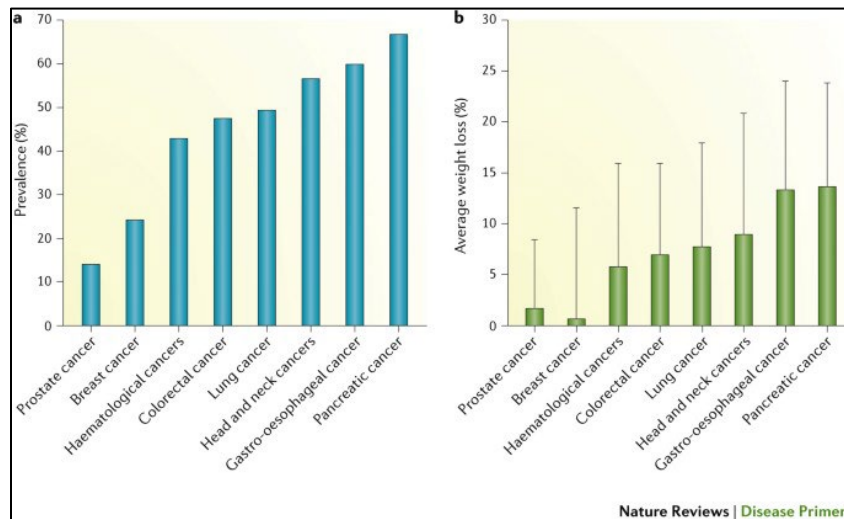


Figure 2: Prevalence of cachexia and intensity of weight loss based on tumor site. (a) The percentage prevalence of cachexia (defined as at least 5% weight loss in the last six months) and **(b)** average percentage weight loss in patients as based on tumor site. Adapted from (Baracos et al., 2018).

1.1.4. Pathogenesis of cancer cachexia

Cancer cachexia is a multifactorial condition defined by involuntary weight loss that results from metabolic dysregulation and anorexia triggered by the tumor in the system. Cachexia-inducing tumors secrete factors (cachexia mediators) that directly influence the metabolism of various organs leading to a multiorgan syndrome (K. C. H. Fearon et al., 2012). Thus, cancer cachexia is a systemic disorder driven by and affecting various organs (Schmidt et al., 2018). Researchers have studied several mediators involved in the pathogenesis of this disorder. The tumor-derived factors and the inflammatory response of the tumor-immune crosstalk elicit catabolic wasting of the target tissues. In response to the systemic alteration, muscle and adipose tissue-derived factors have also been shown to aggravate cachexia development.

Tumor-derived mediators

One of the tumor-derived factors found to deplete adipose tissue mass in cancer patients was zinc- α 2-glycoprotein (ZAG) or lipid mobilizing factor (LMF) (Hirai et al., 1998). ZAG expression and secretion are particularly increased in the adipose tissue of gastrointestinal cancer cachexia patients (Mracek et al., 2011). ZAG was found to be increased in mice bearing the cachexia-inducing MAC16 colon adenocarcinoma (Beck & Tisdale, 1987) and induced the cAMP-mediated lipolysis induction in cultured adipocytes *in vitro* (Hirai et al., 1998). Surprisingly, this factor also depleted fat and decreased body weight in the wildtype and *ob/ob* mice.

Tumor-derived parathyroid hormone-related protein (PTHrP) was shown to induce cachexia in nude mice. Treatment with anti-PTHrP antibodies protected against weight and tissue loss (Iguchi et al., 2001, 2006). PTHrP was recently shown to mediate wasting by regulating the thermogenic gene expression in brown adipose tissue (BAT) (Kir et al., 2014).

Pancreatic cancer-secreted pluripotent hormone adrenomedullin (AM) was shown to induce lipolysis in both human and murine adipocytes by binding to the adrenomedullin receptor (ADMR) and activating the MAPK pathway. Interestingly, blocking AD-ADMR interaction using inhibitors of cancer-induced lipolysis *in vitro* (Sagar et al., 2016). Further, AM has been implicated in impaired insulin secretion and β -cell dysregulation in pancreatic cancer (Javeed et al., 2015). Several other tumors and tumor organoid-secreted factors are reported to be increased in weight-losing cancer patients (Freire et al., 2020; Vaes et al., 2020).

Our lab recently showed tumor- and host-derived phospholipase A2 group VII (PLA2G7) to be particularly increased in mice models of cachexia and cancer cachexia patients. Interestingly, PLA2G7 protein levels and their activity effectively stratified weight-losing and weight-stable cancer patients, suggesting PLA2G7 is a potential cancer cachexia marker (Morigny et al., 2021).

Pro-inflammatory cytokines

Tumor necrosis factor alpha (TNF- α) is a pro-inflammatory cytokine secreted mainly by macrophages. TNF- α can invoke alterations in various biological processes upon binding with its receptors. Furthermore, this critical cytokine is implicated in various disease conditions, including cancer cachexia. TNF- α was shown to induce weight loss in mice (Oliff et al., 1987), and TNF- α receptor-1 (TNFR-1) knockout mice, although had elevated levels of TNF- α displayed slight protection against Lewis lung carcinoma (LLC) induced tissue loss (Llovera et al., 1998). However, anti-TNF- α antibody did not provide any beneficial effects against cachexia in patients (Jatoi et al., 2010), suggesting that blocking one of several cachexia-inducing factors or mediators will not be sufficient to counteract this complex disease.

Interleukin-6 (IL-6) is another critical cytokine found to be specifically increased in cancer patients with reduced survival and increased weight loss (Iwase et al., 2004; Scott et al., 1996). Similar results were also observed in mice models of cachexia; however, it was interesting that systemic treatment of IL-6 increased STAT-3 signaling in muscle but did not induce weight loss or tissue wasting in wildtype mice without tumor-burden (Baltgalvis et al., 2008). These data suggest that the interaction between the pro-inflammatory markers and tumor is critical for developing cachexia phenotype. Like anti-TNF- α , a

humanized anti-IL-6 antibody was also unable to rescue the cancer patients' body weight (Bayliss et al., 2011), substantiating the need for an alternative or multimodal treatment strategy.

Other hosts or tumor-derived cytokines such as TNF-related weak inducer of apoptosis (TWEAK), interleukin-1 β (IL-1 β), interferon-gamma (IFN- γ), leukemia inhibitory factor (LIF), growth/differentiation factor-15 (GDF-15) have also been implicated in the development of cancer cachexia (Braun et al., 2011; Dogra et al., 2007; Lerner et al., 2015; Ma et al., 2017; Seto et al., 2015). It could well be that several cytokines interact and potentiate systemic inflammation during cancer cachexia. Cachexia-inducing tumors have also been reported to secrete pro-inflammatory cytokines (Cahlin et al., 2000; Vaes et al., 2020). Therefore, additional efforts must be made to differentiate the tumor- and host-derived cytokines and their potential to induce cachexia.

Adipokines and myokines

Pro-inflammatory cytokines released from cachexia-inducing tumors or other tissues in the presence of a tumor modulate the expression and release of factors from the adipose tissue (adipokines) and muscle (myokines). Likewise, other systemic and metabolic perturbances influence the expression and release of adipokines and myokines. These factors mediate the inter-organ communication between the adipose tissue and muscle with the other tissues (F. Li et al., 2017). The adipose tissue wasting and muscle atrophy observed in cancer cachexia impair tissue function, thereby altering the adipokines and myokines secretion profile. Although less studied, an altered secretion profile during cachexia development affects the inter-organ crosstalk and impairs the metabolism in other organs (B. Z. C. Weber et al., 2022).

Leptin is one such critical adipokine involved in controlling the appetite and was found to be significantly decreased in cancer cachexia patients and positively correlated with weight loss, appetite score, and insulin resistance (Smiechowska et al., 2010; Weryńska et al., 2009). Similarly, leptin levels were reduced in the rat models of cancer cachexia; however, the mechanism underlying these reduced levels and its contribution to cachexia is not well-studied (Suzuki et al., 2011). Acylated ghrelin secreted by the stomach counteracts the effect of leptin. It negatively correlates with weight change in cancer cachexia patients (Smiechowska et al., 2010).

Adiponectin (AdipoQ) is an abundant adipokine that plays an essential role in the energy metabolism of the adipose tissue. Depending on the type of cancer and the degree of weight loss, AdipoQ levels were increased in cachexia patients (Batista et al., 2013; Mannelli et al., 2020). Other adipokines such as resistin, visfatin, and apelin are less studied in the context of cancer cachexia; however, these factors were found to be altered in weight-losing cancer patients (Mannelli et al., 2020). Increasingly, the role of secreted factors of the BAT (referred to as batokines) is implied in the cachexia progression. Fibroblast growth factor-21 (FGF-21) is significantly increased in cancer cachexia patients (Franz et al., 2019).

Myostatin, also referred to as growth differentiation factor-8 (GDF-8), is one of the earlier myokines studied and was found to be a negative regulator of muscle mass. Myostatin belongs to the transforming growth factor- β (TGF- β) family. It mediates its function through the activin type II receptor (ActRIIB) and SMAD-2/3 signaling pathway (Sartori et al., 2009). Cachexia was induced, and muscle loss was observed in the mice injected with myostatin overexpressing tumor cells (Zimmers et al., 2002). Remarkably, in the mouse model of Duchenne muscular dystrophy (DMD), myostatin-blocking antibodies treatment

improved muscle mass and strength (Bogdanovich et al., 2002). The role of myostatin is beyond muscle tissue, as its levels were remarkably increased in the adipose tissue of obese mice (Allen et al., 2008).

Activin A, another crucial TGF- β family myokine, was found to be increased in metastatic cancer patients (Leto et al., 2006). Signaling through the NF- κ B pathway, increased Activin A levels impaired the myotube function and was rescued upon antibody-mediated blocking of Activin A (Trendelenburg et al., 2012). The role of other myokines such as irisin, myonectin, decorin, and β -aminoisobutyric acid (BAIBA) are increasingly studied and implied in the context of cachexia and other muscle wasting conditions (Manole et al., 2018; Pin et al., 2021). These factors are involved in various metabolic functions and critical in inter-organ communication. Treatment strategies targeting the altered myokines signaling were promising (Benny Klimek et al., 2010; Zhou et al., 2010), and further research is deemed in this area.

1.1.5. Cachexia as a multiorgan syndrome

Cachexia-inducing tumors secrete catabolic factors, and pro-inflammatory cytokines are generated through the crosstalk between the tumor and the host immune system. As mentioned earlier, adipokines from adipose tissue and myokines secretion profiles from muscle are altered in response to metabolic dysregulation (B. Z. C. Weber et al., 2022). These mediators directly affect various organ systems and play an essential role in the loss of target tissues (skeletal muscle, heart, and adipose tissue). Also, they induce metabolic changes in the tissues such as the brain, liver, intestine, and immune system (**Figure 3**). These metabolic perturbations further aggravate the wasting condition through the complex interplay (Schmidt et al., 2018). Thus, cancer cachexia is referred a multiorgan syndrome that affects and is influenced by various organs in the system.

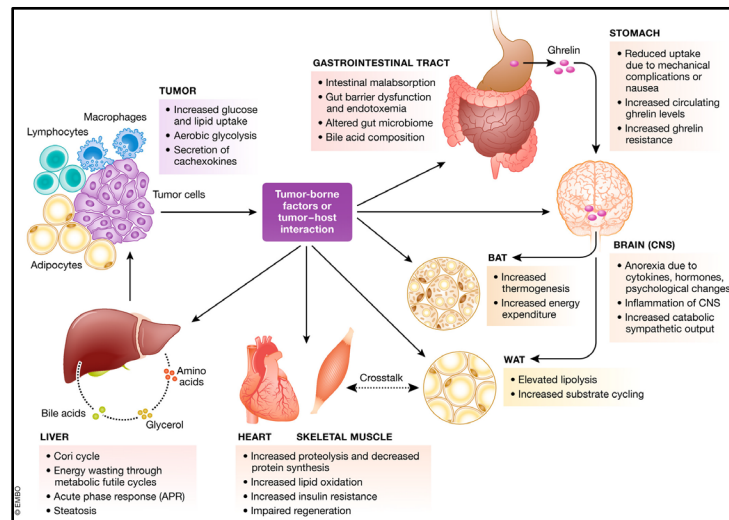


Figure 3: Cachexia as a multiorgan syndrome. Cachexia-inducing tumor and its action on metabolic organs. The physiological processes altered in different organs during cachexia are displayed. Increased lipolysis in adipose tissue and increased proteolysis in skeletal muscle are key features observed in cachexia patients. Adapted from (Rohm et al., 2019).

Skeletal muscle atrophy

Loss of skeletal muscle represents the main clinical manifestation of cancer cachexia (K. Fearon et al., 2011) and is associated with reduced protein synthesis and increased degradation (Smith & Tisdale, 1993). The pro-inflammatory cytokines and myokines described above play a central role in skeletal muscle

wasting. These factors upregulate the expression of critical E3 ligases: Muscle-Specific RING Finger Protein-1 (MuRF-1) and F-Box Only Protein-32 (FBXO-32). MuRF-1 E3 ligases mediate the ubiquitination of myofibrillar proteins and degrade them through the Ubiquitin-Proteasome system (UPS) (Clarke et al., 2007; Cohen et al., 2009). MuRF-1 is remarkably upregulated through NF- κ B signaling, activated by upstream regulators of muscle wasting such as TWEAK (Dogra et al., 2007). FBXO-32, on the other hand, is activated through MAPK signaling by the induction of the CCAAT/enhancer-binding protein (C/EBP)- β transcription factor (Y.-P. Li et al., 2005). FBXO-32 inhibits the protein translation by the ubiquitination of the C-terminal of the initiation factor Eukaryotic translation initiation factor 3 subunit F (eIF3-f). (Csibi et al., 2009). Thus, MuRF-1 and FBXO-32 are highly upregulated during muscle wasting observed in various settings such as cancer cachexia, fasting, denervation, and glucocorticoid-induced (Bedard et al., 2015; Coyne et al., 2018; Rohm et al., 2016). The secreted factors of the cachexia-inducing tumors and tumor-induced altered secretome of the muscle, acting through the NF- κ B and MAPK signaling, contribute to skeletal muscle wasting.

Adipose tissue wasting

According to the consensus (K. Fearon et al., 2011), cancer cachexia is defined as “loss of skeletal muscle mass (with or without loss of fat mass).” However, adipose tissue loss and its role in developing cancer cachexia have been increasingly studied in recent years. In animal models of cancer cachexia, fat mass loss was observed even before the evident body weight loss (Ishiko et al., 1999). Longitudinal assessment of cancer patients with solid gastrointestinal tumors using dual-energy X-ray absorptiometry (DEXA) revealed that patients progressively lost fat tissue more than lean tissue (Fouladiun et al., 2005). The critical mechanism involved in adipose tissue wasting is the increased lipolysis observed in cachexia patients and various animal models of cancer cachexia (Agustsson et al., 2007; Dahlman et al., 2010; Rohm et al., 2016). Apart from the factors mentioned before (*Pathogenesis of cancer cachexia*), catecholamines and natriuretic peptides are reported to induce lipolysis during cachexia (Kalra & Tigas, 2002). The rate-limiting enzymes of lipolysis, the adipose triglyceride lipase (ATGL), and the hormone-sensitive lipase (HSL) are highly upregulated in adipose tissue of weight-losing cancer patients as well as in animal models (Agustsson et al., 2007; Das et al., 2011; Thompson et al., 1993). Apart from the lipases involved in the breakdown of triacylglycerols (TAGs), the β -1 Adrenergic Receptor (ADRB-1) is also increased in the adipose tissue of cachexia patients (Cao et al., 2010). Activation of adenylate cyclase by ADRB-1 increases the accumulation of cyclic adenosine monophosphate (cAMP), which activates protein kinase A (PKA). PKA phosphorylates its target proteins HSL and perilipin-1 (PLIN-1), thereby promoting lipolysis.

1.1.6. Animal models used for cancer cachexia research

The prevalence of cachexia is about 50-80% in end-stage cancer patients, and the mortality rate is estimated at 80% per year in cancer patients (von Haehling & Anker, 2014). Given the rising incidence of cachexia, it is essential to develop effective strategies to counteract the metabolic dysregulation and weight loss associated with it. For effective treatment, a better understanding of the pathogenesis and pathophysiology of the disease is required. Knowledge about the different mechanisms perturbed during cachexia and potential pathways that can be targeted for the therapy were obtained from experiments using various preclinical animal models of cachexia (Ballarò et al., 2016).

Various well-established cancer cachexia models are based on cachexia-inducing rodent cancer cell lines injected subcutaneously, intramuscularly, or intraperitoneally into mice or rats. These models, referred to as the syngenic animal models, are widely used in cancer cachexia research, and the animals develop features observed in cancer cachexia patients. The most commonly used cancer cell lines include colon 26 adenocarcinoma (C26), murine adenocarcinoma 16 (MAC16), LLC, B16 melanoma, Walker 256 carcinosarcoma, and Yoshida ascites hepatoma 130 (AH-130) (A. Sherry et al., 1989; Bennani-Baiti & Walsh, 2011; Tanaka et al., 1990; Toledo, Penna, et al., 2016). Skeletal muscle and fat wasting observed in cancer cachexia patients are evident in these animal models with varying degrees of loss and tumor mass. Although the therapeutic window is relatively short in the C26 cachexia model, significant weight loss and cachexia phenotypes are observed when the tumor mass is about 2% of the carcass weight, which closely reflects the cachexia conditions in human cancer patients (Penna, Busquets, et al., 2016). Systemic inflammation with increased pro-inflammatory cytokines is also observed in these cachexia models. Pototschnig and colleagues recently established a new syngenic mice model for cachexia injecting CHX207 fibrosarcoma intramuscularly. CHX207 cells induced cachexia strongly in mice through IL-6 signaling (Pototschnig et al., 2022).

In orthotopic models, tumor cells are implanted into the organ or tissue of origin of the tumor cells. By injecting the tumor cells into its original tumor site, clinical features of cachexia were better recapitulated than those injected subcutaneously or intraperitoneally (Michaelis et al., 2017). Various research groups established orthotopic models using murine or human pancreatic cancer cells. PANC-1, L3.6pl, S2-013, and COLO-357 are the pancreatic cancer cell lines used to implant into the pancreas of the animals. These animals showed the characteristics of cachexia, such as weight loss, muscle atrophy, and inflammation varyingly (Bruns et al., 1999; Delitto et al., 2017; Henderson et al., 2018; Shukla et al., 2014). However, orthotopic injection requires specialized technical skill, and tumor cells used for injection are not well characterized. Additional research in characterizing tumor cells for injections will enable cancer cachexia researchers to perform experiments using orthotopic models of cancer cachexia and recapitulate clinical features of cachexia *in vivo*.

Genetic-engineered mouse models (GEMMs) for cachexia are increasingly established and studied. The positive aspects of using GEMM for cachexia research are that the tumor develops orthotopically, might extend the therapeutic window, and represents multistep tumorigenesis (Ballarò et al., 2016). In the APC^{Min/+} mice model, a point mutation in the adenomatous polyposis coli (APC) gene induces intestinal polyps. The mice develop cachexia phenotypes at around ten weeks of age. LSL-Kras^{G12D/+}; LSL-Trp53^{R172H/+}; Pdx-1-Cre (KPC) mice and inhibin α -subunit knockout mice (α -KO) are other GEMMs used in cachexia research (Gilabert et al., 2014; Gold et al., 2013; Lee et al., 2016). Recently, an inducible pancreatic cancer cachexia model was developed by Talbert and colleagues. Mice with the genotype Kras^{+G12D}; Ptf1a^{+ER-Cre}; Pten^{fl/fl} (KPP) developed cachexia upon tamoxifen-induced tumorigenesis and closely mimicked the metabolic alterations in the pancreatic ductal adenocarcinoma (PDAC) patients (Talbert et al., 2019).

In our lab, the C26 cancer cachexia model is well-studied in the context of hepatic, cardiac, and adipose dysfunction (Jones et al., 2013; Rohm et al., 2016, 2018; Schäfer et al., 2016). Moreover, the effects of aging and lipid profile alteration were recently studied using the C26 cachexia model (Geppert et al., 2022; Morigny et al., 2020).

1.1.7. Therapeutics developed against cancer cachexia

Since appetite is reduced in cancer cachexia patients, appetite stimulants such as megestrol acetate, cannabinoids, melanocortin-4 receptor antagonists, and ghrelin agonists were tested as treatment strategies against cancer cachexia and found to provide beneficial effects in mice and rat models of cancer cachexia as well as in human trials to a varying degree (Dallmann et al., 2011; Jang et al., 2014; Temel et al., 2015; J. Wang et al., 2019). Particularly, ghrelin receptor agonist anamorelin was shown to be effective in increasing the body weight, lean and fat mass of cancer patients in different phase II trials (Garcia et al., 2015; Temel et al., 2015). Subsequently, anamorelin was approved for cancer cachexia treatment in Japan and marketed as Adlumiz® (Wakabayashi et al., 2021), while other appetite stimulants are still being evaluated in preclinical studies and clinical trials (Argilés et al., 2017). Conceptually, nutritional support is considered an important component of multimodal therapeutic approaches against cachexia. However, the beneficial effect of nutritional support and advice on mortality of weight-losing cancer patients could not be determined, and trials on human patients provided confounding results (Bourdell-Marchasson et al., 2014; De Waele et al., 2015; Prado et al., 2020).

Another important group of drugs developed against cancer cachexia is those that interfere with cachexia-induced metabolic alterations. As mentioned earlier, TNF- α and IL-6 are critical pro-inflammatory cytokines affecting metabolism during cachexia. The research was done to develop antagonists and antibody-mediated therapies against these cytokines; however, the treatments did not provide any beneficial effect against the weight-losing effect of cachexia (Bayliss et al., 2011; Jatoi et al., 2010). ActRIIB is implicated in myostatin-mediated muscle and weight loss, and ADRB-1 levels in the adipose tissue correlated with weight loss in cachexia patients (Cao et al., 2010; Sartori et al., 2009). By using selective agonists against the β -AR and soluble ActRIIB (sActRIIB), researchers have shown rescue muscle wasting in mice models of cachexia (Toledo, Busquets, et al., 2016). The proteasome inhibitor bortezomib was also effective against muscle wasting in the AH-130 and C26 mice cachexia model (Penna, Bonetto, et al., 2016).

As mentioned, GDF-15 levels were particularly increased in weight-losing cancer patients and associated with poor prognosis (Lerner et al., 2015). Interestingly, GDF-15 neutralizing antibodies were shown to be effective against weight, muscle, and fat loss in the mice injected with various cachexia-inducing tumors (Lerner et al., 2016; Suriben et al., 2020), as well as in the chemotherapy (cisplatin) induced weight loss in mice and nonhuman primates (Breen et al., 2020). GDF-15 monoclonal antibody ponesegromab is currently being tested in phase II clinical trials in patients with cancer cachexia. Several other agonists and antagonists were developed against the critical regulators implicated in cachexia pathogenesis. Currently, no drugs have been approved for cancer cachexia treatment effective against metabolic alterations; however, several promising drugs and candidates are assessed in clinical trials. Despite these encouraging results, further research is required to develop effective therapeutics against muscle and fat loss during cachexia (Argilés et al., 2017).

Recently, our lab demonstrated that cell-death-inducing DNA fragmentation factor, alpha subunit-like effector A (CIDEA), interacts with AMP-activated protein kinase (AMPK) and inactivates AMPK activity in the adipose tissue of C26 tumor-bearing mice. An Ampk-Cidea-interfering peptide (ACIP) was developed. Treatment with ACIP prevented cachexia-induced weight and fat loss (Rohm et al., 2016).

Researchers are developing novel and multimodal therapies for effective treatment against cancer cachexia. However, the mechanism behind adipose tissue atrophy and treatment strategies to counteract this dysregulation is less studied and deems additional research in this area.

1.2. Adipose tissue and their function

Adipose tissue primarily comprises adipocytes and is found as different depots throughout the body. As mentioned earlier, adipose tissue is one of the organs significantly affected during cachexia development, and loss of adipose tissue has been proposed as a prognostic marker for cachexia. Adipose tissue stores energy in lipid droplets (LDs) containing neutral triacylglycerols (TAGs) and represents the central energy reservoir in mammals (Luo & Liu, 2016). Two major adipose tissue types, white adipose tissue (WAT) and brown adipose tissue (BAT), have diverse functions. WAT comprises two major depots, subcutaneous WAT (scWAT) and visceral WAT. scWAT are found under the skin and visceral WAT around the organs in the abdominal cavity. In humans, BAT is found around the shoulder and ribs. While WAT functions primarily in energy homeostasis and insulation of intra-abdominal organs, BAT is involved in thermal regulation (Hajer et al., 2008).

1.2.1. Adipocyte physiology

The white and brown adipocytes are the primary cell types in the WAT and BAT, respectively. Their physiology and function govern the distinct roles of these fat depots. The white adipocytes are differentiated from adipogenic Myf5⁻ precursors. The brown adipocytes and myocytes share common myogenic Myf5⁺ precursors (A. Park, 2014). The white adipocytes contain a single unilocular lipid droplet that occupies almost the whole cell. In contrast, the lipid droplets in the brown adipocytes are multilocular. Brown adipocytes have high mitochondria content, similar to muscle cells, and have a high oxidation capacity (Choe et al., 2016). Brown adipocytes express high levels of uncoupling protein-1 (UCP-1), which is an important component of its thermogenic function (A. Park, 2014). On the other hand, white adipocytes are specialized in lipid storage and can expand up to 100 μm in diameter. A new type of adipocyte is increasingly being studied called beige/brite adipocytes, which have both white and brown adipocyte characteristics (J. Wu et al., 2012). Upon cold exposure, beige adipocytes that typically display white adipocyte features adopt an intermediate cell morphology with smaller multilocular lipid droplets surrounding the larger ones. Beige adipocytes have an increased expression of brown adipocyte markers such as UCP-1 and thus its features (A. Park, 2014). Different members of the C/EBP family, bone morphogenetic protein (BMP) family, and peroxisome proliferator-activated receptor gamma (PPAR- γ /PPARG) function in a coordinated way for the differentiation of white and brown adipocytes from their corresponding precursors (Hajer et al., 2008).

1.2.2. Adipose tissue as an energy storage organ

Lipogenesis and lipolysis are critical mechanisms involved in energy homeostasis in adipose tissue (Luo & Liu, 2016). Following food intake, the lipogenic pathway is activated for TAGs synthesis. TAGs can be synthesized by *de novo* lipogenesis (DNL) from the intermediates of the tricarboxylic acid (TCA) cycle and acetyl-coenzyme A (acetyl-CoA). Glucose stimulates the release of pancreatic insulin and induces the expression of the rate-limiting lipogenic enzyme acetyl-CoA carboxylase (ACC). Insulin-mediated glucose uptake into the adipocytes further activates the genes involved in glycolysis and lipogenesis. In addition,

adipocytes can take up free fatty acids (FFAs) from the circulating chylomicrons and very low-density lipoproteins (VLDL) by lipoprotein lipase (LPL). LPL hydrolyses the TGAs in the lipoproteins into FFAs (Mead et al., 2002). FFAs are reesterified by Acyl-CoA Synthetase Long-Chain Family Member-1 (ACSL-1), and diacylglycerol acyltransferase (DGAT) catalyzes the synthesis of TAGs. Thus, as an energy reservoir, adipose tissue buffers the excess FFAs and prevents lipotoxicity in other tissues (Hajer et al., 2008). Lipolysis is activated in WAT during energy-demanding conditions such as fasting, and TGAs are catabolically converted into FFAs and glycerol. Adipocyte triglyceride lipase (ATGL) and hormone-sensitive lipase (HSL) is the critical enzymes involved in the breakdown of TAGs to diacylglycerols (DAGs) and subsequently to monoacylglycerols (MAGs), respectively. Released glycerols can then be used for hepatic gluconeogenesis, and FFAs are oxidized through β -oxidation to produce energy (Zechner et al., 2012).

1.2.3. Adipose tissue as an endocrine organ

Adipose tissue was long considered to be a passive energy storage depot. However, researchers have demonstrated adipose tissue to be a complex and active metabolic and endocrine organ (Kershaw & Flier, 2004). Apart from adipocytes, adipose tissue also contains endothelial cells, blood cells, preadipocytes, macrophages, and several other cell types. These non-adipocyte cells are collectively called the adipose tissue stromal vascular fraction (SVF). The composition and the dynamic interaction of the SVF cells and adipocytes control the function of the adipose tissue (Hajer et al., 2008). Adipokines and cytokines secreted by various cells in the adipose tissue act within adipose tissue and enter the systemic circulation, and, through endocrine action, modulate the metabolism in various organs (**Figure 4**) (Fasshauer & Blüher, 2015; Proença et al., 2014). In addition, lipids secreted by the adipose tissue also influence the metabolism in the liver, muscle, and other tissues (Symonds, 2012). Thus, dysregulation in adipose tissue can exert systemic effects and is observed in various metabolic disorders.

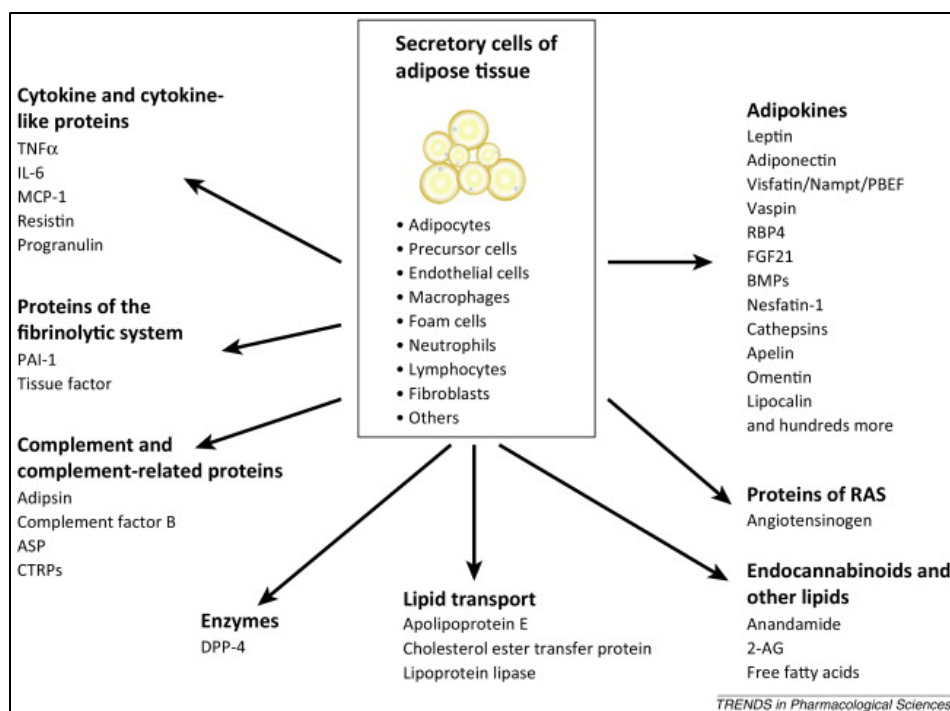


Figure 4: Adipose tissue as an endocrine organ. Important regulatory factors are secreted by various cells in the adipose tissue. Adapted from (Fasshauer & Blüher, 2015).

Leptin was one of the first adipokines discovered (Zhang Y et al., 1994). It was referred to as the satiety hormone because it inhibits hunger and food intake (Elmquist et al., 1999). The plasma leptin levels positively correlate with the body fat mass (Ostlund et al., 1996) and regulate the energy stored in the form of fat by suppressing the appetite. Leptin released by the adipose tissue in response to insulin, glucocorticoids, serotonin, and estrogen crosses the blood-brain barrier and targets the hypothalamus region in the brain (Blüher & Mantzoros, 2015). The leptin receptor and downstream JAK2/STAT3 signaling pathway influence food intake and thus modulate the glucose and fat metabolism in the adipose tissue. Given its important regulatory role in maintaining body weight and energy homeostasis, dysregulation in leptin signaling (referred to as leptin resistance) leads to development of metabolic disorders such as obesity and insulin resistance (Gruzdeva et al., 2019). Increasingly, the role of leptin is demonstrated in the β -cell biology, hepatic metabolism, systemic immune response, and reproduction (Symonds, 2012). Leptin plays a crucial role in angiogenesis, and leptin and its receptor levels were elevated in cancer patients (Luo & Liu, 2016). In the context of cancer cachexia, counterintuitively, leptin levels were particularly decreased in the weight-losing cancer patients (Smiechowska et al., 2010; Weryńska et al., 2009) and animal models of cancer cachexia (Bing et al., 2001; Suzuki et al., 2011). However, the mechanism of decreased leptin levels and its contribution to anorexia and cachexia is less studied.

Another important adipokine that is well-studied is AdipoQ. AdipoQ regulates adipogenesis, insulin sensitivity, and energy homeostasis by binding to its receptors adiponectin receptor-1 and receptor-2 (AdipoR-1 and AdipoR-2) (Ye & Scherer, 2013). The primary target of AdipoQ is the liver, which activates the AMPK and suppresses gluconeogenesis, ultimately enhancing the insulin-sensitizing effect (Nawrocki et al., 2006). Independent of the AMPK, AdipoQ has been shown to improve insulin signaling by acting through ceramide, PPAR- α , and fibroblast growth factor (FGF) signaling (Holland et al., 2011; Y. Wang et al., 2005). AdipoQ also activates the AMPK signaling pathway in the skeletal muscle and improves glucose uptake and fatty acid oxidation. The cardioprotective function of AdipoQ is dependent on the T-cadherin receptor and eNOS (endothelial nitric oxide synthase) signaling (Denzel et al., 2010). Because of these protective effects of AdipoQ, activators of AdipoQ signaling were developed for treating and managing metabolic diseases such as type-2 diabetes (T2D) and its associated complications (Fasshauer & Blüher, 2015). As mentioned earlier, plasma AdipoQ levels were increased in cancer cachexia patients (Batista et al., 2013; Mannelli et al., 2020), suggesting an altered secretion and functioning of adipokines during cancer cachexia.

Other important adipokines that play a critical role in lipolysis, inflammation, insulin resistance, and other metabolism are resistin, FGF-21, apelin, vistafin, TNF α , and IL-6 (Luo & Liu, 2016). Apart from adipocytes, adipose tissue-resident immune cells are the primary source of some adipokines. Thus adipose tissue as an endocrine organ plays an important role in systemic energy homeostasis. Dysregulation in the production, secretion, and functioning of these adipokines in the target tissues is implicated in various metabolic disorders (Fasshauer & Blüher, 2015; Mannelli et al., 2020; Smiechowska et al., 2010). Further, adipose tissue remodeling and dysfunctioning represent the clinical features of cachexia (Dahlman et al., 2010; Rohm et al., 2019). Given the complex endocrine function of adipose tissue and alteration during various disease progressions, pharmacotherapies using or targeting adipokines are being developed (discussed in upcoming sections).

1.2.4. Adipose tissue as thermoregulator

While the WAT functions primarily as an energy regulator and endocrine organ, the role of BAT is predominantly in lipid oxidation and thermoregulation. Unlike the mono-locular lipid droplets in WAT, BAT's lipid droplets are multilocular in nature. BAT is characterized by high mitochondria levels and high expression of mitochondrial UCP-1 (A. Park, 2014). Upon cold exposure, β -adrenergic signaling is activated in the BAT, which stimulates the expression of peroxisome proliferator-activated receptor γ coactivator-1 α (PGC-1 α), and PR Domain-Containing Protein-16 (PRDM-16) and thereby inducing UCP-1 expression. UCP-1 uncouples oxidative phosphorylation (OXPHOS) from ATP synthesis, redirects the proton gradient, and dissipates energy in the form of heat (Luo & Liu, 2016). Recent studies suggest the potential role of WAT in thermoregulation through the remodeling of WAT into a BAT phenotype. This process is called WAT browning, where the mature white adipocytes are transdifferentiated into beige adipocytes capable of thermogenesis (Rosenwald et al., 2013). However, some studies point out that beige adipocytes in WAT, upon cold exposure, are differentiated from a specific precursor cell population (Choe et al., 2016). The role of BAT function and browning of WAT are increasingly studied in the context of cancer cachexia. Particularly, the increased thermogenic activity of adipose tissue was shown to contribute to energy and tissue loss during cancer cachexia (Kir et al., 2014; Kir & Spiegelman, 2016; Petruzzelli et al., 2014). However, our lab showed that the UCP-1 knockout mice develop cancer cachexia, suggesting a UCP-1-independent mechanism of energy wasting in cancer cachexia (Rohm et al., 2016). A better understanding of these mechanisms will help to develop efficient pharmacotreatment strategies against metabolic diseases.

1.2.5. Dysfunction in metabolic syndrome

The effective functioning of adipose tissue is critical in maintaining metabolic homeostasis. Adipose tissue, an energy-storing organ, controls energy homeostasis and lipid mobilization (Luo & Liu, 2016). By secreting lipids and adipokines, adipose tissue functions as an endocrine organ and influences various metabolic pathways in distant organs. Moreover, BAT plays an essential role in non-shivering thermal regulation. Given its diverse role in metabolism, dysregulation of adipose tissue function is implicated in various metabolic disorders (Vegiopoulos et al., 2017). Adipose tissue dysfunction is a hallmark of obesity and is implicated in developing T2D and heart and lung diseases (Hajer et al., 2008). Increasingly, the role of adipose tissue is studied in cancer metabolism and the weight loss associated with it (Rohm et al., 2019; Schmidt et al., 2018).

1.2.6. Therapeutics targeting adipose tissue metabolism

Several pharmacotherapeutics and antibody-based therapies were developed to target adipose tissue and modulate its function in metabolic diseases (Grandl et al., 2020). Because of its role in controlling food intake, recombinant leptin was developed as a treatment strategy for obesity (Heymsfield et al., 1999). Leptin resistance is one of the hallmarks of obese patients. Therefore, treatment with recombinant leptin alone did not provide weight losing effect. However, when co-treated with a leptin sensitizer, amylin, obese patients reduced significant weight and improved lipoprotein and glycemic parameters (Blüher, 2014; Moon et al., 2011). Adiponectin receptor agonist (AdipoRon) improved glucose handling and lifespan of the *db/db* mice fed with a high-fat diet (Kim et al., 2018). Thiazolidinediones (TZDs) regulate

lipid and glucose metabolism by targeting the nuclear transcription factor PPAR- γ . Pioglitazone improved glucose sensitivity in T2D patients (Lincoff et al., 2007). In cachexia, ATGL and HSL-deficient mice showed protection against tumor-induced weight and adipose tissue loss (Das et al., 2011).

1.3. Aim of the study

Loss of adipose tissue is one of the clinical features of cancer cachexia. Increased lipolytic activity is observed in the adipose tissue of weight-losing cancer patients and different animal models of cancer cachexia. Treatment strategies used for cachexia treatment mainly focus on improving appetite or decreasing protein degradation in skeletal muscle. However, these therapeutic options are ineffective in completely counteracting adipose tissue and weight loss, and there is a need to develop better treatment strategies.

This study aimed to identify pharmacological inhibitors of adipose tissue wasting to treat cancer-induced cachexia. For the first part, compounds from a pre-screen will be selected for their antilipolytic properties using *in vitro* adipocyte models such as 3T3-L1, murine primary adipocytes, and the human adipocyte model (hMSC-TERT). The therapeutic potential of selected compounds will then be evaluated on a mouse model of cancer cachexia *in vivo* (Figure 5). Mechanistic understanding of the treatments will potentially reveal novel pathways altered during and relevant for cachexia development. With a long-term goal, developing pharmacotherapies for cancer cachexia will help reduce mortality and prolong life expectancy in patients suffering from this condition.

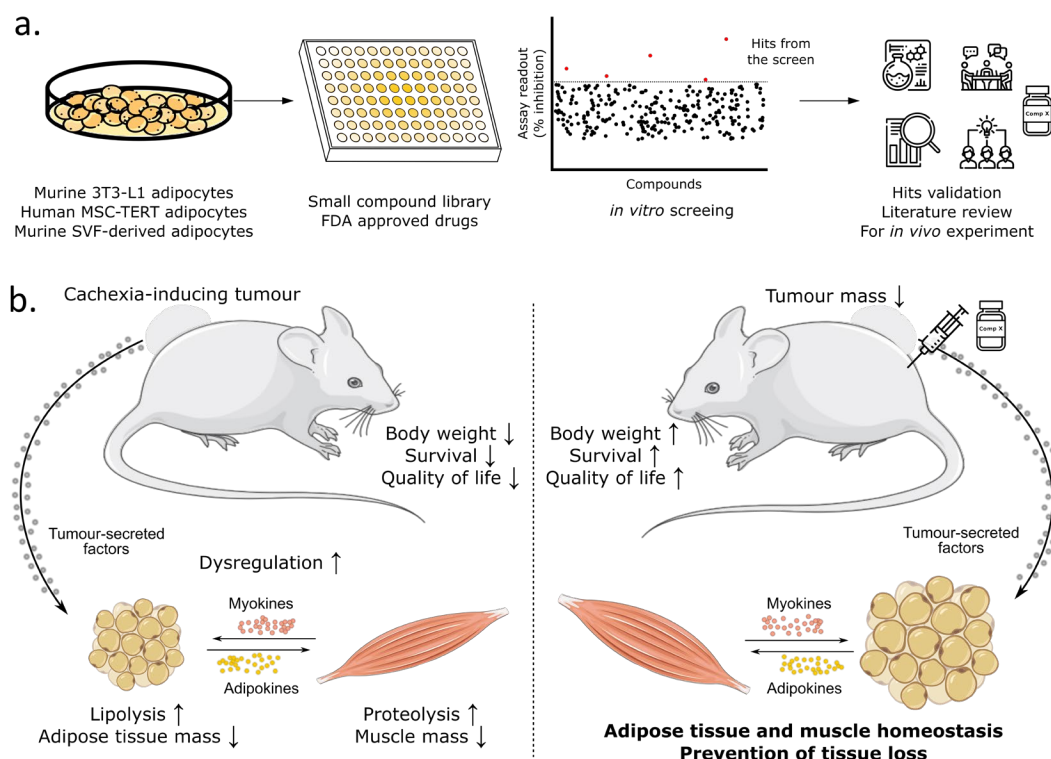


Figure 5: Aim of the study. (a) Screening strategy used in this study for identifying novel antilipolytic compounds, validation, and literature review for further *in vivo* studies. (b) Cachexia-tumor-bearing mice with increased metabolic dysregulation lose body weight, adipose tissue, and muscle mass. When treated with the hit compounds from the screening, we anticipate that the adipose tissue and muscle homeostasis are maintained, and weight and tissue loss are prevented. Created with Inkscape and BioRender.com.

2. RESULTS

2.1. 3T3-L1 adipocytes as a model to screen antilipolytic compounds *in vitro*

Weight-losing cancer cachexia patients and cancer cachexia mouse models exhibit increased white adipose tissue lipolysis compared to weight-stable cancer patients (Agustsson et al., 2007) and control mice groups (Rohm et al., 2016), respectively. Previous research studies have identified several cachexia-inducing factors (cachexokines) implicated in the increased lipolysis and the progression of cachexia (Han et al., 2018; Mracek et al., 2011). Researchers have postulated that inhibitors of rate-limiting lipases and lipolysis, in general, could be a treatment strategy against cancer-induced cachexia (Agustsson et al., 2007; Arner & Langin, 2014). To enable the screening for antilipolytic compounds potentially ameliorating cancer cachexia, it is, therefore, essential to establish *in vitro* readout systems for the lipolytic response of adipocytes.

2.1.1. Establishment of *in vitro* adipocyte system for drug screening

To mimic the increased adipose tissue lipolysis observed in cachexia in an *in vitro* system, I initially used murine 3T3-L1 fibroblasts differentiated into white adipocytes and established the cell culture system for compound screening. Preadipocytes were cultured and differentiated into mature adipocytes, as described in the Methods section (*Differentiation of cells into adipocytes and myotubes*). To investigate the differentiation efficiency, I performed Oil Red O staining. More than 90% of 3T3-L1 fibroblasts were differentiated into adipocytes, as seen by the staining of neutral lipid droplets (**Figure 6a**). The lipid droplet staining was quantified and was observed to be increased compared to the preadipocytes (**Figure 6b**).

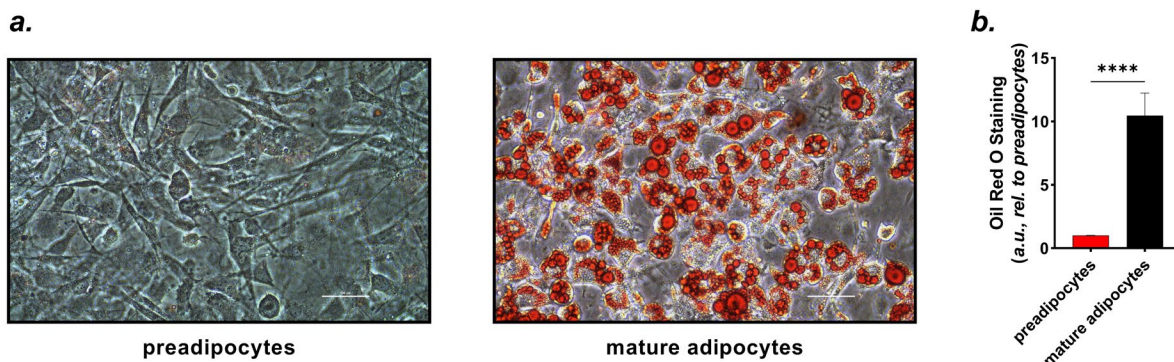


Figure 6: Differentiation of 3T3-L1 fibroblasts into adipocytes. (a) Representative images of the preadipocytes and differentiated 3T3-L1 adipocytes stained for the neutral lipid droplets by Oil Red O staining. Scale bars are 100 μm . (b) Quantification of the staining is shown in **Figure 6a**. $n = 4$, data shown are mean \pm s.e.m, **** $P < 0.0001$; by two-tailed t-test.

2.1.2. Cachexia-inducing TCCM induces adipocytes lipolysis *in vitro*

Morphologically differentiated 3T3-L1 adipocytes were laden with lipid droplets. To investigate their functionality, I treated the mature adipocytes with 10 μM of β -adrenergic receptor ligand isoproterenol (Iso) or tumor-cell-conditioned medium (TCCM) from different cancer cell lines. Murine C26, LLC, or human colorectal 116 carcinoma cell line (HCT116) were previously shown to induce cachexia *in vivo*, and TCCM derived from these cell lines induced adipocyte lipolysis *in vitro* (A. Sherry et al., 1989; Huot et al., 2020; Rohm et al., 2016; Tanaka et al., 1990). However, murine colon 38 adenocarcinoma (MC38) and

human colorectal 29 adenocarcinomas (HT29) did not induce cachexia (Nowakowska et al., 2014; Rosenberg et al., 1986).

Glycerol released into the medium was significantly increased in cells treated with Iso and C26 TCCM (**Figure 7a**). In accordance with previous research (Rohm et al., 2016), proteins involved in the lipolysis inhibition – HSL protein phosphorylated at Ser565 (p-HSL(Ser565)) and phosphorylated acetyl-Coenzyme A carboxylase α (p-ACC α (Ser79)) were significantly downregulated (**Figure 7b, c**). I then compared the effects of TCCM derived from cachexia-inducing C26 and non-cachexia-inducing MC38 on inducing lipolysis *in vitro*. As previously shown by our lab (Rohm et al., 2016), lipolysis was induced when treated with C26 TCCM but not with MC38 TCCM (**Figure 7d**). Similarly, TCCM cachexia-inducing HCT116 induced lipolysis, but non-cachexia-inducing HT29 did not induce lipolysis. However, murine-derived LLC that developed cachexia *in vivo* (A. Sherry et al., 1989) did not significantly increase lipolysis (**Figure 7e**). Using the 3T3-L1 adipocyte model, I can recapitulate the cachexia-induced lipolysis and fundamental metabolic changes observed in the adipocytes of cancer cachexia patients (Agustsson et al., 2007; Rohm et al., 2016). To develop effective pharmacological treatment, it is essential to test the efficacy of the compounds in different systems. Therefore, I established an additional adipocyte model using mouse adipose tissue-derived stromal vascular fraction (SVF) and human mesenchymal-derived stem cells (data not shown).

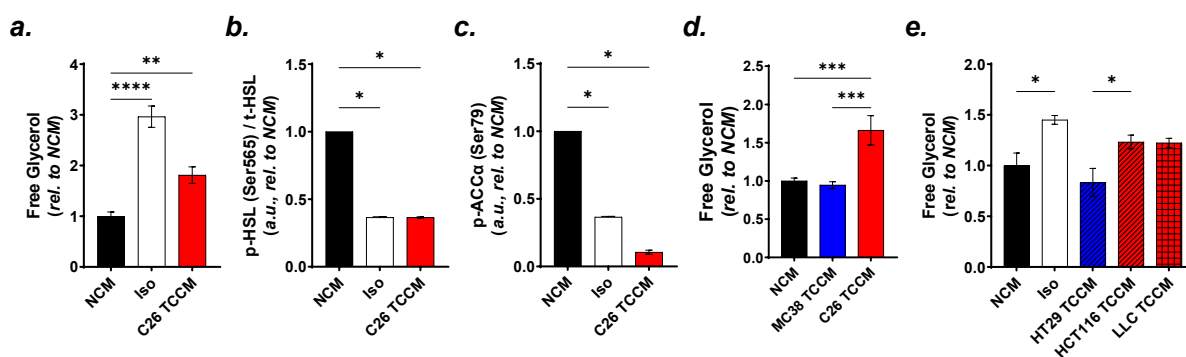


Figure 7: β -adrenergic receptor ligand and TCCM from cachexia-inducing cells induces lipolysis *in vitro*. (a) Free glycerol was released into the medium of the differentiated 3T3-L1 adipocytes treated with either growth medium (NCM), isoproterenol (Iso), or C26 TCCM for 24 hours. (b, c) Proteins extracted from the treated adipocytes were immunoblotted for specific proteins involved in lipolysis. p-HSL(Ser565) levels were normalized with the total HSL and p-ACC α (Ser79) with β -Actin, which was used as the loading control. Free glycerol was released into the medium of the differentiated 3T3-L1 adipocytes treated with either (d) NCM, MC38 TCCM, or C26 TCCM for 24 hours, (e) NCM, Iso, human HT29 TCCM, HCT116 TCCM or LLC TCCM. (a – e) $n = 4$, data shown are mean \pm s.e.m. * $P \leq 0.05$, ** $P \leq 0.01$, *** $P \leq 0.001$, **** $P \leq 0.0001$; by one-way ANOVA with Šidák's multiple-comparison test.

2.2. Screening of compounds *in vitro*

I established three adipocyte systems to screen our compounds and effectively narrow down lead drugs for *in vivo* treatment. After establishing the cell system for adipocyte differentiation, I screened our compounds for their antilipolytic properties in 3T3-L1 adipocytes, mouse primary adipocytes, and human mesenchymal stem cells transduced by a retroviral vector containing the catalytic subunit of human telomerase (hMSC-Tert) differentiated into adipocytes.

2.2.1. Compounds used for the screening

Dr. Katarina Klepac in our lab has previously performed high-throughput screening of compounds *in vitro* on differentiated brown adipocytes (data not shown). She used compounds from the GPCR-targeted library, LOPAC (The Library of Pharmacologically Active Compounds; Sigma-Aldrich), and the Prestwick Chemical Library. Compounds from these libraries are pharmacologically active small molecules that target diverse signaling processes. The United States Food and Drug Administration (FDA), European Medicines Agency (EMA), and other agencies have approved several of the compounds tested. She identified compounds that modulate lipolysis in brown adipocytes while focusing on those that induce lipolysis.

Given that lipolysis is induced in cachexia, I was interested in finding compounds that inhibit the induced lipolysis in white adipocytes. Therefore, we pre-selected fifty-one compounds based on their inhibitory effect in the previous screening performed in brown adipocytes. Literature reviews on these pre-selected compounds revealed that they are agonists or antagonists of important receptors and activators or inhibitors of critical metabolic pathways. I screened these fifty-one compounds for their antilipolytic properties in three *in vitro* white adipocyte models described above (3T3-L1, mouse primary adipocytes, and hMSC-Tert). The compounds, their structure, known functions, and information are presented in the Materials section (**Table 9**).

2.2.2. Tumor-induced lipolysis assay-based compound screening on 3T3-L1 adipocytes

I differentiated murine 3T3-L1 preadipocytes to adipocytes and treated them with either C26 or MC38 TCCM, with 10 μM of the pre-selected 51 compounds or corresponding vehicle control. I also treated the adipocytes with a non-conditioned growth medium (NCM) for 24 hours. After treatment, I quantified the free glycerol released into the medium. The scheme of the experimental procedure is shown in **Figure 8a**. C26 TCCM induced lipolysis up to 40%, measured by the free glycerol released, while NCM or MC38 TCCM treatment did not. Ten compounds significantly inhibited C26 TCCM-induced, and seven inhibited basal (MC38 TCCM) lipolysis (**Figure 8b**). 10 μM of four compounds brought down the glycerol level back to that treated with NCM or MC38 TCCM. In comparison, the remaining six compounds had a substantial antilipolytic effect. I observed five compounds to induce lipolysis in white adipocytes treated with C26 TCCM. However, they had no or less effect when treated with MC38 TCCM. These screening compounds' percentage inhibition (or induction) of lipolysis is represented as a heat map (**Figure 8c**). Most compounds that inhibited lipolysis significantly decreased glycerol levels under C26 and MC38 TCCM treatment conditions.

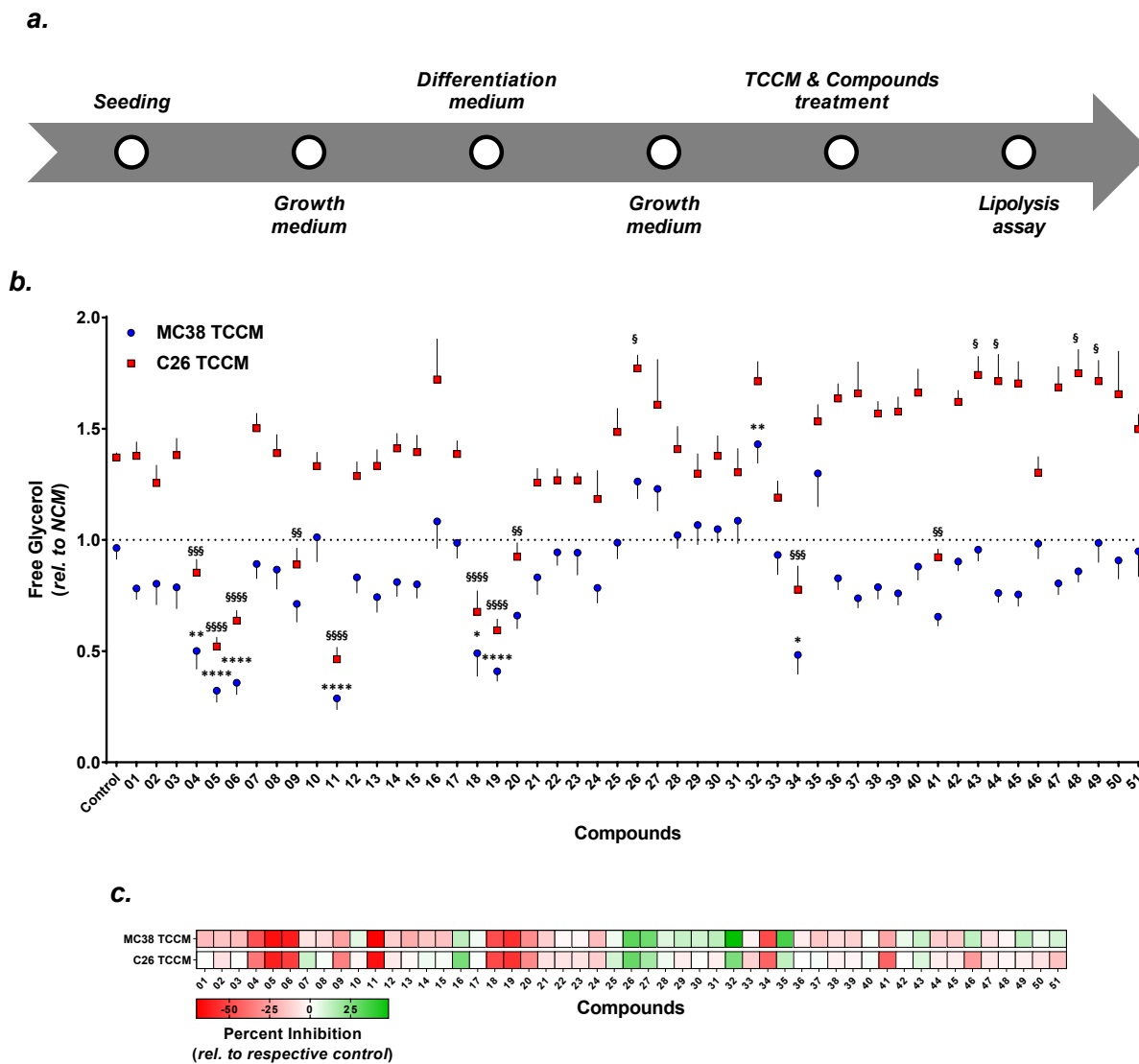


Figure 8: Tumor-induced lipolysis assay-based compound screening on 3T3-L1 adipocytes. (a) Preadipocytes were seeded, grown to confluence and cultured with adipogenesis-inducing differentiation medium, changed every 2-3 days. Differentiated adipocytes were treated with either growth medium and tumor cell-derived conditioned medium (TCCM) with or without 10 μ M of test compounds for 24 hours. Lipolysis was assayed by measuring the non-esterified fatty acid (NEFA) and free glycerol released into the medium. **(b)** Free glycerol was released into the medium of the differentiated 3T3-L1 adipocytes treated with either MC38 TCCM or C26 TCCM together with 10 μ M of the screening compounds for 24 hours. The dotted line represents the reference level of cells treated with NCM. **(c)** Heat map representing the mean percent inhibition of lipolysis relative to respective control. **(b)** $n = 4$, data shown are mean \pm s.e.m., * indicates significance between MC38 TCCM control and specific compound, § indicates significance between C26 TCCM control and specific compound. * $P \leq 0.05$, ** $P \leq 0.01$, *** $P \leq 0.001$, **** $P \leq 0.0001$; by two-way ANOVA with Dunnett's multiple-comparison test.

2.2.3. Tumor-induced lipolysis assay-based compound screening on hMSC-Tert adipocytes

I identified ten compounds that inhibited C26 TCCM-induced lipolysis in the murine white adipocyte model. For developing drugs against human disease, it is also essential to screen and test compounds in human models. Here, I used hMSC-Tert cells differentiated into white adipocytes and C26 TCCM to induce lipolysis. I obtained variable results (not shown) when I cultured the hMSC-Tert adipocytes with TCCM

derived from human cancer cells and MC38 TCCM. For these reasons, I performed the compound screening in this cell model using NCM and C26 TCCM. Like in 3T3-L1 adipocytes, C26 TCCM treatment increased the hMSC-adipocyte lipolysis by 40%, and ten compounds inhibited basal and cachexia-induced lipolysis (**Figure 9a**). Two compounds increased the lipolysis and, thus, the free glycerol levels in the medium. Selected compounds (Compound 04, 05, 11, 18, 19, 20, and 34) that inhibited lipolysis in the 3T3-L1 screen also inhibited lipolysis in the hMSC-Tert model. Interestingly, four compounds (Compounds 01, 06, 07, and 24) inhibited C26 TCCM-induced lipolysis exclusively in the human model; Compounds 06 and 34 significantly inhibited only the C26 TCCM-induced lipolysis. The heat map shows the percentage inhibition of lipolysis to the respective controls (**Figure 9b**).

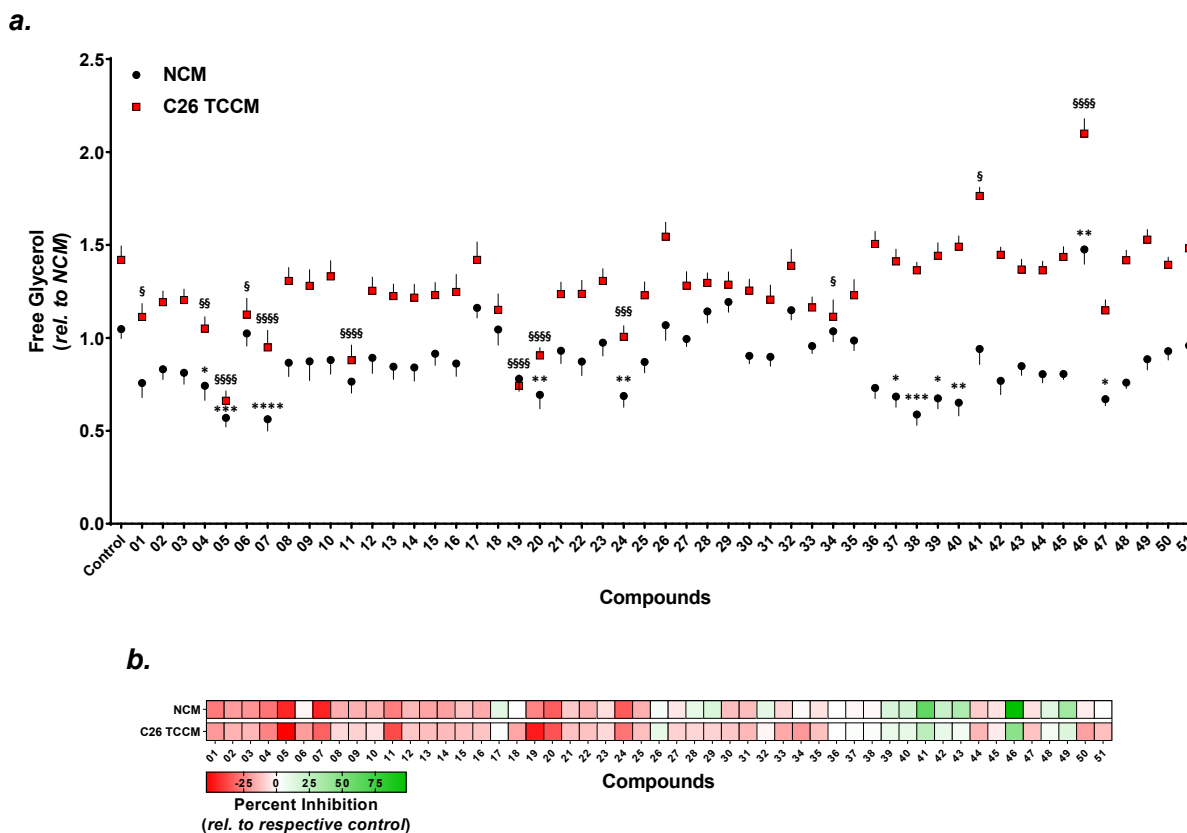


Figure 9: Tumor-induced lipolysis assay-based compound screening on hMSC-Tert adipocytes. (a) Free glycerol was released into the medium of the differentiated hMSC-Tert adipocytes treated with either NCM or C26 TCCM and 10 μ M of the screening compounds for 24 hours. **(b)** Heat map representing the mean percent inhibition of lipolysis relative to respective control. **(a)** $n = 4$, data shown are mean \pm s.e.m., * indicates significance between NCM control and specific compound, \$ indicates significance between C26 TCCM control and specific compound. * $P \leq 0.05$, ** $P \leq 0.01$, *** $P \leq 0.001$, **** $P \leq 0.0001$; by two-way ANOVA with Dunnett's multiple-comparison test.

2.2.4. Tumor-induced lipolysis assay-based compound screening on murine primary adipocytes

Mouse stromal vascular fraction (SVF) isolated from the inguinal white adipose tissue (iWAT) contains progenitor cells that can be differentiated into white adipocytes *in vitro* (Liu et al., 2017). To have more biological references for the compound screening, I used mouse primary adipocytes for the third screening. Freshly isolated SVF was cultured and differentiated into white adipocytes, treated with MC38 TCCM or C26 TCCM and 10 μ M of the screening compounds. Several compounds modulated the glycerol

release in the mouse primary adipocytes (**Figure 10a**). However, due to high variability among different biological replicates, several compounds' effects were insignificant. Compounds 16 and 26 increased the glycerol release significantly, as they did in the 3T3-L1 adipocytes screen. Compounds 04 and 34 significantly and consistently inhibited lipolysis also in this screen. The induction or inhibitory effect of the compounds is not specific to either MC38 TCCM or C26 TCCM treatment, as observed from the heat map (**Figure 10b**).

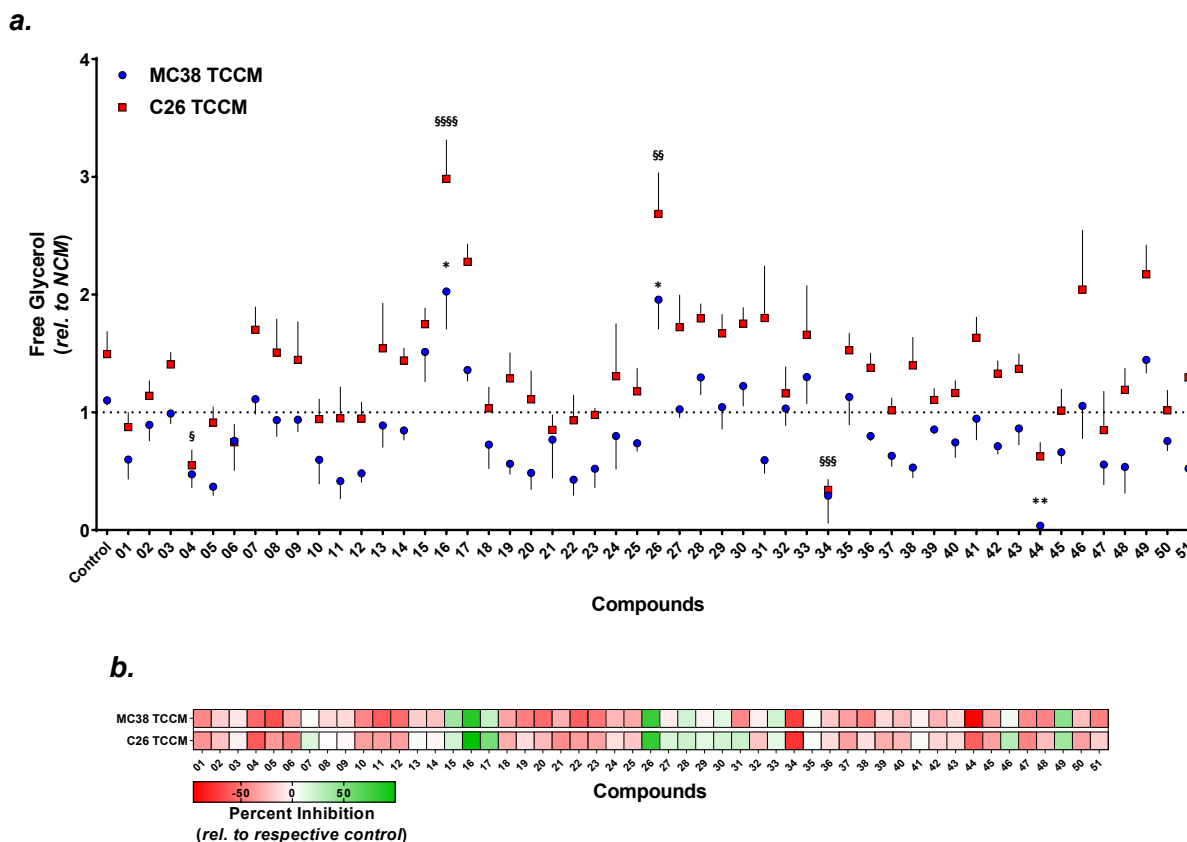


Figure 10: Tumor-induced lipolysis assay-based compound screening on murine primary adipocytes. (a) Free glycerol was released into the medium of the differentiated murine primary adipocytes treated with either MC38 TCCM or C26 TCCM together with 10 μ M of the screening compounds for 24 hours. The dotted line represents the reference level of cells treated with NCM. **(b)** Heat map representing the mean percent inhibition of lipolysis relative to respective control. **(a)** $n = 5$, data shown are mean \pm s.e.m., * indicates significance between MC38 TCCM control and specific compound, § indicates significance between C26 TCCM control and specific compound. * $P \leq 0.05$, ** $P \leq 0.01$, *** $P \leq 0.001$, **** $P \leq 0.0001$; by two-way ANOVA with Dunnett's multiple-comparison test.

2.2.5. Selection of compound for validation

Fifty-one compounds were screened for their antilipolytic properties in three white adipocyte models *in vitro* – murine 3T3-L1, human MSC-Tert, and mouse primary adipocytes. The 16 compounds that significantly inhibited lipolysis in at least one of the conditions tested are represented as a summarizing heat map depicting the percentage inhibition in the three complementary screenings (**Figure 11a**). Next, I selected only the compounds that significantly inhibited C26 TCCM-induced lipolysis in at least two of the three models tested for further experiments. Since there was variability in the mouse primary adipocytes screening and because of their target and biological relevance, I also considered including

compounds 06, 09, and 18 for further analysis, albeit they exerted significant antilipolytic effects only in 3T3-L1 adipocytes. In sum, I selected nine compounds (04, 05, 06, 09, 11, 18, 19, 20, and 34) for subsequent validation experiments.

a.

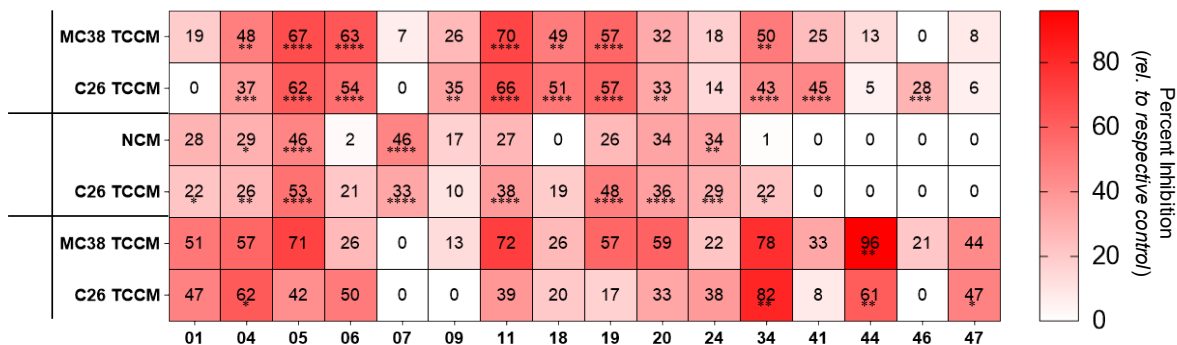


Figure 11: (a) Heat map representing the mean percent inhibition of lipolysis relative to respective control of selected compounds from compounds screening performed using 3T3-L1, mouse primary, and hMSC-Tert adipocytes. The value within the cells indicates the percent inhibition of lipolysis, and the asterisk indicates the significance relative to the respective control.

2.3. Validation of the hit compounds

Based on the tumor-induced lipolysis assay-based compound screening performed in three different cell models, I identified nine compounds that are interesting and potentially effective *in vivo* to counteract the weight loss associated with cancer cachexia. Compounds significantly inhibited lipolysis in at least two of the screens performed were selected for further validation. I performed various *in vitro* validation assays to narrow down the number of the compounds finally selected for *in vivo* testing.

2.3.1. Validation of compounds using human TCCM

To validate the screen and further extend the scope, I used 3T3-L1 adipocytes and treated them with murine TCCM or human TCCM together with the selected compounds. Similar to the screen performed in the 3T3-L1 adipocytes (**Figure 8**), selected compounds significantly inhibited the C26 TCCM-induced lipolysis, and two compounds showed a definite trend in decreasing the induced lipolysis (**Figure 12a**). These results validate the screening performed using fifty-one compounds. Next, I tested the compounds for their antilipolytic property using the TCCM derived from two human colorectal carcinoma cell lines – non-cachexia-inducing HT29 and cachexia-inducing HCT116. Three compounds inhibited the basal (HT29 TCCM) and induced (HCT116 TCCM) lipolysis (**Figure 12b**). Though some compounds decreased the glycerol release, the effect was insignificant, presumably due to technical reasons and high variability. Subcutaneous and intrasplenic injections of HCT116 cells have been shown to induce muscle and fat wasting in mice models (Huot et al., 2020). However, HCT116 cells, when co-cultured with human-derived adipocytes, did not induce the pro-inflammatory cytokines (Nimri et al., 2019). This suggests that TCCM derived from HCT116 might not be as potent and relevant as C26 TCCM for screening and validating the antilipolytic compounds.

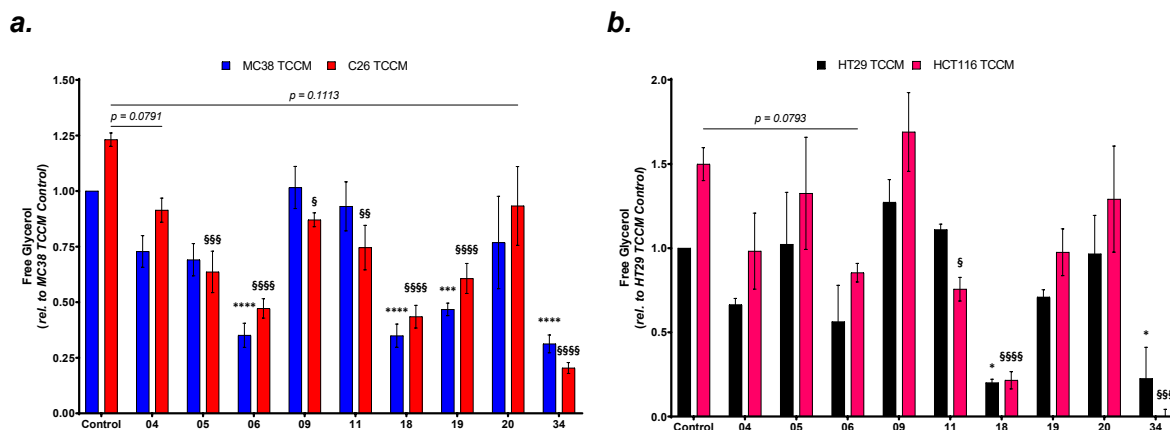
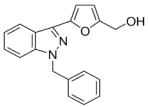
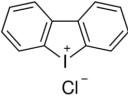
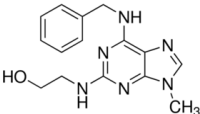
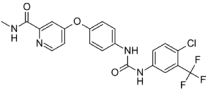


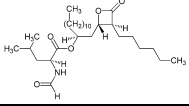
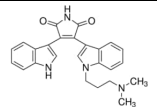
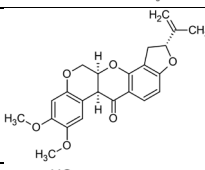
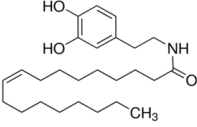
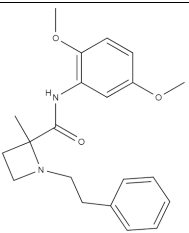
Figure 12: Selected compounds from the screen reduce basal and tumor-induced lipolysis. Free glycerol was released into the medium of the differentiated 3T3-L1 adipocytes treated with either (a) MC38 TCCM or C26 TCCM with 10 μ M of the selected compounds for 24 hours or (b) HT29 TCCM or HCT116 TCCM together with 10 μ M of the selected compounds for 24 hours. $n = 3$, data shown are mean \pm s.e.m., * indicates significance between MC38 TCCM/HT29 TCCM control and specific compound, § indicates significance between C26 TCCM/HCT116 TCCM control and specific compound. * $P \leq 0.05$, ** $P \leq 0.01$, *** $P \leq 0.001$, **** $P \leq 0.0001$; by two-way ANOVA with Dunnett's multiple-comparison test.

2.3.2. Literature review of the selected compounds

I reviewed research articles on the compounds selected from the screening. Several of the selected compounds hold significance as they or their targets are previously implicated in pathways affected by cancer cachexia. Other compounds are equally interesting, as these would help us identify novel mechanisms and targets against cancer cachexia. To determine which compounds to test *in vivo*, I must review them critically before proceeding further. **Table 1** summarizes the selected compounds' structure, target, and known functions.

Table 1: Information about the selected compounds.

Number	Compound name	Structure	Target and function	Reference
04	YC-1		Guanylyl cyclase activator. Inhibited lipolysis and ameliorated C26-induced weight loss.	(Chung et al., 2011)
05	Diphenyleneiodonium chloride (DPI)		NADPH oxidase (NOX) inhibitor. Prevented alcohol-induced liver injury in the rat.	(Kono et al., 2001)
06	Olomoucine		Cyclin-dependent kinases (CDK) inhibitor. Regulated proteins involved in fatty acid metabolism and glycolysis in the medulloblastoma.	(Bhatia et al., 2012)
09	BAY 43-9006 (Sorafenib, Nexavar®)		Broad-spectrum kinase inhibitor. Inhibited tumor growth and angiogenesis.	(Adnane et al., 2006; Wilhelm et al., 2004)

11	Orlistat		Gastric and pancreatic lipases inhibitor. Widely used to treat obesity.	(Gauthier et al., 2008)
18	GF-109203X		Protein Kinase C (PKC) inhibitor. Blunted ERK1/2 activation and the proliferation of colon cancer cells.	(Y. S. Park & Cho, 2012)
19	Rotenone		Mitochondrial NADH: ubiquinone reductase inhibitor. Inhibits the mitochondrial respiratory chain.	(Heinz et al., 2017)
20	<i>N</i> -Oleoylethanolamine (OLDA)		Endogenous transient receptor potential vanilloid-1 (TRPV-1) ligand. Improved glucose homeostasis.	(Z. L. Chu et al., 2010)
34	BioF		No data available	

2.3.3. Dose-response curves for the selected compounds

I used 10 μM of the compounds for the screening and found several compounds to inhibit lipolysis. To find the effectiveness of the compounds, I performed a dose-response experiment and determined the IC_{50} value (**Figure 13**). I measured the glycerol released into the medium after treatment with C26 TCCM and compounds. IC_{50} values were calculated using the least squares fit model and shown in the graph. Due to the known weight-losing effect of orlistat and the cytotoxic nature of rotenone, I excluded these compounds from our further analysis. Together with the remaining seven selected compounds, I also used the ATGL-specific inhibitor Atglistatin (ATGLi), which has an IC_{50} value of 0.7 μM against ATGL (Mayer et al., 2013). ATGLi is highly specific against murine ATGL and was shown to improve glucose handling and prevents HFD-induced obesity and non-alcoholic fatty liver disease (NAFLD) in mice model (Schweiger et al., 2017). Compounds inhibited lipolysis in a dose-dependent manner. Diphenyleneiodonium chloride (DPI) and BioF had an IC_{50} value of less than 1 μM , lower than that of ATGLi. These two compounds are more potent than ATGLi in inhibiting C26-induced lipolysis in 3T3-L1 adipocytes and could potentially be more effective in inhibiting lipolysis *in vivo*.

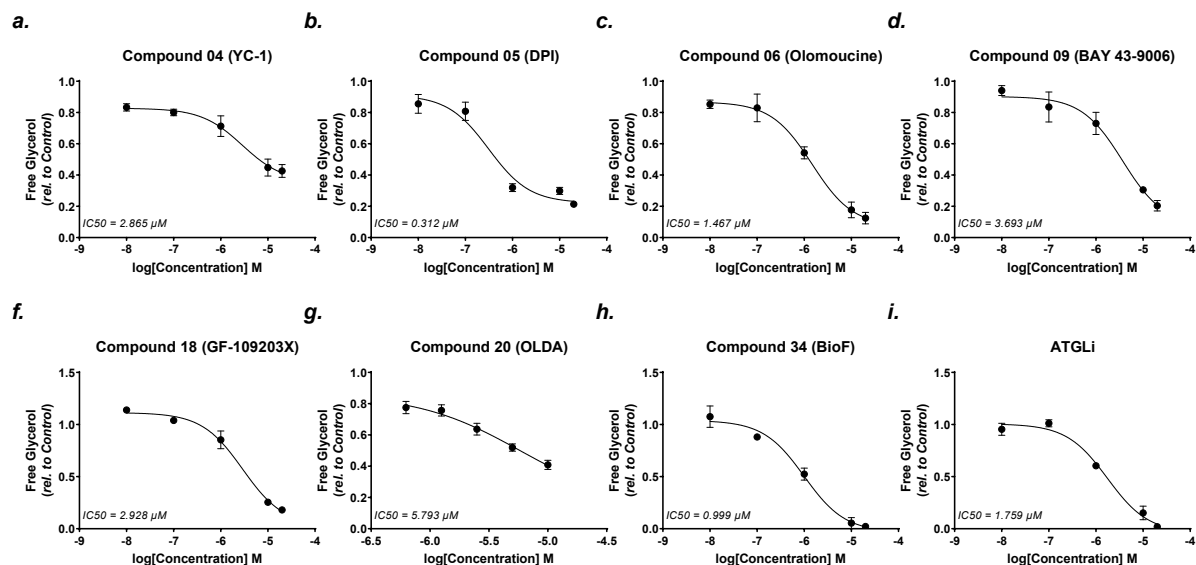


Figure 13: Dose-response curves for the selected compounds. Representative dose-response curves with (a) YC-1, (b) DPI, (c) Olomoucine, (d) BAY 43-9006, (e) GF-109203X, (f) OLDA, (g) BioF and (h) ATGLi. Free glycerol was released into the medium of the differentiated 3T3-L1 adipocytes treated with C26 TCCM with different concentrations of the selected compounds for 24 hours. $n = 3$, data shown are mean \pm s.e.m., IC₅₀ values were calculated by Least squares fit.

2.3.4. cAMP levels are not affected upon C26 TCCM treatment

Previous work has demonstrated that cachexia development in mice and C26 TCCM treatment induced lipolysis and reduced ATP levels in the WAT and 3T3-L1 adipocytes (Rohm et al., 2016). Furthermore, β -adrenergic agonists that induce lipolysis have also been shown to increase intracellular cAMP levels, further activating AMPK and their downstream regulators (Gauthier et al., 2008). Therefore, I must check if the intracellular cAMP levels are affected upon C26 TCCM treatment with the selected compounds. To this end, I measured the intracellular cAMP levels in the differentiated 3T3-L1 adipocytes treated with an adenylyl cyclase activator (forskolin, 10 μ M) as a positive control or with TCCM and selected compounds (EC₅₀ concentration) for four hours. For assay optimization, I found that the cell density of about 5000 cells/well of a 96-well plate showed the maximum induction of cAMP levels upon forskolin treatment (Figure 14a). While forskolin increased cAMP levels, there was a tendency of lowered cAMP levels in the C26 TCCM-treated adipocytes, compared to the control NCM-treated cells (Figure 14b). While both forskolin and C26 TCCM treatment induced lipolysis (data not shown), it was interesting to observe that only forskolin treatment increased cAMP levels. This could be because C26 TCCM induces lipolysis through a cAMP-signaling independent mechanism. Rohm and colleagues' work substantiates this claim that induced-lipolysis observed during cachexia was due to AMPK inactivation during ATP-depleted low energy state (Rohm et al., 2016). However, it will be interesting to see how the cAMP levels were affected after prolonged treatment of the cells with the TCCM and the lipolysis-inhibiting compounds, also if the compounds could inhibit the forskolin-induced cAMP elevation.

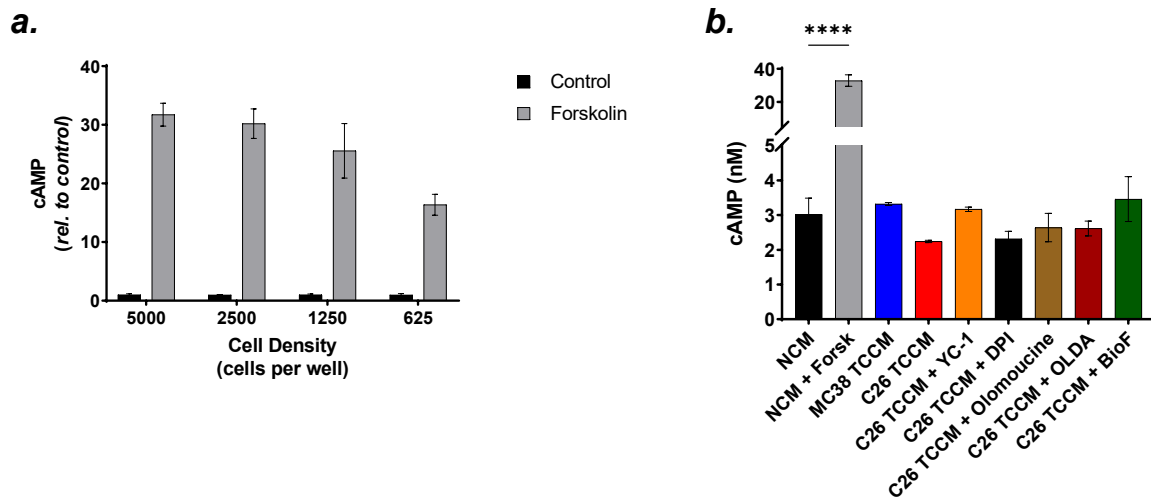


Figure 14: Forskolin treatment induced intracellular cAMP levels. (a) Accumulated intracellular cAMP levels upon treatment with 10 μ M of forskolin (Forsk) for 4 hours in different cell densities of 3T3-L1 adipocytes. (b) cAMP levels of the 3T3-L1 adipocytes were treated with the conditions for 4 hours. (a, b) $n = 3$, data shown are mean \pm s.e.m., **** $P \leq 0.0001$; by one-way ANOVA with Šidák's multiple-comparison test.

2.3.5. The fatty acid uptake of differentiated 3T3-L1 adipocytes

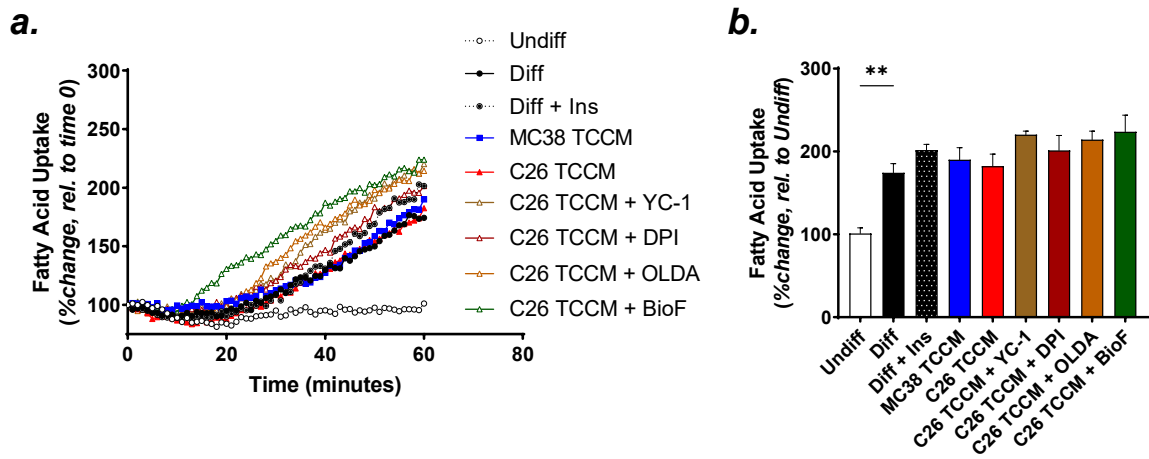


Figure 15: C26 TCCM treatment did not influence fatty acid uptake in the 3T3-L1 adipocytes. The fatty acid uptake over time of the differentiated 3T3-L1 adipocytes after being treated with indicated conditions for 24 hours was assessed using a Varioskan™ LUX multimode microplate reader (Thermo Scientific™). Representative fatty acid uptake is presented as (a) uptake kinetics over time and (b) end-stage uptake value. $n = 3$, data shown are mean \pm s.e.m., ** $P \leq 0.01$; by one-way ANOVA with Šidák's multiple-comparison test.

Researchers have shown an increase in the expression of genes involved in fatty acid uptake and utilization in the brown adipose tissue during cancer cachexia progression (Kliwer et al., 2015; Tsoli et al., 2014). Increased lipolysis leads to the efflux of excessive FFAs into other non-adipose tissue in various metabolic disorders (van Herpen & Schrauwen-Hinderling, 2008). It was demonstrated that there was a parallel increase of lipolysis and lipogenesis in white adipocytes exposed to cachexia-inducing TCCM (Rohm et al., 2016). However, little is known about the uptake of FFA in white adipose tissue under cachexia-inducing

conditions. To check if the increased lipogenesis is accompanied by increased FFA uptake, I performed the FFA uptake assay in the 3T3-L1 adipocytes treated with C26 TCCM. While I observed a clear difference in the FFA uptake between the differentiated and undifferentiated adipocytes, I did not see any effect on TCCM, compound, or insulin treatment (**Figure 15**). 3T3-L1 adipocytes have been used to study fatty acid transporters and uptake using biochemical methods (Lobo et al., 2007); however, I did not observe any effect of insulin upon FFA uptake here. The colorimetric assay used here might not be sensitive to show the difference upon insulin treatment, or the assay condition had to be optimized (to increase insulin concentration and treatment duration) to obtain more informative results. Additional experiments in this direction will provide more information about the alteration (if any) in FFA uptake under cachexia conditions.

2.3.6. The oxygen consumption rate of differentiated 3T3-L1 adipocytes

Previous research in the lab has reported that C26 TCCM treatment in 3T3-L1 adipocytes decreased the maximal respiratory capacity and ATP levels (Rohm et al., 2016). To check if the hit compounds from our screening play a role in mitochondria respiration and if they can rescue this reduced maximal respiratory capacity, I performed a mitochondrial stress test using Seahorse extracellular-flux analyzer.

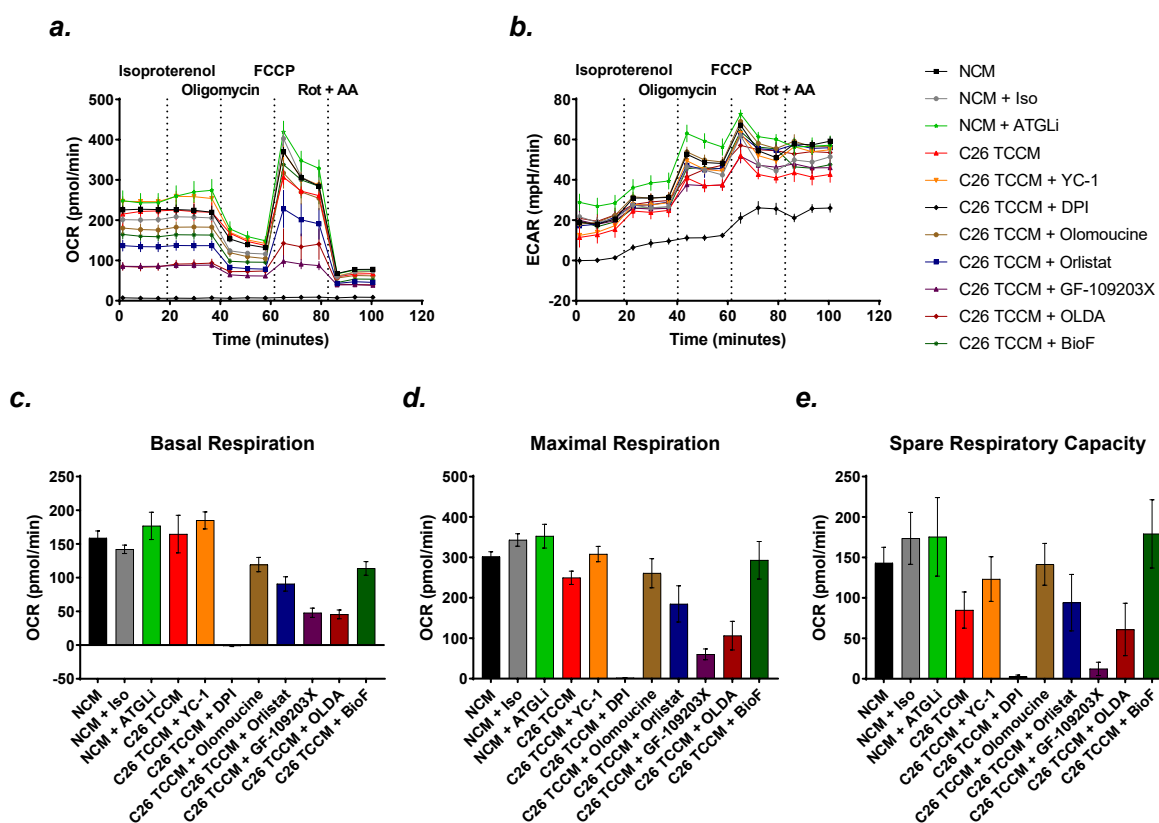


Figure 16: OCR and ECAR measurements of 3T3-L1 adipocytes. The mitochondrial function of differentiated 3T3-L1 adipocytes treated with indicated conditions for 24 hours was assessed using an extracellular flux analyzer (Seahorse Bioscience). Representative (a) OCR and (b) ECAR kinetics are shown. 10 μ M isoproterenol, 4 μ M oligomycin, 0.75 μ M FCCP, and 0.5 μ M rotenone together with 0.5 μ M antimycin A (Rot + AA) were added at the indicated time points. (c) Basal respiration, (d) maximal respiration, and (e) spare respiratory capacity was calculated as mentioned in Methods (Seahorse Mito Stress assay). $n = 6-8$, data shown are mean \pm s.e.m., one-way ANOVA with Šidák's multiple-comparison test was performed.

3T3-L1 adipocytes were treated with C26 TCCM with and without selected compounds for 24 hours. Cells treated with NCM were used as a control, and isoproterenol and ATGLi were used. Lipolysis inducer isoproterenol and inhibitor ATGLi have been previously shown to modulate the genes involved in mitochondrial respiration and oxygen consumption rate of the mature adipocytes or isolated mitochondria (Mukherjee et al., 2015; Schweiger et al., 2017; Xie et al., 2020). After treatment, oxygen consumption rate (OCR) and extracellular acidification rate (ECAR) over time and after treatment with assay compounds were measured (**Figure 16a, b**). Using formulas mentioned in Methods (*Seahorse Mito Stress assay*), I measured the treated adipocytes' basal and maximal respiration and spare respiratory capacity. I represented them as a bar chart (**Figure 16c, d, e**). Though the effects were insignificant, C26 TCCM showed a trend to decrease maximal respiration and spare respiratory capacity. Treatment with compounds like YC-1, olomoucine, and BioF showed a tendency to rescue one or both parameters; however, the effects were insignificant. The low number of technical replicates might explain the variability observed in the experiment and, thus, the insignificant differences. Paradoxically, lipolysis inhibitor ATGLi did not reduce basal respiration, whereas ATGL knockout adipocytes significantly reduced basal respiration (Xie et al., 2020). However, selected compounds significantly reduced basal respiration, which is expected for their antilipolytic property. I observed no significant changes in the OCR values after the acute injection of isoproterenol in the assay. Notably, cells treated with DPI showed close to zero in all measured parameters. When I performed CyQUANT™ Cell Proliferation Assay (data not shown) to quantify and normalize the data to the number of cells, I found that most of the DPI-treated cells were dead, so I obtained these results. The drastic reduction of cell number upon DPI treatment was not observed in the previous experiments (data not shown). The assay plate used for the measurement might influence this observation.

2.3.7. Toxicity of compounds on 3T3-L1 adipocytes and C26 cells

Since I observed cell death upon DPI treatment in the extracellular-flux analysis assay, I wanted to check if the observed inhibition of lipolysis upon compound treatments could be due to an increase in cell death. To address this, I performed the CellTox™ Green Cytotoxicity assay, which gives a reading for both live and dead cells simultaneously. The data can be represented as the ratio of live cells to dead cells. When the differentiated 3T3-L1 adipocytes were treated with C26 TCCM and DPI, the live/dead cells ratio dropped, indicating mild toxicity of the compound (**Figure 17a**). This effect appears to be dose-dependent, as a low concentration of DPI had a slightly better live/dead cells ratio. However, this dead cell percentage does not wholly represent the lipolysis inhibition of DPI (close to 70%). To assess whether the selected compounds could also affect tumor growth, I determined cell proliferation of C26 cells upon treatment with selected compounds by performing crystal violet assays for three different time points. While control cells had increased cell number over time, OLDA treatment reduced the live C26 cells from 24 hours (**Figure 17b**). Interestingly, DPI treatment did not affect the live cell numbers until 24 hours, after which the numbers dropped. Other compounds did not have much effect on the C26 cell proliferation.

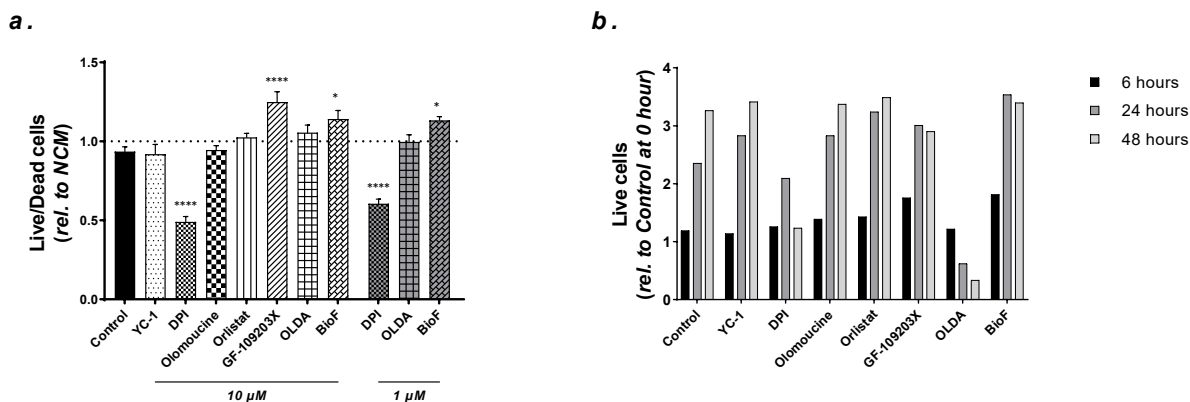


Figure 17: Viability of 3T3-L1 adipocytes and C26 cells. Cells viability was tested **(a)** by CellTox™ Green Cytotoxicity assay on the differentiated 3T3-L1 adipocytes treated with C26 TCCM together with selected compounds for 24 hours and **(b)** by crystal violet assay on the C26 cells treated with selected compounds for different time points. $n = 3$, data shown are **(a)** mean \pm s.e.m. or **(b)** mean, * $P \leq 0.05$, **** $P \leq 0.0001$; by one-way ANOVA with Šidák's multiple-comparison test.

2.4. Effect of antilipolytic compounds *in vivo*

After an extensive literature review of the compounds, their target, and known function, I selected compounds to test their antilipolytic effect *in vivo* in the C26 cancer cachexia mice model. The functional analyses and literature review I performed with these compounds also helped us narrow down the list of compounds I would like to test. DPI and BioF were potent in inhibiting C26 TCCM-induced lipolysis at lower concentrations, and BioF even inhibited the HCT116 TCCM-induced lipolysis in 3T3-L1 adipocytes (**Figure 12 & Figure 13**). OLDA had a significant and consistent antilipolytic effect in the three screenings (**Figure 11**) and showed antitumor effects on C26 cells without any significant cytotoxic effects on the differentiated adipocytes (**Figure 17**). A literature review on these compounds (discussed in the following sections) further corroborated our decision to assess these compounds. Therefore, I tested the effects of three compounds (DPI, OLDA, and BioF) *in vivo* in this study.

2.4.1. Diphenylethylideneiodonium chloride (DPI) is a potential compound to ameliorate cachexia

DPI is a NOX inhibitor that has been shown to prevent liver injury induced by alcohol in rats by inhibiting nuclear factor- κ B (NF- κ B) activation and tumor necrosis factor- α (TNF- α) expression in the liver (Kono et al., 2001). TNF- α mediated NF- κ B signaling is mainly activated during cachexia and is implicated in muscle wasting (Cai et al., 2004; Guttridge et al., 2000). Genetic and pharmacological inhibition of NF- κ B was protective against cancer cachexia (Cai et al., 2004). DPI also inhibited the cytokines induced-lipolysis mediated through NOX3 *in vitro* (Issa et al., 2018). Furthermore, recently, inhibiting or knocking down NOX4 was shown to rescue weight and muscle wasting in tumor-induced cachexia (Dasgupta et al., 2020), thus making DPI a candidate drug to test *in vivo* against cancer cachexia.

Nox3 knockdown inhibited isoproterenol, and C26 TCCM induced lipolysis

Before testing this compound *in vivo*, I checked if knocking down *Nox-3* or *Nox-4* affects lipolysis in 3T3-L1 adipocytes. Interestingly, lentivirus-mediated knockdown of either *Nox-3* or *Nox-4* decreased the free glycerol released into the medium of 3T3-L1 adipocytes (**Figure 18a, b**). However, few shRNA constructs

did not affect the inhibition of lipolysis, possibly due to the lower knockdown efficiency of these constructs (data not shown). I selected lentivirus with shRNA inhibiting lipolysis and treated the 3T3-L1 adipocytes with the TCCM. While *Nox-3* knockdown blunted C26 TCCM-induced lipolysis, *Nox-4* knockdown did not show this effect. However, all three shRNAs used blunted the isoproterenol-induced lipolysis. These data suggest that the knockdown of *Nox-3* exhibit similar inhibition of C26 TCCM-induced lipolysis in 3T3-L1 adipocytes as with the pharmacological inhibition using DPI, though the antilipolytic effect of DPI was much higher. Though DPI inhibits lipolysis in *Nox-3* dependent manner, it is shown that DPI could inhibit other NOX and nitric oxide synthase (NOS) (Stuehr et al., 1991). This could explain why knocking down either *Nox-3* or *Nox-4* alone showed less antilipolytic effect than DPI treatment in 3T3-L1 adipocytes.

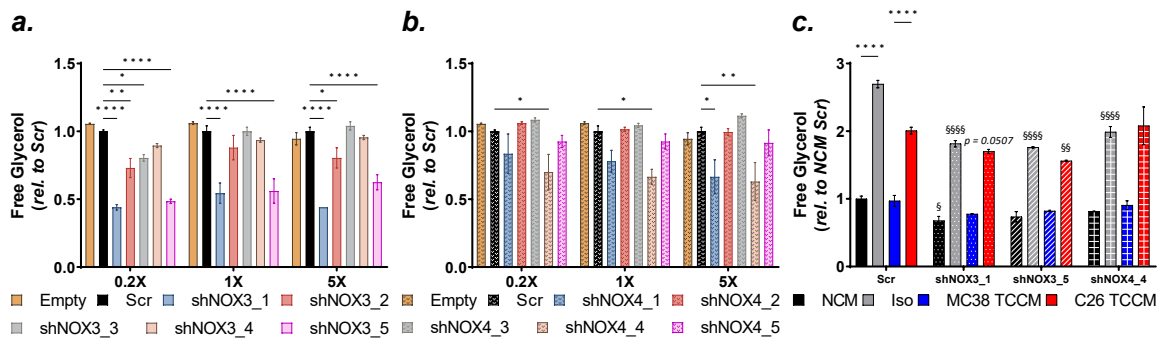


Figure 18: shRNA mediated knockdown of *Nox3* and *Nox4* inhibit lipolysis *in vitro*. 3T3-L1 adipocytes were infected with various concentrations of lentiviruses containing scrambled and shRNAs against (a) *Nox3* and (b) *Nox4*, and a lipolysis assay was performed. (c) 3T3-L1 adipocytes were treated with respective conditions and infected with lentiviruses containing selected shRNAs against *Nox3* and *Nox4*. A lipolysis assay was performed after 24 hours of treatment. $n = 3$, data shown are mean \pm s.e.m., § represents significance against respective Scr samples, * $P \leq 0.05$, ** $P \leq 0.01$, *** $P \leq 0.001$, **** $P \leq 0.0001$; by two-way ANOVA with Tukey's multiple-comparison test.

DPI treatment *in vivo* did not affect the body composition

Before testing the effects of the DPI treatment in C26 tumor-bearing mice, I assessed whether repeated injections of DPI in Balb/c mice would exert any toxicity effects. Repeated injection of 1 mg/kg of DPI was well tolerated in rats, and the lethal dose for mice was shown to be around 8 mg/kg (Cooper et al., 1988; Gatley & Martin, 1979). There was no literature on the recommended or tolerated dose for repeated injection in mice, so I tested half the dosage well tolerated in rats (0.5 mg/kg). I measured the body weight and composition of the seven weeks old Balb/c male mice days before the start of the experiment. I grouped them, and there was no difference in the body weight, fat and lean mass among the groups (Figure 19a). I injected the mice subcutaneously with either 0.5 mg/kg/day of DPI or Vehicle. I collected blood from the tail vein of the animals before treating them with DPI on three different days of the treatment. Four days after the first injection, I sacrificed the animals, collected blood, and selected tissues for further analysis. I did not observe any difference in the percentage of body weight gain (Figure 19b) or food intake, suggesting that the repeated daily injections at the chosen dose did not cause acute toxicity (Figure 19e). Though there was no significant difference in the absolute and relative tissue weights (Figure 19c, d), there was a trend towards increasing the epididymal white adipose tissue (eWAT) weight and decreasing the liver weight upon DPI treatment. There was no difference between the plasma glycerol levels of the mice treated with Vehicle and DPI (Figure 19f). Since the blood was collected after the post-prandial phase, it is difficult to conclude if DPI treatment inhibited lipolysis in wild-type mice. Thus,

repeated injections of 0.5 mg/kg/day of DPI did not elicit acute toxicity or changes in weight, food intake, or blood glycerol levels.

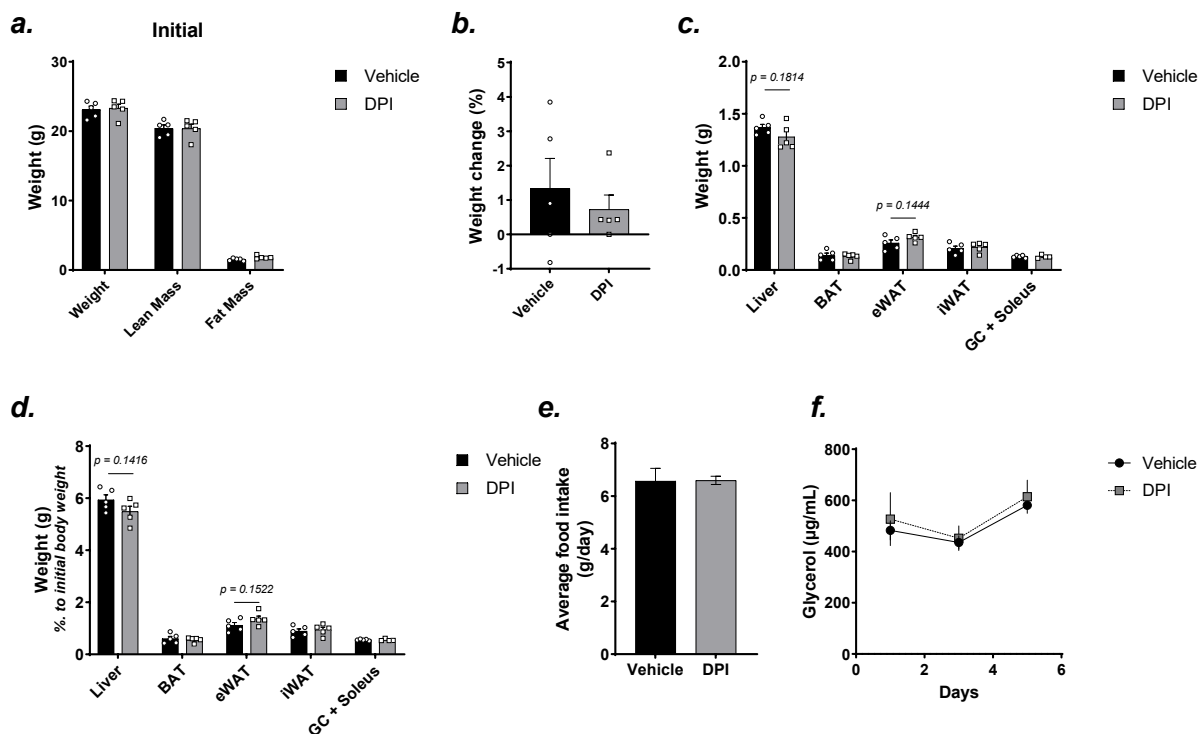


Figure 19: Mice treated with DPI display normal body weight, tissue weight, and plasma glycerol level. Seven weeks old male Balb/c mice were injected subcutaneously with either 0.5 mg/kg of DPI or Vehicle once daily. Mice were sacrificed five days post-injection. **(a)** Initial body composition (body weight, lean and fat mass) measured by Echo-MRI before treatment initiation. **(b)** Percent change in the body weight after the treatment. **(c)** The weight of the tissues (Liver, BAT, eWAT, iWAT, and GC + Soleus) was measured five days after the first injection. **(d)** Tissue weights shown in **Figure 19c** are normalized to the initial body weight. **(e)** Average food consumption of the mice. **(f)** Plasma glycerol levels were measured over the treatment period and before sacrificing the mice. **(a-d, f)** $n = 5$ per group, **(e)** $n = 2$ per group; data shown are mean \pm s.e.m., two-tailed t-test was performed.

DPI treatment increased plasma NEFA levels

As mentioned before, I collected the blood of the animals at the end of the experiment. I then extracted plasma and analyzed the concentration of various metabolites. Since I saw a trend to decrease liver weight (**Figure 19c**) and also to check if the compound elicits any liver toxicity, I quantified the levels of aspartate aminotransferase (AST) and alanine transaminase (ALT). The ratio of the AST to ALT was not different between the groups (**Figure 20a**); also, the values of AST and ALT were not altered upon DPI treatment (data not shown). I also measured the plasma alkaline phosphatase (ALP) and lactate dehydrogenase (LDH) levels to assess any tissue damage upon DPI treatment; however, I did not see any changes in these (**Figure 20b, c**). While I did not observe any significant changes in the random blood glucose levels, cholesterol, or LDL, I saw a substantial increase in the NEFA and a trend to increase the triglycerides in the plasma of the DPI-treated mice (**Figure 20**).

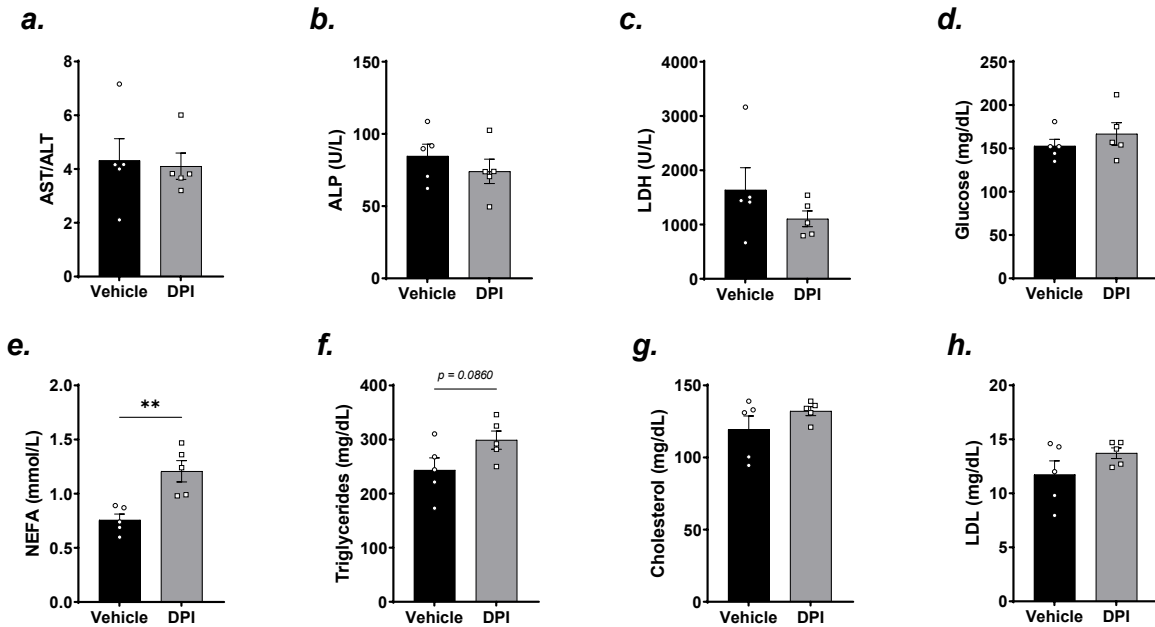


Figure 20: DPI treatment did not elicit liver toxicity. Blood samples were collected from the animals shown in **Figure 19** before sacrificing. Plasma was extracted and analyzed for specific metabolites. **(a)** The ratio of AST to ALT levels, **(b)** ALP, **(c)** LDH, **(d)** random post-prandial glucose, **(e)** NEFA, **(f)** triglycerides, **(g)** cholesterol, and **(h)** LDL levels in the plasma of mice treated with DPI or Vehicle. $n = 5$ per group, data shown are mean \pm s.e.m., $**P \leq 0.01$; by two-tailed t-test.

DPI treatment modulated the genes involved in fatty acid metabolism in iWAT and liver

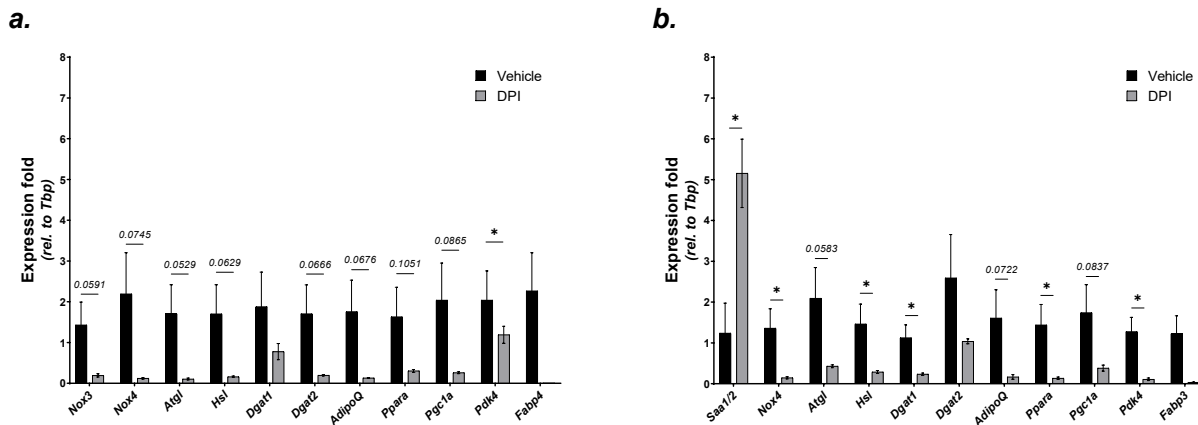


Figure 21: Mice treated with DPI have reduced Nox3 levels in iWAT. Expression levels of genes involved in fatty acid metabolism and DPI targeted genes in the **(a)** iWAT and **(b)** liver of the animals treated with DPI or Vehicle. $n = 5$ per group, data shown are mean \pm s.e.m., $*P \leq 0.05$; by two-tailed t-test.

I extracted RNA from the iWAT and liver of the animals used in the experiment and performed qPCR on selected genes involved in fatty acid metabolism implicated in cancer cachexia. I observed that *Nox-3* and *Nox-4* were significantly reduced in the iWAT of mice treated with DPI. In addition, genes involved in lipolysis (*Atgl*, *Hsl*), and lipogenesis (*Dgat-2*), among others, showed a trend to decrease upon DPI treatment (**Figure 21a**). Like the iWAT, DPI treatment also reduced the levels of genes involved in fatty acid metabolism in the liver (**Figure 21b**). Although I did not observe a change in the plasma levels of AST

to ALT ratio, ALP, and LDH, I saw a significant increase in the transcript levels of serum amyloid A1/2 (*Saa-1/2*) in the liver of DPI-treated mice. The increased liver *Saa-1/2* might indicate an acute phase response upon DPI treatment. However, the *Saa-1/2* transcript is post-transcriptionally regulated, and this could explain why I observed an increase in liver *Saa-1/2* but no changes in the other plasma toxicity markers (Steel et al., 1993).

DPI treatment did not ameliorate C26-induced fat loss

After excluding that repeated injections of DPI at the given dose in wild-type non-tumor bearing mice would exert unacceptable toxic effects, I wanted to test whether DPI treatment could counteract induced lipolysis and ameliorate cachexia development in C26 tumor-bearing Balb/c mice.

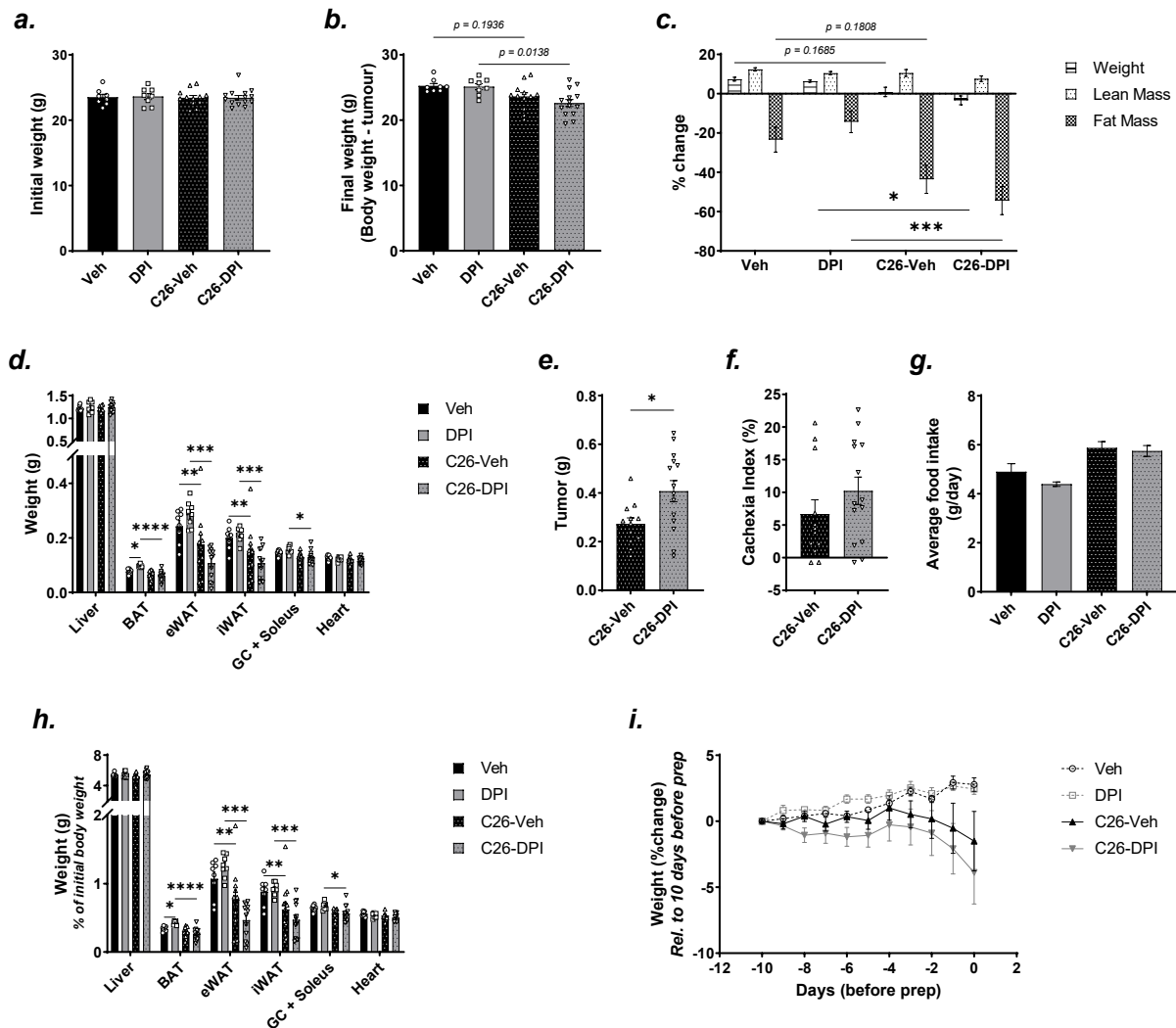


Figure 22: DPI treatment in the C26 tumor-bearing mice did not prevent cachexia development. Eight weeks old male Balb/c mice were injected subcutaneously with either 5×10^5 C26 cells or PBS. 9 days post-inoculation, mice were injected subcutaneously with either 0.5 mg/kg of DPI or Vehicle once daily. Tumor-bearing mice were sacrificed by cervical dislocation after cachexia development, and non-tumor-bearing mice were sacrificed together with the tumor-bearing mice. **(a)** Initial and **(b)** final carcass body weight of the mice. **(c)** Percent change in the body weight, lean and fat mass at the end of the experiment. **(d)** The weight of the tissues (Liver, BAT, eWAT, iWAT, GC + Soleus, heart) and **(e)** tumor were measured at the end of the experiment. **(f)** Cachexia index of the tumor-bearing mice as calculated by the formula mentioned in the Methods (Cachexia index). **(g)** Average food

consumption of the mice. **(h)** Tissue weights shown in **Figure 22d** are normalized to the initial body weight. **(i)** Bodyweight development of the mice in the last ten days before sacrifice depicted as the percentage change in weight relative to that of 10 days before prep. $n = 8$ (Veh, DPI), 12 (C26-Veh) or 14 (C26-DPI), data shown are mean \pm s.e.m., * $P \leq 0.05$, ** $P \leq 0.01$, *** $P \leq 0.001$ and **** $P \leq 0.0001$; by **(a-d, g, h)** one-way ANOVA with Šidák's multiple-comparison test, **(e, f)** by two-tailed t-test or **(i)** two-way ANOVA with Tukey's multiple-comparison test.

For this purpose, I used eight weeks old male Balb/c mice and grouped them before the start of the experiment. The groups did not differ in body weight (**Figure 22a**), fat, and lean mass (data not shown). Mice were inoculated subcutaneously with either 5×10^5 C26 cells prepared in 100 μ L or an equal volume of PBS. Once most of the C26-injected mice developed a palpable tumor, mice were injected once daily subcutaneously with either 0.5 mg/kg of DPI or Vehicle. The endpoint of the experiment and individual mouse was defined when the mouse developed cachexia (lost more than 10% of initial body weight), reached humane endpoint (body condition score, increased tumor burden, and ulceration) or 28 days post tumor cell injection. When sacrificing a tumor-bearing mouse (vehicle or DPI treated) once they reach the endpoint, a mouse with similar tumor size (measured by Vernier capillary) from the other treatment group was matched and sacrificed. At the end of the experiment, tumor-bearing mice showed a trend towards reduced carcass weight compared to non-tumor control groups (**Figure 22b**). Percentage change in weight also showed a trend to decrease, and that of fat mass was significantly reduced in the tumor-bearing mice, suggesting a certain degree of cachexia. However, I observed no change in the lean mass (**Figure 22c**). Tumor-bearing mice displayed hallmark features of cachexia on adipose depots and reduced iWAT and eWAT weight. However, DPI treatment had no protective effect on these parameters. BAT weight was reduced considerably in the DPI-treated tumor-bearing mice; however, DPI treatment in the non-tumor-bearing mice increased BAT weight (**Figure 22d, h**). Although DPI treatment *in vitro* reduced the number of live C26 cells (**Figure 17b**), mice treated with DPI had a slightly increased tumor mass at the end of the experiment (**Figure 22e**). The cachexia index calculates the degree of cachexia development using the initial and final body weight and tumor burden of individual mice and the average weight gain in the control non-tumor-bearing mice (Guarnier et al., 2010). DPI treatment had no protective effect; thus, the cachexia index was not different between the tumor-bearing mice groups (**Figure 22f**). There were no significant differences in the average food intake between the experimental groups; however, there was a trend towards increased food intake in tumor-bearing mice with no difference between the treatment (**Figure 22g**). Although anorexia is observed in cancer cachexia patients (Tisdale, 2009), reduced food intake was not observed in our lab's Balb/c-C26 cancer cachexia model (Jones et al., 2013; Rohm et al., 2016). To depict the kinetics of cachexia development, I plotted the change in body weight of the animals from 10 days before the day of necropsy in each mouse until the day of necropsy (**Figure 22i**).

Previously in our lab, it was shown that Balb/c mice developed cachexia when injected with 5×10^5 C26 cells (data not shown). However, in this experiment, the mice did not wholly develop cachexia phenotype, although I observed that the weight of the fat depots was significantly reduced (**Figure 22d**). Therefore, I decided to inject 1×10^6 C26 cells for the upcoming cancer cachexia experiment. As seen here, DPI treatment did not ameliorate C26-induced weight and fat loss.

Altered plasma metabolite levels in the DPI-treated tumor-bearing mice

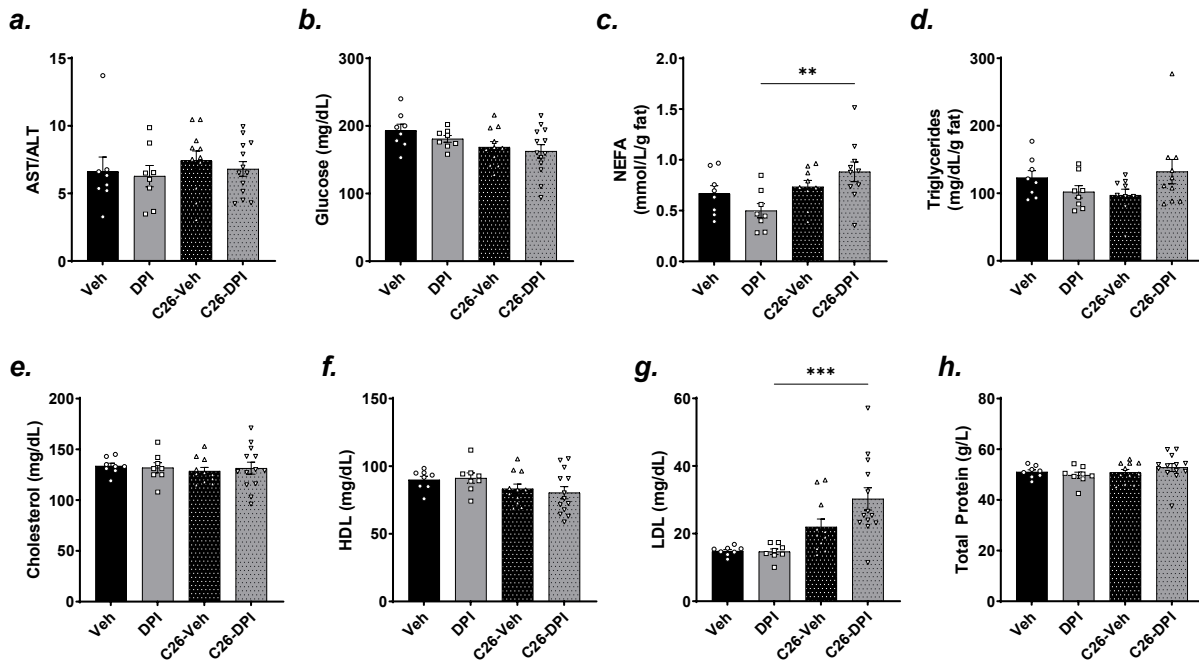


Figure 23: DPI treatment increased NEFA levels in the C26 tumor-bearing mice. Blood samples were collected from the animals shown in **Figure 22** before sacrificing. Plasma was extracted and analyzed for specific metabolites. **(a)** The ratio of AST to ALT levels, **(b)** glucose, **(c)** NEFA, **(d)** triglycerides, **(e)** cholesterol, **(f)** HDL, **(g)** LDL, and **(h)** total protein levels in the plasma of the animals collected before sacrificing. $n = 8$ (Veh, DPI), 12 (C26-Veh) or 14 (C26-DPI), data shown are mean \pm s.e.m., $**P \leq 0.01$ and $***P \leq 0.001$; by one-way ANOVA with Šidák's multiple-comparison test.

The levels of specific metabolites in the circulation can assess cachexia development and its severity. Glucose metabolism is altered, mainly blood glucose and insulin levels, which are lowered in C26 tumor-bearing mice (Asp et al., 2010). Previously our lab also showed elevated NEFA and triglyceride levels in C26 tumor-bearing mice (Rohm et al., 2016). Therefore, I measured glucose, NEFA, and total proteins in the plasma (**Figure 23**). There was no change in the AST to ALT ratio, glucose levels, triglycerides, and cholesterol. NEFA and LDL levels were significantly increased in the tumor-bearing mice treated with DPI. I did not observe increased proteolysis measured by plasma protein levels in the C26 tumor-bearing groups. Even though the mice did not completely develop cachexia phenotype, I observed increased NEFA and LDL levels in tumor-bearing mice without any changes in glucose or protein levels. This could suggest that elevated lipolysis and increased NEFA and LDL levels precede the dysregulation of glucose metabolism and proteolysis.

DPI treatment did not inhibit NADH activity in vivo

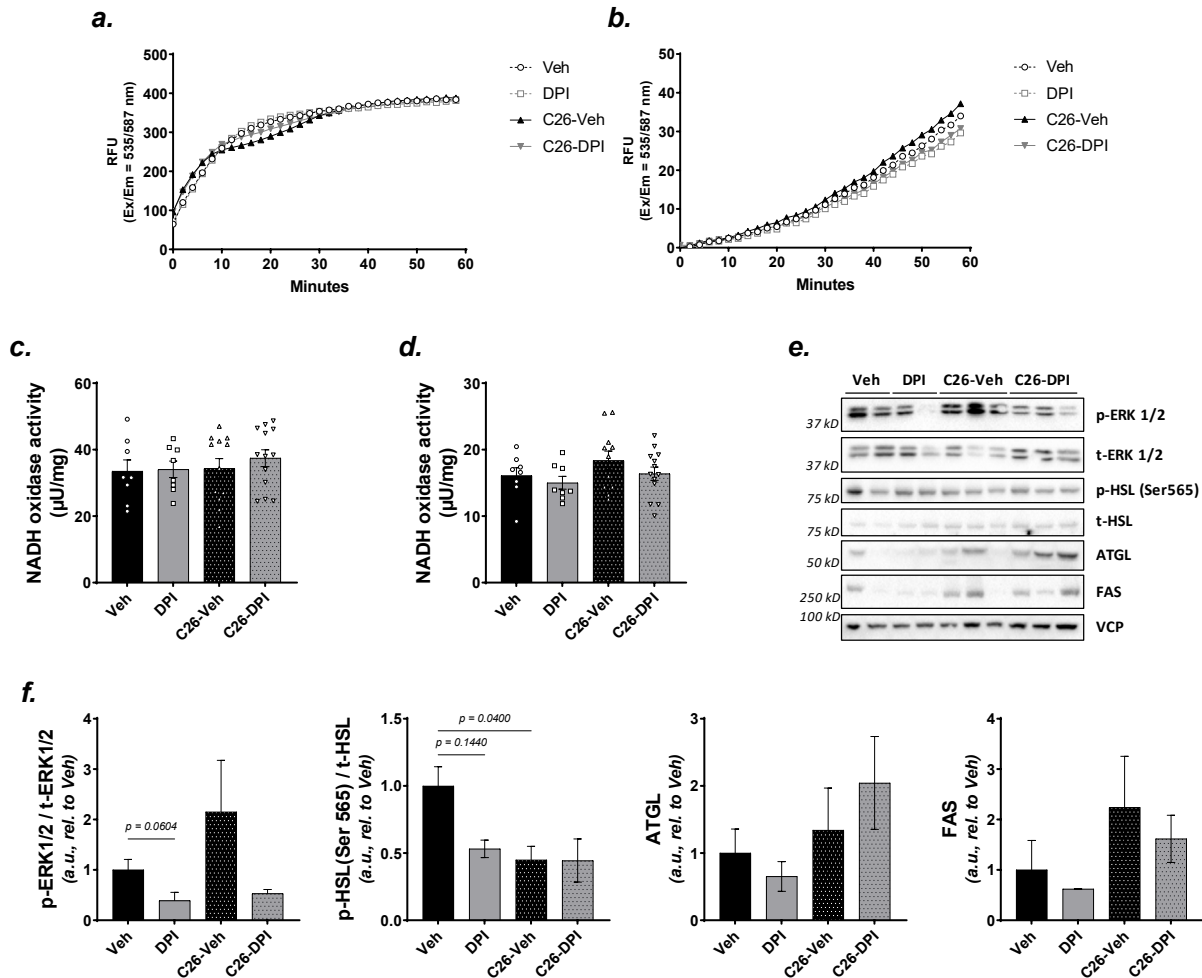


Figure 24: DPI treatment did not inhibit the induced lipolysis in vivo. Reaction kinetics of NADH oxidase activity in (a) iWAT protein lysate and (b) plasma of the mice. NADH oxidase activity was measured in (c) iWAT protein lysate and (d) plasma of the mice. Proteins extracted from iWAT were immunoblotted for specific proteins. (e) Representative immunoblots are shown here, and (f) quantification was performed as mentioned in Methods (SDS-PAGE and immunoblotting). p-HSL(Ser565) levels were normalized with the total HSL and p-ERK1/2 with the total ERK1/2. VCP was used as a loading control. $n = 8$ (Veh, DPI), 12 (C26-Veh) or 14 (C26-DPI), data shown are mean \pm s.e.m., and one-way ANOVA with Šidák's multiple-comparison test was performed.

To check the efficiency of DPI in inhibiting a known target protein, I performed NADH oxidase assay on the iWAT protein extracts and the plasma samples. The reaction kinetics of NADH oxidase activity shows that active NOX proteins were more present in the iWAT protein extract than in the plasma (**Figure 24a, b**). When I looked at the NADH oxidase activity (**Figure 24c, d**), calculated using the formula mentioned in the Methods section (*NADPH Oxidase Activity Assay*), it was clear that the activity of the enzyme was higher in the iWAT (33.53 μ U/mg of protein, Veh) compared to that in the plasma (16.10 μ U/mg of protein, Veh). However, the NADH oxidase activity in the iWAT and plasma was not changed upon DPI treatment nor the C26 tumor burden. I extracted protein from the iWAT of these mice and performed immunoblotting (**Figure 24e**). C26 tumor-bearing mice had significantly less p-HSL(Ser565), also observed in other cachexia studies (Rohm et al., 2016); however, this was not rescued upon DPI

treatment. Surprisingly, DPI treatment also reduced the p-HSL(Ser565) levels, suggesting that lipolysis is induced in the iWAT of DPI-treated and tumor-bearing mice. DPI has previously been shown to affect ERK activity (Kono et al., 2001). Here I saw that DPI treatment decreased the phosphorylated ERK1/2 levels suggesting that the compound worked as anticipated, but that was not enough to counteract cachexia, probably because it also decreased the inhibitory phosphorylated form of HSL (**Figure 24f**). I also measured the levels of adipose triglyceride lipase (ATGL) and fatty acid synthetase (FAS), whose levels are shown to be affected during cachexia (Tsoli et al., 2014). However, I did not see significant changes in the tumor-bearing nor DPI-treated mice (**Figure 24f**). The cachexia development and the degree of weight and fat loss were variable among the tumor-bearing mice, which might explain why I did not see any definite difference in the protein levels.

From this cachexia study testing the compound DPI, I learned that injecting 5×10^5 C26 cells was insufficient to induce significant weight and fat loss. Also, treatment with 0.5 mg/kg/day of DPI did not provide any beneficial effects against tumor-induced cachexia. However, it increased the BAT weight in the non-tumor-bearing mice. DPI treatment inhibited the ERK signaling; however, that was insufficient to prevent the weight loss as the lipolysis induction was unaffected upon DPI treatment.

2.4.2. Testing *N*-Oleoyldopamine (OLDA) for its antilipolytic effect *in vivo*

OLDA is an endogenous fatty acid amide formed by oleic acid and dopamine condensation. OLDA modulates the firing frequency of dopaminergic and histaminergic neurons and partly functions through the cannabinoid receptors (CB1/CB2), fatty acid amide hydrolase, catecholamine, and dopamine uptake (De Luca et al., 2018; Sergeeva et al., 2017). While it is unclear if medicinal cannabinoids improve appetite in cancer cachexia patients with confounding results (Simon et al., 2022; J. Wang et al., 2019), it would be interesting to test if this cannabinoid receptor ligand could provide beneficial effects. OLDA has a more significant effect on the TRPV-1-mediated Ca^{2+} release than other ligands of TRPV-1 and capsaicin (C. J. Chu et al., 2003). It was shown that calcium deposition is particularly increased in the skeletal muscle of cachectic PDAC patients, and calcium handling is disrupted in C26 tumor-bearing mice (Judge et al., 2018; Roberts et al., 2013). Interestingly, TRPV-1 knockout in mice protected against high-fat diet-induced weight gain and adiposity (Motter & Ahern, 2008). OLDA was shown to influence the insulin release and cAMP levels and increase the plasma gastric inhibitory peptide (GIP) through G protein-coupled receptor 119 (GPR-119) and thus improved glucose homeostasis in the mice (Z. L. Chu et al., 2010). It is well known that glucose homeostasis is altered during cachexia (Asp et al., 2010), and OLDA that could improve this dysregulated metabolism could be an ideal drug candidate against cancer cachexia. With all its positive effects and the antilipolytic effects I determined in our *in vitro* screening, I considered OLDA a promising candidate compound for treating cancer cachexia.

OLDA treatment did not affect body composition

Before testing the effect of this compound against C26-induced cachexia, I wanted to check if the mice could tolerate chronic OLDA treatment. When I referred to the literature, three concentrations (5, 10, and 20 mg/kg) were used to inject rats acutely (Konieczny et al., 2009; Przegaliński et al., 2006). Since I did not find literature on the effects of repeated injections of OLDA in mice, I planned to test two dosages (1 and 5 mg/kg/day) of OLDA treatment. I used seven weeks old male Balb/c mice. I stratified them into three

groups with identical body weight (**Figure 25a**) and body composition (data not shown). I injected the mice intraperitoneally with either vehicle, 1 or 5 mg/kg/day of OLDA for four days, then performed an intraperitoneal glucose tolerance test (ipGTT) to determine the effectiveness of the drug as the previous study has shown that acute injection of OLDA to improve glucose tolerance in wild type mice (Z. L. Chu et al., 2010). After the washout period of two days, I again treated them for four more days before collecting the blood and tissues from the animals. OLDA treatment did not influence the final body weight (**Figure 25b**) or the percent change in body composition (**Figure 25c**). At the end of the experiment, there was no change in the food intake (**Figure 25d**) or the weight of the tissues (**Figure 25e, f**). Although there was no difference in the fasting glucose levels (**Figure 25g**), I observed that mice treated with OLDA showed less area under the curve (AUC) of the glucose excursion curve in the ipGTT (**Figure 25h, i**), which is a widely used index for glucose excursion (Sakaguchi et al., 2016). A 5 mg/kg/day dose of OLDA was effective *in vivo* in improving the glucose excursion slightly. In comparison, a 1 mg/kg/day dose only showed a tendency. Therefore, for the cachexia experiment using OLDA, it would be ideal to use the higher dose.

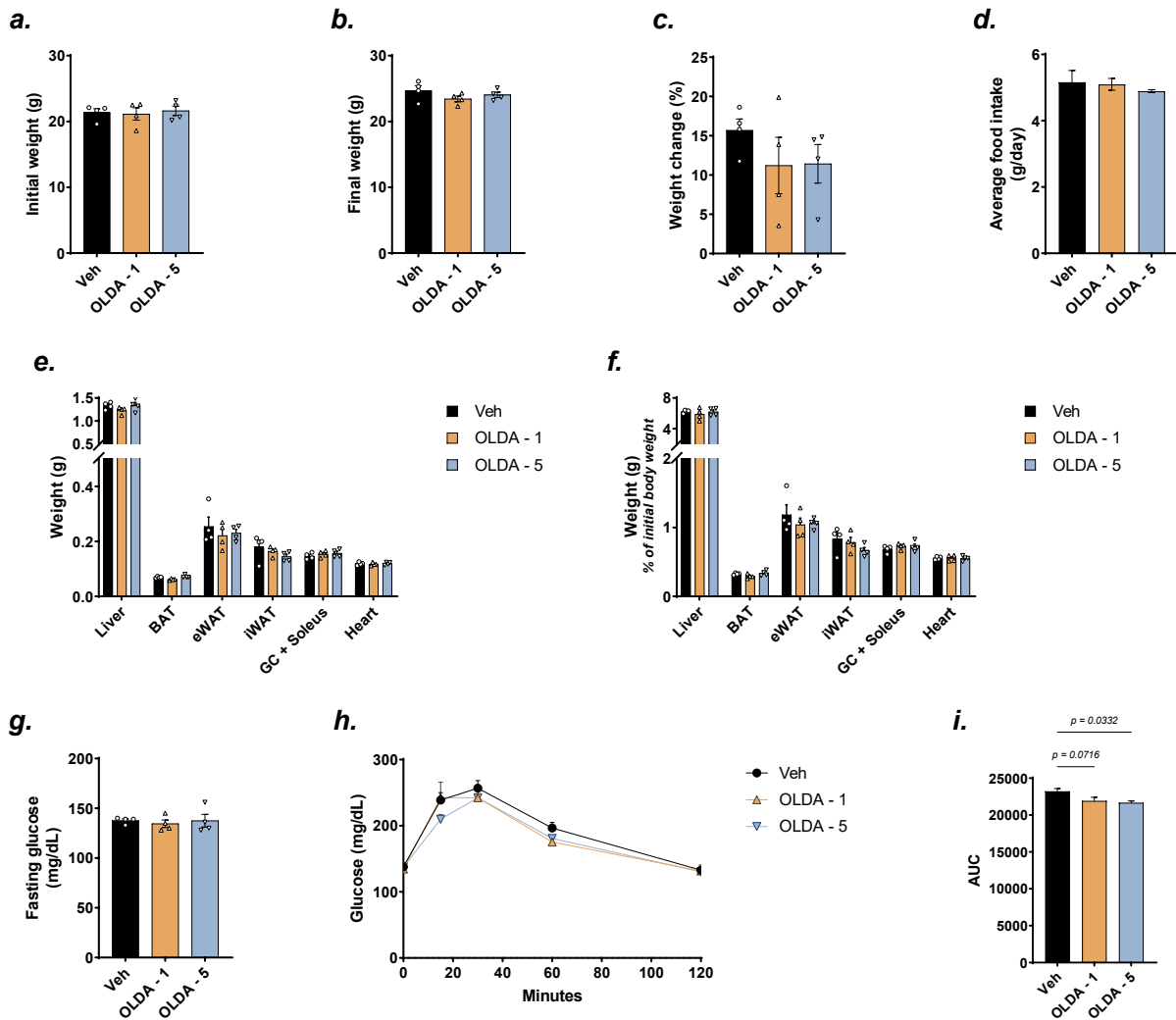


Figure 25: Assessing systemic effects of OLDA treatment. Seven weeks old male Balb/c mice were injected intraperitoneally with either 1 mg/kg, 5 mg/kg of OLDA, or vehicle once daily. ipGTT was performed after four days of treatment, followed by two days of washout before restarting the treatment for another four days. Mice were sacrificed after the treatment. **(a)** Initial and **(b)** final

body weight. (c) Percent change in the body weight after the treatment. (d) Average food consumption of the mice (e) Weight of the tissues (Liver, BAT, eWAT, iWAT, GC + Soleus, and heart) measured at the end of the experiment. (f) Tissue weights shown in **Figure 25e** are normalized to the initial body weight. (g) Glucose levels of the fasted mice before performing ipGTT. (h) Plasma glucose kinetics and (i) area under glucose curve obtained from the ipGTT. (a-c, e-i) $n = 4$ per group, (d) $n = 2$ per group; data shown are mean \pm s.e.m., and one-way ANOVA with Šidák's multiple-comparison test was performed.

OLDA treatment increased plasma NEFA levels

At the end of the experiment, I collected the blood from the animals. I quantified the plasma metabolites to check if the repeated injection of OLDA induced toxicity or brought any changes to the level of important metabolites. There was no change in the liver toxicity marker (AST to ALT ratio), glucose, cholesterol, and other metabolites (**Figure 26**). Surprisingly, there was a trend towards increasing NEFA levels upon OLDA treatment (**Figure 26d**), as I observed the antilipolytic effect of OLDA *in vitro*. The tendency I observed was in the basal condition; however, it is important that the OLDA treatment did not alter the levels of other plasma metabolites.

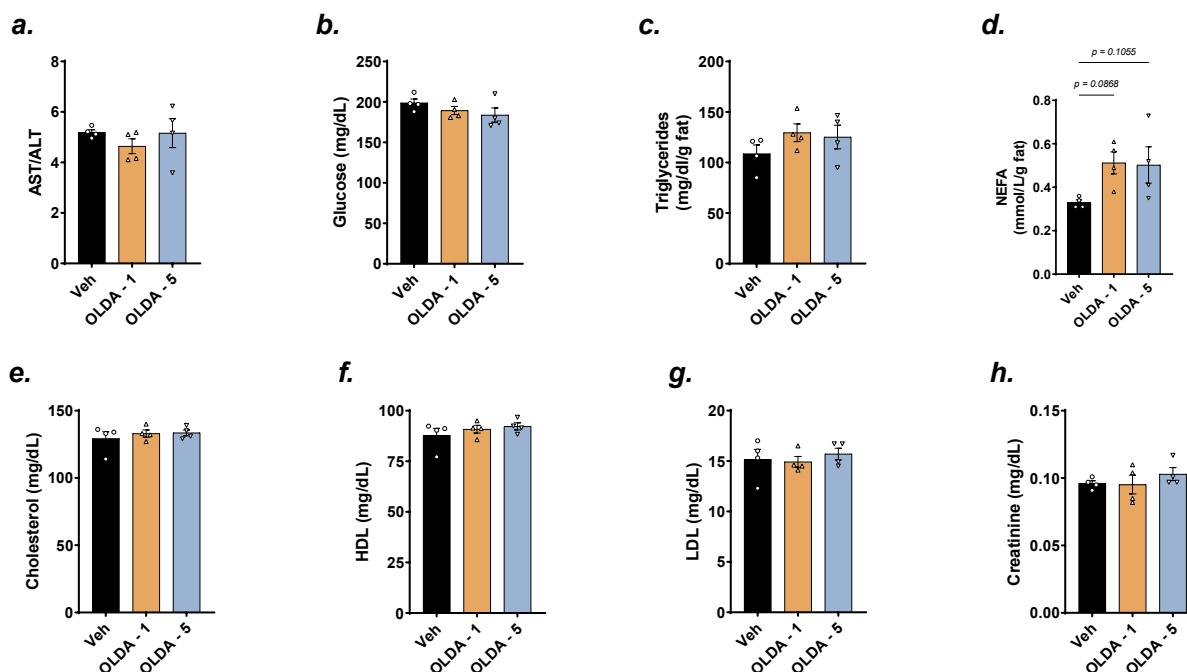


Figure 26: OLDA treatment did not elicit liver toxicity. Blood samples were collected from the animals shown in **Figure 25** before sacrificing. Plasma was extracted and analyzed for specific metabolites. (a) The ratio of AST to ALT levels, (b) random post-prandial glucose, (c) triglycerides, (d) NEFA, (e) cholesterol, (f) HDL, (g) LDL, and (h) creatinine levels in the plasma of mice treated with OLDA or Vehicle. $n = 4$ per group, data shown are mean \pm s.e.m., and one-way ANOVA with Šidák's multiple-comparison test was performed.

OLDA treatment modulates the levels of proteins involved in fatty acid metabolism

To check if the expression of proteins involved in lipid metabolism is altered upon OLDA treatment, I performed immunoblotting on these mice's protein extracts from iWAT and eWAT (**Figure 27a, c**). iWAT and eWAT are the fat depots that are highly affected during cachexia. However, in our lab, I have observed that eWAT is more responsive to β -adrenergic stimuli and TCCM than iWAT in *ex vivo* lipolysis assay (data not shown). FAS levels were decreased, primarily upon high-dose treatment of OLDA. The inhibitory phosphorylation of HSL (p-HSL(Ser565)) was increased (**Figure 27 b, d**), clearly showing that OLDA affects

lipid metabolism in wild-type mice. FAS and p-HSL(Ser565) levels were decreased during cachexia, and it is promising to see that the treatment with a higher dose of OLDA could increase the p-HSL(Ser565) levels in both iWAT and eWAT. Counterintuitively, it was surprising that FAS and p-ACC α (Ser79) levels were decreased in the eWAT upon a higher dose of OLDA treatment. OLDA treatment seems to inhibit the HSL-mediated lipolysis and fatty acid synthesis pathways.

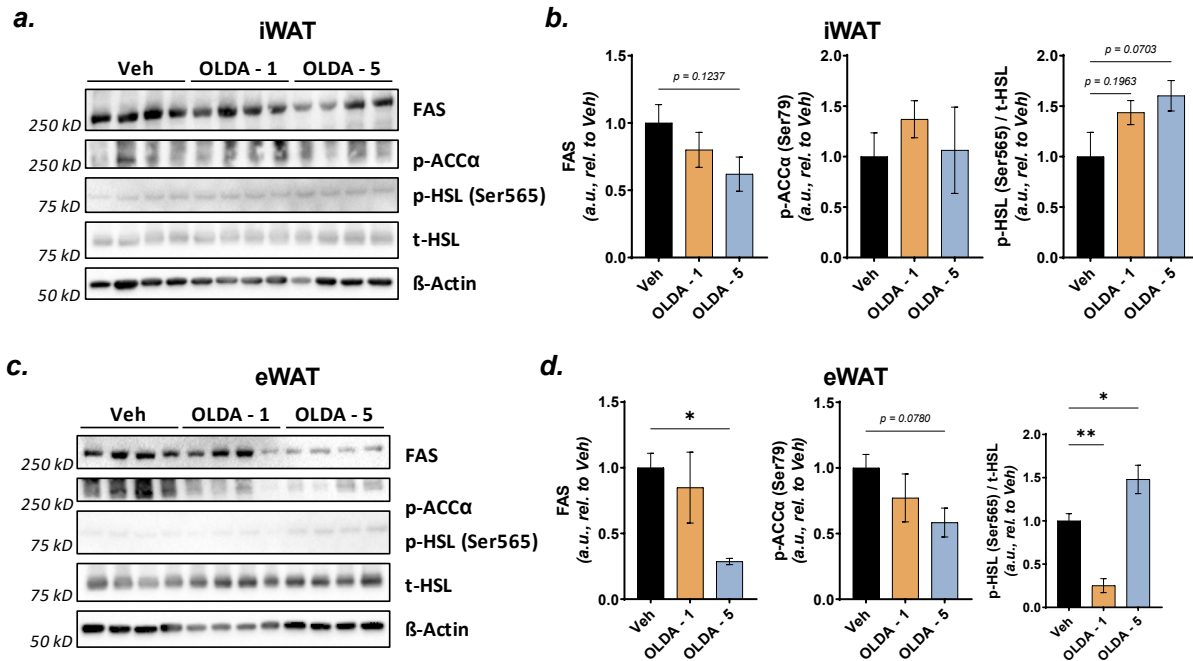


Figure 27: Proteins extracted from iWAT and eWAT were immunoblotted for specific proteins. Immunoblots and quantification of particular proteins separated from (a, b) iWAT and (c, d) eWAT protein extracts. p-HSL(Ser565) levels were normalized with the total HSL and p-ACC α (Ser79) with β -Actin, which was used as the loading control. $n = 4$ per group, data shown are mean \pm s.e.m., * $P \leq 0.05$, and ** $P \leq 0.01$; by one-way ANOVA with Šidák's multiple-comparison test.

OLDA treatment did not ameliorate C26-induced weight and fat loss

5 mg/kg of OLDA treatment slightly improved glucose homeostasis and increased the p-HSL(Ser565) levels in the adipose tissue, so I tested this compound dosage in the C26 tumor-bearing mice. In the previous cachexia experiment, the vehicle-treated C26 tumor-bearing mice did not show significant cachexia development. Therefore, to improve the chance of observing a more pronounced cachexia phenotype, I modified the approach and injected the mice with either 1×10^6 C26 cells (previously 5×10^5 cells) or PBS subcutaneously for this experiment. Most of the animals developed a palpable tumor on day seven post C26 inoculation, so I started the treatment of the animals with vehicle or OLDA (5 mg/kg/day, intraperitoneally). There was no difference in the body weight before the start of the experiment (Figure 28a), and the C26 inoculation induced significant weight loss in both vehicles and OLDA-treated groups (Figure 28b). As a sign of cachexia development, there was a substantial loss in body weight, fat mass (Figure 28c), and tissue weight (Figure 28d, h). The bodyweight development graph of the mice showing the weight change in the last ten days before they were sacrificed also demonstrated that OLDA treatment did not delay cachexia (Figure 28i). Thus, OLDA treatment did not affect cachexia development, severity, or tumor growth, as seen in Figure 28.

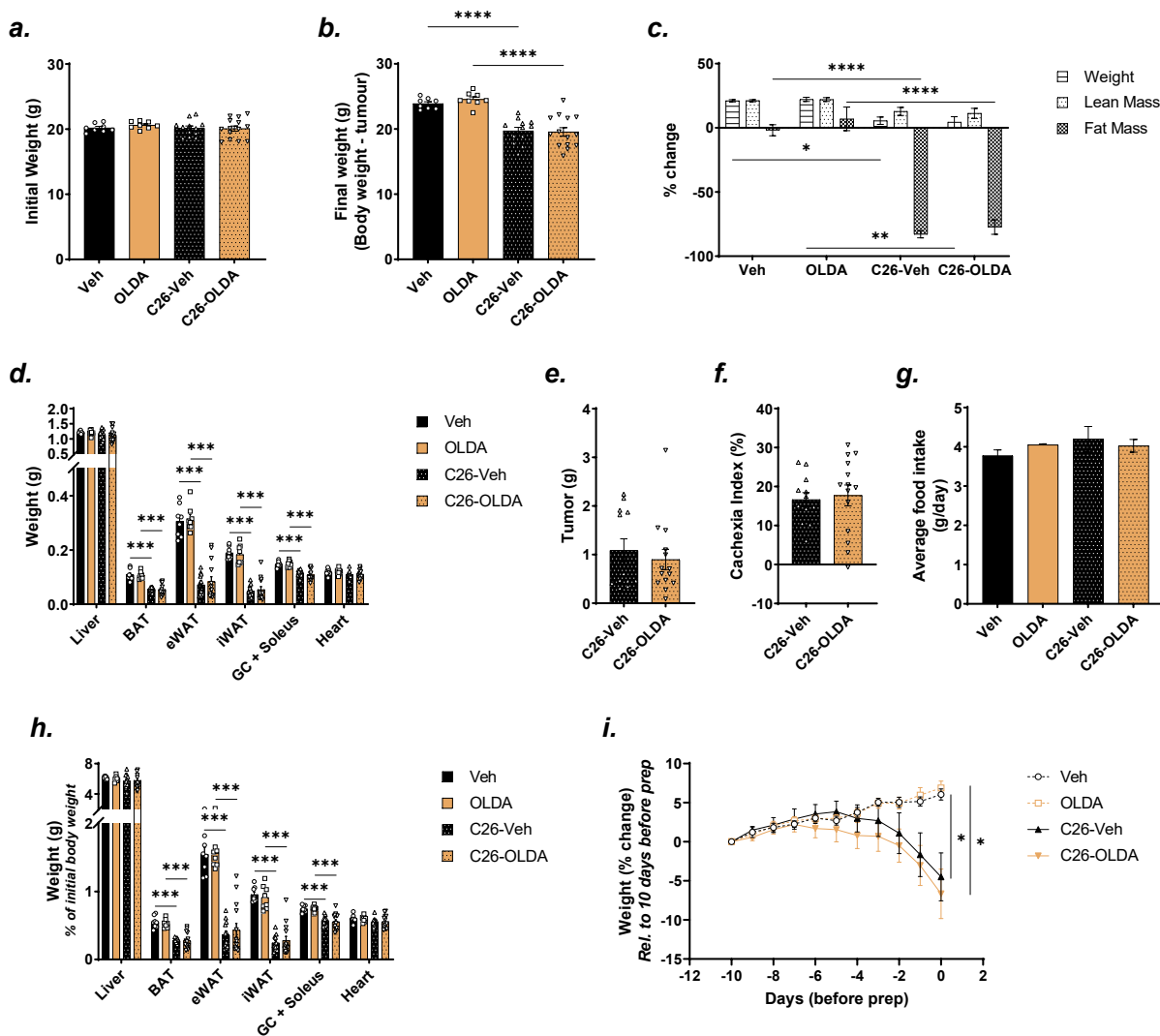


Figure 28: OLDA treatment in the C26 tumor-bearing mice did not prevent cachexia development. Eight weeks old male Balb/c mice were injected subcutaneously with either 1×10^6 C26 cells or PBS. Seven days post-inoculation, mice were injected intraperitoneally with either 5 mg/kg of OLDA or Vehicle once daily. Tumor-bearing mice were sacrificed by cervical dislocation after cachexia development, and non-tumor-bearing mice were sacrificed together with the tumor-bearing mice. **(a)** Initial and **(b)** final carcass body weight of the mice. **(c)** Percent change in the body weight, lean and fat mass at the end of the experiment. **(d)** The weight of the tissues (Liver, BAT, eWAT, iWAT, GC + Soleus, heart) and **(e)** tumor were measured at the end of the experiment. **(f)** Cachexia index of the tumor-bearing mice as calculated by the formula mentioned in the Methods (Cachexia index). **(g)** Average food consumption of the mice. **(h)** Tissue weights shown in **Figure 28d** are normalized to the initial body weight. **(i)** Bodyweight development of the mice in the last ten days before sacrifice depicted as the percentage change in weight relative to that of 10 days before prep. $n = 8$ (Veh, OLDA), 12 (C26-Veh) or 14 (C26-OLDA), data shown are mean \pm s.e.m., * $P \leq 0.05$, ** $P \leq 0.01$, *** $P \leq 0.001$ and **** $P \leq 0.0001$; by **(a-d, g, h)** one-way ANOVA with Sidák's multiple-comparison test, **(e, f)** by two-tailed t-test or **(i)** two-way ANOVA with Tukey's multiple-comparison test.

OLDA treatment did not rescue the increased NEFA levels in tumor-bearing mice

Although OLDA treatment did not ameliorate the C26-induced weight and fat loss, it was still interesting to assess the plasma metabolite levels of these animals. In the pilot experiment, wild-type mice treated with OLDA tended to elevate NEFA in the plasma and altered key lipid metabolism proteins in the fat depots (**Figure 26 & Figure 27**). Moreover, in this experiment, tumor-bearing mice developed a complete

cachexia phenotype (**Figure 28**). Therefore, I wanted to assess if the plasma metabolite levels could reflect the observed cachexia phenotype and if OLDA treatment had any beneficial effect on the metabolite levels. Cachexia development was evident from increased NEFA, triglycerides, glycerol, and LDL levels and decreased plasma glucose levels. OLDA treatment did not have any protective effect against these altered levels of the metabolites (**Figure 29**). However, tumor-bearing mice treated with OLDA had elevated plasma protein levels (**Figure 29h**), suggesting decreased proteolysis or increased protein synthesis. I observed that the AST to ALT ratio was notably increased in the tumor-bearing mice (**Figure 29a**), primarily because of the presence of tumors, as I did not see any significant effect upon OLDA treatment. However, the individual AST and ALT levels were not significantly altered between the groups.

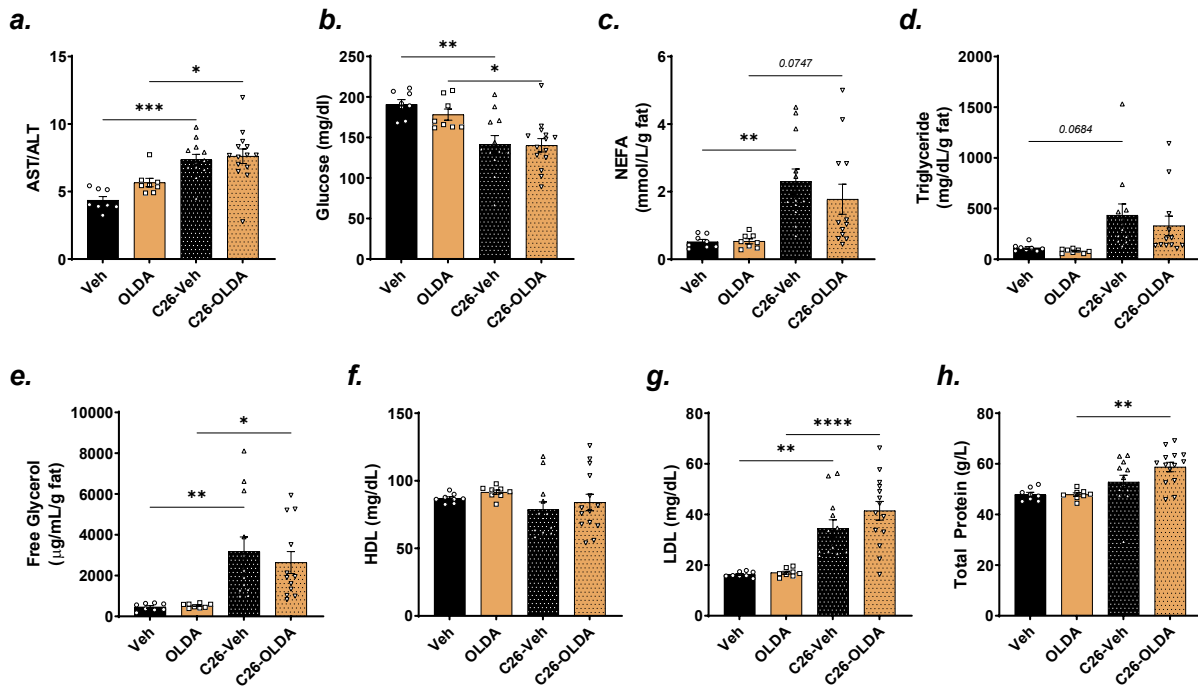


Figure 29: OLDA treatment increased plasma protein levels in the C26 tumor-bearing mice. Blood samples were collected from the animals shown in **Figure 28** before sacrificing. Plasma was extracted and analyzed for specific metabolites. **(a)** The ratio of AST to ALT levels, **(b)** glucose, **(c)** NEFA, **(d)** triglycerides, **(e)** glycerol, **(f)** HDL, **(g)** LDL, and **(h)** total protein levels in the plasma of the animals collected before sacrificing. $n = 8$ (Veh, OLDA), 12 (C26-Veh) or 14 (C26-OLDA), data shown are mean \pm s.e.m., * $P \leq 0.05$, ** $P \leq 0.01$, *** $P \leq 0.001$ and **** $P \leq 0.0001$; by one-way ANOVA with Šidák's multiple-comparison test.

OLDA treatment modulated the levels of proteins involved in fatty acid metabolism

Since fat depots are our target tissues, I extracted proteins and performed immunoblotting with antibodies against the proteins involved in lipid metabolism known to be modulated upon OLDA treatment (**Figure 30a**). Unexpectedly, FAS levels were increased in the tumor-bearing mice treated with vehicle, and this was decreased significantly upon OLDA treatment. A decrease in FAS levels observed upon OLDA treatment in the wild-type mice (**Figure 27**) was not observed in this experiment, possibly because the extended treatment might have a different effect from the pilot experiment. Although the C26-Vehicle group tended to reduce p-ACC α levels signifying the molecular changes upon cachexia development, no effect was observed upon OLDA treatment. TRVP-1 is a target of OLDA, and it is reported that activation of TRVP-1 increases the expression of calcitonin gene-related peptide (CGRP) (Nakanishi

et al., 2010). I observed a tendency to increase the TRVP-1 level in the tumor-bearing mice, and OLDA treatment had no significant effect in the wild-type and tumor-bearing mice. AMPK activity was shown to be reduced, and the levels of phosphorylated AMPK α (p-AMPK α (Thr172)) were reduced in the adipose tissue of the cachexia-inducing tumor-bearing mice (Rohm et al., 2016). However, in this experiment, I did not observe any significant changes in the levels of p-AMPK α (Thr172) (**Figure 30b**). This experiment showed high variability in the tumor burden and cachexia index (**Figure 28**), which might explain the variable molecular changes observed here.

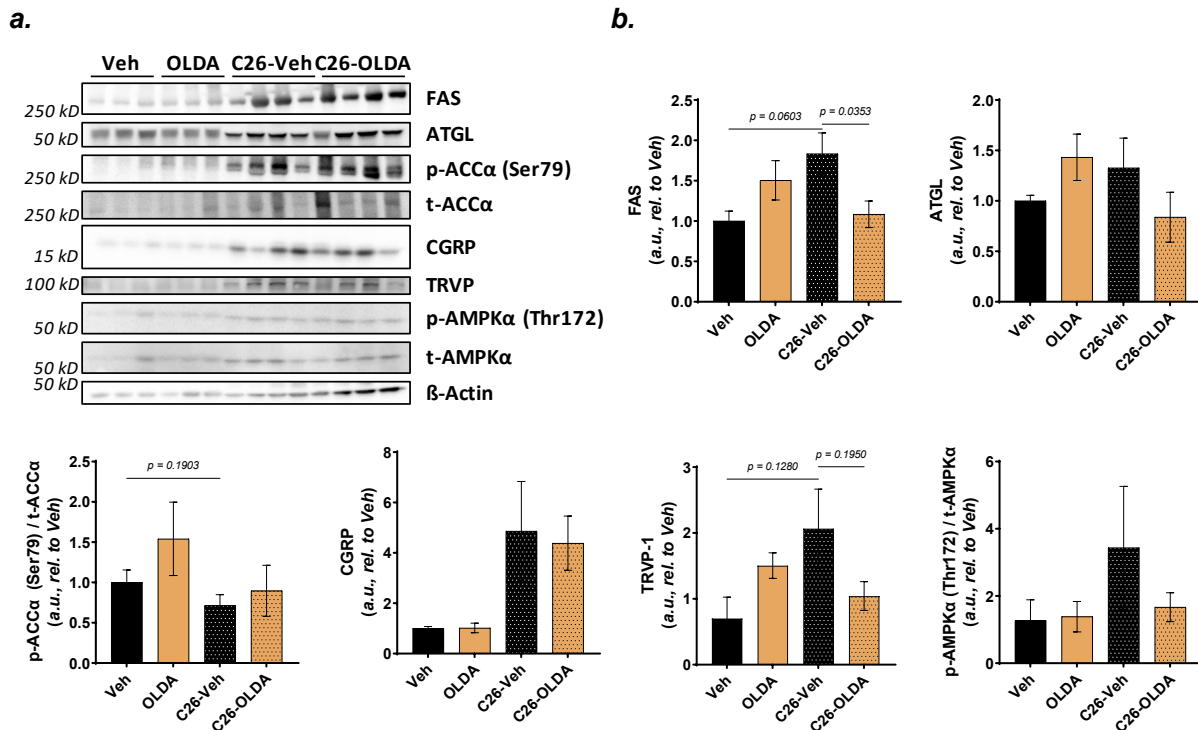


Figure 30: OLDA treatment decreased the TRVP-1 levels in the iWAT of tumor-bearing mice. (a) Immunoblots and **(b)** quantification of specific proteins separated from iWAT protein extracts. p-ACC α (Ser79) levels were normalized with the total ACC α and p-AMPK α (Thr172) with total AMPK α , and β -Actin was used as the loading control. $n = 8$ (Veh, OLDA), 12 (C26-Veh), or 14 (C26-OLDA), data shown are mean \pm s.e.m., one-way ANOVA with Šidák's multiple-comparison test was performed.

Although I observed that 5 mg/kg/day of OLDA treatment was effective and improved glucose excretion in the ipGTT experiment in the wild-type mice (**Figure 25**), I did not observe any significant changes in the measured plasma metabolite levels (**Figure 26**). While Balb/c mice injected with 1×10^6 C26 cells developed cachexia phenotype as observed by muscle and fat mass loss, 5 mg/kg/day of OLDA treatment did not counteract this loss. Levels of selected metabolites, such as glucose, NEFA, glycerol, and LDL, were significantly altered upon cachexia development. However, OLDA treatment did not affect these changes. Molecular changes observed in the iWAT upon cachexia development was not protected upon OLDA treatment. Even though treating with OLDA looked promising in the pilot experiment, it did not provide any beneficial effect against cachexia development.

2.4.3. Effects of BioF treatment in the Balb/c-C26 cachexia model

BioF is a synthetic small molecular weight compound obtained from the Charles River screening library. In the previous screen performed on the brown adipocytes, the BioF compound inhibited lipolysis by 50%. In this study, BioF consistently inhibited lipolysis (20-80%) in all three screenings performed on the white adipocytes. Though not much information is known about this compound, according to the patents database, it is postulated to glucagon-like peptide-1 (GLP-1) receptor ligand. GLP-1 signaling is implicated in anorexia in cancer cachexia patients and specific mice cachexia models (Borner et al., 2018). Interestingly, GLP-1 receptor agonists improved muscle function and ameliorated muscle wasting in mice models of muscle atrophy, such as dexamethasone- and nephrectomy-induced muscle atrophy (Hong et al., 2019). Therefore, I tested this novel compound against tumor-induced cachexia *in vivo*.

BioF treatment ameliorated C26 TCCM-induced C2C12 myotube atrophy

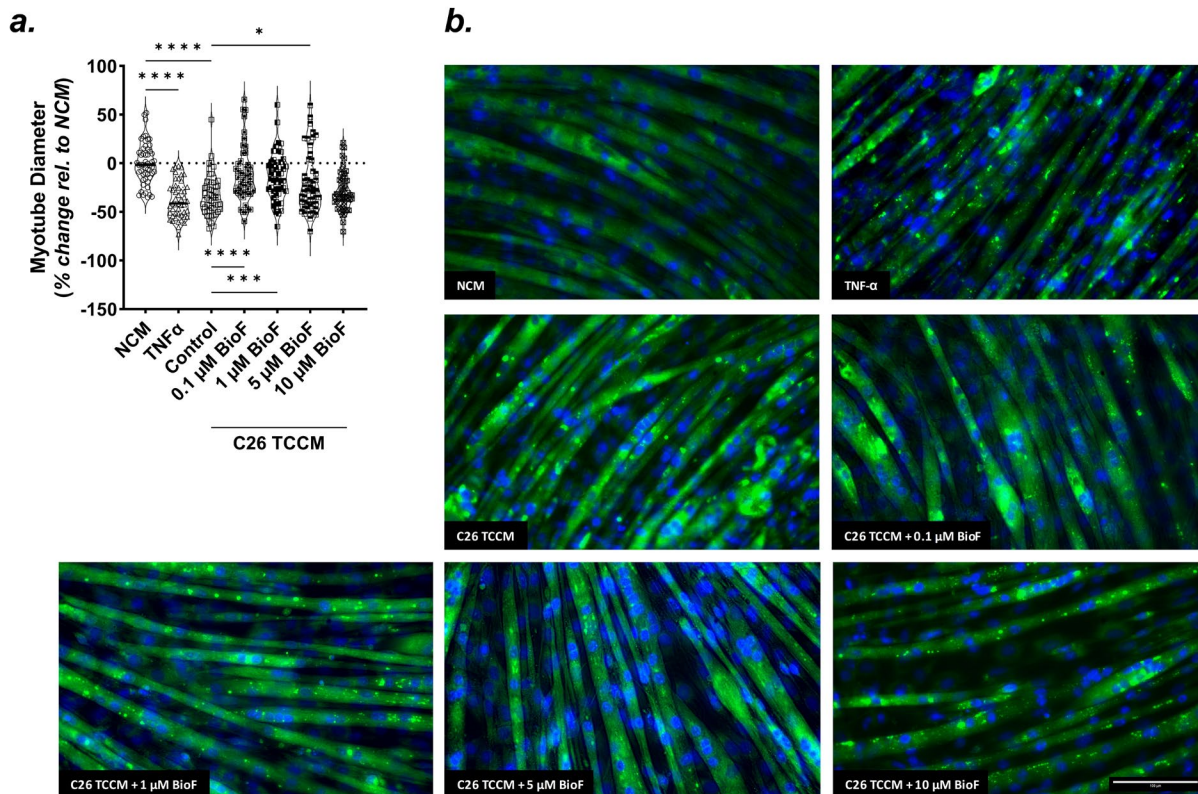


Figure 31: C26 TCCM-induced myotube atrophy is rescued upon BioF treatment. (a) C2C12 myotube diameter was measured using ImageJ as mentioned in the Methods (Staining and analysis of myotube diameter) after treating with indicated conditions for 48 hours. (b) Representative fluorescence images of the C2C12 myotubes. Myotubes are labeled green using MitoTracker™ Green FM dye, and nuclei are labeled blue using DAPI. Scale bar: 100 μ m.

Since I do not have much information about this compound, I performed additional *in vitro* experiments to substantiate that BioF could be a promising candidate compound for testing its efficacy to counteract cancer cachexia *in vivo*. Muscle atrophy is a phenotype observed in cancer cachexia patients and mice models (Argilés et al., 2014), and GLP-1 receptor agonists have been used to ameliorate muscle atrophy (Hong et al., 2019). Therefore, I treated the C2C12 myotubes with C26 TCCM and different concentrations of BioF for 48 hours. As a positive control, I used 20 ng/mL of TNF- α , which like C26 TCCM, induces

myotube atrophy. Interestingly, even at the lowest concentration I tested (0.1 μ M of BioF), co-treatment with BioF inhibited the C26 TCCM-induced myotube atrophy (**Figure 31**).

BioF treatment in healthy mice did not affect the body and tissue weights

In vitro, BioF rescued C26 TCCM-induced lipolysis in different adipocyte models and myotube atrophy in C2C12 cells. However, I did not have any information about the dosage of the BioF compound used previously for *in vivo* experiments. Therefore, I injected intraperitoneally different compound dosages (0.5, 1 mg/kg/day, and 1 mg/kg twice a day) for a treatment period of four days. Nine weeks old Balb/c male mice were used for this experiment, and mice from different groups had similar body weight (**Figure 32a**) and composition (data not shown) before the start of the investigation. After the treatment, the mice had equal weights, and the change in body weight and composition was also not significantly different (**Figure 32b, c**). There was a trend toward increasing the iWAT weight upon BioF treatment, but this effect was insignificant (**Figure 32e, f**). Thus, I did not observe any indications of toxicity or adverse effects on body and tissue weights upon repeated injection of BioF at the given doses.

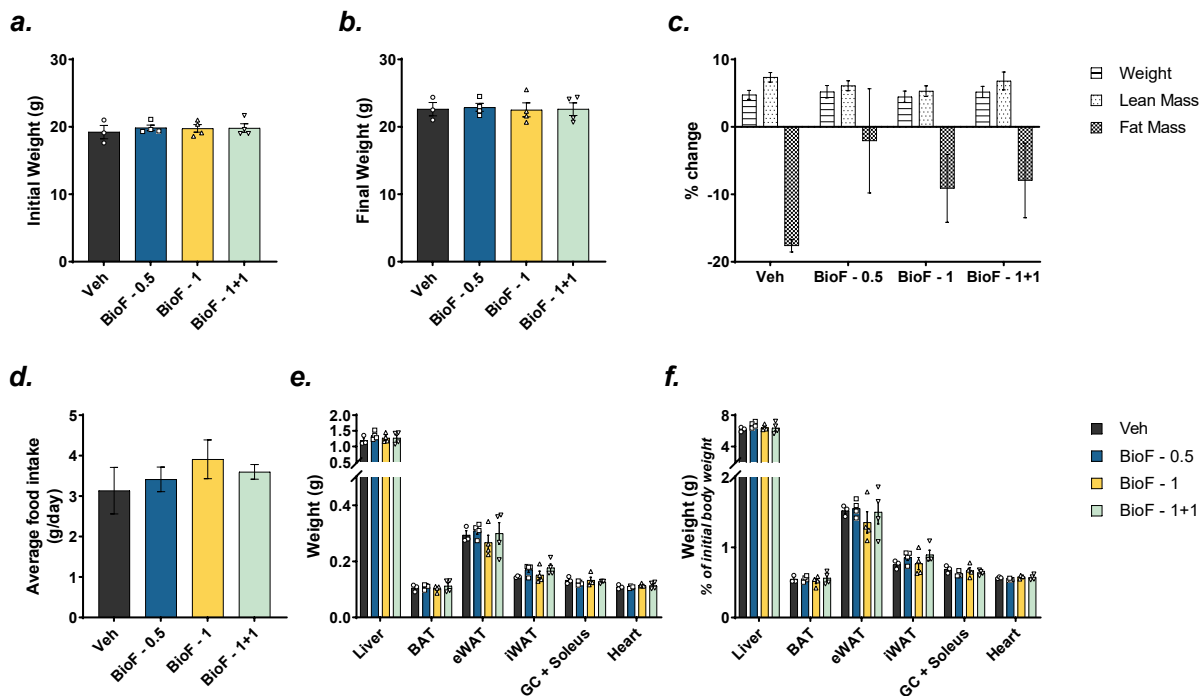


Figure 32: Mice treated with BioF display average body and tissue weight. Nine weeks old male Balb/c mice were injected intraperitoneally with either 0.5 mg/kg, 1 mg/kg of BioF, Vehicle once daily, or 1 mg/kg of BioF twice daily. Mice were sacrificed after four days of treatment. **(a)** Initial and **(b)** final body weight. **(c)** Percent change in the body weight, lean and fat mass after the treatment. **(d)** Average food consumption of the mice **(e)** Weight of the tissues (Liver, BAT, eWAT, iWAT, GC + Soleus, and heart) measured at the end of the experiment. **(f)** Tissue weights shown in **Figure 32e** are normalized to the initial body weight. **(a-c, e, f)** $n = 3$ (Veh) or 4 (BioF - 0.5, 1, 1+1), **(d)** $n = 2$ per group; data shown are mean \pm s.e.m., and one-way ANOVA with Šidák's multiple-comparison test was performed.

BioF treatment-induced plasma triglyceride levels

The repeated injection of BioF in healthy mice did not affect the body and tissue weights; however, assessing whether liver toxicity was induced upon treatment was essential. AST to ALT ratio was not changed (**Figure 33a**), and individual AST and ALT were unaffected (data not shown). However, I only observed an increase in the plasma triglyceride levels in the mice treated with the lowest dosage of 0.5 mg/kg/day BioF (**Figure 33d**). Other parameters were unaltered, though I saw a tendency to decrease the percent change of plasma glycerol in mice treated twice daily (**Figure 33e**). BioF treatment at these doses did not elicit liver toxicity or significantly change the plasma metabolites measured.

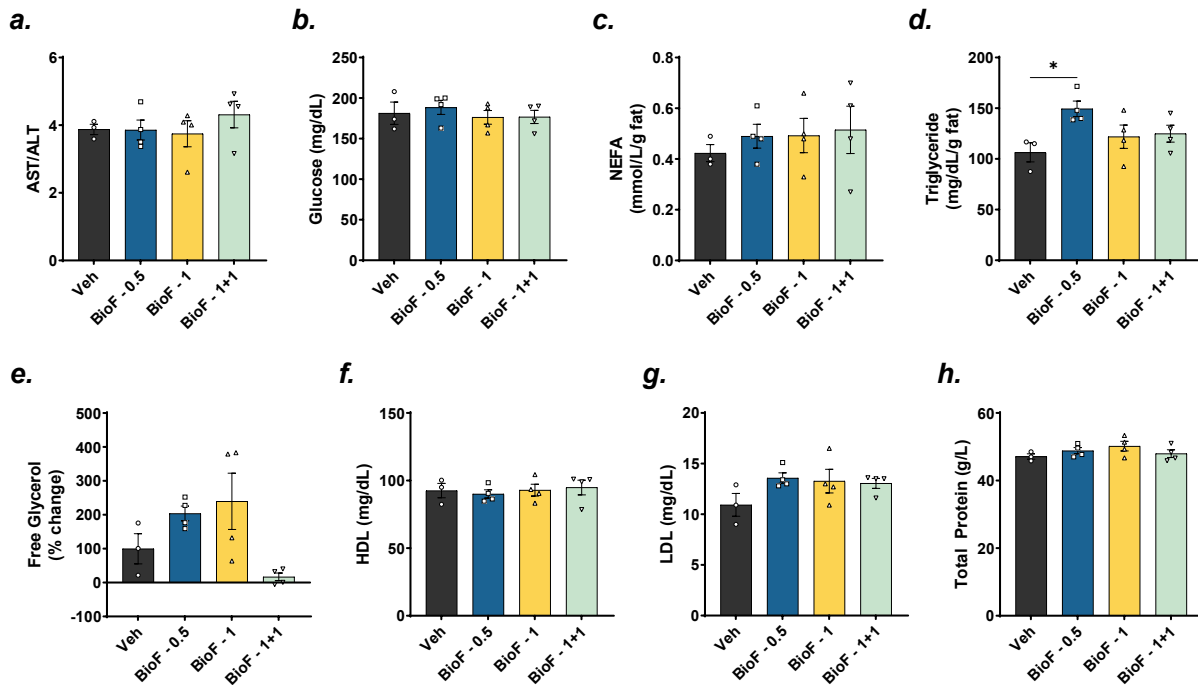


Figure 33: BioF treatment did not elicit liver toxicity. Blood samples were collected from the animals shown in **Figure 32** before sacrificing. Plasma was extracted and analyzed for specific metabolites. (a) The ratio of AST to ALT levels, (b) random post-prandial glucose, (c) triglycerides, (d) NEFA, (e) percent change of glycerol, (f) HDL, (g) LDL, and (h) total protein levels in the plasma of mice treated with BioF or Vehicle. $n = 3$ (Veh) or 4 (BioF - 0.5, 1, 1+1), data shown are mean \pm s.e.m., * $P \leq 0.05$; by one-way ANOVA with Šidák's multiple-comparison test.

High dose of BioF increased weight and lean mass gain

Since I did not observe adverse effects of injecting 0.5-2mg/kg BioF per day, I tested the effects of compound treatment with an even higher dose of 5 mg/kg/day injected intraperitoneally. There was no difference in the initial body weights of the mice. Strikingly, treatment with a higher amount of BioF significantly increased the percent change in the body weight and lean mass at the end of the experiment (**Figure 34a, b, c**). This increase in body weight might well be associated with the trend of increased lean mass. I observed a considerable variation in the percent change in fat mass, possibly due to technical issues (mice handling and injection). Interestingly, there was also a trend of increased iWAT weight of the animals treated with BioF (**Figure 34e, f**). With no effect on food intake (**Figure 34d**) and these beneficial effects observed in body weight, lean mass, and iWAT, it was encouraging for us to use BioF at this dosage for the cachexia experiment.

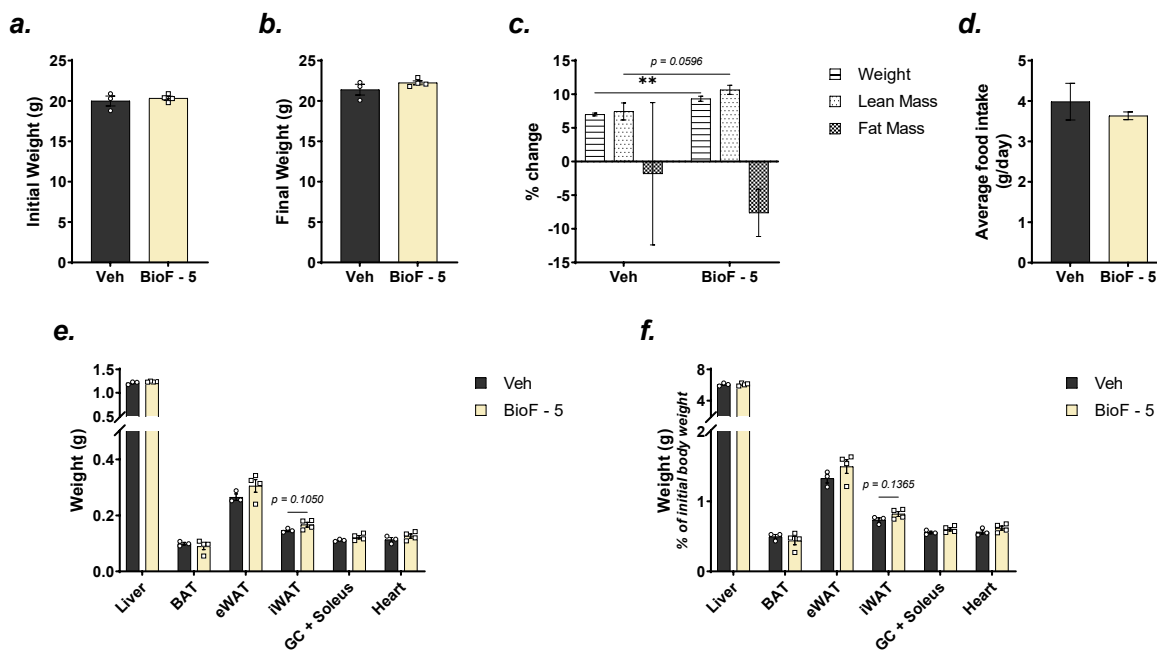


Figure 34: Mice treated with BioF had increased weight gain. Eight weeks old male Balb/c mice were injected intraperitoneally with either 5 mg/kg of BioF or Vehicle once daily. Mice were sacrificed after four days of treatment. **(a)** Initial and **(b)** final body weight. **(c)** Percent change in the body weight, lean and fat mass after the treatment. **(d)** Average food consumption of the mice **(e)** Weight of the tissues (Liver, BAT, eWAT, iWAT, GC + Soleus, and heart) measured at the end of the experiment. **(f)** Tissue weights shown in **Figure 34e** are normalized to the initial body weight. **(a-c, e, f)** $n = 3$ (Veh) or 4 (BioF - 5), **(d)** $n = 2$ per group; data shown are mean \pm s.e.m., $**P < 0.01$; by two-tailed t-test.

A high dose of BioF treatment did not affect the plasma metabolite levels

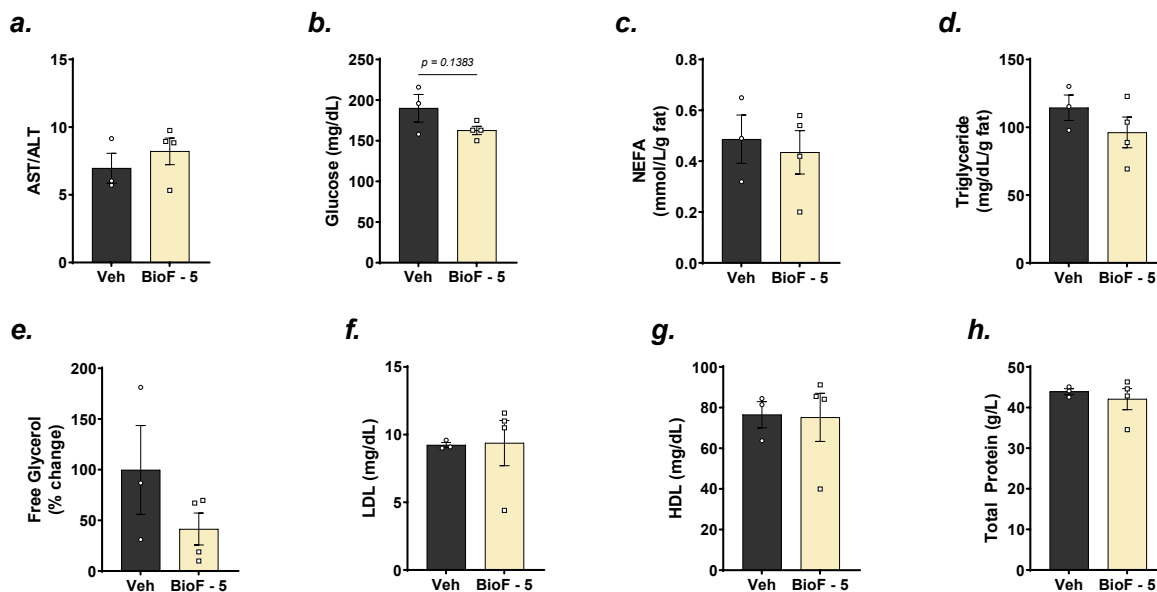


Figure 35: A higher dose of BioF treatment did not elicit liver toxicity. Blood samples were collected from the animals shown in **Figure 34** before sacrificing. Plasma was extracted and analyzed for specific metabolites. **(a)** The ratio of AST to ALT levels, **(b)** random post-prandial glucose, **(c)** triglycerides, **(d)** NEFA, **(e)** percent change of glycerol, **(f)** HDL, **(g)** LDL, and **(h)** total protein

levels in the plasma of mice treated with BioF or Vehicle. $n = 3$ (Veh) or 4 (BioF - 5); data shown are mean \pm s.e.m., and a two-tailed t-test was performed.

I analyzed the plasma of the animals treated with 5 mg/kg/day of BioF to check if the treatment affected the selected metabolites. A higher amount of BioF treatment did not elicit liver toxicity as measured by the ratio of AST to ALT levels (**Figure 35a**). There was a trend towards decreasing plasma glucose levels and changing plasma free glycerol levels. However, the effect was insignificant (**Figure 35b, e**). Other metabolites measured in the plasma were unaffected (**Figure 35**).

BioF treatment increased the expression of adipose tissue markers

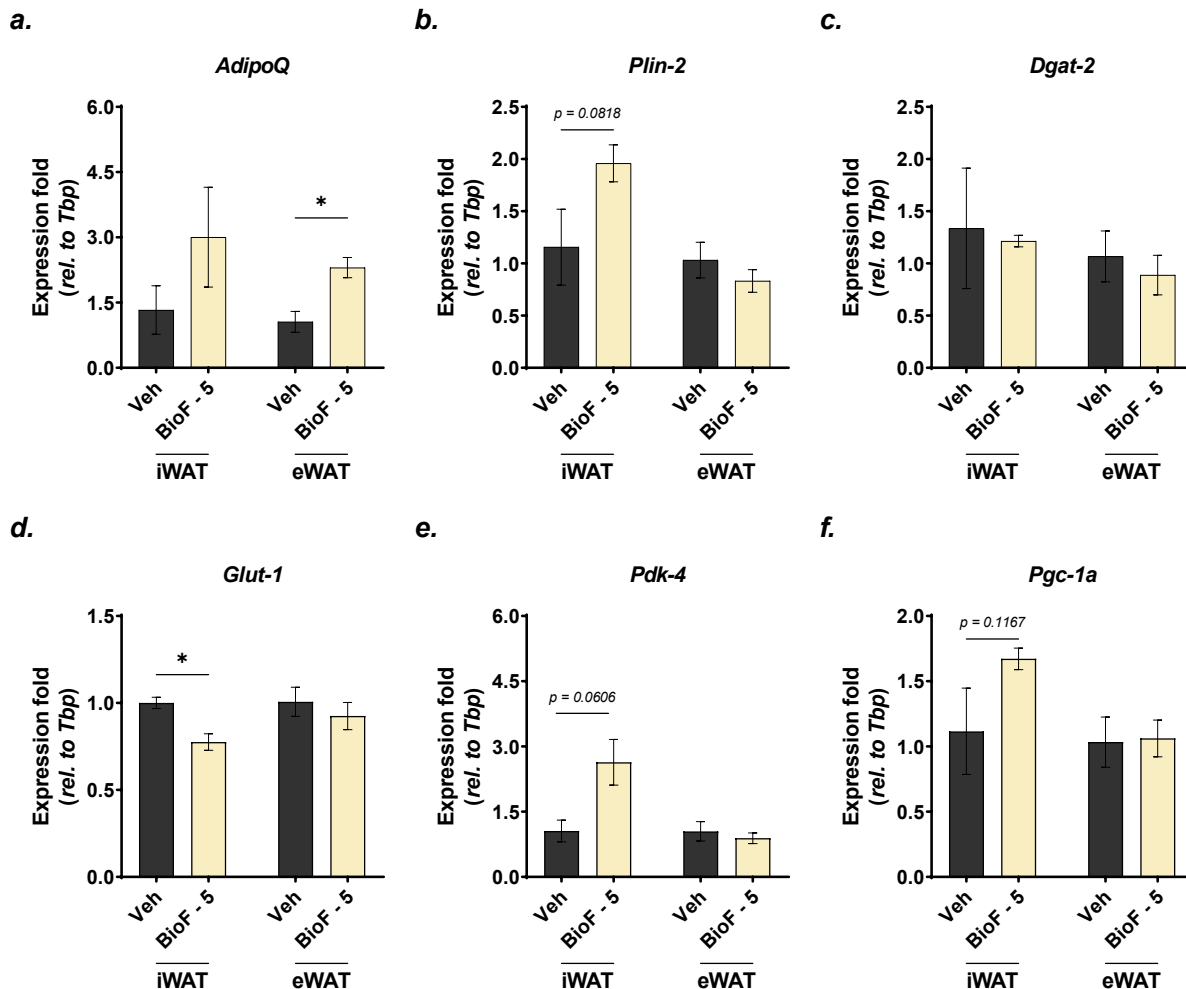


Figure 36: BioF treatment increased the Adiponectin (*AdipoQ*) levels in the iWAT and eWAT. Expression levels of (a) *AdipoQ*, (b) *Plin-2*, (c) *Dgat-2*, (d) *Glut-1*, (e) *Pdk-4*, and (f) *Pgc-1a* transcripts in the iWAT and eWAT of the animals treated with BioF or Vehicle. $n = 3$ (Veh) or 4 (BioF - 5); data shown are mean \pm s.e.m., * $P < 0.05$; by two-tailed t-test.

Since I observed that 5 mg/kg/day of BioF treatment showed a trend to increase iWAT, I wanted to analyze the genes involved in fatty acid metabolism in iWAT and eWAT of the animals. RNA from the iWAT and eWAT was extracted, and qPCR was performed to measure the level of specific transcripts. Adiponectin (*AdipoQ*), Pyruvate dehydrogenase kinase 4 (*Pdk-4*), and PPARG Coactivator 1 α (*Pck-1a*) are important regulators involved in fatty acid and glucose metabolism. *AdipoQ* was shown to rescue high-fat diet-

induced insulin resistance in mice models (Yamauchi et al., 2001). Recently *Pdk-4* was implicated in the development of cancer cachexia, and blocking its activity *in vitro* prevented C2C12 myotube atrophy induced by cachexia-inducing TCCM (Pin et al., 2019). Likewise, *Pck-1 α* overexpression in mice reduced the expression of atrophy markers in muscle (Sandri et al., 2006). The expression levels of these genes (*AdipoQ*, *Pdk-4*, and *Pck-1 α*) were increased in adipose tissue (**Figure 36**). Glucose Transporter Type-1 (*Glut-1*) levels involved in the glucose transport and uptake were decreased in the iWAT of animals treated with BioF (**Figure 36d**); however, it would be interesting to check if the GLUT-4 translocation is altered. Perilipin-2 (*Plin-2*) coats the lipid droplets, and this gene's expression showed a trend toward increasing in BioF-treated iWAT. Diacylglycerol O-Acyltransferase 2 (*Dgat-2*) is involved in the fatty acid synthesis and was shown to be downregulated during cachexia (Tsoli et al., 2014). BioF treatment did not alter the expression of *Dgat-2*. Overall, 5 mg/kg/day BioF treatment positively changed the expression of selected genes involved in fatty acid and glucose metabolism in the iWAT and eWAT.

BioF treatment did not delay cachexia development

5 mg/kg/day treatment of BioF increased the body weight (**Figure 34**) and altered (or showed a tendency to) the expression of genes involved in fatty acid and glucose metabolism in iWAT and eWAT (**Figure 36**). Therefore, I used this dosage for the cachexia experiment. As indicated in the Methods (*C26 cachexia model*), cachexia-inducing C26 cells were injected. After eight days, I injected the mice intraperitoneally with 5 mg/kg of BioF or the vehicle daily. Tumor-bearing mice developed cachexia as observed from the final body weight and the change in fat mass and weight (**Figure 37b, c**). Although the BioF treatment showed a trend to increase body weight in the non-tumor-bearing mice, it did not provide any protective effect in the tumor-bearing mice. The C26-induced cachexia also affected the weight of the adipose tissues and skeletal muscle, and the treatment with the compound had no significant effect on these parameters (**Figure 37d, h**). Although there was no difference between the tumor weight and the cachexia index (**Figure 37e, f**), the tumor-bearing mice treated with BioF had increased average food intake (**Figure 37g**). When I looked at the food intake over time (data not shown), I could observe that the mice started to eat more food towards the end of the cachexia-induced weight loss. Together, these results suggest that even though BioF treatment increased body weight change in wild-type mice, at this concentration, BioF had no effect in delaying or counteracting cachexia development.

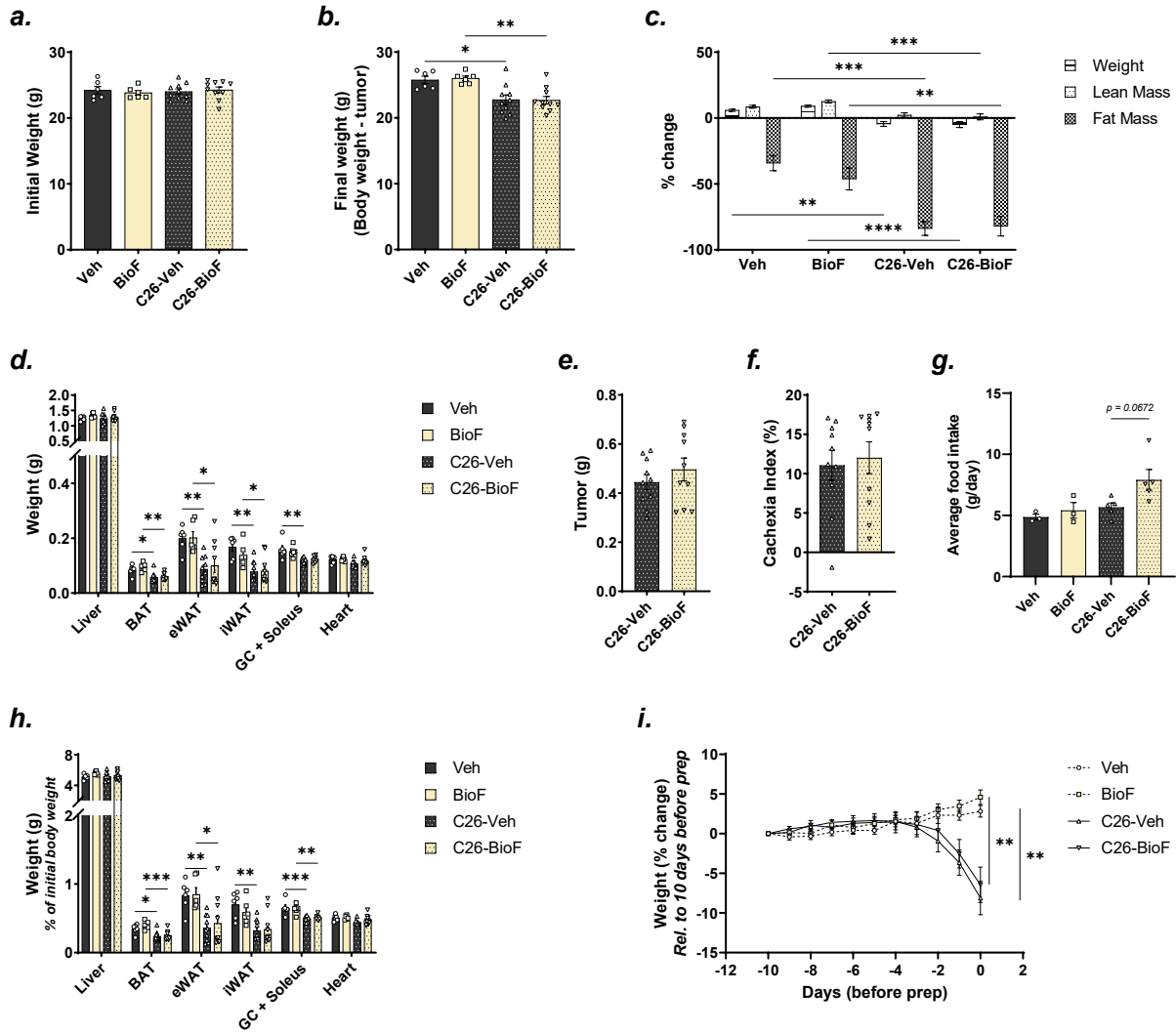


Figure 37: BioF treatment in the C26 tumor-bearing mice did not prevent cachexia development. Eight weeks old male Balb/c mice were injected subcutaneously with either 1×10^6 C26 cells or PBS. Seven days post-inoculation, mice were injected intraperitoneally with either 5 mg/kg of BioF or Vehicle once daily. Tumor-bearing mice were sacrificed by cervical dislocation after cachexia development, and non-tumor-bearing mice were sacrificed together with the tumor-bearing mice. **(a)** Initial and **(b)** final carcass body weight of the mice. **(c)** Percent change in the body weight, lean and fat mass at the end of the experiment. **(d)** The weight of the tissues (Liver, BAT, eWAT, iWAT, GC + Soleus, heart) and **(e)** tumor were measured at the end of the experiment. **(f)** Cachexia index of the tumor-bearing mice as calculated by the formula mentioned in the Methods (Cachexia index). **(g)** Average food consumption of the mice. **(h)** Tissue weights shown in **Figure 37d** are normalized to the initial body weight. **(i)** Bodyweight development of the mice in the last ten days before sacrifice depicted as the percentage change in weight relative to that of 10 days before prep. $n = 6$ (Veh, BioF), or 10 (C26-Veh, C26-BioF), data shown are mean \pm s.e.m., $*P \leq 0.05$, $**P \leq 0.01$, $***P \leq 0.001$ and $****P \leq 0.0001$; by **(a-d, g, h)** one-way ANOVA with Šidák's multiple-comparison test, **(e, f)** by two-tailed t-test or **(i)** two-way ANOVA with Tukey's multiple-comparison test.

BioF treatment did not affect the altered plasma metabolites

To assess and validate cachexia development, I analyzed the plasma collected from the experiment and quantified the levels of critical metabolites. I observed changes in the key markers of cachexia, such as decreased glucose levels and increased NEFA, triglycerides, glycerol, and LDL levels (**Figure 38**). BioF treatment showed a tendency to decrease the glucose levels in the non-tumor-bearing mice as in the

previous experiment using BioF (**Figure 35**) and to rescue the decreased glucose level in the tumor-bearing mice; however, the effect was insignificant. I observed no protective effect of BioF treatment in the plasma metabolite levels in the tumor-bearing mice.

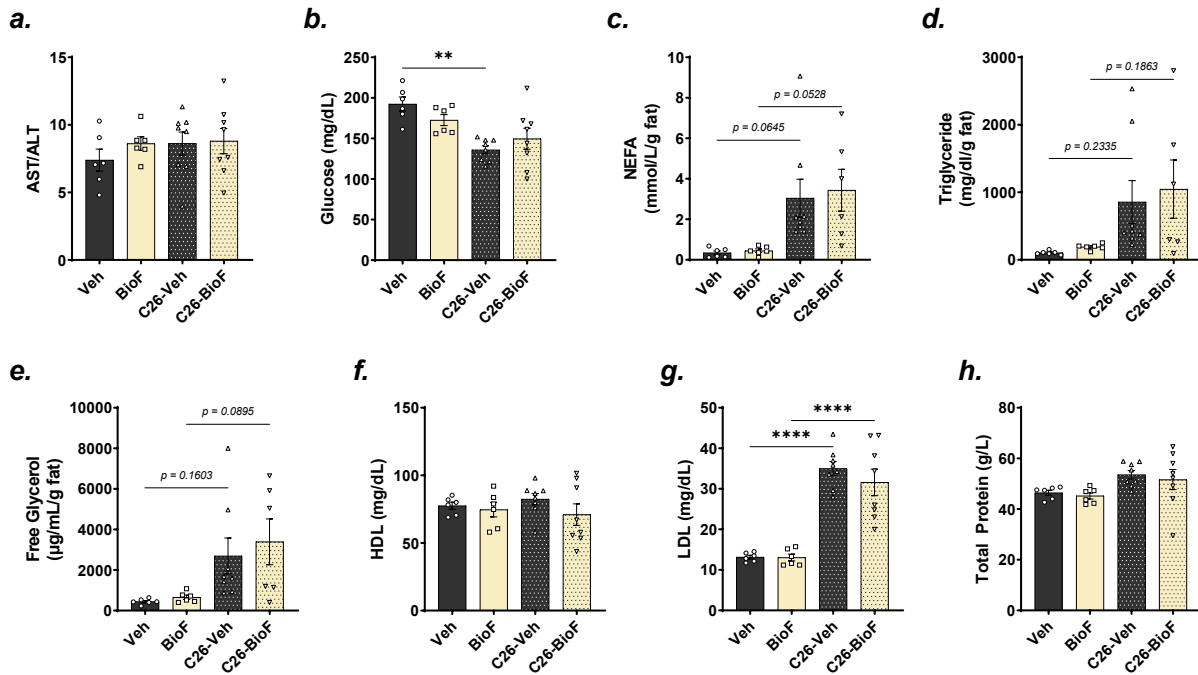


Figure 38: BioF treatment did not inhibit the C26-induced increase in NEFA levels. Blood samples were collected from the animals shown in **Figure 37** before sacrificing. Plasma was extracted and analyzed for specific metabolites. **(a)** The ratio of AST to ALT levels, **(b)** random post-prandial glucose, **(c)** NEFA, **(d)** triglycerides, **(e)** free glycerol, **(f)** HDL, **(g)** LDL, and **(h)** total protein levels in the plasma of the animals. $n = 6$ (Veh, BioF), 10 (C26-Veh), or 8 (C26-BioF); data shown are mean \pm s.e.m., $**P \leq 0.01$, and $***P \leq 0.0001$; by one-way ANOVA with Šídák's multiple-comparison test.

BioF treatment modulated the levels of proteins involved in lipolysis

Since I observed molecular changes upon BioF treatment in the previous experiment (**Figure 36**), I extracted proteins from the target tissues iWAT and eWAT and performed immunoblotting experiments. BioF treatment increased the levels of inhibitory phosphorylation of HSL (p-HSL(Ser565)) and decreased the activatory phosphorylation (p-HSL(Ser563)) in the iWAT of the tumor-bearing mice (**Figure 39a, b**). Although I did not see an effect on the p-HSL(Ser565) levels in the eWAT, BioF treatment decreased the p-HSL(Ser563) levels in the eWAT (**Figure 39c, d**), implying that the BioF treatment inhibited the lipolysis mechanism *in vivo*. However, this inhibition of HSL-mediated lipolysis in the iWAT and eWAT upon BioF did not affect the altered metabolite levels in the plasma nor protect against weight and fat mass loss. I did not observe significant changes in the levels of FAS.

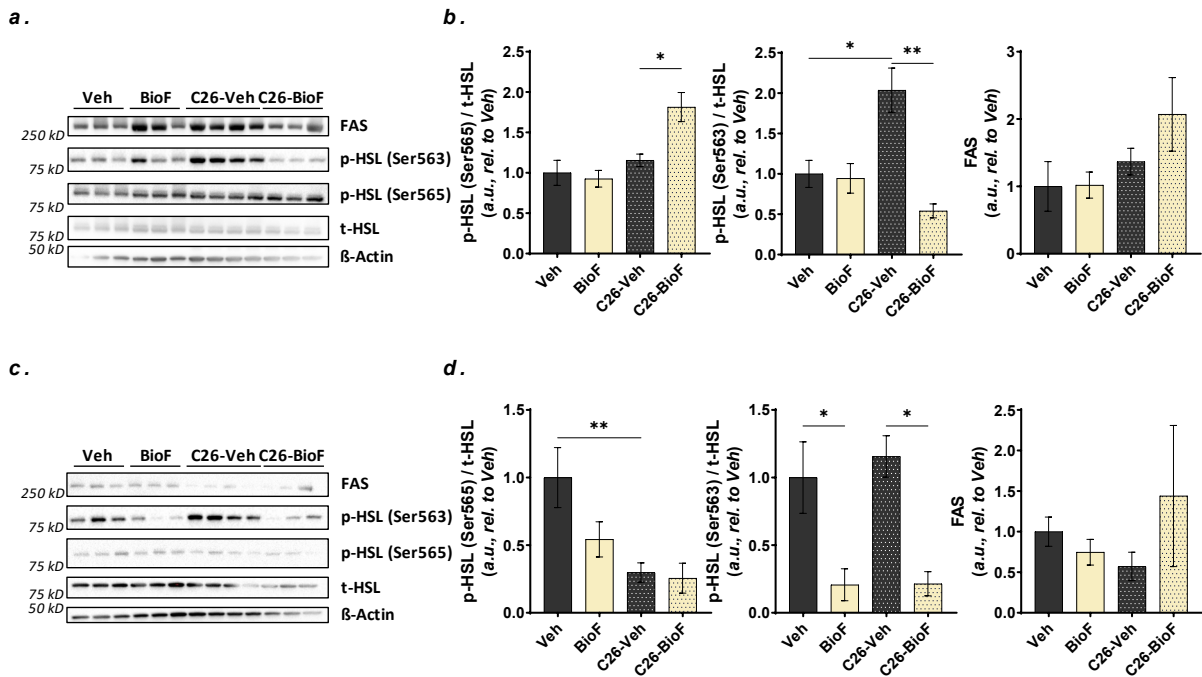


Figure 39: BioF treatment decreased the p-HSL(Ser563) levels in the iWAT and eWAT. (a, c) Immunoblots and (b, d) quantification of specific proteins separated from (a, b) iWAT and (c, d) eWAT protein extracts. p-HSL(Ser565) and p-HSL(Ser563) levels were normalized with the total HSL, and β-Actin was used as the loading control. $n = 6$ (Veh, BioF), 10 (C26-Veh), or 8 (C26-BioF), data shown are mean \pm s.e.m., * $P \leq 0.05$ and ** $P \leq 0.01$; by one-way ANOVA with Šidák's multiple-comparison test.

Atrophy markers were increased in the tumor-bearing mice

Muscle atrophy is a key characteristic of cancer cachexia, and tumor-bearing mice lost significant muscle mass in the cachexia experiment (Figure 37). *In vitro*, I observed that treatment with BioF ameliorated the C26-induced C2C12 myotube atrophy (Error! Reference source not found.). To check if BioF treatment modulated the expression of genes involved in muscle atrophy, I analyzed the transcript levels of atrophy-related genes in the GC muscle. F-Box Protein 32 (*Fbxo-32*), Forkhead Box Protein O1 (*Foxo-1*), BCL2 Interacting Protein-3 (*Bnip-3*), and *Pdk-4* levels were previously shown to be increased during cachexia in the muscle (Brown et al., 2017; Pin et al., 2019; Reed et al., 2012). Transcript levels of *Fbxo-32*, *Foxo-1*, and *Bnip-3* were significantly increased in the tumor-bearing mice, and the compound treatment had no significant effect. Interestingly, BioF treatment showed a trend to reduce the increased expression of *Pdk-4* levels in the GC muscle (Figure 40). PDK-4 inhibition showed a positive effect against C2C12 myotube atrophy (Pin et al., 2019); however, the compound did not confer any beneficial effect, even though *Pdk-4* levels were reduced upon BioF treatment in the GC muscle. The insulin-sensitive Glucose Transporter Type-4 (Glut-4) transcript levels were largely unaffected in tumor-bearing and BioF-treated mice.

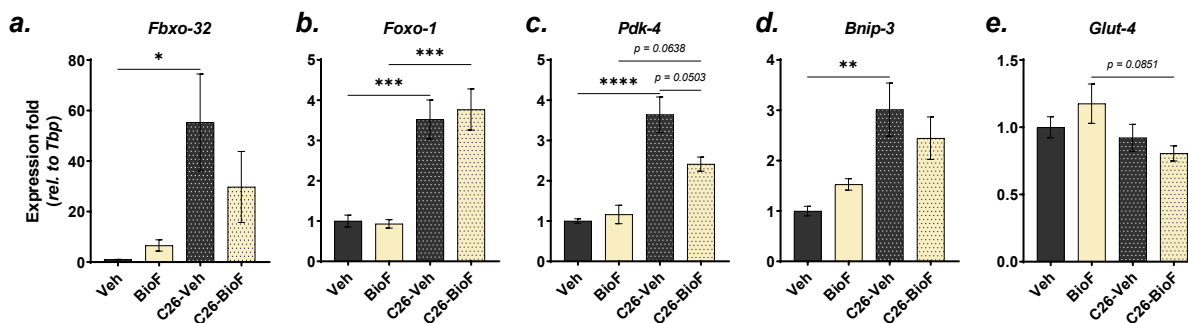


Figure 40: BioF treatment decreased the Pdk-4 transcript levels in tumor-bearing mice. Expression levels of (a) *Fbxo-32*, (b) *Foxo-1*, (c) *Pdk-4*, (d) *Bnip-3*, and (e) *Glut-4* transcripts in the GC muscle of the animals. $n = 6$ (Veh, BioF), or 10 (C26-Veh), or 8 (C26-BioF), data shown are mean \pm s.e.m., * $P \leq 0.05$, ** $P \leq 0.01$, *** $P \leq 0.001$ and **** $P \leq 0.0001$; by one-way ANOVA with Šidák's multiple-comparison test.

Taken together, the data from this cachexia study showed that even though the BioF treatment altered the levels of critical proteins and genes involved in cachexia development, the dosage used was insufficient to counteract the cachexia-induced weight and fat loss. Therefore, it would be interesting to test this compound in a different experimental setup or with a higher dose.

BioF treatment did not prevent cachexia development in mice held at the thermoneutral condition

I observed that treatment with BioF, even though it brought changes in the levels of critical molecular regulators and inhibited lipolysis *in vitro* and *in vivo*, did not provide a beneficial effect against the tissue and weight loss associated with cancer cachexia. In previous cachexia experiments, I often observed a tendency for the compounds to increase the BAT weight in the non-tumor-bearing mice groups. I speculated that the effect of the compounds might be masked in the tumor-bearing mice due to the holding temperature. Therefore, I wanted to perform an experiment to rule out the possible involvement of BAT metabolism. To that end, I designed an experiment in which mice were acclimatized to 30 °C. I induced cachexia by injecting C26 cells and treated them with either vehicle or 5 mg/kg/day of BioF. Compound treatment in the mice held at 30 °C did not prevent the cachexia development or the severity of the cachexia. Tumor-bearing mice lost significant weight, lean, and fat mass (Figure 41c). I observed C26-induced muscle and heart atrophy, and the weights of fat depots were significantly reduced (Figure 41d, h). Like in the previous cachexia experiment using BioF (Figure 37), I did not observe any protective effect against weight and tissue loss. Interestingly, I did not observe the increased food intake in the C26-BioF groups I saw in the previous cachexia experiment using the BioF compound (Figure 37). BioF treatment did not mitigate the cachexia index or the tumor growth (Figure 41e, f); in fact, the BioF-treated mice seemed to lose weight and develop cachexia before the vehicle-treated tumor-bearing mice (Figure 41i).

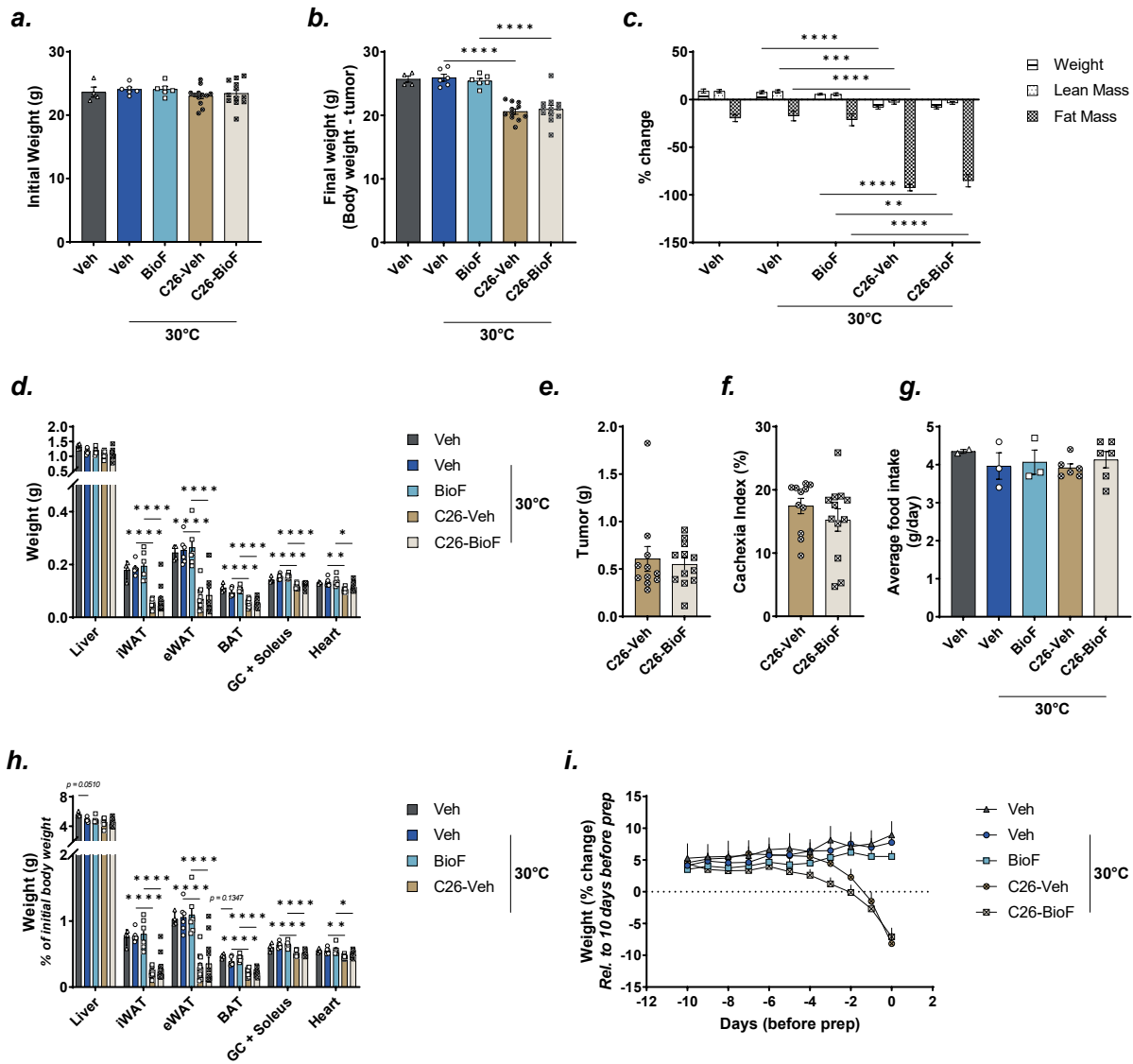


Figure 41: Effects of holding C26 tumor-bearing mice in thermoneutral condition. Twelve weeks old male Balb/c mice were allowed to acclimatize to the thermoneutral condition (30 °C) for a week. Control mice were housed in a housing temperature of 21 °C. Mice were injected subcutaneously with either 1 x 10⁶ C26 cells or PBS. From the next day onwards, they were injected intraperitoneally with either 5 mg/kg of BioF or Vehicle once daily. Tumor-bearing mice were sacrificed by cervical dislocation after cachexia development, and non-tumor-bearing mice were sacrificed together with the tumor-bearing mice. **(a)** Initial and **(b)** final carcass body weight of the mice. **(c)** Percent change in the body weight, lean and fat mass at the end of the experiment. **(d)** The weight of the tissues (Liver, BAT, eWAT, iWAT, GC + Soleus, heart) and **(e)** tumor were measured at the end of the experiment. **(f)** Cachexia index of the tumor-bearing mice as calculated by the formula mentioned in the Methods (Cachexia index). **(g)** Average food consumption of the mice. **(h)** Tissue weights shown in **Figure 41d** are normalized to the initial body weight. **(i)** Bodyweight development of the mice in the last ten days before sacrifice depicted as the percentage change in weight relative to that of 10 days before prep. n = 4 (Veh); 6 (Veh, BioF), or 12 (C26-Veh, C26-BioF) at 30 °C, data shown are mean ± s.e.m., *P ≤ 0.05, **P ≤ 0.01, ***P ≤ 0.001 and ****P ≤ 0.0001; by **(a-d, g, h)** one-way ANOVA with Šidák's multiple-comparison test, **(e, f)** by two-tailed t-test or **(i)** two-way ANOVA with Tukey's multiple-comparison test.

Changes in the plasma metabolites in mice held at the thermoneutral condition

Even though BioF treatment did not ameliorate the tissue and weight loss in the C26 cachexia model in thermoneutral conditions, I observed a trend to counteract the levels of individual plasma metabolites

upon compound treatment. The tumor-bearing mice had increased cholesterol and LDL levels in their plasma samples, and the treatment with BioF showed a tendency to reduce these levels (**Figure 42e, g**). However, BioF treatment did not affect the levels of other altered metabolites in the plasma, such as glucose, NEFA, triglycerides, and proteins (**Figure 42**).

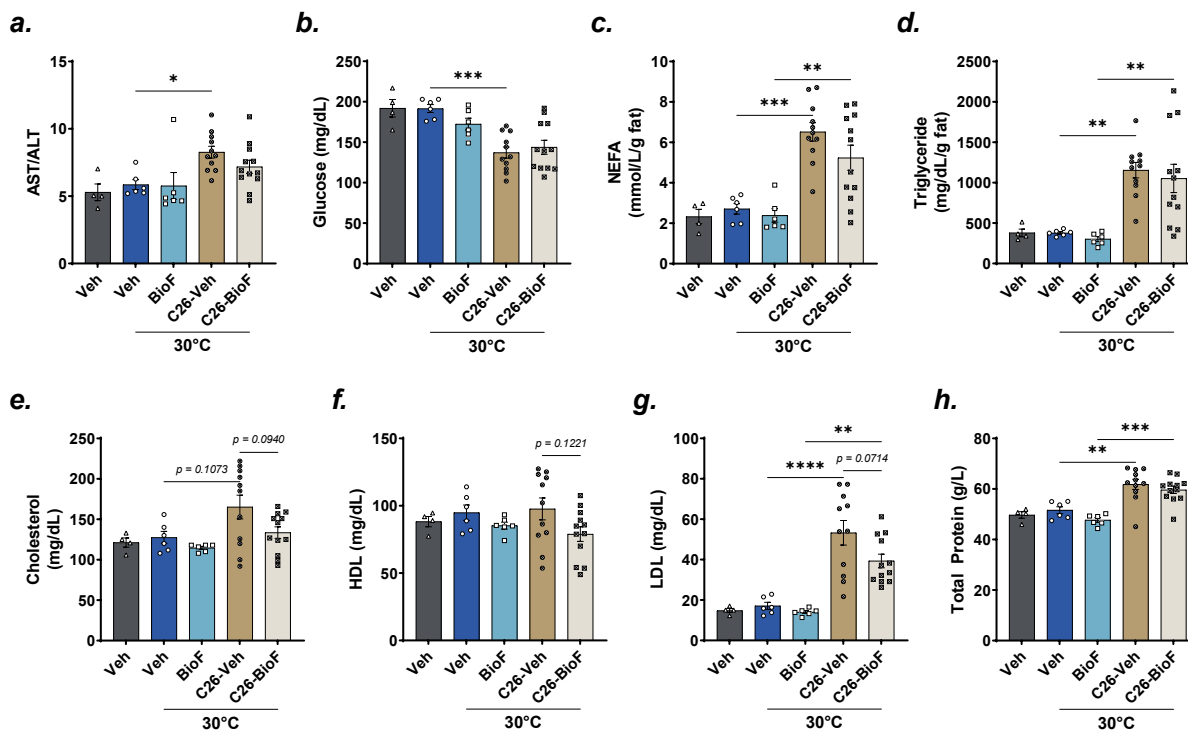


Figure 42: BioF treatment in thermoneutral conditions reduced the C26-induced increase in cholesterol levels. Blood samples were collected from the animals shown in **Figure 41** before sacrificing. Plasma was extracted and analyzed for specific metabolites. **(a)** The ratio of AST to ALT levels, **(b)** random post-prandial glucose, **(c)** NEFA, **(d)** triglycerides, **(e)** cholesterol, **(f)** HDL, **(g)** LDL, and **(h)** total protein levels in the plasma of the animals. $n = 4$ (Veh); 6 (Veh, BioF), or 12 (C26-Veh, C26-BioF) at 31 °C; data shown are mean \pm s.e.m., * $P \leq 0.05$, ** $P \leq 0.01$, *** $P \leq 0.001$ and **** $P \leq 0.0001$; by one-way ANOVA with Šidák's multiple-comparison test.

3. DISCUSSION

3.1. Targeting lipolysis as a treatment strategy against cancer cachexia

Research on cancer cachexia was focused extensively on deciphering the mechanism of muscle wasting and methods to prevent cachexia-induced protein degradation in the muscle. However, studies in our lab and by other researchers have demonstrated the critical involvement of adipose tissue biology and wasting during cachexia (Das et al., 2011; Rohm et al., 2016). In the animal models of cachexia and the weight-losing gastrointestinal cancer patients cohort, adipose tissue wasting was observed even before an absolute reduction in the lean mass and body weight (Byerley et al., 2010; Fouladiun et al., 2005; Ishiko et al., 1999). These data supported the need for extensive research on altered adipose tissue metabolism during cachexia. One of the critical mechanisms implicated in adipose tissue wasting is cachexia-induced lipolysis. Tumor-derived factors such as ZAG were reported to be increased in weight-loss cancer patients, and treatment of ZAG induced lipolysis *in vitro* and reduced weight gain in obese *ob/ob* mice (Hirai et al., 1998; T. Todorov et al., 1998). Several tumor-derived factors and pro-inflammatory cytokines exhibiting elevated levels in the presence of a cachexia-inducing tumor were shown to play a critical role in the induction of lipolysis and tissue and weight loss during cachexia (Mannelli et al., 2020). The adipose tissue of cancer cachexia patients was more sensitive to the lipolytic stimuli and had increased expression and activity of HSL (Agustsson et al., 2007; Dahlman et al., 2010). Recently, our lab showed that the cachexia-inducing tumor impaired energy homeostasis and induced lipolysis in the metabolically dysregulated WAT. Furthermore, treatment with ACIP, which was developed to block AMPK-CIDEA interaction, counteracted tumor-induced lipolysis and reduced adipose tissue wasting and weight loss in cachexia-inducing tumor-bearing mice (Rohm et al., 2016). Therefore, previous research suggested that inhibiting cachexia-induced lipolysis could prevent fat loss and, ultimately, the weight loss observed in weight-losing cancer patients.

Lipolysis is a highly regulated process, and several lipases and their coactivators are involved in the sequential breakdown of TGA into FFA and glycerol (Luo & Liu, 2016). Small molecule inhibitors were developed against the rate-limiting lipase ATGL and HSL and were shown to be highly-specific and effective (Mayer et al., 2013; Schweiger et al., 2006). The ATGL-specific inhibitor Atglistatin (ATGLi) inhibited lipolysis and thus FFA mobilization *in vitro* in mature 3T3-L1 adipocytes and wildtype mice by up to 50% (Mayer et al., 2013). Interestingly, ATGLi treatment prevented metabolic dysregulation upon high-fat diet feeding in the wildtype mice as well as in the genetic obesity *ob/ob* mouse model. Furthermore, ATGLi treatment counteracted insulin resistance, reversed adipose tissue inflammation, and reduced NAFLD development in mice fed a high-fat diet (Schweiger et al., 2017). Likewise, ATGLi and adipose tissue-specific knockout of ATGL (*atATGL-KO*) was shown to modulate cardiac metabolism and protect against heart failure, while *atATGL-KO* mice also increased body and fat mass (Parajuli et al., 2019). Altered glucose, lipid metabolism, and inflammation are also hallmark features of adipose tissue during cachexia (Rohm et al., 2019; Schmidt et al., 2018). Interestingly, ATGL or HSL knockout mice were protected against the loss of weight, fat, and muscle mass associated with LLC and B16 melanoma (B16) to varying degrees (Das et al., 2011). However, ATGLi did not inhibit human ATGL (Schweiger et al., 2017) and thus could not be an effective drug for cancer cachexia patients. Therefore, in this study, I screened

for novel lipolysis inhibitors that could be potentially used against weight and tissue loss during cancer cachexia.

Dr. Katarina Klepac previously screened for lipolysis regulators in the brown adipocytes using compounds from three libraries (more than 11000 compounds). She found over 200 of them to either increase or decrease basal lipolysis in the brown adipocytes. Since lipolysis is increased in the adipose tissue of the cancer cachexia patients as well as in mouse models (Dahlman et al., 2010), we have pre-selected the compounds that inhibited lipolysis in the previous screen. Fifty-one compounds were thus selected for the screening process (**Table 9**). These small molecule compounds have diverse functions and target enzymes involved in various metabolic pathways. Some of the pathways were shown to be affected during cachexia, while the mechanism of other compounds needs to be studied extensively in the context of cancer cachexia if proven effective. From the screening using three different adipocyte models and the selection criteria of inhibiting lipolysis in at least two models, nine compounds were selected for further validation.

YC-1, an activator for the guanylyl cyclase, was a hit compound that inhibited lipolysis in all three adipocyte models used and had an IC_{50} value of about 3 μ M in 3T3-L1 adipocytes treated with C26 TCCM (**Figure 11 & Figure 13**). In addition to promoting adipogenesis in the 3T3-L1 preadipocytes, YC-1 was previously shown to inhibit TNF- α and C26 TCCM-induced lipolysis in mature adipocytes. Interestingly, YC-1, by inhibiting lipolysis *in vivo*, rescued the C26 tumor-induced weight loss (Chung et al., 2011). YC-1 brought out this beneficial effect against weight loss by modulating the AKT, ERK, and PPAR- γ signaling. Finding YC-1 as a hit compound in our tumor-induced lipolysis assay-based screening validated our screening technique and our hypothesis that inhibiting lipolysis could be beneficial against weight loss during cancer cachexia. Several kinase inhibitors were found in this screening that inhibited C26 TCCM-induced lipolysis, and I also found compounds such as DPI and OLDA that target NOX and TRPV-1, respectively. BioF, a synthetic compound, consistently inhibited lipolysis in all three models tested. The IC_{50} value for BioF was 1 μ M in 3T3-L1 adipocytes treated with C26 TCCM, less than that of the ATGLi (**Figure 13**). Thus the applied screening identified lipolysis inhibitors that are more potent than ATGLi, a known inhibitor of ATGL and lipolysis.

Catecholamines are neurotransmitters that play a critical role in regulating lipolysis in the adipose tissue by acting on the β -adrenergic receptors (β -ARs) (Collins, 2012). In humans, insulin, catecholamines, and natriuretic peptides (paracrine hormone) regulate lipolysis. Particularly, β -ARs signaling increases the intracellular accumulation of cAMP, which activates PKA and furthers the lipolytic pathway (Arner & Langin, 2014). Circulating catecholamines levels were increased, while insulin that inhibit lipolysis was decreased in cancer cachexia patients and animal models of cancer cachexia (Asp et al., 2010; Bastos et al., 2018; Xie et al., 2022). Xie and colleagues recently demonstrated that the levels of catecholamines were remarkably increased in the adipose tissue of the cachexia-inducing tumor-bearing mice. In contrast, the levels were not increased in the serum (Xie et al., 2022). I anticipated that cAMP accumulation in the adipocytes would be increased upon C26 TCCM treatment. However, in this study, C26 TCCM treatment on the mature 3T3-L1 adipocytes did not elicit induction of intracellular cAMP levels, while the β -AR agonist forskolin did (**Figure 14**). This implies that factors secreted by the cachexia-inducing C26 tumor cells induce lipolysis through cAMP-independent mechanisms. It was shown by previous research that the

adipose tissue of cancer cachexia patients is more prone to catecholamines and natriuretic peptides-induced lipolysis and that the expression of ATGL and HSL are increased (Agustsson et al., 2007). It would be interesting to test the involvement of other upstream regulators of ATGL and HSL during cachexia.

Although it was shown that the lipogenic pathway is activated in the WAT of the cachexia-inducing tumor-bearing mice (Mulligan & Tisdale, 1991; Rohm et al., 2016), in human cancer patients, no change in the lipogenesis but increased lipolysis was observed (Rydén et al., 2008). Interestingly, in animal models of cachexia, fatty acid uptake and utilization were increased in the kidney, BAT, and liver (López-Soriano et al., 1996; Mulligan & Tisdale, 1991; Tsoli et al., 2014). No significant differences were observed when fatty acid uptake was assessed in the white adipocytes upon C26 TCCM treatment (**Figure 15**). Possibly, the 3T3-L1 adipocytes system used for this assay was not the optimal system to check the alteration in fatty acid uptake, or the colorimetric assay was not as sensitive as the biochemical methods described in 3T3-L1 adipocytes (Lobo et al., 2007). As stated before, compelling studies show that lipogenesis is increased along with lipolysis during cachexia, which might lead to energy-demanding futile substrate cycling (Rohm et al., 2019). Research from our lab showed that this process is mediated through impaired AMPK signaling during cachexia (Rohm et al., 2016). The assay performed here only assessed the fatty acid uptake into the cells, which will be reesterified and incorporated into lipid droplets. DNL is not assessed, so it would be interesting to check if the DNL pathway is affected upon C26 TCCM treatment. However, this was beyond the scope of the present work focusing on identifying antilipolytic compounds.

One of the critical regulators of energy metabolism and mitochondrial function, PGC-1 α , is significantly modulated in various disease conditions such as T2D, neurodegeneration, heart failure, kidney dysfunction, and cancer (Bost & Kaminski, 2019; Sweeney & Song, 2016; H. Wu et al., 2016). Increasingly, the role of PGC-1 α and disturbed mitochondrial function is described in cancer cachexia (Beltrà et al., 2021). PGC-1 α is reduced in various metabolic tissues during cachexia (Baltgalvis et al., 2008; White et al., 2012), and PGC-1 α overexpression protects against muscle atrophy (Sandri et al., 2006). In muscles, mitochondria DNA content and the mitochondria dynamics and function regulators are impaired during cachexia (Baltgalvis et al., 2008; van der Ende et al., 2018). In the liver, the mitochondrial function is dysregulated during cachexia (Halle et al., 2019). Although C26 tumor-bearing mice had increased mitochondria function in WAT, it was shown that C26 TCCM treatment on mature adipocytes impaired basal and maximal respiration (Halle et al., 2019; Rohm et al., 2016). When I assessed the mitochondrial function upon C26 TCCM treatment of the 3T3-L1 adipocytes, mitochondrial respiration or its maximal capacity was not altered (**Figure 16**). However, differentiation of the adipocytes in the Seahorse assay plate was difficult as the mature adipocytes tended to detach from the plates during the treatment and incubation with assay medium/buffer. Even though there was no effect upon C26 TCCM treatment, treatment with compounds such as DPI, olomoucine, orlistat, GF-109203X, and OLDA reduced basal and maximal respiration. Given the increased mitochondrial respiration observed by Halle and colleagues in the cachectic WAT, using these compounds would be beneficial in counteracting cachexia conditions (Halle et al., 2019).

Therapeutics developed against cancer cachexia focus on improving appetite or interfering with the altered metabolism in response to a cachexia-inducing tumor (Argilés et al., 2017). Taking into account the increasingly recognized important role of adipose tissue wasting in cachexia, I screened to identify

novel lipolysis inhibitors, the latter of which is elevated during cachexia. However, in the context of primary malignant disease, it was relevant to assess whether these compounds could affect tumor cell proliferation and growth. Since I observed a complete loss of mitochondrial activity upon DPI treatment, I first examined the cytotoxicity of the compounds in mature adipocytes. Although cytotoxicity is increased upon DPI treatment, the percent loss of cells was less than the percent inhibition of lipolysis, and the cytotoxic effect does not entirely represent the antilipolytic effect of the compound. Apart from their antilipolytic properties, compounds like DPI and OLDA reduced the growth of C26 cells *in vitro* (**Figure 17**). These findings suggest that the candidate compounds might exert anti-tumorigenic effects *in vivo*, which would be beneficial in the context of a cancer disease.

3.2. Inhibition of NOX using DPI in cancer cachexia

Reactive oxygen species (ROS) are highly reactive molecules that function as signaling molecules for effective cellular mechanisms. ROS is a collective term for different reactive molecules such as hydrogen peroxide (H_2O_2), ozone (O_3), superoxide anion radical (O_2^-), and Hydroxyl radical ($\cdot\text{OH}$), among others (Sies & Jones, 2020). Given their reactive property, ROS homeostasis is tightly regulated by various proteins, antioxidants, and reduction-oxidation (redox) relays. The primary source of ROS is the OXPHOS and the protein family NADPH oxidases (NOX). NOX functions primarily in the generation of H_2O_2 and O_2^- , and increased expression of this family of proteins is observed in cancer initiation and progression (Block & Gorin, 2012). Particularly, NOX-2 levels are increased in the tumors of gastric patients, and patients with a high level of NOX-2 presented a poor 5-year survival rate (P. Wang et al., 2015). In cancer cachexia, oxidative stress plays an important role, and treatment with antioxidants that scavenges ROS was successful in ameliorating cachexia-induced muscle atrophy (Abrigo et al., 2018; Buck & Chojkier, 1996; Wijaya et al., 2021). Recently, Dasgupta and colleagues demonstrated that activation of SIRT-1 by inhibiting oxidative stress combatted muscle wasting *in vitro* and *in vivo* (Dasgupta et al., 2020; Zhang et al., 2017). They also showed that NOX-4 functions as a downstream regulator of SIRT-1, and genetic and pharmacological inhibition of NOX-4 also protects against cachexia-induced weight and tissue loss (Dasgupta et al., 2020).

Since DPI, a NOX inhibitor was a hit compound from the screening; I was interested in testing its effect in the mice model of cancer cachexia. DPI treatment and shRNA-mediated knockdown of *Nox-3* in the differentiated 3T3-L1 adipocytes inhibited basal, isoproterenol, and C26 TCCM-induced lipolysis (**Figure 18**). DPI effectively inhibited the C26 TCCM-induced with the IC_{50} value of $0.3 \mu\text{M}$ (**Figure 13**). Although DPI treatment had a cytotoxic effect on the differentiated adipocytes, the cytotoxic effects were markedly reduced at a lower concentration. Interestingly, DPI inhibited the C26 cell proliferation *in vitro* (**Figure 17**). In the wild-type mice, DPI did not affect the body weight or the weights of the metabolic tissues. Though DPI treatment tended to improve eWAT weight, the effect was small and insignificant (**Figure 19**). It was important to see that the repeated DPI treatment in a respective pilot experiment did not elicit obvious harmful toxicity in mice (**Figure 20**). Surprisingly, DPI treatment reduced the PDK-4 transcript levels in the iWAT and liver. In cultured myotubes, PDK-4 overexpression and treatment with a PDK-4 activator (WY-14643) induced atrophy. In line with this, shRNA-mediated knockdown rescued the myotube atrophy (Pin et al., 2019). DPI treatment reduces the expression of genes involved in lipolysis and lipogenesis (**Figure 21**). As discussed earlier, both pathways are increased during cancer cachexia (Mulligan & Tisdale, 1991;

Rohm et al., 2016). Overall, these data encouraged me to assess the effects of DPI treatment in the C26-induced cachexia mouse model.

Previously, in our lab, injection of 5×10^5 C26 cells into the flanks of the Balb/c mice induced a pronounced cachexia phenotype (data not shown). In the DPI treatment cachexia experiment, 5×10^5 C26 cells were insufficient to induce a significant body weight loss in the vehicle-treated tumor-bearing mice at the end of the experiment (28 days post C26 cells inoculation and other termination criteria, refer to page number 32). However, tumor-bearing mice had significantly reduced adipose tissue and muscle mass (**Figure 22**), displaying a precachectic condition. Tumor-bearing mice treated with DPI had a significant percent loss in weight and fat mass, suggesting that DPI treatment aggravated the cachexia development and had a bigger tumor (**Figure 22**). Several small molecule inhibitors of NOX were developed and used in cancer research. Some of these inhibitors also inhibited tumor cell growth and metastasis in mice models (Konaté et al., 2020). DPI inhibited the growth of C26 *in vitro* (**Figure 17**); however, 0.5 mg/kg/day of DPI in Balb/c increased the mass of the C26 tumor. Anorexia is often observed in cancer cachexia patients but not consistently in mouse models of cancer cachexia (Ezeoke & Morley, 2015). In this experiment using DPI, I observed an insignificant trend toward increased food intake in the tumor-bearing mice. However, I observed increased amounts of small pieces of food inside the cage of the animals developing a cachexia phenotype, which might be the reason for the observed result. The tumor-bearing mice did not develop complete cachexia phenotypes as there was no increase in the plasma NEFA, triglycerides, or LDL, which were increased in different cancer cachexia animal models and patients. The DPI treatment aggravated the cachexia development as NEFA, and LDL levels were significantly increased in the tumor-bearing mice treated with DPI but not in the vehicle-treated tumor-bearing mice (**Figure 23**). In a mice model of cachexia using MAC13 tumor cells, $O_2^{\cdot-}$ levels were notably increased in the skeletal muscle of the weight-losing cachexia mice. Counterintuitively, the levels of NOX-2 and their catabolic subunits were reduced (Sullivan-Gunn et al., 2011). This demonstrates the complex role and regulation of different members of the NOX family during cachexia. NADH oxidase assay performed on the iWAT and serum samples suggested that the applied dose was insufficient to inhibit the overall NOX activity (**Figure 24**). However, one of the downstream regulators of NOX activity, p-ERK-1/2 levels, was decreased in the DPI-treated mice. This implies that the DPI treatment was effective in eliciting the molecular changes, but this was insufficient to counteract the observed components of a cachexia phenotype. C26 tumor-bearing mice had reduced fat mass, which was reflected in the lower inhibitory p-HSL(Ser565) levels in iWAT (**Figure 24**). The loss in adipose tissue and molecular changes seems to precede the absolute weight and lean mass loss in this study.

Although DPI significantly inhibited basal and TCCM-induced adipocyte lipolysis *in vitro* (**Figure 11**), it was ineffective in ameliorating cachexia-induced weight and fat loss (**Figure 22**). As expected, central regulators of lipolysis were modulated in the tumor-bearing mice, and DPI treatment affects the ERK-1/2 phosphorylation (**Figure 24**). However, these molecular changes did not affect the altered levels of the plasma metabolites or the weight loss. Testing an increased dose of DPI or using a more specific NOX inhibitor will be required to further understand the role of NOX in cancer cachexia.

3.3. Testing endogenous fatty acid amide OLDA in cancer cachexia

Following up on the next hit compounds from the screening, I tested the effect of an endogenous fatty acid amide OLDA in wild-type and cachexia-inducing tumor-bearing mice. OLDA has been shown to bind to or function through various receptor signaling pathways such as CB1/CB2, TRPV-1, and GPR-119 (C. J. Chu et al., 2003; Z. L. Chu et al., 2010; De Luca et al., 2018; Sergeeva et al., 2017). Furthermore, interestingly, these pathways were implicated in one or other hallmark features of cachexia. As early as the 1980s, one of the foremost effective constituents of cannabis, delta-9-tetrahydrocannabinol (delta-9-THC), was used in cancer patients undergoing chemotherapy (Nelson et al., 1994). At a maximum dose of 15 mg/day, delta-9-THC improved weight gain significantly in advanced cancer patients (Gorter, 1999). Later, several other pieces of research also confirmed their ability to stimulate appetite (Dariš et al., 2019; Dejesus et al., 2007). Because of its proven effect, a synthetic form of delta-9-THC (dronabinol) was used to manage anorexia in weight loss AIDS and cancer patients (Badowski & Perez, 2016; Badowski & Yanful, 2018). TRPV-1 levels were shown to be modulated in cancer patients with varying results, so their role in cancer development is unknown (Bujak et al., 2019). However, because of its role in inflammation and calcium signaling (C. J. Chu et al., 2003), which is highly disrupted in cachexia patients and animal models (Judge et al., 2018), it was interesting to test TRPV-1 agonists in the context of cancer cachexia. OLDA is increasingly studied for its anti-inflammatory effects in endotoxemic and septic mice as well as against TNF- α (Joffre et al., 2022; Spicarova & Palecek, 2010). Additionally, OLDA targets GPR-119 and improves glucose homeostasis in wild-type mice (Z. L. Chu et al., 2010), and glucose metabolism is disrupted during cachexia development (Asp et al., 2010). These functional implications and the antilipolytic effects observed *in vitro* make OLDA a promising choice for *in vivo* testing against cancer cachexia.

Since limited literature was available about the applicability of repeated injections of OLDA in mice, I tested two different concentrations (1 and 5 mg/kg/day) to check if mice could tolerate it and that the compound did not induce obvious toxicity. Injection of OLDA at both concentrations for four days did not elicit an adverse effect (**Figure 25 & Figure 26**). 5 mg/kg/day of OLDA slightly improved glucose excursion in the wild-type mice (**Figure 25**). Chu and colleagues showed that a single dose of 100 mg/kg of OLDA by oral gavage before the ipGTT improved glucose tolerance in lean wildtype mice (Z. L. Chu et al., 2010), validating that 5 mg/kg/day of OLDA dosing was effective *in vivo*. OLDA treatment in the wild-type mice increased inhibitory p-HSL(Ser565) (**Figure 27**), suggesting that a higher dose of OLDA inhibits lipolysis in the adipose tissue. As mentioned earlier, HSL transcript and protein levels, as well as the p-HSL(Ser565) levels, were shown to be increased in the adipose tissue of cancer cachexia patients and animal models (Agustsson et al., 2007; Dahlman et al., 2010; Rohm et al., 2016). This further motivated us to test this compound in tumor-bearing mice.

Since 5×10^5 C26 cells did not wholly induce a cachexia phenotype in the previous cachexia experiment (**Figure 22**), for the cachexia experiment using OLDA, I injected the mice with 1×10^6 C26 cells. Indeed, C26-induced cachexia development was evident in the tumor-bearing mice as they lost significant weight and fat mass. The body weight loss was also reflected in muscle atrophy and fat wasting (**Figure 28**). Cardiac atrophy, often associated with cancer cachexia (Murphy, 2016), was not observed in the C26-Balb/c model in this study. Although TRPV-1 and their ligands, including capsaicin and OLDA, play a critical role in tumor initiation and progression (L. Li et al., 2021; L. V. Weber et al., 2016), OLDA treatment did

not affect the C26 tumor growth in the Balb/c mice (**Figure 28**). OLDA treatment affected the expression of critical enzymes involved in glucose and lipid metabolism (**Figure 30**); however, they did not exert any beneficial effect against the C26-induced cachexia, as evident from the percent change in weight and fat mass, muscle atrophy, and cachexia index. The animals show changes in the assessed plasma metabolite levels compared to the previous cachexia experiment. As a sign of cachexia development, lipolysis was increased, and metabolites such as NEFA, glycerol, and triglycerides in the plasma were significantly increased (**Figure 29**). OLDA significantly inhibited the C26 TCCM-induced lipolysis in both human and murine-derived adipocytes (**Figure 11**). In contrast, 5 mg/kg/day treatment with OLDA did not exert a similar antilipolytic effect observed *in vitro*. However, in the pilot experiment using non-tumor-bearing mice, OLDA treatment increased the expression of p-HSL(Ser565) (**Figure 27**). When the levels of the critical proteins involved in cachexia progression were assessed in the iWAT of the animal, FAS and p-ACC α were modulated in the tumor-bearing mice, and the OLDA treatment had no effect (**Figure 30**).

Thus, OLDA treatment that showed a good effect *in vitro* (**Figure 11**), as well as in the pilot experiment on the wild-type mice (**Figure 25**), did not exhibit a protective effect against the C26-induced cachexia *in vivo* (**Figure 28**). Importantly, OLDA did not affect food intake, suggesting that 5 mg/kg/day treatment of OLDA did not affect appetite regulation through CB1/CB2-related pathways. In various literature, OLDA was administered acutely, and the kinetics of the drug need to be understood thoroughly (Z. L. Chu et al., 2010; Konieczny et al., 2009; Przegaliński et al., 2006). Therefore, it would be essential to determine the pharmacokinetics of OLDA in more depth in order to reassess its potential efficacy in counteracting cachexia development.

3.4. Effect of novel BioF compound against cancer cachexia

The last hit compound from the initial screen, which was tested *in vivo*, was BioF, a novel compound synthesized by Charles River. BioF consistently inhibited lipolysis in all three screens performed in this study and in the previous screening in brown adipocytes performed by Dr. Katarina Klepac. Apart from the antilipolytic effect in adipocytes, BioF treatment also protected against the C26 TCCM-induced C2C12 myotube atrophy, suggesting that BioF could exert anti-cachectic functions in different cell types. Based on the chemical structure of BioF, it was predicted to act as a GLP-1 receptor ligand. Various GLP-1 receptor agonists are used to treat T2D and are proposed to be effective against obesity and its associated metabolic conditions (Drucker, 2022; Grandl et al., 2020; Quarta et al., 2022). Interestingly, exendin-4, a GLP-1 receptor agonist widely used for diabetes treatment, was shown to rescue dexamethasone-and nephrectomy-induced muscle atrophy (Hong et al., 2019).

Since not much information is available about this compound, I performed *in vivo* pilot experiments testing different dosages of the compound. In different experiments, I treated the mice with either 0.5, 1, 2 (1 + 1), and 5 mg/kg/day of BioF for four days, and at the end of the experiments, I did not observe induction in the toxicity markers (**Figure 33 & Figure 35**). Lower doses of BioF did not affect the body or tissue weight (**Figure 32**). Interestingly, 5 mg/kg/day of BioF increased the weight and lean mass gain without affecting the food intake (**Figure 34**). The determined plasma metabolites of the animal treated with BioF had no difference compared with the vehicle group (**Figure 33 & Figure 35**). As discussed earlier, AdipoQ is one of the crucial adipokines that play a critical role in lipid and glucose metabolism, and its expression is downregulated in various metabolic disease conditions (Fasshauer & Blüher, 2015). The

transcript levels of AdipoQ and other regulators, such as PDK-4 and PCK-1 α , increased upon a higher dose of BioF treatment in the adipose tissue (**Figure 36**). Thus, the treatment with BioF *in vivo* positively altered the expression of key lipid and glucose metabolism regulators. Therefore, I decided to test the effect of 5 mg/kg/day of BioF against cachexia.

Compounds used for treatment can affect the metabolism in various organs. BAT thermogenesis and browning of WAT have been proposed as important drivers of cancer cachexia (Kir et al., 2014; Kir & Spiegelman, 2016). In contrast, the mice lacking UCP-1, the central component of BAT thermogenesis, did not prevent cachexia development (Rohm et al., 2016).

BAT mass tended to increase in the non-tumor-bearing mice treated with DPI and BioF (**Figure 22 & Figure 37**). Targets of the candidate compound tested *in vivo* (NOX, TRPV-1, and GLP-1 receptor for DPI, OLDA, and BioF, respectively) were shown to play a critical role in enhancing BAT thermogenesis (Beiroa et al., 2014; Kawabata et al., 2009; Y. Li et al., 2012). Since BAT and its thermogenic function, and WAT browning are implicated in the development of cachexia (Kir et al., 2014; Kir & Spiegelman, 2016; Petruzzelli et al., 2014), I speculated that involvement of the BAT metabolism might mask the antilipolytic effect of the compounds against cancer cachexia. So, I tested the effect of BioF on the tumor-bearing mice held at a thermoneutral temperature, which eliminates BAT activation (Vegiopoulos et al., 2010). In the previous cachexia experiments, I treated the mice once the tumor was palpable. Therefore, it was interesting to check if starting the treatment earlier might be beneficial, as it has been done for other compounds such as YC-1 (Chung et al., 2011), which was also a hit on my screen. Although the increased cholesterol and LDL levels in the tumor-bearing mice were reduced upon BioF treatment, no protective effect of the compound was observed on weight loss and muscle and fat atrophy. When housed at the thermoneutral temperature, tumor-bearing mice displayed heart atrophy and lost significant lean mass, which was not observed in the other cachexia experiments in this study. Also, the weight loss progression was less steep than the mice held at sub-thermal conditions, giving a wider therapeutic window. Tumor growth is influenced by the holding temperature, where mice held at thermoneutral conditions had slower progression of tumor growth (Kokolus et al., 2013). It is difficult to compare the tumor weights from the two independent experiments; however, the tumor mass and the cachexia index seemed to be increased in the thermoneutral experiment. Therefore, it would be interesting to test the effect of holding temperature on cachexia progression.

BioF treatment inhibited C26 TCCM-induced adipocyte lipolysis and myotube atrophy *in vitro*. In the pilot experiment, BioF treatment showed a promising effect on weight gain in wild-type mice. However, it did not exhibit a protective effect against the C26-induced weight and tissue loss. Also, 5 mg/kg/day of BioF was proven ineffective in the thermoneutral condition. Additional experiments studying the temperature effect on tumor and cachexia development, pharmacokinetics of BioF, and finding its target will be essential to study the effect of BioF against cancer cachexia.

3.5. Main conclusions and outlook

In summary, this study described an effective screening strategy to identify novel antilipolytic compounds using different adipocyte models *in vitro*. The hit compounds identified in this study demonstrated robust and consistent antilipolytic effects against basal and C26 TCCM-induced lipolysis. DPI, olomoucine, and

BioF were more potent in inhibiting lipolysis and had an IC_{50} value less than that of known lipolysis inhibitor ATGLi. Apart from their antilipolytic properties, selected compounds such as DPI and OLDA inhibited C26 tumor cell proliferation *in vitro*.

Based on the literature review concerning known mechanisms of action and further *in vitro* analyses of the hit compounds from the screening, three compounds were selected for further assessment of their potential to counteract weight loss in a cancer cachexia mouse model based on the implantation of cachexia-inducing C26 cells. DPI, OLDA, and BioF were tested using different concentrations. In addition, the BioF compound was also tested at a thermoneutral temperature condition and applied an earlier treatment initiation. However, these compounds, at the tested conditions, did not provide a beneficial effect against weight loss, adipose tissue wasting, and muscle atrophy. Interestingly, the compounds altered the levels of important proteins involved in lipolysis and the plasma metabolite levels of cachexia markers. Therefore, further investigations of the hit compounds are required to assess their potential to exert antilipolytic effects, prevent adipose tissue loss *in vivo*, and provide proof-of-concept for adipose tissue-targeted pharmacotherapy against cancer cachexia.

In this line of approach, we will assess the pharmacokinetics and pharmacodynamics of the compounds in more depth. Knowledge about the absorption, distribution, metabolism, and excretion of the compounds in the system will help us to optimize the administration route and drug doses. Eventually, this will help us understand the compound's mechanism of action and possibly find novel targets involved in cachexia progression.

As discussed earlier (*Animal models used for cancer cachexia research*), researchers have developed various cachexia animal models. Every model has their advantages over other models and has limitations. One of the critical limitations of the C26 cachexia model tested in this study is that the tumor-bearing mice do not develop anorexia and have a relatively narrow therapeutic window. Therefore, it would be interesting to test the compounds in other cachexia models, for example, in LLC and KPP mice models, as well as in aged mice, which better reflect cachexia development in humans. Although not discussed extensively in this study, metabolic disorders such as obesity, although representing the conversed state with respect to energy homeostasis, share common mechanisms that are altered during cachexia, including systemic inflammation and induced adipose tissue lipolysis. Consequently, testing these candidate compounds in mouse models of obesity and diabetes might represent an interesting approach to improve the tissue-specific and systemic metabolic state.

Researchers have postulated that multimodal therapies are required to treat cachexia-induced metabolic alterations and weight loss efficiently. This primarily refers to the combination of nutritional support, adapted exercise, and novel pharmacotherapies. However, combinatorial approaches might also be required for the pharmacotherapy component of novel anti-cachexia treatment approaches. Although co-treatment of DPI and OLDA did not synergize their antilipolytic effects *in vitro* (data not shown), it would be interesting to check if the combinatorial treatment of the hit compounds with regulators of lipogenesis or muscle atrophy will protect against the cachexia-induced weight loss. Finally, using human or patient-derived adipocytes and validating the effects of the compounds and combinatorial treatment will further substantiate the need for targeting multiple mechanisms to counteract the metabolic dysregulation caused by the cachexia-inducing tumor.

4. METHODS

4.1. Molecular Biology

4.1.1. Preparation of Luria broth medium and agar plates

Luria broth (LB) medium was prepared by dissolving 5 g of yeast extract, 10 g of peptone, and 10 g of NaCl into sterile water and made up to 1 L. Using a magnetic stirrer, the components were stirred, and the pH was adjusted to 7.0 using 1 N NaOH or 1 N HCl. On a liquid cycle, the medium was autoclaved for 20 minutes at 15 pounds per square inch (psi) (1.05 kg/cm²). Sterilized LB medium was stored at room temperature until used.

For LB agar, just before autoclaving the LB medium, 15 g/L of Bacto agar was added and mixed. On a liquid cycle, the medium was autoclaved for 20 minutes at 15 psi (1.05 kg/cm²). Autoclaved LB agar was allowed to cool to ~50 °C before adding appropriate antibiotics and pouring it into plates. Approximately 30 mL LB agar was poured per 10 cm plate and allowed to harden. Once the medium had completely hardened, plates were stored in an inverted position at 4°C until used.

4.1.2. Revival of *E. coli* glycerol stock

MISSION® shRNA bacterial clones containing shRNA plasmid targeted against mouse NOX3, NOX4, or non-mammalian control were obtained from Sigma-Aldrich as glycerol stocks. Before reviving the glycerol stocks, LB agar plates with appropriate antibiotics were brought to room temperature. Using a sterile pipette tip, frozen bacteria were scraped off from the top and streaked onto the prepared LB agar plates. Streaked plates were incubated in an inverted position at 37 °C overnight. Sterility was maintained by wiping the lab bench with 70% ethanol before and after working, and bacteria handling was handled near a Bunsen burner.

4.1.3. Transformation of *E. coli*

Lentivirus packaging and envelop vectors (pRSV-Rev, pCMV-Eco, and pCgpV) from the ViraSafe™ Lentiviral Packaging System, Ecotropic (Cell Biolabs, Inc.) were already available in the lab. Packaging and envelop vectors were transformed into *E. coli* by heat shock transformation method. 50 µL of chemically competent *E. coli* were thawed on ice. 0.1-1 µg of plasmid DNA was added to the cells, mixed with a gentle flick, and incubated for 30 minutes on ice. A heat shock was applied for 30 seconds at 42 °C. 250 µL of SOC medium was added to each vial and were incubated for 1 hour at 37 °C under vigorous shaking (~300 rpm). The medium was plated onto LB agar plates containing the appropriate antibiotic.

4.1.4. Bacterial liquid cultures

Single colonies obtained from the plating or streaking were inoculated into an LB medium supplemented with the appropriate antibiotic. Single colonies were inoculated into a 2 mL medium for extracting plasmid DNA for sequencing and a 50 to 200 mL medium for extracting transfection-grade plasmid DNA. The cultures were incubated overnight at 37 °C under vigorous shaking (~160 rpm).

4.1.5. Determination of DNA and RNA concentration

DNA and RNA concentrations were measured using NanoDrop 2000 spectrophotometer. Before the sample measurements, the sample type was selected as dsDNA or RNA. Blank measurement was done using the elution solution used, and 1 μL of the blank or the samples were used for each measurement. The absorbance ratio from 260 nm to 280 nm indicated protein contamination.

4.1.6. DNA sequencing

DNA sequencing was performed using the LightRun Tube service (Eurofins Genomics). 5 μL of the purified plasmid DNA (50-100 ng/ μL) was mixed with 5 μL of sequencing primer (pmol/ μL). The sequencing sample was labeled with a prepaid barcode and submitted. The sequencing results were downloaded from <https://eurofinsgenomics.eu/> by logging into the account. The sequencing results were then visualized and analyzed using the cloud-based tool <https://benchling.com/>.

4.1.7. RNA extraction

From mammalian cells

Cells were washed with ice-cold PBS, and 1 mL of Trizol was added under the laminar fume hood. Handling of samples was performed under the laminar fume hood. Cells were harvested into RNase-free 1.5 mL centrifugation tubes and incubated for 5 minutes at room temperature. 200 μL of chloroform was added and vortexed vigorously for 30 seconds to mix the phases. The mixture was incubated for 15 minutes at room temperature and centrifuged for 10 minutes at 10000 *rcf* at 4 °C. The aqueous upper phase was transferred to RNase-free 1.5 mL centrifugation tubes and placed on ice. 0.6 volume (of the upper phase) of 100% ethanol was added and vortexed briefly. The mixture was loaded into an EconoSpin® all-in-one silica membrane mini spin column (Epoch Life Science, Inc.) and centrifuged for 30 seconds at 13000 *rcf*. The flow through was discarded, and the column was washed three times with 500 μL RPE buffer (Qiagen) and centrifuged for 30 seconds at 13000 *rcf*. After the last RPE buffer wash, the column was centrifuged for 2 minutes at 13000 *rcf* to remove residual buffer. The column was then transferred to a new RNase-free 1.5 mL centrifugation tube. The tube was incubated with the lid open for 10 minutes at room temperature. 50 μL of RNase-free water was added to the center of the column, incubated for 2 minutes, and centrifuged for 2 minutes at 9000 *rcf*. Eluted RNA was quantified, quality checked and stored at -80 °C until used.

From tissues

On dry ice, one clean stainless steel bead was placed into every 2 mL centrifugation tube. Approximately 5 mg of frozen tissue was sliced, transferred to the tubes with beads, and placed on dry ice. 1 mL of Trizol was added under the laminar fume hood, and the tissue was lysed using the TissueLyser II (Qiagen) for 60 sec at a frequency of 30 Hz twice. Handling of samples was performed under the laminar fume hood. Lysed tissue in Trizol was incubated for 5 minutes at room temperature. Steps from adding chloroform were performed as previously described (*From mammalian cells*) until RNA elution. 100 μL of RNase-free water was added to the center of the column, incubated for 2 minutes, and centrifuged for 2 minutes at 9000 *rcf*. Eluted RNA was quantified, quality checked and stored at -80 °C until used.

4.1.8. cDNA synthesis

cDNA was synthesized from the extracted RNA using the Quantitect Reverse Transcription kit (Qiagen). 500-1000 ng of RNA was prepared in PCR tubes and made up to 9 μ L using RNase-free water. Non-template control (NTC) was also included, in which RNase-free water was used instead of the RNA sample. 1.5 μ L of gDNA wipeout buffer was added to each sample and incubated for 2 minutes at 42 °C. To each sample, 0.75 μ L of quantiscript reverse transcriptase, 3 μ L of quantiscript RT buffer, and 0.75 μ L of RT primer mix were added. The master mix was prepared to avoid the technical error of pipetting a small volume. PCR tubes were gently flicked and then spun down briefly. Samples were incubated for 30 minutes at 42 °C, followed by 3 minutes at 95 °C. 100 μ L of RNase-free water was added to each sample and stored at -20 °C until used.

4.1.9. Quantitative PCR

For every primer pair and gene quantified, an individual master mix was prepared. The master mix contained 4 μ L of SYBR™ Green PCR Master Mix, 0.5 μ L of RNase-free water, 0.25 μ L of 5 μ M forward primer, and 0.25 μ L of 5 μ M reverse primer for every individual reaction. 5.5 μ L of the prepared master mix was applied to the appropriate wells. 2.5 μ L of diluted cDNA was added to the respective well in MicroAmp™ Optical 384-Well Reaction Plate (Applied Biosystems™). 384-well plate was spun briefly, and quantitative PCR was performed using Quantstudio 6/7 Flex (Thermo Fisher Scientific). Technical duplicates of all samples were performed.

4.2. Cell Biology

4.2.1. Cell culture conditions and media

All experiments with eukaryotic cells were performed under sterile conditions. Cells were cultured at 37 °C, 5% CO₂, and 95% humidity. All media and additives were warmed to 37 °C before use. A list of the media used for cell culture experiments is shown in **Table 2**.

Table 2: Cell culture medium and their composition

Name	Medium
Growth medium	DMEM, high glucose, GlutaMAX™ Supplement, pyruvate + 10% FBS + 1% P/S
3T3-L1 differentiation medium 1 (3T3-L1 DM1)	Growth medium + 1 μ g/ml insulin + 0.5 mM IBMX + 0.25 μ M dexamethasone + 1/1000 volume ABP stock solution
3T3-L1 differentiation medium 2 (3T3-L1 DM2)	Growth medium + 1 μ g/ml insulin + 1/1000 volume ABP stock solution
iWA digestion buffer	DMEM, high glucose, GlutaMAX™ Supplement, pyruvate + 1.5 mg/ml type II collagenase + 0.5% BSA
iWA induction medium	DMEM, high glucose, GlutaMAX™ Supplement, pyruvate + 5% FBS + 1% P/S + 0.172 mM insulin + 0.5 mM IBMX + 0.25 μ M dexamethasone + 1 nM triiodothyronine (T3) + 1/1000 ABP stock solution
iWA maintenance medium	DMEM, high glucose, GlutaMAX™ Supplement, pyruvate + 5% FBS + 1% P/S + 0.172 mM insulin + 1 nM triiodothyronine (T3) + 1/1000 ABP stock solution

hMSC differentiation medium 1 (hMSC DM1)	DMEM, high glucose, GlutaMAX™ Supplement, pyruvate + 5% FBS + 1% P/S + 2 μM insulin + 0.5 mM IBMX + 0.1 μM dexamethasone + 1 μM rosiglitazone + 1 μM U0126
hMSC differentiation medium 2 (hMSC DM2)	DMEM, high glucose, GlutaMAX™ Supplement, pyruvate + 5% FBS + 1% P/S + 2 μM insulin + 0.5 mM IBMX + 0.1 μM dexamethasone + 1 μM U0126
C2C12 DM	DMEM, high glucose, GlutaMAX™ Supplement, pyruvate + 2% HS + 1% P/S + 1 μM insulin
HEK medium	Growth medium + 1% NEAA
HEK-HEPES medium	Growth medium + 1% NEAA + 10 mM HEPES
Lenti medium	DMEM, high glucose, GlutaMAX™ Supplement, pyruvate + 25 mM HEPES

4.2.2. Freezing and thawing of cells

For freezing, cells were washed with 1X PBS and trypsinized for 3 minutes. Detached cells were collected in a fresh growth medium and made up to 10 mL. The cells were counted in a Countess™ cell counting chamber slide (Invitrogen™). The cells were pelleted by centrifugation for 10 minutes at 1000 *rcf* and resuspended in an appropriate volume of the freezing medium. The freezing medium and the frozen cell number for each cell line are represented in **Table 3**. The cells were then aliquoted into 1 mL each in 2 mL CryoPure tubes (Sarstedt, Inc.). The tubes were placed into Mr. Frosty™ Freezing Container (Thermo Scientific™) and placed into a -80 °C freezer. The next day, the tubes were moved to a liquid nitrogen tank (for an extended storage period) or to a -80 °C freezer (for a shorter storage period).

For thawing, tubes were placed at 37 °C. The cells were seeded onto 15 cm cell culture plates containing a 20 mL growth medium. 24 hours after seeding, cells were refreshed with a fresh growth medium.

Table 3: The freezing medium and the frozen cell number for each cell line

Cell line	Freezing medium	Cell concentration
3T3-L1 fibroblasts	Growth medium + 5% DMSO	5 x 10 ⁵ cells per mL
hMSC-Tert	Growth medium + 10% DMSO	5 x 10 ⁵ cells per mL
C2C12 myotubes	Growth medium + 5% DMSO	1 x 10 ⁶ cells per mL
C26	Growth medium + 10% DMSO	5 x 10 ⁶ cells per mL
MC38	Growth medium + 10% DMSO	5 x 10 ⁶ cells per mL
HCT116	Growth medium + 10% DMSO	5 x 10 ⁶ cells per mL
HT29	Growth medium + 10% DMSO	5 x 10 ⁶ cells per mL
LLC	Growth medium + 10% DMSO	5 x 10 ⁶ cells per mL
HEK293LTV	Growth medium + 10% DMSO	1 x 10 ⁶ cells per mL

4.2.3. Culturing of cells

Culturing of 3T3-L1 fibroblasts

5 x 10⁵ 3T3-L1 fibroblasts were cultured on 15 cm tissue culture plates in a 20 mL growth medium. 3T3-L1 cells were maintained at less than 70% confluency and low passage (less than passage 15) to avoid reduced differentiation potential.

For subculturing, the cells were washed with 1X PBS and trypsinized for 3 minutes. Detached cells were collected in a fresh growth medium and made up to 10 mL. The cells were counted in a Countess™ cell counting chamber slide (Invitrogen™). The cells were pelleted by centrifugation for 10 minutes at 1000 *rcf* and resuspended in a 1 mL growth medium. 0.5×10^6 cells were seeded onto a 15 cm tissue culture dish containing a 20 mL medium. Cells were subcultured every 3-4 days.

Culturing of hMSC-Tert

5×10^5 hMSC-Tert cells were cultured on 15 cm tissue culture plates in a 20 mL growth medium. hMSC-Tert cells were maintained at less than 70% confluency to avoid reduced differentiation potential. Cells were subcultured as described for 3T3-L1 cells.

Culturing of mouse and human cancer cells

5×10^6 mouse and human cancer cell lines were cultured on 15 cm tissue culture plates in a 20 mL growth medium. Cells were subcultured as described for 3T3-L1 cells. Cells were maintained at a confluency of not more than 90%.

Culturing of C2C12 myoblasts

1×10^6 C2C12 cells were cultured on 15 cm tissue culture plates in a 20 mL growth medium. C2C12 cells were maintained at less than 70% confluency and low passage (less than passage 15) to avoid reduced differentiation potential. Cells were subcultured as described for 3T3-L1 cells.

Culturing of HEK293LTV cells

1×10^6 HEK293LTV cells were cultured on 15 cm tissue culture plates in a 20 mL growth medium. Cells were subcultured as described for 3T3-L1 cells. Cells were maintained at a confluency of not more than 90%.

4.2.4. Isolation of preadipocytes from adipose tissue

Preadipocytes were isolated from the stromal vascular fraction (SVF) of inguinal white adipose tissue (iWAT) depots of male C57BL6/N mice aged approximately seven weeks. Mice were sacrificed by cervical dislocation and sterilized with 70% ethanol. iWAT depots were dissected, and lymph nodes were removed. Dissected iWAT depots were washed with ice-cold 1X PBS, transferred to a 5 mL centrifugation tube, and chopped into small pieces using scissors. ~1 g of tissue was transferred into a 15 mL falcon tube containing a 7 mL filter sterilized iWA digestion buffer. iWAT was digested for 1 hour at 37 °C and 180 rpm with frequent vortex. Once digested, 7 ml growth medium was added to stop the collagenase activity and incubated for 10 minutes at room temperature. The SVF was harvested by centrifugation at 1000 rpm, for 10 minutes, at room temperature. The cell pellet was resuspended in a growth medium, filtered through a 100 μ m nylon filter, and cells were seeded to 96 well plates. The next day, the cells were washed with 1X PBS and refreshed with a fresh growth medium. Cells were washed every second day with a growth medium until they reached confluency.

4.2.5. Differentiation of cells into adipocytes and myotubes

Differentiation of 3T3-L1 fibroblasts into adipocytes

3T3-L1 fibroblasts for differentiation were seeded in desired plates at a cell density of 3×10^4 cells/cm². Two days after confluency (denoted as D0), preadipocytes were differentiated into mature white adipocytes by maintaining the cells in the 3T3-L1 DM1 for four days, followed by keeping them in the 3T3-L1 DM2 for two days. Differentiated 3T3-L1 adipocytes were then maintained in the growth medium, and experiments were performed 8 to 12 days after the initiation of differentiation.

Differentiation of primary preadipocytes into adipocytes

Preadipocytes were cultured until they reached confluency. Two days after confluency (denoted as D0), preadipocytes were differentiated into mature white adipocytes by maintaining the cells in the iWA induction medium for four days, followed by keeping them in the iWA maintenance medium for two days. Differentiated primary adipocytes were then maintained in a growth medium, and experiments were performed 8 to 12 days after the initiation of differentiation.

Differentiation of hMSC-Tert into adipocytes

hMSC-Tert cells for differentiation were seeded in desired plates at a cell density of 3×10^4 cells/cm². On the day of confluency (denoted as D0), cells were differentiated into mature white adipocytes by maintaining the cells in the hMSC DM1 for 12 days, followed by keeping the cells in the hMSC DM2 for seven days. The cells were refreshed with differentiation medium three times a week. Differentiated hMSC-Tert adipocytes were then maintained in a growth medium, and experiments were performed 21 to 24 days after initiation of differentiation.

Differentiation of C2C12 myoblasts into myotubes

C2C12 for differentiation were seeded in desired plates at a cell density of 3×10^4 cells/cm². Two days after seeding (denoted as D0), myoblasts were differentiated into mature myotubes by maintaining the cells in the C2C12 DM for eight days. The cells were refreshed with differentiation medium three times a week. Differentiated C2C12 myotubes were then maintained in the growth medium, and experiments were performed 10 to 12 days after the initiation of differentiation.

4.2.6. Preparation of tumor cell conditioned medium (TCCM)

5×10^6 cancer cells were seeded on 15 cm tissue culture plates in a 20 mL growth medium. 24 hours after seeding, cells were washed with 1X PBS and refreshed with a growth medium. 48 hours post-seeding, the culture medium was collected and filtered through a 0.45 μ m surfactant-free cellulose acetate (SFCA) membrane filter (Corning®). Freshly prepared conditioned medium was used for assays performed on the same day or aliquoted and stored at -80°C.

4.2.7. Treatment of adipocytes and myotubes

Differentiated adipocytes and myotubes were maintained in a growth medium for at least 24 hours before the treatment. Differentiated adipocytes were treated with TCCM and 10 μ M of compounds (unless mentioned) for 24 hours, and myotubes were treated for 48 hours.

4.2.8. Oil Red O staining and quantification

3 mg/mL Oil Red O (ORO) solution was prepared freshly from 5 mg/mL stock solution using sterile water and filtered two times through a paper filter. Cells were washed with PBS and fixed with 4% ROTI®Histofix (Carl Roth GmbH & Co. KG) for 1 hour at room temperature. The fixation solution was removed and washed three times with PBS. The prepared ORO solution was added and incubated for 1 hour at room temperature. After staining, the cells were washed with distilled water and imaged using ECLIPSE Ts2 inverted microscope (Nikon Instruments Inc.).

For quantification of the staining, cells were washed three times for 5 minutes with 60% isopropanol with gentle rocking. ORO stain was extracted by adding 100% isopropanol for 5 minutes with gentle rocking. Absorbance was measured at 492 nm using the Varioskan™ LUX multimode microplate reader (Thermo Scientific™), and 100% isopropanol was used as blank control.

4.2.9. Lipolysis assay

For the lipolysis assay, adipocytes were treated with appropriate treatment conditions, as mentioned before (*Treatment of adipocytes and myotubes*). NEFA and glycerol were measured using commercial kits from the cell culture supernatants (FUJIFILM Wako Chemicals and Sigma-Aldrich).

NEFA measurement

R1 and R2 reagents were prepared by mixing one bottle of Color A and Solvent A (R1 reagent) and Color B and Solvent B (R2 reagent). Prepared R1 and R2 reagents were stored at 4 °C and used within one month. 5 – 10 µL of the supernatants, diluted standards, and blank were added to the 96-well plate in duplicates. 100 µL of the R1 reagent was added, and the plate was incubated for 5 minutes at 37 °C. 50 µL of the R2 reagent was added, and the plate was incubated for 5 minutes at 37 °C. Absorbance was read at 546 nm using the Varioskan™ LUX multimode microplate reader (Thermo Scientific™). NEFA concentration of the samples was calculated using the known concentration of the standards.

Glycerol measurement

Free glycerol reagent was reconstituted by adding 40 mL of distilled water, stored at 4 °C, and used within two months. 5 – 10 µL of the supernatants, diluted standards, and blank were added to the 96-well plate in duplicates. 100 µL of the reconstituted free glycerol reagent was added, and the plate was incubated for 5 minutes at 37 °C. Absorbance was read at 540 nm using the Varioskan™ LUX multimode microplate reader (Thermo Scientific™). The free glycerol concentration of the samples was extrapolated from the known concentration of the standards.

4.2.10. cAMP assay

cAMP levels were measured following the protocol of the cAMP Gs dynamic kit (Cisbio Bioassays SAS). Reagents for the assays were prepared and stored according to the manufacturer's protocol. Differentiated 3T3-L1 adipocytes were trypsinized and reseeded at different cell densities (5000, 2500, 1250, and 625 cells per well of 96-well white-walled, clear bottom plate (Corning™)). The assay was performed using negative controls without reagents addition, non-treated controls, and cells treated with appropriate conditions. Likewise, provided cAMP standard was used after dilutions. Homogeneous Time

Resolved Fluorescence (HTRF) signals were measured at 620 and 665 nm at the end of the assay using Varioskan™ LUX multimode microplate reader (Thermo Scientific™). The HTRF ratio was determined by using the formula below.

$$HTRF \text{ ratio} = \frac{\text{Signal at 665 nm}}{\text{Signal at 620 nm}} \times 104$$

A standard graph was plotted between the HTRF ratio and the cAMP standards concentration. Unknown samples' cAMP concentrations were extrapolated from it.

4.2.11. Fatty acid uptake assay

Fatty acid uptake was measured following the protocol of the Fatty Acid Uptake Assay Kit (Abcam). Reagents for the assays were prepared and stored according to the manufacturer's protocol. 3T3-L1 preadipocytes were seeded and differentiated on a 96-well black-walled, clear bottom plate (Corning™). Differentiated adipocytes were starved using the serum-free, phenol-red-free medium for 1 hour at 37 °C. After serum starvation, adipocytes were treated with the test compounds and incubated for 30 minutes at 37 °C, 5% CO₂, and 95% humidity. The quenched uptake reaction mix was prepared freshly and added to the cells. Fluorescence (Ex/Em = 488/523 nm) was measured using Varioskan™ LUX multimode microplate reader (Thermo Scientific™) in kinetic mode for 60 minutes at 37 °C using the 'bottom read' function. Percentage activity was calculated using the formula below.

$$\% \text{ activity} = \frac{RFU_{\text{Compound}} - RFU_{\text{Blank}}}{RFU_{\text{Vehicle}} - RFU_{\text{Blank}}} \times 100$$

4.2.12. Seahorse Mito Stress assay

Differentiation and treatment of 3T3-L1 in XF96 microplate

3T3-L1 fibroblasts were seeded onto an XF96 microplate (Agilent Technologies) at a cell density of 3 X 10⁴ cells/cm² in 100 µL of growth medium. Only growth medium was added to the four edges (A1, A12, H1, and H12) of the plates, and they served as reference wells. Cells were differentiated into adipocytes, as mentioned before (*Differentiation of 3T3-L1 fibroblasts into adipocytes*).

Before the day of the assay

The day before the assay, differentiated adipocytes were treated with appropriate conditions for 24 hours. XF96 Analyzer, its computer, and the prep station were switched on at least 12h before the assay. About 12 hours before the end of the treatment period, the XF Sensor cartridge was hydrated by adding 200 µL of sterile water to each well of the XF Utility plate. The XF Sensor cartridge was placed on top of the XF Utility Plate and incubated at 37 °C without CO₂. An assay protocol was created using the parameters shown in **Table 4** in the Seahorse Wave Desktop Software.

Table 4: Assay protocol for the Seahorse Mito Stress assay

Command	Time	Measurements
Calibrate Probes	25 minutes	
Equilibrate	12 minutes	
Baseline measurement - Loop Start (3X)		1-3
Mix	4 minutes	

Measure	3 minutes	
Inject Port A		
Loop Start (3X)		4-6
Mix	4 minutes	
Measure	3 minutes	
Loop End		
Inject Port B		
Loop Start (3X)		7-9
Mix	4 minutes	
Measure	3 minutes	
Loop End		
Inject Port C		
Loop Start (3X)		10-12
Mix	4 minutes	
Measure	3 minutes	
Loop End		
Inject Port D		
Loop Start (3X)		13-15
Mix	4 minutes	
Measure	3 minutes	
Loop End		

On the day of the assay

The assay medium was prepared, as shown in **Table 5**. The pH was adjusted to 7.2 – 7.4 and sterile-filtered. After 24 hours of treatment, 3T3-L1 adipocytes were carefully washed twice with the assay medium. 180 μ L of assay medium was added to each well of the plate. The assay plate was incubated at 37 °C without CO₂ for 1 hour before the assay. In the meantime, 10X concentrated assay compounds were prepared using the assay medium. They were loaded into the respective ports of the hydrated XF Sensor cartridge. The assay compounds, their concentration, and the volumes loaded are provided in the **Table 6**.

Table 5: Composition of the Seahorse Mito Stress assay medium

Component	Final concentration
Seahorse XF DMEM assay medium (pH 7.4)	
Pyruvate	2 mM
Glucose	2.5 mM
Glutamine	1 mM

Table 6: Volume of the assay compounds loaded into the ports of the XF Sensor cartridge

Port	Compound	Working conc.	Volume loaded	Conc. on cells
A	Isoproterenol	100 μ M	20 μ L	10 μ M
B	Oligomycin A	40 μ M	22 μ L	4 μ M

C	FCCP	7.5 μ M	25 μ L	750 nM
D	Antimycin A + Rotenone	5 μ M (each)	28 μ L	500 nM (each)

The compounds loaded XF Sensor cartridge was inserted into the XF96 extracellular flux analyzer, and the assay protocol was initiated. The analyzer calibrates the XF Sensor cartridge, and the XF Utility Plate is ejected. After 1 hour of incubation, the XF96 microplate containing the treated adipocytes was loaded into the analyzer. The output from the software was processed using Microsoft Excel and analyzed using the formula described. Graphs were prepared, and statistical analysis was performed using GraphPad Prism software.

Assay calculation formula

Non mitochondrial respiration rate = Minimum rate after rotenone & antimycin A injection

Basal respiration = Last rate before first injection – Non mitochondrial respiration rate

Maximal respiration = Max. rate after FCCP injection – Non mitochondrial respiration rate

Spare respiratory capacity = Maximal respiration – Basal respiration

4.2.13. Cytotoxicity assay

CellTox™ green cytotoxicity assay

Cytotoxicity was measured following the protocol of the CellTox™ Green Cytotoxicity Assay (Promega). Reagents for the assays were prepared and stored according to the manufacturer's protocol. Differentiated adipocytes were treated with the appropriate conditions and incubated at 37 °C, 5% CO₂, and 95% humidity. After treatment, CellTox™ Green reagent was added to the adipocytes, and the plate was mixed for 1 minute by orbital shaking (700 – 900 rpm). The plate was incubated for 15 minutes at room temperature and shielded from ambient light. Fluorescence (Ex/Em = 488/523 nm) was measured using Varioskan™ LUX multimode microplate reader (Thermo Scientific™).

Crystal violet assay

C26 cells were treated appropriately and incubated at 37 °C, 5% CO₂, and 95% humidity. Crystal violet solution was prepared by dissolving 0.125 grams of crystal violet powder in 50 mL of 20% methanol. The lysis solution was prepared by dissolving 5.88 grams of sodium citrate in 200 mL of 25% ethanol (pH 4.2). After treatment, cells were washed once with PBS, and the crystal violet solution was added. Cells were incubated for 10 minutes at room temperature. Cells were washed thrice with PBS, and lysis solution was added. The plate was incubated on a rocking shaker for 30 minutes at room temperature. Absorbance was read at 590 nm using the Varioskan™ LUX multimode microplate reader (Thermo Scientific™).

4.2.14. Staining and analysis of myotube diameter

After treating the differentiated myotubes as mentioned (*Treatment of adipocytes and myotubes*), myotubes were washed with PBS and fixed with 4% ROTI® Histofix for 1 hour at room temperature. The fixation solution was removed and washed three times with PBS. 500 nM of MitoTracker™ Green FM and 1 μ M of 4',6-diamidino-2-phenylindole (DAPI) were prepared in PBS. The fixed myotubes were incubated with the prepared solution for 30 minutes at room temperature. The staining solution was removed, and

cells were washed three times with PBS and maintained in PBS. The myotubes were imaged immediately or stored at 4 °C until used.

ECLIPSE Ts2 inverted microscope (Nikon Instruments Inc.) was used to obtain myotube images. The images were exported as Tag Image File Format (TIFF), and the myotube diameter was measured using the ImageJ software. Ten measurements were made using the line tool for every myotube, and the average value was calculated as the diameter. At least 100 myotubes were quantified for each treatment condition.

4.2.15. Lentivirus production and concentration

Two days before transfection, 5×10^5 HEK293LTV cells were seeded on 10 cm tissue culture plates in a 10 mL HEK medium. Cells were prepared at 70-80% confluency in a 10 mL Lenti medium. A transfection mix was prepared for each reaction, as shown in **Table 7**. The Lipoflex mix was incubated for 15 minutes at room temperature. After incubation, the mix was gently added to the respective 10 cm dishes and incubated at 37 °C, 5% CO₂, and 95% humidity.

Table 7: Composition of the lipoflex mix

Components		Required amount
PolyFect		100 µL
Pure DMEM		100 µL
Packaging and envelop vector	pRSV-Rev	1 µg
	pCMV-Eco	1 µg
	pCgpV	1 µg
Transfer vector		3 µg

24 hours after transfection, cells were refreshed with HEK-HEPES medium. 48 hours and 72 hours after transfection, viral supernatant was collected and filtered through a 0.45 µm surfactant-free cellulose acetate (SFCA) membrane filter (Corning®). One volume of cold PEG-it Virus Precipitation Solution (System Biosciences) was added to every four volumes of lentivirus-containing supernatant and stored at 4 °C for at least 12 hours. Lentivirus particles were centrifuged for 30 minutes at 6000 *rcf* at 4 °C. The supernatant was transferred to a fresh tube and centrifuged for 30 minutes at 6000 *rcf* at 4 °C. Lentivirus pellets were combined in 1/50th of the total lentivirus-containing supernatant using Lenti medium to produce 50X concentrated lentivirus particles. 50X lentivirus was aliquoted into vials and stored at - 80 °C until use.

4.2.16. Transduction of 3T3-L1 adipocytes with lentiviruses

3T3-L1 fibroblasts were differentiated into adipocytes, as mentioned (*Differentiation of 3T3-L1 fibroblasts into adipocytes*). Different lentivirus particles were prepared from the 50X concentrated lentivirus particles using the growth medium containing 10 µg/mL of polybrene. The transfection mix was incubated for 15 minutes at room temperature and added to the differentiated adipocytes. After 48-72 hours of transfection, cells were collected for the experiment or treated with TCCM and isoproterenol for 24 hours.

4.3. Biochemistry

4.3.1. Protein extraction

From mammalian cells

One tablet of cOMplete™, Mini, EDTA-free Protease Inhibitor Cocktail (Roche), and one tablet of PhosSTOP™ (Roche) was freshly added to 10 mL of RIPA Lysis and Extraction Buffer (Thermo Scientific™). Cells were washed once with PBS, and an appropriate volume of the prepared lysis buffer was added. Cells were scrapped off using a cell scrapper, collected in 1.5 mL centrifugation tubes, and incubated for 15 minutes on ice. Cells were lysed using the Sonopuls™ HD 2070 Homogenisator (Bandelin Electronic™) for 10 seconds at 20 kHz and 70% power. After sonication, cells were incubated for 5 minutes on ice and centrifuged for 1 hour at 10000 *rcf* at 4 °C. Supernatant was transferred to a new 1.5 mL centrifugation tube, protein concentration was measured, and stored at - 20°C until use.

From tissues

Lysis buffer was prepared as mentioned in the last section (*From mammalian cells*). On dry ice, one clean stainless steel bead was placed into every 2 mL centrifugation tube. Approximately 5 mg of frozen tissue was sliced, transferred to the tubes with beads, and placed on dry ice. 100 µL of prepared lysis buffer was added, and the tissue was lysed using the TissueLyser II (Qiagen) for 60 sec at a frequency of 30 Hz twice. Lysates were centrifuged for 1 hour at 10000 *rcf* at 4 °C. The supernatant was transferred to a new 1.5 mL centrifugation tube, protein concentration was measured, and stored at - 20°C until use.

4.3.2. Determination of protein concentration

Extracted protein was quantified using Pierce™ BCA Protein Assay Kit (Thermo Scientific™). The working solution was freshly prepared by mixing 50 parts of reagent A with 1 part of reagent B. Lysates from the mammalian cells were diluted 1:2 – 1:5, and tissue lysates were diluted 1:10 – 1:20 using PBS. In a 96-well plate, 10 µL of diluted samples, standards, and blank PBS solution were added in duplicate. 200 µL per well of the working solution was added and incubated for 30 minutes at 37 °C. Absorbance was measured at 562 nm using the Varioskan™ LUX multimode microplate reader (Thermo Scientific™). Using the known concentration of the standards, the protein concentration of the samples was calculated.

4.3.3. SDS-PAGE and immunoblotting

SDS-PAGE

Protein samples were supplemented with 5X Laemmli Sample Buffer and incubated for 5 minutes at 95°C. 20 – 30 µg of the protein was loaded onto Novex™ WedgeWell™ 8 to 16%, Tris-Glycine, 1.0 mm, Mini Protein Gels (Invitrogen™). Precision Plus Protein™ Kaleidoscope™ Prestained Protein Standards (Bio-Rad Laboratories) was used as a protein ladder. Proteins were separated at a constant 70 V for 30 minutes and 100 V for 1 – 1.5 hours using a 1X SDS running buffer.

Protein transfer

Separated proteins were transferred onto 0.2 µm nitrocellulose membranes using a Trans-Blot Turbo RTA transfer kit (Bio-Rad Laboratories). 1X transfer buffer was freshly prepared by mixing 10 mL of 100%

ethanol, 10 mL of 5x transfer buffer, and 30 mL of Milli-Q water. The blotting sandwich was assembled according to the manufacturer's instructions. Using the Trans-Blot Turbo Transfer System (Bio-Rad Laboratories), proteins were transferred for 15 minutes at 12 V and constant 2.5 A.

Ponceau S staining

Membranes were stained for 5 minutes with Ponceau S to check the transfer efficiency. The background was removed by washing it with distilled water.

Immunoblotting and detection

Membranes were blocked for 1 hour in 5% milk in TBST. The blocking solution was removed and washed briefly with 1X Tris-Buffered Saline (TBS) containing 0.1% Tween[®] 20 (TBST). If required, the membrane was cut and incubated with respective primary antibodies prepared in 5% bovine serum albumin (BSA) in TBST at 4 °C overnight. Membranes were washed thrice with TBST for 10 minutes. Horseradish peroxidase (HRP)-conjugated secondary antibody prepared in 5% BSA in TBST was added to the respective membranes and incubated for 1 hour at room temperature. Membranes were washed thrice with TBST for 10 minutes. Pierce™ ECL Plus Western Blotting Substrate (Thermo Scientific™) was freshly prepared by mixing the solutions in a 1:1 ratio. Proteins were detected using the ChemiDoc Imaging System (Bio-Rad Laboratories). Primary and secondary antibodies and their dilutions used are represented in **Table 10**.

Quantification of immunoblots

Densitometric analysis of the immunoblots was performed using either the Image Lab Software (Bio-Rad Laboratories) or ImageJ software.

4.3.4. NADPH Oxidase Activity Assay

NADPH oxidase activity was quantified using NADH Oxidase Activity Assay Kit (Fluorometric) (Abcam). Reagents for the assays were prepared and stored according to the manufacturer's protocol. 5 – 10 mg of iWAT was homogenized using the provided lysis buffer. In duplicates, diluted iWAT and plasma samples, standards, and positive controls were added to the 96-well white-walled, clear bottom plate (Corning™). Following the manufacturer's protocol, the assay was performed, and fluorescence (Ex/Em = 535/587 nm) was measured in kinetic mode for 60 minutes at room temperature. NOX activity was determined using the following equation. ΔT = Reaction time ($T_2 - T_1$) (in minutes), P = Amount of protein in the sample (mg). NOX activity was reported as $\mu\text{U}/\text{mg}$.

$$\text{NOX activity} = \frac{\text{Lactate standard}}{(\Delta T \times P)}$$

4.4. Animal experiments

Balb/c and C57BL6/N mice were procured from either Charles River Laboratories, Germany, or Janvier Labs, France. Mice were housed according to international standard conditions under pathogen-free conditions with a 12-hour light-dark cycle at 22 or 31 °C. Mice had unrestricted access to rodent chow diet (Kliba Nafag #3437, Provimi Kliba AG, Switzerland; Kaiseraugst, Switzerland) and water. Animal handling and experimentation were performed following the institutional animal welfare officer. The licenses were

obtained from the state ethics committee and the government of Upper Bavaria (ROB-55.2-2532.Vet_02-18-93).

For each animal experiment, body composition analysis of mice was performed and stratified into groups. Body weight and composition were similar between groups, as confirmed by statistical analysis. The number of mice used for each experiment is indicated in the figure legends. Unless otherwise mentioned, at the end of the experiment, mice were killed by cervical dislocation, and blood was collected after decapitation. Organs including liver, adipose tissues (iWAT, eWAT, and scapular BAT), GC and soleus muscles, heart, and tumor were collected, weighed, snap-frozen in liquid nitrogen, and used for further analysis.

4.4.1. Mice for isolation of primary preadipocytes

Eight weeks old male C57BL6/N mice purchased from Janvier Labs, France, were used to isolate primary preadipocytes. Mice were then sacrificed to excise adipose tissue and isolated preadipocytes for culture as detailed before (*Isolation of preadipocytes from adipose tissue*).

4.4.2. Testing the toxicity of the compounds

Six to seven weeks old male Balb/c mice purchased from Charles River Laboratories, Germany, were let to acclimatize in the animal facility for at least a week. For the individual experiment, mice were injected with either vehicle or different concentrations of the compound at a particular time of the day throughout the experiment. DPI, OLDA, and BioF compounds dissolved in DMSO were prepared freshly in their respective solvent for the treatment (**Table 8**).

Table 8: Solvents used for preparing the compounds for injection and the injection site used for in vivo experiments.

Compound	Solvent	Injection site
DPI	PBS	Subcutaneous
OLDA	80% of 0.9% NaCl 10% Tween 80 10% ethanol	Intraperitoneal
BioF	98% of 0.9% NaCl 2% Tween 80	Intraperitoneal

4.4.3. C26 cachexia model

Six to seven weeks old male Balb/c mice purchased from Charles River Laboratories, Germany, were let to acclimatize in the animal facility for at least a week. 0.5 or 1×10^6 C26 cells prepared in $100 \mu\text{L}$ PBS were injected subcutaneously into the right flank for tumor induction. Non-tumor-bearing mice groups were injected with $100 \mu\text{L}$ of PBS. Mice were monitored for four weeks after tumor cell implantation, and the scoring of animals was performed according to the animal license.

For the thermoneutrality experiment, mice were injected with 1×10^6 C26 cells or PBS. From the next day onwards, mice were treated with either vehicle or 5 mg/kg/day of BioF. For other cachexia experiments, once tumor cell injected mice developed a palpable tumor, body weight was measured. Mice were treated with either vehicle or compound every day. The tumor growth and food intake were recorded every other

day for the initial two weeks and daily afterward. Body composition analysis was performed one week before the start of the experiment, 14 and 21 days after tumor inoculation, and before sacrificing the mice.

Mice were sacrificed when they reached one or more of four termination criteria: 28 days after injection, ulceration, tumor diameter more than 1.5 cm, or cachexia as defined by body weight loss more than 10-15% or body condition score (BCS) less than 2. When a tumor-bearing mouse treated with the vehicle or compound is sacrificed, mice with similar tumor sizes from the other treatment group are matched and sacrificed for comparison. Non-tumor-bearing mice were sacrificed together with the tumor-bearing mice throughout the experiment.

4.4.4. Cachexia index

The cachexia index of the tumor-bearing mice was calculated using the formula mentioned below (Viana et al., 2016). *Bmg* = body mass gain of the non-tumor-bearing vehicle-treated mice.

$$\text{Cachexia index} = \frac{[(\text{initial body mass} - \text{carcass mass} + \text{tumor weight} + \text{bmg})]}{(\text{initial body mass} + \text{bmg})} \times 100\%$$

4.4.5. Intraperitoneal glucose tolerance test

The intraperitoneal glucose tolerance test was performed on the Balb/c mice treated with vehicle or 1 and 5 mg/kg/day of OLDA for four days. Mice were fasted for 6 hours, body weight was measured, and 2 g/kg of glucose prepared in 0.9% NaCl was injected intraperitoneally. A small amount of venous blood from the tail was obtained using a razor blade. Blood glucose level was measured before (fasting glucose) and 15, 30, 60, and 120 minutes after glucose injection using glucometer strips. AUC of the glucose excursion curve was calculated, having the fasted blood glucose concentration as the baseline.

4.4.6. Body composition analysis

Body composition was determined using magnetic resonance (EchoMRI, Echo Medical Systems, Houston).

4.4.7. Blood plasma extraction

Blood samples were collected in Micro sample tubes K3 EDTA, 1.3 ml, push cap, EU (Sarstedt, Inc.). Blood samples were centrifuged for 5 minutes at 10000 *rcf* at 4°C. The blood plasma (upper phase) was transferred to a fresh 1.5 ml safe-lock tube and stored at -80°C.

4.5. Statistical Analysis

Data were collected or inputted in Microsoft Excel and processed using Excel functions. Figures were prepared, and statistical analysis was performed using GraphPad Prism. Two-tailed unpaired t-test, one or two-way analysis of variance (ANOVA) was performed with Šídák's (One way ANOVA), Tukey's, or Dunnett's (Two way ANOVA) posthoc multiple-comparison test. $p < 0.05$ was considered statistically significant. * $p < 0.05$, ** $p < 0.01$, *** $p < 0.001$, and **** $p < 0.0001$.

5. MATERIALS

5.1. Compounds used in the screen

Table 9: Compounds screened in this study.

ID	Name	Molecular weight (Da)	Company	Product ID
01	Quercetin Dihydrate	338.27	Santa Cruz Biotechnology	sc-203225
02	L-(-)- α -Methyldopa	211.22	Santa Cruz Biotechnology	sc-203092
03	Clozapine	326.8	Biomol	Cay12059-50
04	YC-1	304.3	Biomol	Cay81560-5
05	Diphenyleneiodonium Chloride (DPI)	314.55	Sigma-Aldrich	D2926-10MG
06	Olomoucine	298.3	Biomol	Cay10010240-5
07	Piceatannol	244.2	Biomol	Cay10009366-5
08	Hispidin	246.2	Biomol	Cay10012605-5
09	BAY 43-9006	464.8	Biomol	AG-CR1-0025-M005
10	(-)-Epicatechin	290.3	Biomol	Cay11807-5
11	Orlistat	495.7	Biomol	Cay10005426-50
12	N-6-2-(4-Aminophenyl) ethyladenosine	386.41	Santa Cruz Biotechnology	sc-253170
13	Olanzapine	312.43	Sigma-Aldrich	O1141-10MG
14	Fenipentol	164.25	BioCat	T0857-25mg-TM
15	Estramustine	440.4	Enzo Life Sciences	LKT-E7578-M100
16	FSCPX	506.55	Santa Cruz Biotechnology	sc-252841A
17	2',4'-Dichlorobenzamil • HCl	425.1	Santa Cruz Biotechnology	sc-200197
18	GF-109203X	412.48	BIOZOL Diagnostica Vertrieb	SCM-P61-900-10
19	Rotenone	394.4	Biomol	Cay13995-1
20	N-Oleoyldopamine (OLDA)	417.62	Santa Cruz Biotechnology	sc-201456
21	(\pm)-Taxifolin	304.25	Santa Cruz Biotechnology	sc-202828
22	Praziquantel	312.4	Biomol	Cay20508-1
23	FPL 64176	347.4	Biomol	Cay20122-5
24	Caffeic acid phenethyl ester	284.31	Santa Cruz Biotechnology	sc-200800
25	rac α -Methyl DOPA	211.21	Santa Cruz Biotechnology	sc-219872
26	Dipyridamole	504.63	Santa Cruz Biotechnology	sc-200717
27	Lavendustin A	381.4	Biomol	Cay10010268-5

28	Donepezil	379.5	Biomol	Cay13245-10
29	(+)-Catechin	290.27	Sigma-Aldrich	C1788-500MG
30	6-Hydroxymelatonin	248.28	Santa Cruz Biotechnology	sc-217347
31	Sanguinarine (chloride)	367.8	Enzo Life Sciences	Cay16951-5
32	Niguldipine (hydrochloride)	646.2	Biomol	Cay19534-5
33	Loperamide Hydrochloride	513.5	VWR International	EHERC14647000
34	BioFocus_AZD01 (BioF) 405_5923_8723	354.45	Charles River Laboratories	T-065998
35	BioFocus_SFG17 389_7751_5941_0263_8170	458.606	Charles River Laboratories	T-061532
36	L-750,667 trihydrochloride	527.66	Santa Cruz Biotechnology	sc-300865
37	2-Methylserotonin Maleate	306.31	Santa Cruz Biotechnology	SML0640-5MG
38	Hydroxyzine Dihydrochloride	447.83	Enzo Life Sciences	LKT-H9717-G001
39	Bupivacaine Hydrochloride	342.9	Th. Geyer	10433852
40	Nipecotic acid	129.16	Santa Cruz Biotechnology	sc-257909
41	Benzethonium chloride, 97%	448.08	Th. Geyer	11789400
42	Dicyclomine (hydrochloride)	346	Biomol	Cay23867-500
43	Thionicotinamide adenine dinucleotide phosphate potassium salt	796.56	Santa Cruz Biotechnology	sc-394300
44	Caffeic acid	180.16	Sigma-Aldrich	C0625-2G
45	(+)-Catechin (hydrate)	290.3	Biomol	Cay70940-1
46	Antimycin A	548.633	VWR International	J63522.X0
47	N-Acetyl-5-hydroxytryptamine	292.4	Enzo Life Sciences	ALX-550-208-M500
48	Rutin trihydrate	664.56	Santa Cruz Biotechnology	sc-204897
49	L-750,667 trihydrochloride	527.66	Santa Cruz Biotechnology	sc-300865
50	Erbstatin analog	194.2	Biomol	Cay10010238-5
51	N-6-Phenyladenosine	343.34	Enzo Life Sciences	JBS-N-1073

5.2. Animals

Strain	Origin
Balb/c	Charles River Laboratories, Germany
C57BL6/N	Charles River Laboratories, Germany

5.3. Antibodies

Table 10: Primary and secondary antibodies used in this study

Antibodies	Dilution	Host	Company	Product ID
Anti-Erk1/2	1:1000	Rabbit	Cell Signaling Technology	4695

Anti-phospho-Erk1/2 (Thr202/Tyr204)	1:1000	Rabbit	Cell Signaling Technology	9101
Anti-HSL	1:1000	Rabbit	Cell Signaling Technology	4107S
Anti-phospho-HSL (Ser565)	1:1000	Rabbit	Cell Signaling Technology	4137S
Anti-phospho-HSL (Ser563)	1:1000	Rabbit	Cell Signaling Technology	4139S
Anti-ATGL	1:1000	Rabbit	Cell Signaling Technology	2138S
Anti-FAS	1:1000	Rabbit	Cell Signaling Technology	3180S
Anti-VCP	1:10000	Mouse	Abcam	ab11433
Anti-ACC α	1:1000	Rabbit	Abcam	ab72046
Anti-phospho-ACC α (Ser79)	1:1000	Rabbit	Cell Signaling Technology	3661
Anti- β -actin	1:10000	Mouse	Sigma-Aldrich	A5441
Anti-CGRP	1:1000	Mouse	Santa Cruz Biotechnology	sc-57053
Anti-TRVP	1:1000	Rabbit	Thermo Fisher Scientific	PA1-748
Anti-AMPK α	1:1000	Rabbit	Cell Signaling Technology	2532
Anti-phospho-AMPK α (Thr172)	1:1000	Rabbit	Cell Signaling Technology	2531
Anti-Rabbit IgG(H+L) HRP	1:5000	Goat	Bio-Rad Laboratories	1721019
Anti-Mouse IgG, HRP	1:5000	Goat	Biomol	BCT-RSA1122-M001

5.4. Chemicals and Reagents

Chemical/Reagents	Company
Yeast extract	Sigma-Aldrich
Peptone	Sigma-Aldrich
Sodium chloride	Sigma-Aldrich
Sodium hydroxide	Sigma-Aldrich
Hydrochloric acid	Sigma-Aldrich
Bacto agar	Thermo Fisher Scientific
SOC medium	Sigma-Aldrich
Ampicillin	Sigma-Aldrich
Trizol	Life Technologies
Chloroform	Sigma-Aldrich
Ethanol	Sigma-Aldrich
Methanol	Sigma-Aldrich
DMEM, high glucose, GlutaMAX Supplement, pyruvate	Thermo Fisher Scientific
DMEM/F-12, GlutaMAX Supplement	Life Technologies
Fetal bovine serum	Sigma-Aldrich
Penicillin-Streptomycin	Thermo Fisher Scientific
Insulin	Sigma-Aldrich
3-Isobutyl-1-methylxanthine	Sigma-Aldrich
Dexamethasone	Sigma-Aldrich
(+)-Sodium L-ascorbate	Sigma-Aldrich
D-Pantothenic acid hemicalcium	Sigma-Aldrich
Biotin	Sigma-Aldrich
Type II collagenase	Life Technologies
Bovine Serum Albumin	Sigma-Aldrich

3,3',5'-Triiodo-L-thyronine	Sigma-Aldrich
Rosiglitazone	Sigma-Aldrich
U0126	Merck Millipore
NEAA	Life Technologies
HEPES	Biozym
DMSO	Sigma-Aldrich
Trypsin	Sigma-Aldrich
Oil Red O solution	Sigma-Aldrich
ROTI®Histofix	Carl Roth GmbH & Co. KG
isopropanol	Sigma-Aldrich
Seahorse XF DMEM assay medium (pH 7.4)	Agilent Technologies
Pyruvate	Thermo Fisher Scientific
Glucose	Thermo Fisher Scientific
Glutamine	Thermo Fisher Scientific
Norepinephrine	Sigma-Aldrich
Forskolin	Biomol
Isoproterenol	Santa Cruz Biotechnology
Atglistatin	Sigma-Aldrich
Oligomycin A	Sigma-Aldrich
FCCP	Sigma-Aldrich
Antimycin A	Sigma-Aldrich
Rotenone	Sigma-Aldrich
MitoTracker™ Green FM	Thermo Fisher Scientific
DAPI	Thermo Fisher Scientific
PolyFect Transfection Reagent	Qiagen
PEG-it Virus Precipitation Solution	Biocat
Polybrene Transfection Reagent	Merck Millipore
cOmplete™, Mini, EDTA-free Protease Inhibitor Cocktail	Roche Holding AG
PhosSTOP™	Roche Holding AG
RIPA Lysis and Extraction Buffer	Thermo Fisher Scientific
5X Laemmli Sample Buffer	Nectagen, Inc.
Precision Plus Protein™ Kaleidoscope™ Prestained Protein Standards	Bio-Rad Laboratories
Ponceau S	Thermo Fisher Scientific
Milk powder	Sigma-Aldrich
Tween-20	Santa Cruz Biotechnology, Inc.
Tween-80	Santa Cruz Biotechnology, Inc.
Pierce™ ECL Plus Western Blotting Substrate	Thermo Fisher Scientific
RPE buffer	Qiagen
PBS	Life Technologies
Rodent chow diet	Altromin Spezialfutter GmbH & Co. KG

5.5. Kits

Kits	Company	Product ID
QIAprep Spin Miniprep Kit	Qiagen	27106
QIAGEN Plasmid Plus Midi Sample Kit	Qiagen	12943
Quantitect Reverse Transcription kit	Qiagen	205311
SYBR™ Green PCR Master Mix	Thermo Fisher Scientific	4309155
Pierce™ BCA Protein Assay Kit	Thermo Fisher Scientific	23225
cAMP Gs dynamic kit	Cisbio Bioassays SAS	62AM4PEB
NADH Oxidase Activity Assay Kit (Fluorometric)	Abcam	ab273345
Fatty Acid Uptake Assay Kit	Abcam	ab287857
CellTox™ Green Cytotoxicity Assay	Promega	G8743
Free glycerol reagent	Sigma-Aldrich	F6428-40ML
Glycerol standard solution	Sigma-Aldrich	G7793-5ML
NEFA-HR(2) Assay Reagent 1 Set	FUJIFILM Wako Chemicals Europe GmbH	434-91795
NEFA-HR(2) Assay Reagent 2 Set	FUJIFILM Wako Chemicals Europe GmbH	436-91995
NEFA-HR(2) Assay Standard	FUJIFILM Wako Chemicals Europe GmbH	270-77000

5.6. Plasmids

Plasmid	Resistance	Company	Product ID
pRSV-Rev Packaging Vector	Ampicillin	Cell Biolabs, Inc.	320022
pCMV-Eco Envelope Vector	Ampicillin	Cell Biolabs, Inc.	320026
pCgpV Packaging Vector	Ampicillin	Cell Biolabs, Inc.	320024

5.7. qPCR primers

Primer name	Sequence (5' → 3')	Target
m_No3_F	CACAGGCTCAAATGGACGGA	Nox-3
m_No3_R	CTGCCAGCCATAAGAGAGCA	
m_No4_F	CCAAATGTTGGGCGATTGTGT	Nox-4
m_No4_R	GGCTACATGCACACCTGAGA	
mPnpla2_Fwd	GGATGGCGGCATTTTCAGACA	Atgl
mPnpla2_Rev	CAAAGGGTTGGGTTGGTTCAG	
mLipe_fwd	CCAGCCTGAGGGCTTACTG	Hsl
mLipe_Rev	CTCCATTGACTGTGACATCTCG	
mDgat1_F	GGTCCGTGTTTGCTCTGGCAT	Dgat-1
mDgat1_R	CCACTGACCTTCTCCCTGTAG	
mDgat2_F	CGAGACACCATAGACTACTTGCT	Dgat-2
mDgat2_R	GCGGTTCTTCAGGGTGACTG	
mAdiponectin F	GCACTGGCAAGTTCTACTGCAA	AdipoQ
mAdiponectin R	GTAGGTGAAGAGAACGGCCTTGT	
mPpara_F	ACCACTACGGAGTTCACGCATG	Ppara
mPpara_R	GAATCTTGACGCTCCGATCACAC	
mPgc1a-F	CCCTGCCATTGTTAAGACC	Pgc-1α
mPgc1a-R	TGCTGCTGTTCTGTTTTTTC	

mPdk4_F	GTCGAGCATCAAGAAAACCGTCC	<i>Pdk-4</i>
mPdk4_R	GCGGTCAGTAATCCTCAGAGGA	
mSaa1/2_F	TCTCAAAGGCATGGGCAGAG	<i>Saa-1/2</i>
mSaa1/2_R	TCATGTCAGTGTAGGCTCGC	
mFabp3_Fw	ACCTGGAAGCTAGTGGACAG	<i>Fabp-3</i>
mFabp3_Rv	TGATGGTAGTAGGCTTGGTCAT	
mFabp4_F	CTTTGCCACAAGGAAAGTGG	<i>Fabp-4</i>
mFabp4_R	TCCCCATTTACGCTGATGAT	
mPlin2-F	CTTGTGTCCTCCGCTTATGTC	<i>Plin-2</i>
mPlin2-R	GCAGAGGTCACGGTCTTCAC	
mGLUT1_F	TCAACACGGCCTTCACTG	<i>Glut-1</i>
mGLUT1_R	CACGATGCTCAGATAGGACATC	
mGLUT4_F	CGTCGGGCTTCCAACAGATA	<i>Glut-4</i>
mGLUT4_R	CACCGCAGAGAACACAGCAA	
mFbxo32_F	CAGCTTCGTGAGCGACCTC	<i>Fbxo-32</i>
mFbxo32_R	GGCAGTCGAGAAGTCCAGTC	
mFOXO1_F	CCCAGGCCGGAGTTAACC	<i>Foxo-1</i>
mFOXO1_R	GTTGTCATAAAGTCGGTGCT	
mBnip3_F	GCTCCAAGAGTTCTCACTGTGAC	<i>Bnip-3</i>
mBnip3_R	GTTTTTCTCGCCAAAGCTGTGGC	
mTbp_F	GCTCTGAAATTGTACCGCAG	<i>Tbp</i>
mTbp_R	CTGGCTCATAGCTCTTGGCTC	

5.8. shRNAs

shRNA ID (in this study)	Target	Accession number	Product ID
shNOX3_1	Mouse <i>Nox-3</i>	NM_198958	TRCN0000443443
shNOX3_2	Mouse <i>Nox-3</i>	NM_198958	TRCN0000420088
shNOX3_3	Mouse <i>Nox-3</i>	NM_198958	TRCN0000431231
shNOX3_4	Mouse <i>Nox-3</i>	NM_198958	TRCN0000437719
shNOX3_5	Mouse <i>Nox-3</i>	NM_198958	TRCN0000413465
shNOX4_1	Mouse <i>Nox-4</i>	NM_015760	TRCN0000076583
shNOX4_2	Mouse <i>Nox-4</i>	NM_015760	TRCN0000076585
shNOX4_3	Mouse <i>Nox-4</i>	NM_015760	TRCN0000076584
shNOX4_4	Mouse <i>Nox-4</i>	NM_015760	TRCN0000076586
shNOX4_5	Mouse <i>Nox-4</i>	NM_015760	TRCN0000076587

5.9. Software

Software/Tool	Version	Company
Prism	8.0.2 and above	GraphPad Software, Inc.
ImageJ	1.52k and above	Wayne Rasband (retired from NIH)
Image Lab Software	6.1	Bio-Rad Laboratories
Office (Word, Excel, Powerpoint)	Professional Plus 2016	Microsoft Corporation
Seahorse Wave Desktop Software	2.6.1	Agilent Technologies

6. APPENDIX

6.1. Abbreviations

·OH	-	Hydroxyl radical
3T3-L1 DM1	-	3T3-L1 differentiation medium 1
3T3-L1 DM2	-	3T3-L1 differentiation medium 2
ABP	-	Ascorbate, Biotin, Pantothenic acid
ACC	-	Acetyl-CoA carboxylase
Acetyl-CoA	-	Acetyl-coenzyme A
ACIP	-	Ampk-Cidea-interfering peptide
ACSL-1	-	Acyl-CoA Synthetase Long-Chain Family Member-1
ActRIIB	-	Activin type II receptor
AdipoQ	-	Adiponectin
AdipoR-1	-	Adiponectin receptor-1
AdipoR-2	-	Adiponectin receptor-2
AdipoRon	-	Adiponectin receptor agonist
ADMR	-	Adrenomedullin receptor
ADRB-1	-	β -1 Adrenergic Receptor
AH-130	-	Ascites hepatoma 130
AIDS	-	Autoimmune deficiency syndrome
ALP	-	Alkaline phosphatase
ALT	-	Alanine transaminase
AM	-	Adrenomedullin
AMPK	-	AMP-activated protein kinase
APC	-	Adenomatous polyposis coli
AST	-	Aspartate aminotransferase
atATGL-KO	-	Adipose tissue-specific knockout of ATGL
ATGL	-	Adipose triglyceride lipase
ATGLi	-	Atglistatin
ATP	-	Adenosine triphosphate
AUC	-	The area under the curve
BAIBA	-	β -aminoisobutyric acid
BAT	-	Brown adipose tissue
BMI	-	Body mass index
BMP	-	Bone morphogenetic protein
Bnip-3	-	BCL2 Interacting Protein-3
C/EBP	-	CCAAT/enhancer-binding protein
C26	-	Colon 26 adenocarcinoma
cAMP	-	Cyclic adenosine monophosphate
CB1/CB2	-	Cannabinoid receptors
CDK	-	Cyclin-dependent kinases
cDNA	-	Complementary DNA

CGRP	-	Calcitonin gene-related peptide
CHF	-	Chronic heart failure
CIDEA	-	Cell-death-inducing DNA fragmentation factor, alpha subunit-like effector A
CKD	-	Chronic kidney disease
COPD	-	Chronic obstructive pulmonary disease
DAGs	-	Diacylglycerols
delta-9-THC	-	Delta-9-tetrahydrocannabinol
DEXA	-	Dual-energy X-ray absorptiometry
DGAT	-	Diacylglycerol acyltransferase
Dgat-2	-	Diacylglycerol O-Acyltransferase 2
DM	-	Differentiation medium
DMD	-	Duchenne muscular dystrophy
DNA	-	Deoxyribonucleic acid
DNL	-	De novo lipogenesis
DPI	-	Diphenyleiodonium chloride
dsDNA	-	Double-stranded deoxyribonucleic acid
E. coli	-	Escherichia coli
ECAR	-	Extracellular acidification rate
eIF3-f	-	Eukaryotic translation initiation factor 3 subunit F
EMA	-	European Medicines Agency
eNOS	-	Endothelial nitric oxide synthase
eWAT	-	Epididymal white adipose tissue
FAS	-	Fatty acid synthetase
FBXO-32	-	F-box only protein-32
FDA	-	Food and Drug Administration
FFAs	-	Free fatty acids
FGF	-	Fibroblast growth factor
FGF-21	-	Fibroblast growth factor-21
Foxo-1	-	Forkhead Box Protein O1
GDF-15	-	Growth/differentiation factor-15
GDF-8	-	Growth differentiation factor-8
GEMMs	-	Genetic-engineered mouse models
GIP	-	Gastric inhibitory peptide
GLP-1	-	Glucagon-like peptide-1
Glut-1	-	Glucose Transporter Type-1
Glut-4	-	Glucose Transporter Type-4
GPCR	-	G-protein coupled receptor
GPR-119	-	G protein-coupled receptor 119
H ₂ O ₂	-	Hydrogen peroxide
HCl	-	Hydrochloric acid
HCT116	-	Human colorectal 116 carcinoma cell line
HDL	-	High-density lipoprotein
hMSC DM1	-	hMSC differentiation medium 1

hMSC DM2	-	hMSC differentiation medium 2
hMSC-Tert	-	Human mesenchymal stem cells
HSL	-	Hormone-sensitive lipase
HT29	-	Human colorectal 29 adenocarcinomas
IC ₅₀	-	Half maximal inhibitory concentration
IFN- γ	-	Interferon-gamma
IL-1 β	-	Interleukin-1 β
IL-6	-	Interleukin-6
ipGTT	-	Intraperitoneal glucose tolerance test
Iso	-	Isoproterenol
iWAT	-	Inguinal white adipose tissue
KPC	-	LSL-KrasG12D/+; LSL-Trp53R172H/+; Pdx-1-Cre
KPP	-	Kras+/G12D; Ptf1a+/ER-Cre; Ptenfl/fl
LB	-	Luria broth
LDH	-	Lactate dehydrogenase
LDL	-	Low-density lipoprotein
LDs	-	Lipid droplets
LIF	-	Leukemia inhibitory factor
LLC	-	Lewis lung carcinoma
LMF	-	Lipid mobilizing factor
LOPAC	-	The Library of Pharmacologically Active Compounds
LPL	-	Lipoprotein lipase
MAC16	-	Murine adenocarcinoma 16
MAGs	-	Monoacylglycerols
MC38	-	Murine colon 38 adenocarcinoma
MuRF-1	-	Muscle-Specific RING Finger Protein-1
NaCl	-	Sodium chloride
NADH	-	Nicotinamide adenine dinucleotide hydrogen
NaOH	-	Sodium hydroxide
NCM	-	Non-conditioned growth medium
NEFA	-	Non-esterified fatty acid
NF- κ B	-	Nuclear factor- κ B
NOS	-	Nitric oxide synthase
NOX	-	NADPH oxidase
NTC	-	Non-template control
O ₂ ⁻	-	Superoxide anion radical
O ₃	-	Ozone
OCR	-	Oxygen consumption rate
OLDA	-	N-Oleoyldopamine
OXPHOS	-	Oxidative phosphorylation
PBS	-	Phosphate-buffered saline
PDAC	-	Pancreatic ductal adenocarcinoma
Pdk-4	-	Pyruvate dehydrogenase kinase 4

PGC-1 α	-	Peroxisome proliferator-activated receptor γ coactivator-1 α
PKA	-	Protein kinase A
PLIN-1	-	Perilipin-1
Plin-2	-	Perilipin-2
PPAR- γ /PPARG	-	Peroxisome proliferator-activated receptor gamma
PRDM-16	-	PR Domain-Containing Protein-16
PTHrP	-	Parathyroid hormone-related protein
rcf	-	Relative centrifugal force
redox	-	Reduction-oxidation
RNA	-	Ribonucleic acid
ROS	-	Reactive oxygen species
Saa- 1/2	-	Serum amyloid A1/2
sActRIIB	-	Soluble ActRIIB
scWAT	-	Subcutaneous WAT
SDS	-	Sodium dodecyl sulfate
SDS-Page	-	SDS polyacrylamide gel electrophoresis
SFCA	-	Surfactant-free cellulose acetate
shRNA	-	Short hairpin RNA
SOC	-	Super Optimal broth with Catabolite repression
SVF	-	Stromal vascular fraction
T2D	-	Type-2 diabetes
TAGs	-	Triacylglycerols
TBS	-	Tris-Buffered Saline
TBST	-	TBS, 0.1% Tween [®] 20
TCCM	-	Tumor cell conditioned medium
TGF- β	-	Transforming growth factor- β
TIFF	-	Tag Image File Format
TNFR-1	-	TNF- α receptor-1
TNF- α	-	Tumor necrosis factor-alpha
TRPV-1	-	Transient Receptor Potential Vanilloid-1
TWEAK	-	TNF-related weak inducer of apoptosis
TZDs	-	Thiazolidinediones
UCP-1	-	Uncoupling protein-1
UPS	-	Ubiquitin-Proteasome system
WAT	-	White adipose tissue
ZAG	-	Zinc- α 2- glycoprotein
α -KO	-	Inhibin α -subunit knockout mice
β -ARs	-	β -adrenergic receptors

6.2. List of Figures

- Figure 1: Stages of cancer cachexia.** The cancer cachexia spectrum represents the different stages of the disease progression adapted from (K. Fearon et al., 2011). BMI – body mass index.1
- Figure 2: Prevalence of cachexia and intensity of weight loss based on tumor site. (a)** The percentage prevalence of cachexia (defined as at least 5% weight loss in the last six months) and **(b)** average percentage weight loss in patients as based on tumor site. Adapted from (Baracos et al., 2018).2
- Figure 3: Cachexia as a multiorgan syndrome.** Cachexia-inducing tumor and its action on metabolic organs. The physiological processes altered in different organs during cachexia are displayed. Increased lipolysis in adipose tissue and increased proteolysis in skeletal muscle are key features observed in cachexia patients. Adapted from (Rohm et al., 2019).5
- Figure 4: Adipose tissue as an endocrine organ.** Important regulatory factors are secreted by various cells in the adipose tissue. Adapted from (Fasshauer & Blüher, 2015).10
- Figure 5: Aim of the study. (a)** Screening strategy used in this study for identifying novel antilipolytic compounds, validation, and literature review for further in vivo studies. **(b)** Cachexia-tumor-bearing mice with increased metabolic dysregulation lose body weight, adipose tissue, and muscle mass. When treated with the hit compounds from the screening, we anticipate that the adipose tissue and muscle homeostasis are maintained, and weight and tissue loss are prevented. Created with Inkscape and BioRender.com.13
- Figure 6: Differentiation of 3T3-L1 fibroblasts into adipocytes. (a)** Representative images of the preadipocytes and differentiated 3T3-L1 adipocytes stained for the neutral lipid droplets by Oil Red O staining. Scale bars are 100 μm . **(b)** Quantification of the staining is shown in **Figure 6a**. $n = 4$, data shown are mean \pm s.e.m, **** $P < 0.0001$; by two-tailed t-test.14
- Figure 7: β -adrenergic receptor ligand and TCCM from cachexia-inducing cells induces lipolysis in vitro. (a)** Free glycerol was released into the medium of the differentiated 3T3-L1 adipocytes treated with either growth medium (NCM), isoproterenol (Iso), or C26 TCCM for 24 hours. **(b, c)** Proteins extracted from the treated adipocytes were immunoblotted for specific proteins involved in lipolysis. p-HSL(Ser565) levels were normalized with the total HSL and p-ACCa(Ser79) with β -Actin, which was used as the loading control. Free glycerol was released into the medium of the differentiated 3T3-L1 adipocytes treated with either **(d)** NCM, MC38 TCCM, or C26 TCCM for 24 hours, **(e)** NCM, Iso, human HT29 TCCM, HCT116 TCCM or LLC TCCM. **(a – e)** $n = 4$, data shown are mean \pm s.e.m. * $P \leq 0.05$, ** $P \leq 0.01$, *** $P \leq 0.001$, **** $P \leq 0.0001$; by one-way ANOVA with Šidák's multiple-comparison test.15
- Figure 8: Tumor-induced lipolysis assay-based compound screening on 3T3-L1 adipocytes. (a)** Preadipocytes were seeded, grown to confluence and cultured with adipogenesis-inducing differentiation medium, changed every 2-3 days. Differentiated adipocytes were treated with either growth medium and tumor cell-derived conditioned medium (TCCM) with or without 10 μM of test compounds for 24 hours. Lipolysis was assayed by measuring the non-esterified fatty acid (NEFA) and free glycerol released into the medium. **(b)** Free glycerol was released into the medium of the differentiated 3T3-L1 adipocytes treated with either MC38 TCCM or C26 TCCM together with 10 μM of the screening compounds for 24 hours. The dotted line represents the reference level of cells treated with NCM. **(c)** Heat map representing the mean percent inhibition of lipolysis relative to respective control. **(b)** $n = 4$, data shown are mean \pm s.e.m., * indicates significance between MC38 TCCM control and specific compound, § indicates significance between C26 TCCM control and specific compound. * $P \leq 0.05$, ** $P \leq 0.01$, *** $P \leq 0.001$, **** $P \leq 0.0001$; by two-way ANOVA with Dunnett's multiple-comparison test.17
- Figure 9: Tumor-induced lipolysis assay-based compound screening on hMSC-Tert adipocytes. (a)** Free glycerol was released into the medium of the differentiated hMSC-Tert adipocytes treated with either NCM or C26 TCCM and 10 μM of the screening compounds for 24 hours. **(b)** Heat map representing the mean percent inhibition of lipolysis relative to respective control. **(a)** $n = 4$, data shown are mean \pm s.e.m., * indicates significance between NCM control

and specific compound, § indicates significance between C26 TCCM control and specific compound. * $P \leq 0.05$, ** $P \leq 0.01$, *** $P \leq 0.001$, **** $P \leq 0.0001$; by two-way ANOVA with Dunnett's multiple-comparison test.18

Figure 10: Tumor-induced lipolysis assay-based compound screening on murine primary adipocytes. (a) Free glycerol was released into the medium of the differentiated murine primary adipocytes treated with either MC38 TCCM or C26 TCCM together with 10 μM of the screening compounds for 24 hours. The dotted line represents the reference level of cells treated with NCM. (b) Heat map representing the mean percent inhibition of lipolysis relative to respective control. (a) $n = 5$, data shown are mean \pm s.e.m., * indicates significance between MC38 TCCM control and specific compound, § indicates significance between C26 TCCM control and specific compound. * $P \leq 0.05$, ** $P \leq 0.01$, *** $P \leq 0.001$, **** $P \leq 0.0001$; by two-way ANOVA with Dunnett's multiple-comparison test.19

Figure 11: (a) Heat map representing the mean percent inhibition of lipolysis relative to respective control of selected compounds from compounds screening performed using 3T3-L1, mouse primary, and hMSC-Tert adipocytes. The value within the cells indicates the percent inhibition of lipolysis, and the asterisk indicates the significance relative to the respective control.20

Figure 12: Selected compounds from the screen reduce basal and tumor-induced lipolysis. Free glycerol was released into the medium of the differentiated 3T3-L1 adipocytes treated with either (a) MC38 TCCM or C26 TCCM with 10 μM of the selected compounds for 24 hours or (b) HT29 TCCM or HCT116 TCCM together with 10 μM of the selected compounds for 24 hours. $n = 3$, data shown are mean \pm s.e.m., * indicates significance between MC38 TCCM/HT29 TCCM control and specific compound, § indicates significance between C26 TCCM/HCT116 TCCM control and specific compound. * $P \leq 0.05$, ** $P \leq 0.01$, *** $P \leq 0.001$, **** $P \leq 0.0001$; by two-way ANOVA with Dunnett's multiple-comparison test.21

Figure 13: Dose-response curves for the selected compounds. Representative dose-response curves with (a) YC-1, (b) DPI, (c) Olomoucine, (d) BAY 43-9006, (e) GF-109203X, (f) OLDA, (g) BioF and (h) ATGLi. Free glycerol was released into the medium of the differentiated 3T3-L1 adipocytes treated with C26 TCCM with different concentrations of the selected compounds for 24 hours. $n = 3$, data shown are mean \pm s.e.m., IC_{50} values were calculated by Least squares fit.23

Figure 14: Forskolin treatment induced intracellular cAMP levels. (a) Accumulated intracellular cAMP levels upon treatment with 10 μM of forskolin (Forsk) for 4 hours in different cell densities of 3T3-L1 adipocytes. (b) cAMP levels of the 3T3-L1 adipocytes were treated with the conditions for 4 hours. (a, b) $n = 3$, data shown are mean \pm s.e.m., **** $P \leq 0.0001$; by one-way ANOVA with Šídák's multiple-comparison test.24

Figure 15: C26 TCCM treatment did not influence fatty acid uptake in the 3T3-L1 adipocytes. The fatty acid uptake over time of the differentiated 3T3-L1 adipocytes after being treated with indicated conditions for 24 hours was assessed using a Varioskan™ LUX multimode microplate reader (Thermo Scientific™). Representative fatty acid uptake is presented as (a) uptake kinetics over time and (b) end-stage uptake value. $n = 3$, data shown are mean \pm s.e.m., ** $P \leq 0.01$; by one-way ANOVA with Šídák's multiple-comparison test.24

Figure 16: OCR and ECAR measurements of 3T3-L1 adipocytes. The mitochondrial function of differentiated 3T3-L1 adipocytes treated with indicated conditions for 24 hours was assessed using an extracellular flux analyzer (Seahorse Bioscience). Representative (a) OCR and (b) ECAR kinetics are shown. 10 μM isoproterenol, 4 μM oligomycin, 0.75 μM FCCP, and 0.5 μM rotenone together with 0.5 μM antimycin A (Rot + AA) were added at the indicated time points. (c) Basal respiration, (d) maximal respiration, and (e) spare respiratory capacity was calculated as mentioned in Methods (Seahorse Mito Stress assay). $n = 6-8$, data shown are mean \pm s.e.m., one-way ANOVA with Šídák's multiple-comparison test was performed.25

Figure 17: Viability of 3T3-L1 adipocytes and C26 cells. Cells viability was tested (a) by CellTox™ Green Cytotoxicity assay on the differentiated 3T3-L1 adipocytes treated with C26 TCCM together with selected compounds for 24 hours and (b) by crystal violet assay on the C26 cells treated with selected compounds for different time points. $n = 3$, data shown are (a) mean \pm s.e.m. or (b) mean, * $P \leq 0.05$, **** $P \leq 0.0001$; by one-way ANOVA with Šídák's multiple-comparison test.27

Figure 18: shRNA mediated knockdown of Nox3 and Nox4 inhibit lipolysis in vitro. 3T3-L1 adipocytes were infected with various concentrations of lentiviruses containing scrambled and shRNAs against (a) Nox3 and (b) Nox4, and a lipolysis assay was performed. (c) 3T3-L1 adipocytes were treated with respective conditions and infected with lentiviruses containing selected shRNAs against Nox3 and Nox4. A lipolysis assay was performed after 24 hours of treatment. $n = 3$, data shown are mean \pm s.e.m., § represents significance against respective Scr samples, $*P \leq 0.05$, $**P \leq 0.01$, $***P \leq 0.001$, $****P \leq 0.0001$; by two-way ANOVA with Tukey's multiple-comparison test.28

Figure 19: Mice treated with DPI display normal body weight, tissue weight, and plasma glycerol level. Seven weeks old male Balb/c mice were injected subcutaneously with either 0.5 mg/kg of DPI or Vehicle once daily. Mice were sacrificed five days post-injection. (a) Initial body composition (body weight, lean and fat mass) measured by Echo-MRI before treatment initiation. (b) Percent change in the body weight after the treatment. (c) The weight of the tissues (Liver, BAT, eWAT, iWAT, and GC + Soleus) was measured five days after the first injection. (d) Tissue weights shown in **Figure 19c** are normalized to the initial body weight. (e) Average food consumption of the mice. (f) Plasma glycerol levels were measured over the treatment period and before sacrificing the mice. (a-d, f) $n = 5$ per group, (e) $n = 2$ per group; data shown are mean \pm s.e.m., two-tailed t-test was performed.29

Figure 20: DPI treatment did not elicit liver toxicity. Blood samples were collected from the animals shown in **Figure 19** before sacrificing. Plasma was extracted and analyzed for specific metabolites. (a) The ratio of AST to ALT levels, (b) ALP, (c) LDH, (d) random post-prandial glucose, (e) NEFA, (f) triglycerides, (g) cholesterol, and (h) LDL levels in the plasma of mice treated with DPI or Vehicle. $n = 5$ per group, data shown are mean \pm s.e.m., $**P \leq 0.01$; by two-tailed t-test.30

Figure 21: Mice treated with DPI have reduced Nox3 levels in iWAT. Expression levels of genes involved in fatty acid metabolism and DPI targeted genes in the (a) iWAT and (b) liver of the animals treated with DPI or Vehicle. $n = 5$ per group, data shown are mean \pm s.e.m., $*P \leq 0.05$; by two-tailed t-test.30

Figure 22: DPI treatment in the C26 tumor-bearing mice did not prevent cachexia development. Eight weeks old male Balb/c mice were injected subcutaneously with either 5×10^5 C26 cells or PBS. 9 days post-inoculation, mice were injected subcutaneously with either 0.5 mg/kg of DPI or Vehicle once daily. Tumor-bearing mice were sacrificed by cervical dislocation after cachexia development, and non-tumor-bearing mice were sacrificed together with the tumor-bearing mice. (a) Initial and (b) final carcass body weight of the mice. (c) Percent change in the body weight, lean and fat mass at the end of the experiment. (d) The weight of the tissues (Liver, BAT, eWAT, iWAT, GC + Soleus, heart) and (e) tumor were measured at the end of the experiment. (f) Cachexia index of the tumor-bearing mice as calculated by the formula mentioned in the Methods (Cachexia index). (g) Average food consumption of the mice. (h) Tissue weights shown in **Figure 22d** are normalized to the initial body weight. (i) Bodyweight development of the mice in the last ten days before sacrifice depicted as the percentage change in weight relative to that of 10 days before prep. $n = 8$ (Veh, DPI), 12 (C26-Veh) or 14 (C26-DPI), data shown are mean \pm s.e.m., $*P \leq 0.05$, $**P \leq 0.01$, $***P \leq 0.001$ and $****P \leq 0.0001$; by (a-d, g, h) one-way ANOVA with Šidák's multiple-comparison test, (e, f) by two-tailed t-test or (i) two-way ANOVA with Tukey's multiple-comparison test.31

Figure 23: DPI treatment increased NEFA levels in the C26 tumor-bearing mice. Blood samples were collected from the animals shown in **Figure 22** before sacrificing. Plasma was extracted and analyzed for specific metabolites. (a) The ratio of AST to ALT levels, (b) glucose, (c) NEFA, (d) triglycerides, (e) cholesterol, (f) HDL, (g) LDL, and (h) total protein levels in the plasma of the animals collected before sacrificing. $n = 8$ (Veh, DPI), 12 (C26-Veh) or 14 (C26-DPI), data shown are mean \pm s.e.m., $**P \leq 0.01$ and $***P \leq 0.001$; by one-way ANOVA with Šidák's multiple-comparison test.33

Figure 24: DPI treatment did not inhibit the induced lipolysis in vivo. Reaction kinetics of NADH oxidase activity in (a) iWAT protein lysate and (b) plasma of the mice. NADH oxidase activity was measured in (c) iWAT protein lysate and (d) plasma of the mice. Proteins extracted from iWAT were immunoblotted for specific proteins. (e) Representative immunoblots are shown here, and (f) quantification was performed as mentioned in Methods (SDS-PAGE and immunoblotting). p-HSL(Ser565) levels were normalized with the total HSL and p-ERK1/2 with the total

ERK1/2. VCP was used as a loading control. $n = 8$ (Veh, DPI), 12 (C26-Veh) or 14 (C26-DPI), data shown are mean \pm s.e.m., and one-way ANOVA with Šidák's multiple-comparison test was performed.....34

Figure 25: Assessing systemic effects of OLDA treatment. Seven weeks old male Balb/c mice were injected intraperitoneally with either 1 mg/kg, 5 mg/kg of OLDA, or vehicle once daily. ipGTT was performed after four days of treatment, followed by two days of washout before restarting the treatment for another four days. Mice were sacrificed after the treatment. **(a)** Initial and **(b)** final body weight. **(c)** Percent change in the body weight after the treatment. **(d)** Average food consumption of the mice **(e)** Weight of the tissues (Liver, BAT, eWAT, iWAT, GC + Soleus, and heart) measured at the end of the experiment. **(f)** Tissue weights shown in **Figure 25e** are normalized to the initial body weight. **(g)** Glucose levels of the fasted mice before performing ipGTT. **(h)** Plasma glucose kinetics and **(i)** area under glucose curve obtained from the ipGTT. **(a-c, e-i)** $n = 4$ per group, **(d)** $n = 2$ per group; data shown are mean \pm s.e.m., and one-way ANOVA with Šidák's multiple-comparison test was performed.....36

Figure 26: OLDA treatment did not elicit liver toxicity. Blood samples were collected from the animals shown in **Figure 25** before sacrificing. Plasma was extracted and analyzed for specific metabolites. **(a)** The ratio of AST to ALT levels, **(b)** random post-prandial glucose, **(c)** triglycerides, **(d)** NEFA, **(e)** cholesterol, **(f)** HDL, **(g)** LDL, and **(h)** creatinine levels in the plasma of mice treated with OLDA or Vehicle. $n = 4$ per group, data shown are mean \pm s.e.m., and one-way ANOVA with Šidák's multiple-comparison test was performed.37

Figure 27: Proteins extracted from iWAT and eWAT were immunoblotted for specific proteins. Immunoblots and quantification of particular proteins separated from **(a, b)** iWAT and **(c, d)** eWAT protein extracts. p-HSL(Ser565) levels were normalized with the total HSL and p-ACC α (Ser79) with β -Actin, which was used as the loading control. $n = 4$ per group, data shown are mean \pm s.e.m., * $P \leq 0.05$, and *** $P \leq 0.01$; by one-way ANOVA with Šidák's multiple-comparison test.38

Figure 28: OLDA treatment in the C26 tumor-bearing mice did not prevent cachexia development. Eight weeks old male Balb/c mice were injected subcutaneously with either 1×10^6 C26 cells or PBS. Seven days post-inoculation, mice were injected intraperitoneally with either 5 mg/kg of OLDA or Vehicle once daily. Tumor-bearing mice were sacrificed by cervical dislocation after cachexia development, and non-tumor-bearing mice were sacrificed together with the tumor-bearing mice. **(a)** Initial and **(b)** final carcass body weight of the mice. **(c)** Percent change in the body weight, lean and fat mass at the end of the experiment. **(d)** The weight of the tissues (Liver, BAT, eWAT, iWAT, GC + Soleus, heart) and **(e)** tumor were measured at the end of the experiment. **(f)** Cachexia index of the tumor-bearing mice as calculated by the formula mentioned in the Methods (Cachexia index). **(g)** Average food consumption of the mice. **(h)** Tissue weights shown in **Figure 28d** are normalized to the initial body weight. **(i)** Bodyweight development of the mice in the last ten days before sacrifice depicted as the percentage change in weight relative to that of 10 days before prep. $n = 8$ (Veh, OLDA), 12 (C26-Veh) or 14 (C26-OLDA), data shown are mean \pm s.e.m., * $P \leq 0.05$, ** $P \leq 0.01$, *** $P \leq 0.001$ and **** $P \leq 0.0001$; by **(a-d, g, h)** one-way ANOVA with Šidák's multiple-comparison test, **(e, f)** by two-tailed t-test or **(i)** two-way ANOVA with Tukey's multiple-comparison test.39

Figure 29: OLDA treatment increased plasma protein levels in the C26 tumor-bearing mice. Blood samples were collected from the animals shown in **Figure 28** before sacrificing. Plasma was extracted and analyzed for specific metabolites. **(a)** The ratio of AST to ALT levels, **(b)** glucose, **(c)** NEFA, **(d)** triglycerides, **(e)** glycerol, **(f)** HDL, **(g)** LDL, and **(h)** total protein levels in the plasma of the animals collected before sacrificing. $n = 8$ (Veh, OLDA), 12 (C26-Veh) or 14 (C26-OLDA), data shown are mean \pm s.e.m., * $P \leq 0.05$, ** $P \leq 0.01$, *** $P \leq 0.001$ and **** $P \leq 0.0001$; by one-way ANOVA with Šidák's multiple-comparison test.40

Figure 30: OLDA treatment decreased the TRVP-1 levels in the iWAT of tumor-bearing mice. **(a)** Immunoblots and **(b)** quantification of specific proteins separated from iWAT protein extracts. p-ACC α (Ser79) levels were normalized with the total ACC α and p-AMPK α (Thr172) with total AMPK α , and β -Actin was used as the loading control. $n = 8$ (Veh, OLDA), 12 (C26-Veh), or 14 (C26-OLDA), data shown are mean \pm s.e.m., one-way ANOVA with Šidák's multiple-comparison test was performed.....41

Figure 31: C26 TCCM-induced myotube atrophy is rescued upon BioF treatment. (a) C2C12 myotube diameter was measured using ImageJ as mentioned in the Methods (Staining and analysis of myotube diameter) after treating with indicated conditions for 48 hours. (b) Representative fluorescence images of the C2C12 myotubes. Myotubes are labeled green using MitoTracker™ Green FM dye, and nuclei are labeled blue using DAPI. Scale bar: 100 μ m.42

Figure 32: Mice treated with BioF display average body and tissue weight. Nine weeks old male Balb/c mice were injected intraperitoneally with either 0.5 mg/kg, 1 mg/kg of BioF, Vehicle once daily, or 1 mg/kg of BioF twice daily. Mice were sacrificed after four days of treatment. (a) Initial and (b) final body weight. (c) Percent change in the body weight, lean and fat mass after the treatment. (d) Average food consumption of the mice (e) Weight of the tissues (Liver, BAT, eWAT, iWAT, GC + Soleus, and heart) measured at the end of the experiment. (f) Tissue weights shown in Figure 32e are normalized to the initial body weight. (a-c, e, f) n = 3 (Veh) or 4 (BioF - 0.5, 1, 1+1), (d) n = 2 per group; data shown are mean \pm s.e.m., and one-way ANOVA with Šídák's multiple-comparison test was performed.43

Figure 33: BioF treatment did not elicit liver toxicity. Blood samples were collected from the animals shown in Figure 32 before sacrificing. Plasma was extracted and analyzed for specific metabolites. (a) The ratio of AST to ALT levels, (b) random post-prandial glucose, (c) triglycerides, (d) NEFA, (e) percent change of glycerol, (f) HDL, (g) LDL, and (h) total protein levels in the plasma of mice treated with BioF or Vehicle. n = 3 (Veh) or 4 (BioF - 0.5, 1, 1+1), data shown are mean \pm s.e.m., *P \leq 0.05; by one-way ANOVA with Šídák's multiple-comparison test.44

Figure 34: Mice treated with BioF had increased weight gain. Eight weeks old male Balb/c mice were injected intraperitoneally with either 5 mg/kg of BioF or Vehicle once daily. Mice were sacrificed after four days of treatment. (a) Initial and (b) final body weight. (c) Percent change in the body weight, lean and fat mass after the treatment. (d) Average food consumption of the mice (e) Weight of the tissues (Liver, BAT, eWAT, iWAT, GC + Soleus, and heart) measured at the end of the experiment. (f) Tissue weights shown in Figure 34e are normalized to the initial body weight. (a-c, e, f) n = 3 (Veh) or 4 (BioF - 5), (d) n = 2 per group; data shown are mean \pm s.e.m., **P < 0.01; by two-tailed t-test.45

Figure 35: A higher dose of BioF treatment did not elicit liver toxicity. Blood samples were collected from the animals shown in Figure 34 before sacrificing. Plasma was extracted and analyzed for specific metabolites. (a) The ratio of AST to ALT levels, (b) random post-prandial glucose, (c) triglycerides, (d) NEFA, (e) percent change of glycerol, (f) HDL, (g) LDL, and (h) total protein levels in the plasma of mice treated with BioF or Vehicle. n = 3 (Veh) or 4 (BioF - 5); data shown are mean \pm s.e.m., and a two-tailed t-test was performed.45

Figure 36: BioF treatment increased the Adiponectin (AdipoQ) levels in the iWAT and eWAT. Expression levels of (a) AdipoQ, (b) Plin-2, (c) Dgat-2, (d) Glut-1, (e) Pdk-4, and (f) Pgc-1a transcripts in the iWAT and eWAT of the animals treated with BioF or Vehicle. n = 3 (Veh) or 4 (BioF - 5); data shown are mean \pm s.e.m., *P \leq 0.05; by two-tailed t-test.46

Figure 37: BioF treatment in the C26 tumor-bearing mice did not prevent cachexia development. Eight weeks old male Balb/c mice were injected subcutaneously with either 1×10^6 C26 cells or PBS. Seven days post-inoculation, mice were injected intraperitoneally with either 5 mg/kg of BioF or Vehicle once daily. Tumor-bearing mice were sacrificed by cervical dislocation after cachexia development, and non-tumor-bearing mice were sacrificed together with the tumor-bearing mice. (a) Initial and (b) final carcass body weight of the mice. (c) Percent change in the body weight, lean and fat mass at the end of the experiment. (d) The weight of the tissues (Liver, BAT, eWAT, iWAT, GC + Soleus, heart) and (e) tumor were measured at the end of the experiment. (f) Cachexia index of the tumor-bearing mice as calculated by the formula mentioned in the Methods (Cachexia index). (g) Average food consumption of the mice. (h) Tissue weights shown in Figure 37d are normalized to the initial body weight. (i) Bodyweight development of the mice in the last ten days before sacrifice depicted as the percentage change in weight relative to that of 10 days before prep. n = 6 (Veh, BioF), or 10 (C26-Veh, C26-BioF), data shown are mean \pm s.e.m., *P \leq 0.05, **P \leq 0.01, ***P \leq 0.001 and ****P \leq 0.0001; by (a-d, g, h) one-way ANOVA with Šídák's multiple-comparison test, (e, f) by two-tailed t-test or (i) two-way ANOVA with Tukey's multiple-comparison test.48

Figure 38: BioF treatment did not inhibit the C26-induced increase in NEFA levels. Blood samples were collected from the animals shown in **Figure 37** before sacrificing. Plasma was extracted and analyzed for specific metabolites. **(a)** The ratio of AST to ALT levels, **(b)** random post-prandial glucose, **(c)** NEFA, **(d)** triglycerides, **(e)** free glycerol, **(f)** HDL, **(g)** LDL, and **(h)** total protein levels in the plasma of the animals. $n = 6$ (Veh, BioF), 10 (C26-Veh), or 8 (C26-BioF); data shown are mean \pm s.e.m., $**P \leq 0.01$, and $****P \leq 0.0001$; by one-way ANOVA with Šidák's multiple-comparison test.....49

Figure 39: BioF treatment decreased the p-HSL(Ser563) levels in the iWAT and eWAT. **(a, c)** Immunoblots and **(b, d)** quantification of specific proteins separated from **(a, b)** iWAT and **(c, d)** eWAT protein extracts. p-HSL(Ser565) and p-HSL(Ser563) levels were normalized with the total HSL, and β -Actin was used as the loading control. $n = 6$ (Veh, BioF), 10 (C26-Veh), or 8 (C26-BioF), data shown are mean \pm s.e.m., $*P \leq 0.05$ and $**P \leq 0.01$; by one-way ANOVA with Šidák's multiple-comparison test.....50

Figure 40: BioF treatment decreased the Pdk-4 transcript levels in tumor-bearing mice. Expression levels of **(a)** Fbxo-32, **(b)** Foxo-1, **(c)** Pdk-4, **(d)** Bnip-3, and **(e)** Glut-4 transcripts in the GC muscle of the animals. $n = 6$ (Veh, BioF), or 10 (C26-Veh), or 8 (C26-BioF), data shown are mean \pm s.e.m., $*P \leq 0.05$, $**P \leq 0.01$, $***P \leq 0.001$ and $****P \leq 0.0001$; by one-way ANOVA with Šidák's multiple-comparison test.51

Figure 41: Effects of holding C26 tumor-bearing mice in thermoneutral condition. Twelve weeks old male Balb/c mice were allowed to acclimatize to the thermoneutral condition (30 °C) for a week. Control mice were housed in a housing temperature of 21 °C. Mice were injected subcutaneously with either 1×10^6 C26 cells or PBS. From the next day onwards, they were injected intraperitoneally with either 5 mg/kg of BioF or Vehicle once daily. Tumor-bearing mice were sacrificed by cervical dislocation after cachexia development, and non-tumor-bearing mice were sacrificed together with the tumor-bearing mice. **(a)** Initial and **(b)** final carcass body weight of the mice. **(c)** Percent change in the body weight, lean and fat mass at the end of the experiment. **(d)** The weight of the tissues (Liver, BAT, eWAT, iWAT, GC + Soleus, heart) and **(e)** tumor were measured at the end of the experiment. **(f)** Cachexia index of the tumor-bearing mice as calculated by the formula mentioned in the Methods (Cachexia index). **(g)** Average food consumption of the mice. **(h)** Tissue weights shown in **Figure 41d** are normalized to the initial body weight. **(i)** Bodyweight development of the mice in the last ten days before sacrifice depicted as the percentage change in weight relative to that of 10 days before prep. $n = 4$ (Veh); 6 (Veh, BioF), or 12 (C26-Veh, C26-BioF) at 30 °C, data shown are mean \pm s.e.m., $*P \leq 0.05$, $**P \leq 0.01$, $***P \leq 0.001$ and $****P \leq 0.0001$; by **(a-d, g, h)** one-way ANOVA with Šidák's multiple-comparison test, **(e, f)** by two-tailed t-test or **(i)** two-way ANOVA with Tukey's multiple-comparison test.....52

Figure 42: BioF treatment in thermoneutral conditions reduced the C26-induced increase in cholesterol levels. Blood samples were collected from the animals shown in **Figure 41** before sacrificing. Plasma was extracted and analyzed for specific metabolites. **(a)** The ratio of AST to ALT levels, **(b)** random post-prandial glucose, **(c)** NEFA, **(d)** triglycerides, **(e)** cholesterol, **(f)** HDL, **(g)** LDL, and **(h)** total protein levels in the plasma of the animals. $n = 4$ (Veh); 6 (Veh, BioF), or 12 (C26-Veh, C26-BioF) at 31 °C; data shown are mean \pm s.e.m., $*P \leq 0.05$, $**P \leq 0.01$, $***P \leq 0.001$ and $****P \leq 0.0001$; by one-way ANOVA with Šidák's multiple-comparison test.....53

6.3. List of Tables

Table 1: Information about the selected compounds.	21
Table 2: Cell culture medium and their composition	65
Table 3: The freezing medium and the frozen cell number for each cell line	66
Table 4: Assay protocol for the Seahorse Mito Stress assay	70
Table 5: Composition of the Seahorse Mito Stress assay medium	71
Table 6: Volume of the assay compounds loaded into the ports of the XF Sensor cartridge	71
Table 7: Composition of the lipoflex mix	73
Table 8: Solvents used for preparing the compounds for injection and the injection site used for in vivo experiments.	76
Table 9: Compounds screened in this study.	78
Table 10: Primary and secondary antibodies used in this study.	79

6.4. Bibliography

- A. Sherry, B., GELIN, J., FONG, Y., MARANO, M., WEI, H., CERAMI, A., F. LOWRY, S., G. LUNDHOLM, K., & L. MOLDAWER, L. (1989). Anticachectin / tumor attenuate tumor models necrosis antibodies in development of cachexia. *The FASEB Journal*, *3*, 1956–1962.
- Abrigo, J., Elorza, A. A., Riedel, C. A., Vilos, C., Simon, F., Cabrera, D., Estrada, L., & Cabello-Verrugio, C. (2018). Role of oxidative stress as key regulator of muscle wasting during cachexia. *Oxidative Medicine and Cellular Longevity*, *2018*. <https://doi.org/10.1155/2018/2063179>
- Adnane, L., Trail, P. A., Taylor, I., & Wilhelm, S. M. (2006). Sorafenib (BAY 43-9006, Nexavar®), a Dual-Action Inhibitor That Targets RAF/MEK/ERK Pathway in Tumor Cells and Tyrosine Kinases VEGFR/PDGFR in Tumor Vasculature. *Methods in Enzymology*, *407*(05), 597–612. [https://doi.org/10.1016/S0076-6879\(05\)07047-3](https://doi.org/10.1016/S0076-6879(05)07047-3)
- Agustsson, T., Rydén, M., Hoffstedt, J., Van Harmelen, V., Dicker, A., Laurencikiene, J., Isaksson, B., Permert, J., & Arner, P. (2007). Mechanism of increased lipolysis in cancer cachexia. *Cancer Research*, *67*(11), 5531–5537. <https://doi.org/10.1158/0008-5472.CAN-06-4585>
- Allen, D. L., Cleary, A. S., Speaker, K. J., Lindsay, S. F., Uyenishi, J., Reed, J. M., Madden, M. C., & Mehan, R. S. (2008). Myostatin, activin receptor IIb, and follistatin-like-3 gene expression are altered in adipose tissue and skeletal muscle of obese mice. *American Journal of Physiology - Endocrinology and Metabolism*, *294*(5), 918–927. <https://doi.org/10.1152/ajpendo.00798.2007>
- Argilés, J. M., Busquets, S., Stemmler, B., & López-Soriano, F. J. (2014). Cancer cachexia: Understanding the molecular basis. *Nature Reviews Cancer*, *14*(11), 754–762. <https://doi.org/10.1038/nrc3829>
- Argilés, J. M., López-Soriano, F. J., Stemmler, B., & Busquets, S. (2017). Novel targeted therapies for cancer cachexia. *Biochemical Journal*, *474*(16), 2663–2678. <https://doi.org/10.1042/BCJ20170032>
- Arner, P., & Langin, D. (2014). Lipolysis in lipid turnover, cancer cachexia, and obesity-induced insulin resistance. *Trends in Endocrinology and Metabolism*, *25*(5), 255–262. <https://doi.org/10.1016/j.tem.2014.03.002>
- Asp, M. L., Tian, M., Wendel, A. A., & Belury, M. A. (2010). Evidence for the contribution of insulin resistance to the development of cachexia in tumor-bearing mice. *International Journal of Cancer*, *126*(3), 756–763. <https://doi.org/10.1002/ijc.24784>
- Badowski, M. E., & Perez, S. E. (2016). Clinical utility of dronabinol in the treatment of weight loss associated with HIV and AIDS. *HIV/AIDS - Research and Palliative Care*, *8*, 37–45. <https://doi.org/10.2147/HIV.S81420>
- Badowski, M. E., & Yanful, P. K. (2018). Dronabinol oral solution in the management of anorexia and weight loss in AIDS and cancer. *Therapeutics and Clinical Risk Management*, *14*, 643–651. <https://doi.org/10.2147/TCRM.S126849>
- Ballarò, R., Costelli, P., & Penna, F. (2016). Animal models for cancer cachexia. *Current Opinion in Supportive and Palliative Care*, *10*(4), 281–287. <https://doi.org/10.1097/SPC.0000000000000233>
- Baltgalvis, K. A., Berger, F. G., Pena, M. M. O., Davis, J. M., Muga, S. J., & Carson, J. A. (2008). Interleukin-6 and cachexia in ApcMin/+ mice. *American Journal of Physiology - Regulatory Integrative and Comparative Physiology*, *294*(2), 393–401. <https://doi.org/10.1152/ajpregu.00716.2007>
- Baracos, V. E., Martin, L., Korc, M., Guttridge, D. C., & Fearon, K. C. H. (2018). Cancer-associated cachexia. *Nature Reviews Disease Primers*, *4*, 1–18. <https://doi.org/10.1038/nrdp.2017.105>
- Bastos, D. B., Sarafim-Silva, B. A. M., Sundefeld, M. L. M. M., Ribeiro, A. A., Brandão, J. D. P., Biasoli, É. R., Miyahara, G. I., Casarini, D. E., & Bernabé, D. G. (2018). Circulating catecholamines are associated with biobehavioral factors and anxiety symptoms in head and neck cancer patients. *PLoS ONE*, *13*(8), 1–18. <https://doi.org/10.1371/journal.pone.0202515>
- Batista, M. L., Oliven, M., Alcantara, P. S. M., Sandoval, R., Peres, S. B., Neves, R. X., Silverio, R., Maximiano, L. F., Otoch, J. P., & Seelaender, M. (2013). Adipose tissue-derived factors as potential biomarkers in

- cachectic cancer patients. *Cytokine*, 61(2), 532–539. <https://doi.org/10.1016/j.cyto.2012.10.023>
- Bayliss, T. J., Smith, J. T., Schuster, M., Dragnev, K. H., & Rigas, J. R. (2011). A humanized anti-IL-6 antibody (ALD518) in non-small cell lung cancer. *https://doi.org/10.1517/14712598.2011.627850*, 11(12), 1663–1668. <https://doi.org/10.1517/14712598.2011.627850>
- Bedard, N., Jammoul, S., Moore, T., Wykes, L., L. Hallauer, P., E. M. Hastings, K., Stretch, C., Baracos, V., Chevalier, S., Plourde, M., Coyne, E., & S. Wing, S. (2015). Inactivation of the ubiquitin-specific protease 19 deubiquitinating enzyme protects. *FASEB Journal*, 29, 3889–3898.
- Beiroa, D., Imbernon, M., Gallego, R., Senra, A., Herranz, D., Villarroya, F., Serrano, M., Fernø, J., Salvador, J., Escalada, J., Dieguez, C., Lopez, M., Frühbeck, G., & Nogueiras, R. (2014). GLP-1 agonism stimulates brown adipose tissue thermogenesis and browning through hypothalamic AMPK. *Diabetes*, 63(10), 3346–3358. <https://doi.org/10.2337/db14-0302>
- Beltrà, M., Pin, F., Ballarò, R., Costelli, P., & Penna, F. (2021). Mitochondrial dysfunction in cancer cachexia: Impact on muscle health and regeneration. *Cells*, 10(11), 1–18. <https://doi.org/10.3390/cells10113150>
- Bennani-Baiti, N., & Walsh, D. (2011). Animal models of the cancer anorexia-cachexia syndrome. *Supportive Care in Cancer*, 19(9), 1451–1463. <https://doi.org/10.1007/s00520-010-0972-0>
- Benny Klimek, M. E., Aydogdu, T., Link, M. J., Pons, M., Koniaris, L. G., & Zimmers, T. A. (2010). Acute inhibition of myostatin-family proteins preserves skeletal muscle in mouse models of cancer cachexia. *Biochemical and Biophysical Research Communications*, 391(3), 1548–1554. <https://doi.org/10.1016/j.bbrc.2009.12.123>
- Bhatia, B., Potts, C. R., Guldal, C., Choi, S. P., Korshunov, A., Pfister, S., Kenney, A. M., & Nahlé, Z. A. (2012). Hedgehog-mediated regulation of PPARc controls metabolic patterns in neural precursors and shh-driven medulloblastoma. *Acta Neuropathologica*, 123(4), 587–600. <https://doi.org/10.1007/s00401-012-0968-6>
- Bing, C., Taylor, S., Tisdale, M. J., & Williams, G. (2001). Cachexia in MAC16 adenocarcinoma: Suppression of hunger despite normal regulation of leptin, insulin and hypothalamic neuropeptide Y. *Journal of Neurochemistry*, 79(5), 1004–1012. <https://doi.org/10.1046/j.1471-4159.2001.00639.x>
- Block, K., & Gorin, Y. (2012). Aiding and abetting roles of NOX oxidases in cellular transformation. *Nature Reviews Cancer*, 12(9), 627–637. <https://doi.org/10.1038/nrc3339>
- Blüher, M. (2014). Adipokines - removing road blocks to obesity and diabetes therapy. *Molecular Metabolism*, 3(3), 230–240. <https://doi.org/10.1016/j.molmet.2014.01.005>
- Blüher, M., & Mantzoros, C. S. (2015). From leptin to other adipokines in health and disease: Facts and expectations at the beginning of the 21st century. *Metabolism: Clinical and Experimental*, 64(1), 131–145. <https://doi.org/10.1016/j.metabol.2014.10.016>
- Bogdanovich, S., Krag, T. O. B., Barton, E. R., Morris, L. D., Whittemore, L. A., Ahima, R. S., & Khurana, T. S. (2002). Functional improvement of dystrophic muscle by myostatin blockade. *Nature*, 420(6914), 418–421. <https://doi.org/10.1038/nature01154>
- Borner, T., Liberini, C. G., Lutz, T. A., & Riediger, T. (2018). Brainstem GLP-1 signalling contributes to cancer anorexia-cachexia syndrome in the rat. *Neuropharmacology*, 131, 282–290. <https://doi.org/10.1016/J.NEUROPHARM.2017.12.024>
- Bost, F., & Kaminski, L. (2019). The metabolic modulator PGC-1 α in cancer. *American Journal of Cancer Research*, 9(2), 198–211. <http://www.ncbi.nlm.nih.gov/pubmed/30906622> <http://www.pubmedcentral.nih.gov/articlerender.fcgi?artid=PMC6405967>
- Bourdel-Marchasson, I., Blanc-Bisson, C., Doussau, A., Germain, C., Blanc, J. F., Dauba, J., Lahmar, C., Terrebonne, E., Lecaille, C., Ceccaldi, J., Cany, L., Lavau-Denes, S., Houede, N., Chomy, F., Durrieu, J., Soubeyran, P., Senesse, P., Chene, G., & Fonck, M. (2014). Nutritional advice in older patients at risk of malnutrition during treatment for chemotherapy: A two-year randomized controlled trial. *PLoS*

- ONE, 9(9). <https://doi.org/10.1371/journal.pone.0108687>
- Braun, T. P., Zhu, X., Szumowski, M., Scott, G. D., Grossberg, A. J., Levasseur, P. R., Graham, K., Khan, S., Damaraju, S., Colmers, W. F., Baracos, V. E., & Marks, D. L. (2011). Central nervous system inflammation induces muscle atrophy via activation of the hypothalamic-pituitary-adrenal axis. *Journal of Experimental Medicine*, 208(12), 2449–2463. <https://doi.org/10.1084/jem.20111020>
- Breen, D. M., Kim, H., Bennett, D., Calle, R. A., Collins, S., Esquejo, R. M., He, T., Joaquim, S., Joyce, A., Lambert, M., Lin, L., Pettersen, B., Qiao, S., Rossulek, M., Weber, G., Wu, Z., Zhang, B. B., & Birnbaum, M. J. (2020). GDF-15 Neutralization Alleviates Platinum-Based Chemotherapy-Induced Emesis, Anorexia, and Weight Loss in Mice and Nonhuman Primates. *Cell Metabolism*, 32(6), 938–950.e6. <https://doi.org/10.1016/j.cmet.2020.10.023>
- Brown, J. L., Rosa-Caldwell, M. E., Lee, D. E., Blackwell, T. A., Brown, L. A., Perry, R. A., Haynie, W. S., Hardee, J. P., Carson, J. A., Wiggs, M. P., Washington, T. A., & Greene, N. P. (2017). Mitochondrial degeneration precedes the development of muscle atrophy in progression of cancer cachexia in tumour-bearing mice. *Journal of Cachexia, Sarcopenia and Muscle*, 8(6), 926–938. <https://doi.org/10.1002/jcsm.12232>
- Bruns, C. J., Harbison, M. T., Kuniyasu, H., Eue, I., & Fidler, I. J. (1999). In vivo selection and characterization of metastatic variants from human pancreatic adenocarcinoma by using orthotopic implantation in nude mice. *Neoplasia (New York, N.Y.)*, 1(1), 50–62. <https://doi.org/10.1038/sj.neo.7900005>
- Buck, M., & Chojkier, M. (1996). Muscle wasting and dedifferentiation induced by oxidative stress in a murine model of cachexia is prevented by inhibitors of nitric oxide synthesis and antioxidants. *EMBO Journal*, 15(8), 1753–1765. <https://doi.org/10.1002/j.1460-2075.1996.tb00524.x>
- Bujak, J. K., Kosmala, D., Szopa, I. M., Majchrzak, K., & Bednarczyk, P. (2019). Inflammation, Cancer and Immunity—Implication of TRPV1 Channel. *Frontiers in Oncology*, 9(October), 1–16. <https://doi.org/10.3389/fonc.2019.01087>
- Byerley, L. O., Lee, S. H., Redmann, S., Culberson, C., Clemens, M., & Lively, M. O. (2010). Evidence for a novel serum factor distinct from zinc alpha-2 glycoprotein that promotes body fat loss early in the development of cachexia. *Nutrition and Cancer*, 62(4), 484–494. <https://doi.org/10.1080/01635580903441220>
- Cahlin, C., Körner, A., Axelsson, H., Wang, W., Lundholm, K., & Svanberg, E. (2000). Experimental Cancer Cachexia: The Role of Host-derived Cytokines Interleukin (IL)-6, IL-12, Interferon- γ , and Tumor Necrosis Factor α Evaluated in Gene Knockout, Tumor-bearing Mice on C57 Bl Background and Eicosanoid-dependent Cachexia1. *Cancer Research*, 60(19), 5488–5493.
- Cai, D., Frantz, J. D., Tawa, N. E., Melendez, P. A., Oh, B. C., Lidov, H. G. W., Hasselgren, P. O., Frontera, W. R., Lee, J., Glass, D. J., & Shoelson, S. E. (2004). IKK β /NF- κ B activation causes severe muscle wasting in mice. *Cell*, 119(2), 285–298. <https://doi.org/10.1016/j.cell.2004.09.027>
- Cao, D. xing, Wu, G. hao, Yang, Z. ang, Zhang, B., Jiang, Y., Han, Y. song, He, G. dong, Zhuang, Q., Wang, Y. fu, Huang, Z. lin, & Xi, Q. lei. (2010). Role of β 1-adrenoceptor in increased lipolysis in cancer cachexia. *Cancer Science*, 101(7), 1639–1645. <https://doi.org/10.1111/j.1349-7006.2010.01582.x>
- Choe, S. S., Huh, J. Y., Hwang, I. J., Kim, J. I., & Kim, J. B. (2016). Adipose tissue remodeling: Its role in energy metabolism and metabolic disorders. *Frontiers in Endocrinology*, 7(APR), 1–16. <https://doi.org/10.3389/fendo.2016.00030>
- Chu, C. J., Huang, S. M., De Petrocellis, L., Bisogno, T., Ewing, S. A., Miller, J. D., Zipkin, R. E., Daddario, N., Appendino, G., Di Marzo, V., & Walker, J. M. (2003). N-oleoyldopamine, a novel endogenous capsaicin-like lipid that produces hyperalgesia. *Journal of Biological Chemistry*. <https://doi.org/10.1074/jbc.M211231200>
- Chu, Z. L., Carroll, C., Chen, R., Alfonso, J., Gutierrez, V., He, H., Lucman, A., Xing, C., Sebring, K., Zhou, J., Wagner, B., Unett, D., Jones, R. M., Behan, D. P., & Leonard, J. (2010). N-oleoyldopamine enhances glucose homeostasis through the activation of GPR119. *Molecular Endocrinology*, 24(1), 161–170.

- <https://doi.org/10.1210/me.2009-0239>
- Chung, T. H., Yen-Ping Kuo, M., Chen, J. K., & Huang, D. M. (2011). YC-1 rescues cancer cachexia by affecting lipolysis and adipogenesis. *International Journal of Cancer*, *129*(9), 2274–2283. <https://doi.org/10.1002/ijc.26174>
- Clarke, B. A., Drujan, D., Willis, M. S., Murphy, L. O., Corpina, R. A., Burova, E., Rakhilin, S. V., Stitt, T. N., Patterson, C., Latres, E., & Glass, D. J. (2007). The E3 Ligase MuRF1 Degrades Myosin Heavy Chain Protein in Dexamethasone-Treated Skeletal Muscle. *Cell Metabolism*, *6*(5), 376–385. <https://doi.org/10.1016/j.cmet.2007.09.009>
- Cohen, S., Brault, J. J., Gygi, S. P., Glass, D. J., Valenzuela, D. M., Gartner, C., Latres, E., & Goldberg, A. L. (2009). During muscle atrophy, thick, but not thin, filament components are degraded by MuRF1-dependent ubiquitylation. *Journal of Cell Biology*, *185*(6), 1083–1095. <https://doi.org/10.1083/jcb.200901052>
- Collins, S. (2012). β -Adrenoceptor signaling networks in adipocytes for recruiting stored fat and energy expenditure. *Frontiers in Endocrinology*, *3*(JAN), 1–7. <https://doi.org/10.3389/fendo.2011.00102>
- Cooper, J. M., Petty, R. K. H., Hayes, D. J., Challiss, R. A. J., Brosnan, M. J., Shoubridge, E. A., Radda, G. K., Morgan-Hughes, J. A., & Clark, J. B. (1988). An animal model of mitochondrial myopathy: A biochemical and physiological investigation of rats treated in vivo with the NADH-CoQ reductase inhibitor, diphenyleneiodonium. *Journal of the Neurological Sciences*. [https://doi.org/10.1016/0022-510X\(88\)90079-2](https://doi.org/10.1016/0022-510X(88)90079-2)
- Coyne, E. S., Bedard, N., Wykes, L., Stretch, C., Jammoul, S., Li, S., Zhang, K., Sladek, R. S., Bathe, O. F., Jagoe, R. T., Posner, B. I., & Wing, S. S. (2018). Knockout of USP19 deubiquitinating enzyme prevents muscle wasting by modulating insulin and glucocorticoid signaling. *Endocrinology*, *159*(8), 2966–2977. <https://doi.org/10.1210/en.2018-00290>
- Csibi, A., Leibovitch, M. P., Cornille, K., Tintignac, L. A., & Leibovitch, S. A. (2009). MAFbx/Atrogin-1 controls the activity of the initiation factor eIF3-fin skeletal muscle atrophy by targeting multiple C-terminal lysines. *Journal of Biological Chemistry*, *284*(7), 4413–4421. <https://doi.org/10.1074/jbc.M807641200>
- Dahlman, I., Mejhert, N., Linder, K., Agustsson, T., Mutch, D. M., Kulyte, A., Isaksson, B., Permert, J., Petrovic, N., Nedergaard, J., Sjölin, E., Brodin, D., Clement, K., Dahlman-Wright, K., Rydén, M., & Arner, P. (2010). Adipose tissue pathways involved in weight loss of cancer cachexia. *British Journal of Cancer*, *102*(10), 1541–1548. <https://doi.org/10.1038/sj.bjc.6605665>
- Dallmann, R., Weyermann, P., Anklin, C., Boroff, M., Bray-French, K., Cardel, B., Courdier-Fruh, I., Deppe, H., Dubach-Powell, J., Erb, M., Haefeli, R. H., Henneböhle, M., Herzner, H., Hufschmid, M., Marks, D. L., Nordhoff, S., Papp, M., Rummey, C., Santos, G., ... Feurer, A. (2011). The orally active melanocortin-4 receptor antagonist BL-6020/979: a promising candidate for the treatment of cancer cachexia. *Journal of Cachexia, Sarcopenia and Muscle*, *2*(3), 163–174. <https://doi.org/10.1007/s13539-011-0039-1>
- Dariš, B., Verboten, M. T., Knez, Ž., & Ferk, P. (2019). Cannabinoids in cancer treatment: Therapeutic potential and legislation. *Bosnian Journal of Basic Medical Sciences*, *19*(1), 14–23. <https://doi.org/10.17305/BJBMS.2018.3532>
- Das, S. K., Eder, S., Schauer, S., Diwoky, C., Temmel, H., Guertl, B., Gorkiewicz, G., Tamilarasan, K. P., Kumari, P., Trauner, M., Zimmermann, R., Vesely, P., Haemmerle, G., Zechner, R., & Hoefler, G. (2011). Adipose triglyceride lipase contributes to cancer-associated cachexia. *Science (New York, N.Y.)*, *333*(6039), 233–238. <https://doi.org/10.1126/science.1198973>
- Dasgupta, A., Shukla, S. K., Vernucci, E., King, R. J., Abrego, J., Mulder, S. E., Mullen, N. J., Graves, G., Buettner, K., Thakur, R., Murthy, D., Attri, K. S., Wang, D., Chaika, N. V., Pacheco, C. G., Rai, I., Engle, D. D., Grandgenett, P. M., Punsoni, M., ... Singh, P. K. (2020). Sirt1–nox4 signaling axis regulates cancer cachexia. *Journal of Experimental Medicine*, *217*(7). <https://doi.org/10.1084/jem.20190745>

- De Luca, R., Mazur, K., Kernder, A., Suvorava, T., Kojda, G., Haas, H. L., & Sergeeva, O. A. (2018). Mechanisms of N-oleoyldopamine activation of central histaminergic neurons. *Neuropharmacology*, *143*, 327–338. <https://doi.org/10.1016/j.neuropharm.2018.09.006>
- De Waele, E., Mattens, S., Honoré, P., Spapen, H., De Grève, J., & Pen, J. J. (2015). Nutrition therapy in cachectic cancer patients. The Tight Caloric Control (TiCaCo) pilot trial. *Appetite*, *91*, 298–301. <https://doi.org/10.1016/j.appet.2015.04.049>
- Dejesus, E., Rodwick, B. M., Bowers, D., Cohen, C. J., & Pearce, D. (2007). Use of dronabinol improves appetite and reverses weight loss in HIV/AIDS-infected patients. *Journal of the International Association of Physicians in AIDS Care*, *6*(2), 95–100. <https://doi.org/10.1177/1545109707300157>
- Delitto, D., Judge, S. M., Delitto, A. E., Nosacka, R. L., Rocha, F. G., DiVita, B. B., Gerber, M. H., George, T. J., Behrns, K. E., Hughes, S. J., Wallet, S. M., Judge, A. R., & Trevino, J. G. (2017). Human pancreatic cancer xenografts recapitulate key aspects of cancer cachexia. *Oncotarget*, *8*(1), 1177–1189. <https://doi.org/10.18632/oncotarget.13593>
- Denzel, M. S., Scimia, M. C., Zumstein, P. M., Walsh, K., Ruiz-Lozano, P., & Ranscht, B. (2010). T-cadherin is critical for adiponectin-mediated cardioprotection in mice. *Journal of Clinical Investigation*, *120*(12), 4342–4352. <https://doi.org/10.1172/JCI43464>
- Doehner, W., & Anker, S. D. (2002). Cardiac cachexia in early literature: A review of research prior to Medline. *International Journal of Cardiology*, *85*(1), 7–14. [https://doi.org/10.1016/S0167-5273\(02\)00230-9](https://doi.org/10.1016/S0167-5273(02)00230-9)
- Dogra, C., Changotra, H., Wedhas, N., Qin, X., Wergedal, J. E., & Kumar, A. (2007). TNF-Related Weak inducer of Apoptosis (TWEAK) is a potent skeletal muscle-wasting cytokine. *FASEB Journal : Official Publication of the Federation of American Societies for Experimental Biology*, *21*(8), 1857. <https://doi.org/10.1096/FJ.06-7537COM>
- Elmqvist, J. K., Elias, C. F., & Saper, C. B. (1999). From lesions to leptin: Hypothalamic control of food intake and body weight. *Neuron*, *22*(2), 221–232. [https://doi.org/10.1016/S0896-6273\(00\)81084-3](https://doi.org/10.1016/S0896-6273(00)81084-3)
- Ezeoke, C. C., & Morley, J. E. (2015). Pathophysiology of anorexia in the cancer cachexia syndrome. *Journal of Cachexia, Sarcopenia and Muscle*, *6*(4), 287–302. <https://doi.org/10.1002/jcsm.12059>
- Fasshauer, M., & Blüher, M. (2015). Adipokines in health and disease. *Trends in Pharmacological Sciences*, *36*(7), 461–470. <https://doi.org/10.1016/j.tips.2015.04.014>
- Fearon, K. C. H., Glass, D. J., & Guttridge, D. C. (2012). Cancer cachexia: Mediators, signaling, and metabolic pathways. *Cell Metabolism*, *16*(2), 153–166. <https://doi.org/10.1016/j.cmet.2012.06.011>
- Fearon, K., Strasser, F., Anker, S. D., Bosaeus, I., Bruera, E., Fainsinger, R. L., Jatoi, A., Loprinzi, C., MacDonald, N., Mantovani, G., Davis, M., Muscaritoli, M., Ottery, F., Radbruch, L., Ravasco, P., Walsh, D., Wilcock, A., Kaasa, S., & Baracos, V. E. (2011). Definition and classification of cancer cachexia: An international consensus. *The Lancet Oncology*, *12*(5), 489–495. [https://doi.org/10.1016/S1470-2045\(10\)70218-7](https://doi.org/10.1016/S1470-2045(10)70218-7)
- Fouladiun, M., Körner, U., Bosaeus, I., Daneryd, P., Hyltander, A., & Lundholm, K. G. (2005). Body composition and time course changes in regional distribution of fat and lean tissue in unselected cancer patients on palliative care - Correlations with food intake, metabolism, exercise capacity, and hormones. *Cancer*, *103*(10), 2189–2198. <https://doi.org/10.1002/cncr.21013>
- Franz, K., Ost, M., Otten, L., Herpich, C., Coleman, V., Endres, A. S., Klaus, S., Müller-Werdan, U., & Norman, K. (2019). Higher serum levels of fibroblast growth factor 21 in old patients with cachexia. *Nutrition*, *63–64*, 81–86. <https://doi.org/10.1016/j.nut.2018.11.004>
- Freire, P. P., Fernandez, G. J., Moraes, D., Cury, S. S., Dal Pai-Silva, M., Reis, P. P., Rogatto, S. R., & Carvalho, R. F. (2020). The expression landscape of cachexia-inducing factors in human cancers. *Journal of Cachexia, Sarcopenia and Muscle*, *11*(4), 947–961. <https://doi.org/10.1002/jcsm.12565>
- Garcia, J. M., Boccia, R. V., Graham, C. D., Yan, Y., Duus, E. M., Allen, S., & Friend, J. (2015). Anamorelin for patients with cancer cachexia: An integrated analysis of two phase 2, randomised, placebo-

- controlled, double-blind trials. *The Lancet Oncology*, 16(1), 108–116. [https://doi.org/10.1016/S1470-2045\(14\)71154-4](https://doi.org/10.1016/S1470-2045(14)71154-4)
- Gatley, S. J., & Martin, J. L. (1979). Some aspects of the pharmacology of diphenylethylideneiodonium, a bivalent iodine compound. *Xenobiotica*. <https://doi.org/10.3109/00498257909042319>
- Gauthier, M. S., Miyoshi, H., Souza, S. C., Cacicedo, J. M., Saha, A. K., Greenberg, A. S., & Ruderman, N. B. (2008). AMP-activated protein kinase is activated as a consequence of lipolysis in the adipocyte: Potential mechanism and physiological relevance. *Journal of Biological Chemistry*, 283(24), 16514–16524. <https://doi.org/10.1074/jbc.M708177200>
- Geppert, J., Walth, A. A., Expósito, R. T., Kaltenecker, D., Morigny, P., Machado, J., Becker, M., Simoes, E., Lima, J. D. C. C., Daniel, C., Diaz, M. B., Herzig, S., Seelaender, M., & Rohm, M. (2022). Aging aggravates cachexia in tumor-bearing mice. *Cancers*, 14(1). <https://doi.org/10.3390/cancers14010090>
- Gilabert, M., Calvo, E., Airoldi, A., Hamidi, T., Moutardier, V., Turrini, O., & Iovanna, J. (2014). Pancreatic Cancer-Induced Cachexia Is Jak2-Dependent in Mice. *Journal of Cellular Physiology*, 229(10), 1437–1443. <https://doi.org/10.1002/jcp.24580>
- Gold, E., Marino, F. E., Harrison, C., Makanji, Y., & Risbridger, G. (2013). Activin- β c reduces reproductive tumour progression and abolishes cancer-associated cachexia in inhibin-deficient mice. *The Journal of Pathology*, 229(4), 599–607. <https://doi.org/10.1002/path.4142>
- Gorter, R. W. (1999). Cancer cachexia and cannabinoids. *Forschende Komplementarmedizin*, 6(SUPPL. 3), 21–22. <https://doi.org/10.1159/000057152>
- Grandl, G., Novikoff, A., Dimarchi, R., Tschöp, M. H., & Müller, T. D. (2020). Gut peptide agonism in the treatment of obesity and diabetes. *Comprehensive Physiology*, 10(1), 99–124. <https://doi.org/10.1002/cphy.c180044>
- Gruzdeva, O., Borodkina, D., Uchasova, E., Dyleva, Y., & Barbarash, O. (2019). Leptin resistance: Underlying mechanisms and diagnosis. *Diabetes, Metabolic Syndrome and Obesity: Targets and Therapy*, 12, 191–198. <https://doi.org/10.2147/DMSO.S182406>
- Guarnier, F. A., Cecchini, A. L., Suzukawa, A. A., Maragno, A. L. G. C., Simão, A. N. C., Gomes, M. D., & Cecchini, R. (2010). Time course of skeletal muscle loss and oxidative stress in rats with Walker 256 solid tumor. *Muscle and Nerve*, 42(6), 950–958. <https://doi.org/10.1002/mus.21798>
- Guttridge, D. C., Mayo, M. W., Madrid, L. V., Wang, C. Y., & Baldwin, J. (2000). NF- κ B-induced loss of MyoD messenger RNA: Possible role in muscle decay and cachexia. *Science*, 289(5488), 2363–2365. <https://doi.org/10.1126/science.289.5488.2363>
- Hajer, G. R., Van Haeften, T. W., & Visseren, F. L. J. (2008). Adipose tissue dysfunction in obesity, diabetes, and vascular diseases. *European Heart Journal*, 29(24), 2959–2971. <https://doi.org/10.1093/eurheartj/ehn387>
- Halle, J. L., Pena, G. S., Paez, H. G., Castro, A. J., Rossiter, H. B., Visavadiya, N. P., Whitehurst, M. A., & Khamoui, A. V. (2019). Tissue-specific dysregulation of mitochondrial respiratory capacity and coupling control in colon-26 tumor-induced cachexia. *American Journal of Physiology - Regulatory Integrative and Comparative Physiology*, 317(1), R68–R82. <https://doi.org/10.1152/ajpregu.00028.2019>
- Han, J., Meng, Q., Shen, L., & Wu, G. (2018). Interleukin-6 induces fat loss in cancer cachexia by promoting white adipose tissue lipolysis and browning. *Lipids in Health and Disease*, 17(1), 1–8. <https://doi.org/10.1186/s12944-018-0657-0>
- Heinz, S., Freyberger, A., Lawrenz, B., Schladt, L., Schmuck, G., & Ellinger-Ziegelbauer, H. (2017). Mechanistic Investigations of the Mitochondrial Complex I Inhibitor Rotenone in the Context of Pharmacological and Safety Evaluation. *Scientific Reports*, 7(October 2016), 1–13. <https://doi.org/10.1038/srep45465>
- Henderson, S. E., Makhijani, N., & Mace, T. A. (2018). Pancreatic Cancer-Induced Cachexia and Relevant

- Mouse Models. *Pancreas*, 47(8), 937–945. <https://doi.org/10.1097/MPA.0000000000001124>
- Heymsfield, S. B., Greenberg, A. S., Fujioka, K., Dixon, R. M., Kushner, R., Hunt, T., Lubina, J. A., Patane, J., Self, B., Hunt, P., & McCamish, M. (1999). Recombinant Leptin for Weight Loss in Obese and Lean Adults. *JAMA*, 282(16), 1568. <https://doi.org/10.1001/jama.282.16.1568>
- Hirai, K., J. Hussey, H., D. Barber, M., A. Price, S., & J. Tisdale, M. (1998). Biological Evaluation of a Lipid-mobilizing Factor Isolated from the Urine of Cancer Patients1 | Cancer Research | American Association for Cancer Research. *Cancer Research*, 58(11), 2359–2365. <https://aacrjournals.org/cancerres/article/58/11/2359/504087/Biological-Evaluation-of-a-Lipid-mobilizing-Factor>
- Holland, W. L., Miller, R. A., Wang, Z. V., Sun, K., Barth, B. M., Bui, H. H., Davis, K. E., Bikman, B. T., Halberg, N., Rutkowski, J. M., Wade, M. R., Tenorio, V. M., Kuo, M. S., Brozinick, J. T., Zhang, B. B., Birnbaum, M. J., Summers, S. A., & Scherer, P. E. (2011). Receptor-mediated activation of ceramidase activity initiates the pleiotropic actions of adiponectin. *Nature Medicine*, 17(1), 55–63. <https://doi.org/10.1038/nm.2277>
- Hong, Y., Han Lee, J., Won Jeong, K., Soo Choi, C., & Jun, H.-S. (2019). Amelioration of muscle wasting by glucagon-like peptide-1 receptor agonist in muscle atrophy. *Journal of Cachexia, Sarcopenia and Muscle*, 10, 903–918. <https://onlinelibrary.wiley.com/doi/epdf/10.1002/jcsm.12434>
- Huot, J. R., Novinger, L. J., Pin, F., & Bonetto, A. (2020). HCT116 colorectal liver metastases exacerbate muscle wasting in a mouse model for the study of colorectal cancer cachexia. *DMM Disease Models and Mechanisms*, 13(1), 1–10. <https://doi.org/10.1242/dmm.043166>
- Iguchi, H., Aramaki, Y., Maruta, S., & Takiguchi, S. (2006). Effects of anti-parathyroid hormone-related protein monoclonal antibody and osteoprotegerin on PTHrP-producing tumor-induced cachexia in nude mice. *Journal of Bone and Mineral Metabolism*, 24(1), 16–19. <https://doi.org/10.1007/s00774-005-0640-5>
- Iguchi, H., Onuma, E., Sato, K., Sato, K., & Ogata, E. (2001). Involvement of parathyroid hormone-related protein in experimental cachexia induced by a human lung cancer-derived cell line established from a bone metastasis specimen. *International Journal of Cancer*, 94(1), 24–27. <https://doi.org/10.1002/ijc.1425>
- Ishiko, O., Nishimura, S., Yasui, T., Sumi, T., Hirai, K., Honda, K. I., & Ogita, S. (1999). Metabolic and morphologic characteristics of adipose tissue associated with the growth of malignant tumors. *Japanese Journal of Cancer Research*, 90(6), 655–659. <https://doi.org/10.1111/j.1349-7006.1999.tb00797.x>
- Issa, N., Lachance, G., Bellmann, K., Laplante, M., Stadler, K., & Marette, A. (2018). Cytokines promote lipolysis in 3T3-L1 adipocytes through induction of NADPH oxidase 3 expression and superoxide production. *Journal of Lipid Research*. <https://doi.org/10.1194/jlr.M086504>
- Iwase, S., Murakami, T., Saito, Y., & Nakagawa, K. (2004). Steep elevation of blood interleukin-6 (IL-6) associated only with late stages of cachexia in cancer patients. *European Cytokine Network*, 15(4), 312–316. <https://pubmed.ncbi.nlm.nih.gov/15627639/>
- Jang, K., Yoon, S., Kim, S. E., Cho, J. Y., Yoon, S. H., Lim, K. S., Yu, K. S., Jang, I. J., & Lee, H. (2014). Novel nanocrystal formulation of megestrol acetate has improved bioavailability compared with the conventional micronized formulation in the fasting state. *Drug Design, Development and Therapy*, 8, 851–858. <https://doi.org/10.2147/DDDT.S62176>
- Jatoi, A., Ritter, H. L., Dueck, A., Nguyen, P. L., Nikcevich, D. A., Luyun, R. F., Mattar, B. I., & Loprinzi, C. L. (2010). A Placebo-Controlled, Double Blind Trial of Infliximab for Cancer-Associated Weight Loss in Elderly and/or Poor Performance Non-Small Cell Lung Cancer Patients (N01C9). *Lung Cancer (Amsterdam, Netherlands)*, 68(2), 234. <https://doi.org/10.1016/J.LUNGCAN.2009.06.020>
- Javeed, N., Sagar, G., Dutta, S. K., Smyrk, T. C., Lau, J. S., Bhattacharya, S., Truty, M., Petersen, G. M., Kaufman, R. J., Chari, S. T., & Mukhopadhyay, D. (2015). Pancreatic cancer-derived exosomes cause

- paraneoplastic β -cell dysfunction. *Clinical Cancer Research*, 21(7), 1722–1733. <https://doi.org/10.1158/1078-0432.CCR-14-2022>
- Joffre, J., Wong, E., Lawton, S., Lloyd, E., Nguyen, N., Xu, F., Sempio, C., Kobzik, L., Zlatanova, I., Schumacher, M., Klawitter, J., Su, H., Rabl, K., Wilhelmsen, K., Yeh, C. C., & Hellman, J. (2022). N - Oleoyl dopamine induces IL-10 via central nervous system TRPV1 and improves endotoxemia and sepsis outcomes. *Journal of Neuroinflammation*, 19(1), 1–21. <https://doi.org/10.1186/s12974-022-02485-z>
- Jones, A., Friedrich, K., Rohm, M., Schäfer, M., Algire, C., Kulozik, P., Seibert, O., Müller-Decker, K., Sijmonsma, T., Strzoda, D., Sticht, C., Gretz, N., Dallinga-Thie, G. M., Leuchs, B., Kögl, M., Stremmel, W., Diaz, M. B., & Herzig, S. (2013). TSC22D4 is a molecular output of hepatic wasting metabolism. *EMBO Molecular Medicine*, 5(2), 294–308. <https://doi.org/10.1002/emmm.201201869>
- Judge, S. M., Nosacka, R. L., Delitto, D., Gerber, M. H., Cameron, M. E., Trevino, J. G., & Judge, A. R. (2018). Skeletal Muscle Fibrosis in Pancreatic Cancer Patients with Respect to Survival. *JNCI Cancer Spectrum*, 2(3), 1–13. <https://doi.org/10.1093/jncics/pky043>
- Kalra, P. R., & Tigas, S. (2002). Regulation of lipolysis: Natriuretic peptides and the development of cachexia. *International Journal of Cardiology*, 85(1), 125–132. [https://doi.org/10.1016/S0167-5273\(02\)00241-3](https://doi.org/10.1016/S0167-5273(02)00241-3)
- Kawabata, F., Inoue, N., Masamoto, Y., Matsumura, S., Kimura, W., Kadowaki, M., Higashi, T., Tominaga, M., Inoue, K., & Fushiki, T. (2009). Non-pungent capsaicin analogs (capsinoids) increase metabolic rate and enhance thermogenesis via gastrointestinal TRPV1 in mice. *Bioscience, Biotechnology and Biochemistry*, 73(12), 2690–2697. <https://doi.org/10.1271/bbb.90555>
- Kern, K. A., & Norton, J. A. (1988). Cancer cachexia. *Journal of Parenteral and Enteral Nutrition*, 12(3), 286–298. <https://doi.org/10.1177/0148607188012003286>
- Kershaw, E. E., & Flier, J. S. (2004). Adipose tissue as an endocrine organ. *Journal of Clinical Endocrinology and Metabolism*, 89(6), 2548–2556. <https://doi.org/10.1210/jc.2004-0395>
- Kim, Y., Lim, J. H., Kim, M. Y., Kim, E. N., Yoon, H. E., Shin, S. J., Choi, B. S., Kim, Y. S., Chang, Y. S., & Park, C. W. (2018). The adiponectin receptor agonist AdipoRon ameliorates diabetic nephropathy in a model of type 2 diabetes. *Journal of the American Society of Nephrology*, 29(4), 1108–1127. <https://doi.org/10.1681/ASN.2017060627>
- Kir, S., & Spiegelman, B. M. (2016). Cachexia and Brown Fat: A Burning Issue in Cancer. *Trends in Cancer*, 2(9), 461–463. <https://doi.org/10.1016/j.trecan.2016.07.005>
- Kir, S., White, J. P., Kleiner, S., Kazak, L., Cohen, P., Baracos, V. E., & Spiegelman, B. M. (2014). Tumour-derived PTH-related protein triggers adipose tissue browning and cancer cachexia. *Nature* 2014 513:7516, 513(7516), 100–104. <https://doi.org/10.1038/nature13528>
- Kliewer, K. L., Ke, J. Y., Tian, M., Cole, R. M., Andridge, R. R., & Belury, M. A. (2015). Adipose tissue lipolysis and energy metabolism in early cancer cachexia in mice. *Cancer Biology and Therapy*, 16(6), 886–897. <https://doi.org/10.4161/15384047.2014.987075>
- Kokolus, K. M., Capitano, M. L., Lee, C. T., Eng, J. W. L., Waight, J. D., Hylander, B. L., Sexton, S., Hong, C. C., Gordon, C. J., Abrams, S. I., & Repasky, E. A. (2013). Baseline tumor growth and immune control in laboratory mice are significantly influenced by subthermoneutral housing temperature. *Proceedings of the National Academy of Sciences of the United States of America*, 110(50), 20176–20181. <https://doi.org/10.1073/pnas.1304291110>
- Konaté, M. M., Antony, S., & Doroshov, J. H. (2020). Inhibiting the Activity of NADPH Oxidase in Cancer. *Antioxidants and Redox Signaling*, 33(6), 435–454. <https://doi.org/10.1089/ars.2020.8046>
- Konieczny, J., Przegaliński, E., & Pokorski, M. (2009). N-oleoyl-dopamine decreases muscle rigidity induced by reserpine in rats. *International Journal of Immunopathology and Pharmacology*. <https://doi.org/10.1177/039463200902200104>
- Kono, H., Rusyn, I., Uesugi, T., Yamashina, S., Connor, H. D., Dikalova, A., Mason, R. P., & Thurman, R. G.

- (2001). Diphenyleneiodonium sulfate, an NADPH oxidase inhibitor, prevents early alcohol-induced liver injury in the rat. *American Journal of Physiology - Gastrointestinal and Liver Physiology*. <https://doi.org/10.1152/ajpgi.2001.280.5.g1005>
- Lee, J. W., Komar, C. A., Bengsch, F., Graham, K., & Beatty, G. L. (2016). Genetically Engineered Mouse Models of Pancreatic Cancer: The KPC Model (LSL-Kras G12D/+ ;LSL-Trp53 R172H/+ ;Pdx-1-Cre), Its Variants, and Their Application in Immuno-oncology Drug Discovery. *Current Protocols in Pharmacology*, 73(1), 1–28. <https://doi.org/10.1002/cpph.2>
- Lerner, L., Hayes, T. G., Tao, N., Krieger, B., Feng, B., Wu, Z., Nicoletti, R., Isabel Chiu, M., Gyuris, J., & Garcia, J. M. (2015). Plasma growth differentiation factor 15 is associated with weight loss and mortality in cancer patients. *Journal of Cachexia, Sarcopenia and Muscle*, 6(4), 317–324. <https://doi.org/10.1002/jcsm.12033>
- Lerner, L., Tao, J., Liu, Q., Nicoletti, R., Feng, B., Krieger, B., Mazsa, E., Siddiquee, Z., Wang, R., Huang, L., Shen, L., Lin, J., Vigano, A., Chiu, M. I., Weng, Z., Winston, W., Weiler, S., & Gyuris, J. (2016). MAP3K11/GDF15 axis is a critical driver of cancer cachexia. *Journal of Cachexia, Sarcopenia and Muscle*, 7(4), 467–482. <https://doi.org/10.1002/jcsm.12077>
- Leto, G., Incorvaia, L., Badalamenti, G., Tumminello, F. M., Gebbia, N., Flandina, C., Crescimanno, M., & Rini, G. (2006). Activin A circulating levels in patients with bone metastasis from breast or prostate cancer. *Clinical and Experimental Metastasis*, 23(2), 117–122. <https://doi.org/10.1007/s10585-006-9010-5>
- Li, F., Li, Y., Duan, Y., Hu, C. A. A., Tang, Y., & Yin, Y. (2017). Myokines and adipokines: Involvement in the crosstalk between skeletal muscle and adipose tissue. *Cytokine and Growth Factor Reviews*, 33, 73–82. <https://doi.org/10.1016/j.cytogfr.2016.10.003>
- Li, L., Chen, C., Chiang, C., Xiao, T., Chen, Y., Zhao, Y., & Zheng, D. (2021). The impact of trpv1 on cancer pathogenesis and therapy: A systematic review. *International Journal of Biological Sciences*, 17(8), 2034–2049. <https://doi.org/10.7150/ijbs.59918>
- Li, Y.-P., Chen, Y., John, J., Moylan, J., Jin, B., Mann, D. L., & Reid, M. B. (2005). TNF- α acts via p38 MAPK to stimulate expression of the ubiquitin ligase atrogin1/MAFbx in skeletal muscle. *The FASEB Journal*, 19(3), 362–370. <https://doi.org/10.1096/fj.04-2364com>
- Li, Y., Mouche, S., Sajic, T., Veyrat-Durebex, C., Supale, R., Pierroz, D., Ferrari, S., Negro, F., Hasler, U., Feraille, E., Moll, S., Meda, P., Deffert, C., Montet, X., Krause, K. H., & Szanto, I. (2012). Deficiency in the NADPH oxidase 4 predisposes towards diet-induced obesity. *International Journal of Obesity*. <https://doi.org/10.1038/ijo.2011.279>
- Lincoff, A. M., Wolski, K., Nicholls, S. J., & Nissen, S. E. (2007). Pioglitazone and risk of cardiovascular events in patients with type 2 diabetes mellitus: A meta-analysis of randomized trials. *Jama*, 298(10), 1180–1188. <https://doi.org/10.1001/jama.298.10.1180>
- Liu, L., D. Zheng, L., R. Donnelly, S., P. Emont, M., Wu, J., & Cheng, Z. (2017). Isolation of Mouse Stromal Vascular Cells for Monolayer Culture. In *Thermogenic Fat* (pp. 9–16).
- Llovera, M., García-Martínez, C., López-Soriano, J., Carbó, N., Agell, N., López-Soriano, F. J., & Argiles, J. M. (1998). Role of TNF receptor 1 in protein turnover during cancer cachexia using gene knockout mice. *Molecular and Cellular Endocrinology*, 142(1–2), 183–189. [https://doi.org/10.1016/S0303-7207\(98\)00105-1](https://doi.org/10.1016/S0303-7207(98)00105-1)
- Lobo, S., Wiczer, B. M., Smith, A. J., Hall, A. M., & Bernlohr, D. A. (2007). Fatty acid metabolism in adipocytes: Functional analysis of fatty acid transport proteins 1 and 4. *Journal of Lipid Research*, 48(3), 609–620. <https://doi.org/10.1194/jlr.M600441-JLR200>
- López-Soriano, J., Argilés, J. M., & López-Soriano, F. J. (1996). Lipid metabolism in rats bearing the Yoshida AH-130 ascites hepatoma. *Molecular and Cellular Biochemistry*, 165(1), 17–23. <https://doi.org/10.1007/bf00229741>
- Luo, L., & Liu, M. (2016). Adipose tissue in control of metabolism. *Journal of Endocrinology*, 231(3), R77–

- R99. <https://doi.org/10.1530/JOE-16-0211>
- Ma, J. F., Sanchez, B. J., Hall, D. T., Tremblay, A. K., Di Marco, S., & Gallouzi, I. (2017). STAT3 promotes IFN γ /TNF α -induced muscle wasting in an NF- κ B-dependent and IL-6-independent manner. *EMBO Molecular Medicine*, *9*(5), 622–637. <https://doi.org/10.15252/emmm.201607052>
- Mannelli, M., Gamberi, T., Magherini, F., & Fiaschi, T. (2020). The Adipokines in Cancer Cachexia. *International Journal of Molecular Sciences*, *21*(14). <https://doi.org/10.3390/ijms21144860>
- Manole, E., Ceafalan, L. C., Popescu, B. O., Dumitru, C., & Bastian, A. E. (2018). Myokines as possible therapeutic targets in cancer cachexia. *Journal of Immunology Research*, *2018*. <https://doi.org/10.1155/2018/8260742>
- Mayer, N., Schweiger, M., Romauch, M., Grabner, G. F., Eichmann, T. O., Fuchs, E., Ivkovic, J., Heier, C., Mrak, I., Lass, A., Höfler, G., Fledelius, C., Zechner, R., Zimmermann, R., & Breinbauer, R. (2013). Development of small-molecule inhibitors targeting adipose triglyceride lipase. *Nature Chemical Biology*, *9*(12), 785–787. <https://doi.org/10.1038/nchembio.1359>
- Mead, J. R., Irvine, S. A., & Ramji, D. P. (2002). Lipoprotein lipase: Structure, function, regulation, and role in disease. *Journal of Molecular Medicine*, *80*(12), 753–769. <https://doi.org/10.1007/s00109-002-0384-9>
- Michaelis, K. A., Zhu, X., Burfeind, K. G., Krasnow, S. M., Levasseur, P. R., Morgan, T. K., & Marks, D. L. (2017). Establishment and characterization of a novel murine model of pancreatic cancer cachexia. *Journal of Cachexia, Sarcopenia and Muscle*, *8*(5), 824–838. <https://doi.org/10.1002/jcsm.12225>
- Moon, H. S., Chamberland, J. P., Diakopoulos, K. N., Fiorenza, C. G., Ziemke, F., Schneider, B., & Mantzoros, C. S. (2011). Leptin and amylin act in an additive manner to activate overlapping signaling pathways in peripheral tissues: In vitro and ex vivo studies in humans. *Diabetes Care*, *34*(1), 132–138. <https://doi.org/10.2337/dc10-0518>
- Morigny, P., Kaltenecker, D., Zuber, J., Machado, J., Mehr, L., Tsokanos, F. F., Kuzi, H., Hermann, C. D., Voelkl, M., Monogarov, G., Springfield, C., Laurent, V., Engelmann, B., Friess, H., Zörnig, I., Krüger, A., Krijgsveld, J., Prokopchuk, O., Fisker Schmidt, S., ... Berriel Diaz, M. (2021). Association of circulating PLA2G7 levels with cancer cachexia and assessment of darapladib as a therapy. *Journal of Cachexia, Sarcopenia and Muscle*, *12*(5), 1333–1351. <https://doi.org/10.1002/jcsm.12758>
- Morigny, P., Zuber, J., Haid, M., Kaltenecker, D., Riols, F., Lima, J. D. C., Simoes, E., Otoch, J. P., Schmidt, S. F., Herzig, S., Adamski, J., Seelaender, M., Berriel Diaz, M., & Rohm, M. (2020). High levels of modified ceramides are a defining feature of murine and human cancer cachexia. *Journal of Cachexia, Sarcopenia and Muscle*, 1–17. <https://doi.org/10.1002/jcsm.12626>
- Motter, A. L., & Ahern, G. P. (2008). TRPV1-null mice are protected from diet-induced obesity. *FEBS Letters*. <https://doi.org/10.1016/j.febslet.2008.05.021>
- Mracek, T., Stephens, N. A., Gao, D., Bao, Y., Ross, J. A., Rydén, M., Arner, P., Trayhurn, P., Fearon, K. C. H., & Bing, C. (2011). Enhanced ZAG production by subcutaneous adipose tissue is linked to weight loss in gastrointestinal cancer patients. *British Journal of Cancer*, *104*(3), 441–447. <https://doi.org/10.1038/sj.bjc.6606083>
- Mukherjee, D., Ghosh, A. K., Dutta, M., Mitra, E., Mallick, S., Saha, B., Reiter, R. J., & Bandyopadhyay, D. (2015). Mechanisms of isoproterenol-induced cardiac mitochondrial damage. *Journal of Pineal Research*, *58*, 275–290.
- Mulligan, H. D., & Tisdale, M. J. (1991). Lipogenesis in tumour and host tissues in mice bearing colonic adenocarcinomas. *British Journal of Cancer*, *63*(5), 719–722. <https://doi.org/10.1038/bjc.1991.162>
- Murphy, K. T. (2016). The pathogenesis and treatment of cardiac atrophy in cancer cachexia. *American Journal of Physiology - Heart and Circulatory Physiology*, *310*(4), H466–H477. <https://doi.org/10.1152/ajpheart.00720.2015>
- Nakanishi, M., Hata, K., Nagayama, T., Sakurai, T., Nishisho, T., Wakabayashi, H., Hiraga, T., Ebisu, S., & Yoneda, T. (2010). Acid activation of Trpv1 leads to an up-regulation of calcitonin gene-related

- peptide expression in dorsal root ganglion neurons via the CaMK-CREB cascade: A potential mechanism of inflammatory pain. *Molecular Biology of the Cell*, 21(15), 2568–2577. <https://doi.org/10.1091/mbc.E10-01-0049>
- Nawrocki, A. R., Rajala, M. W., Tomas, E., Pajvani, U. B., Saha, A. K., Trumbauer, M. E., Pang, Z., Chen, A. S., Ruderman, N. B., Chen, H., Rossetti, L., & Scherer, P. E. (2006). Mice lacking adiponectin show decreased hepatic insulin sensitivity and reduced responsiveness to peroxisome proliferator-activated receptor γ agonists. *Journal of Biological Chemistry*, 281(5), 2654–2660. <https://doi.org/10.1074/jbc.M505311200>
- Nelson, K., Walsh, D., Deeter, P., & Sheehan, F. (1994). A phase II study of delta-9-tetrahydrocannabinol for appetite stimulation in cancer-associated anorexia. *Journal of Palliative Care*, 10(1), 14–18. <https://doi.org/10.1177/082585979401000105>
- Nimri, L., Peri, I., Yehuda-Shnaidman, E., & Schwartz, B. (2019). Adipocytes Isolated from Visceral and Subcutaneous Depots of Donors Differing in BMI Crosstalk with Colon Cancer Cells and Modulate their Invasive Phenotype. *Translational Oncology*, 12(11), 1404–1415. <https://doi.org/10.1016/j.tranon.2019.07.010>
- Nowakowska, M., Pospiech, K., Lewandowska, U., Piastowska-Ciesielska, A. W., & Bednarek, A. K. (2014). Diverse effect of WWOX overexpression in HT29 and SW480 colon cancer cell lines. *Tumor Biology*, 35(9), 9291–9301. <https://doi.org/10.1007/s13277-014-2196-2>
- Oliff, A., Defeo-Jones, D., Boyer, M., Martinez, D., Kiefer, D., Vuocolo, G., Wolfe, A., & Socher, S. H. (1987). Tumors secreting human TNF/cachectin induce cachexia in mice. *Cell*, 50(4), 555–563. [https://doi.org/10.1016/0092-8674\(87\)90028-6](https://doi.org/10.1016/0092-8674(87)90028-6)
- Ostlund, R. E., Yang, J. W., Klein, S., & Gingerich, R. (1996). Relation between plasma leptin concentration and body fat, gender, diet, age, and metabolic covariates. *The Journal of Clinical Endocrinology & Metabolism*, 81(11), 3909–3913. <https://doi.org/10.1210/jcem.81.11.8923837>
- Parajuli, N., Takahara, S., Matsumura, N., T. Kim, T., Ferdaoussi, M., K. Migglautsch, A., Zechner, R., Breinbauer, R., E. Kershaw, E., & RB Dyck, J. (2019). Atglistatin Ameliorates Functional Decline in Heart Failure via Adipocyte-specific Inhibition of Adipose Triglyceride Lipase. *Journal of Chemical Information and Modeling*, 53(9), 1689–1699. <https://doi.org/10.1017/CBO9781107415324.004>
- Park, A. (2014). Distinction of white, beige and brown adipocytes derived from mesenchymal stem cells. *World Journal of Stem Cells*, 6(1), 33. <https://doi.org/10.4252/wjsc.v6.i1.33>
- Park, Y. S., & Cho, N. J. (2012). EGFR and PKC are involved in the activation of ERK1/2 and p90 RSK and the subsequent proliferation of SNU-407 colon cancer cells by muscarinic acetylcholine receptors. *Molecular and Cellular Biochemistry*, 370(1–2), 191–198. <https://doi.org/10.1007/S11010-012-1410-Z/FIGURES/6>
- Penna, F., Bonetto, A., Aversa, Z., Minero, V. G., Rossi Fanelli, F., Costelli, P., & Muscaritoli, M. (2016). Effect of the specific proteasome inhibitor bortezomib on cancer-related muscle wasting. *Journal of Cachexia, Sarcopenia and Muscle*, 7(3), 345–354. <https://doi.org/10.1002/jcsm.12050>
- Penna, F., Busquets, S., & Argilés, J. M. (2016). Experimental cancer cachexia: Evolving strategies for getting closer to the human scenario. *Seminars in Cell and Developmental Biology*, 54, 20–27. <https://doi.org/10.1016/j.semcd.2015.09.002>
- Petruzzelli, M., Schweiger, M., Schreiber, R., Campos-Olivas, R., Tsoi, M., Allen, J., Swarbrick, M., Rose-John, S., Rincon, M., Robertson, G., Zechner, R., & Wagner, E. F. (2014). A switch from white to brown fat increases energy expenditure in cancer-associated cachexia. *Cell Metabolism*, 20(3), 433–447. <https://doi.org/10.1016/j.cmet.2014.06.011>
- Pin, F., Bonewald, L. F., & Bonetto, A. (2021). Role of myokines and osteokines in cancer cachexia. *Experimental Biology and Medicine*, 246(19), 2118–2127. <https://doi.org/10.1177/15353702211009213>
- Pin, F., Novinger, L. J., Huot, J. R., Harris, R. A., Couch, M. E., O’Connell, T. M., & Bonetto, A. (2019). PDK4

- drives metabolic alterations and muscle atrophy in cancer cachexia. *FASEB Journal*, 33(6), 7778–7790. <https://doi.org/10.1096/fj.201802799R>
- Pototschnig, I., Feiler, U., Diwoy, C., Vesely, P. W., Rauchenwald, T., Paar, M., Bakiri, L., Pajed, L., Hofer, P., Kashofer, K., Sukhbaatar, N., Schoiswohl, G., Weichhart, T., Hoefler, G., Bock, C., Pichler, M., Wagner, E. F., Zechner, R., & Schweiger, M. (2022). Interleukin-6 initiates muscle- and adipose tissue wasting in a novel C57BL/6 model of cancer-associated cachexia. *Journal of Cachexia, Sarcopenia and Muscle*. <https://doi.org/10.1002/jcsm.13109>
- Prado, C. M., Purcell, S. A., & Laviano, A. (2020). Nutrition interventions to treat low muscle mass in cancer. *Journal of Cachexia, Sarcopenia and Muscle*, 11(2), 366–380. <https://doi.org/10.1002/jcsm.12525>
- Proença, A. R. G., Sertié, R. A. L., Oliveira, A. C., Campaña, A. B., Caminhotto, R. O., Chimin, P., & Lima, F. B. (2014). New concepts in white adipose tissue physiology. *Brazilian Journal of Medical and Biological Research*, 47(3), 192–205. <https://doi.org/10.1590/1414-431X20132911>
- Przegaliński, E., Filip, M., Zajac, D., & Pokorski, M. (2006). N-oleoyl-dopamine increases locomotor activity in the rat. *International Journal of Immunopathology and Pharmacology*, 19(4), 897–904. <https://doi.org/10.1177/039463200601900419>
- Reed, S. A., Sandesara, P. B., Senf, S. M., & Judge, A. R. (2012). Inhibition of FoxO transcriptional activity prevents muscle fiber atrophy during cachexia and induces hypertrophy. *The FASEB Journal*, 26(3), 987–1000. <https://doi.org/10.1096/fj.11-189977>
- Roberts, B. M., Ahn, B., Smuder, A. J., Al-Rajhi, M., Gill, L. C., Beharry, A. W., Powers, S. K., Fuller, D. D., Ferreira, L. F., & Judge, A. R. (2013). Diaphragm and ventilatory dysfunction during cancer cachexia. *FASEB Journal*, 27(7), 2600–2610. <https://doi.org/10.1096/fj.12-222844>
- Rohm, M., Savic, D., Ball, V., Curtis, M. K., Bonham, S., Fischer, R., Legrave, N., MacRae, J. I., Tyler, D. J., & Ashcroft, F. M. (2018). Cardiac dysfunction and metabolic inflexibility in a mouse model of diabetes without dyslipidemia. *Diabetes*, 67(6), 1057–1067. <https://doi.org/10.2337/db17-1195>
- Rohm, M., Schäfer, M., Laurent, V., Üstünel, B. E., Niopek, K., Algire, C., Hautzinger, O., Sijmonsma, T. P., Zota, A., Medrikova, D., Pellegata, N. S., Ryden, M., Kulyte, A., Dahlman, I., Arner, P., Petrovic, N., Cannon, B., Amri, E.-Z., Kemp, B. E., ... Herzig, S. (2016). An AMP-activated protein kinase-stabilizing peptide ameliorates adipose tissue wasting in cancer cachexia in mice. *Nature Medicine*, 22(10), 1120–1130. <https://doi.org/10.1038/nm.4171>
- Rohm, M., Zeigerer, A., Machado, J., & Herzig, S. (2019). Energy metabolism in cachexia. *EMBO Reports*. <https://doi.org/10.15252/embr.201847258>
- Rosenberg, S. A., Spiess, P., & Lafreniere, R. (1986). A new approach to the adoptive immunotherapy of cancer with tumor-infiltrating lymphocytes. *Science*, 233(4770), 1318–1321. <https://doi.org/10.1126/science.3489291>
- Rosenwald, M., Perdikari, A., Rüllicke, T., & Wolfrum, C. (2013). Bi-directional interconversion of brite and white adipocytes. *Nature Cell Biology*, 15(6), 659–667. <https://doi.org/10.1038/ncb2740>
- Rydén, M., Agustsson, T., Laurencikiene, J., Britton, T., Sjölin, E., Isaksson, B., Permert, J., & Arner, P. (2008). Lipolysis - not inflammation, cell death, or lipogenesis - is involved in adipose tissue loss in cancer cachexia. *Cancer*, 113(7), 1695–1704. <https://doi.org/10.1002/cncr.23802>
- Sagar, G., Sah, R. P., Javeed, N., Dutta, S. K., Smyrk, T. C., Lau, J. S., Giorgadze, N., Tchkonja, T., Kirkland, J. L., Chari, S. T., & Mukhopadhyay, D. (2016). Pathogenesis of pancreatic cancer exosome-induced lipolysis in adipose tissue. *Gut*, 65(7), 1165–1174. <https://doi.org/10.1136/gutjnl-2014-308350>
- Sakaguchi, K., Takeda, K., Maeda, M., Ogawa, W., Sato, T., Okada, S., Ohnishi, Y., Nakajima, H., & Kashiwagi, A. (2016). Glucose area under the curve during oral glucose tolerance test as an index of glucose intolerance. *Diabetology International*, 7(1), 53–58. <https://doi.org/10.1007/s13340-015-0212-4>
- Sandri, M., Lin, J., Handschin, C., Yang, W., Arany, Z. P., Lecker, S. H., Goldberg, A. L., & Spiegelman, B. M. (2006). PGC-1 α protects skeletal muscle from atrophy by suppressing FoxO3 action and atrophy-

- specific gene transcription. *Proceedings of the National Academy of Sciences of the United States of America*, 103(44), 16260–16265. <https://doi.org/10.1073/pnas.0607795103>
- Sartori, R., Milan, G., Patron, M., Mammucari, C., Blaauw, B., Abraham, R., & Sandri, M. (2009). Smad2 and 3 transcription factors control muscle mass in adulthood. *American Journal of Physiology - Cell Physiology*, 296(6), 1248–1257. <https://doi.org/10.1152/ajpcell.00104.2009>
- Schäfer, M., Oeing, C. U., Rohm, M., Baysal-Temel, E., Lehmann, L. H., Bauer, R., Volz, H. C., Boutros, M., Sohn, D., Sticht, C., Gretz, N., Eichelbaum, K., Werner, T., Hirt, M. N., Eschenhagen, T., Müller-Decker, K., Strobel, O., Hackert, T., Krijgsveld, J., ... Herzig, S. (2016). Ataxin-10 is part of a cachexokine cocktail triggering cardiac metabolic dysfunction in cancer cachexia. *Molecular Metabolism*, 5(2), 67–78. <https://doi.org/10.1016/j.molmet.2015.11.004>
- Schmidt, S. F., Rohm, M., Herzig, S., & Berriel Diaz, M. (2018). Cancer Cachexia: More Than Skeletal Muscle Wasting. *Trends in Cancer*, 4(12), 849–860. <https://doi.org/10.1016/j.trecan.2018.10.001>
- Schweiger, M., Romauch, M., Schreiber, R., Grabner, G. F., Hütter, S., Kotzbeck, P., Benedikt, P., Eichmann, T. O., Yamada, S., Knittelfelder, O., Diwoky, C., Doler, C., Mayer, N., De Cecco, W., Breinbauer, R., Zimmermann, R., & Zechner, R. (2017). Pharmacological inhibition of adipose triglyceride lipase corrects high-fat diet-induced insulin resistance and hepatosteatosis in mice. *Nature Communications*, 8(May 2016). <https://doi.org/10.1038/ncomms14859>
- Schweiger, M., Schreiber, R., Haemmerle, G., Lass, A., Fledelius, C., Jacobsen, P., Tornqvist, H., Zechner, R., & Zimmermann, R. (2006). Adipose triglyceride lipase and hormone-sensitive lipase are the major enzymes in adipose tissue triacylglycerol catabolism. *Journal of Biological Chemistry*, 281(52), 40236–40241. <https://doi.org/10.1074/jbc.M608048200>
- Scott, H. R., McMillan, D. C., Crilly, A., McArdle, C. S., & Milroy, R. (1996). The relationship between weight loss and interleukin 6 in non-small-cell lung cancer. *British Journal of Cancer*, 73(12), 1560–1562. <https://doi.org/10.1038/bjc.1996.294>
- Sergeeva, O. A., De Luca, R., Mazur, K., Chepkova, A. N., Haas, H. L., & Bauer, A. (2017). N-oleoyldopamine modulates activity of midbrain dopaminergic neurons through multiple mechanisms. *Neuropharmacology*, 119, 111–122. <https://doi.org/10.1016/j.neuropharm.2017.04.011>
- Seto, D. N., Kandarian, S. C., & Jackman, R. W. (2015). A key role for leukemia inhibitory factor in C26 cancer cachexia. *Journal of Biological Chemistry*, 290(32), 19976–19986. <https://doi.org/10.1074/jbc.M115.638411>
- Shukla, S. K., Gebregiorgis, T., Purohit, V., Chaika, N. V., Gunda, V., Radhakrishnan, P., Mehla, K., Pipinos, I. I., Powers, R., Yu, F., & Singh, P. K. (2014). Erratum to: Metabolic reprogramming induced by ketone bodies diminishes pancreatic cancer cachexia. *Cancer & Metabolism*, 2(1), 1–19. <https://doi.org/10.1186/2049-3002-2-22>
- Sies, H., & Jones, D. P. (2020). Reactive oxygen species (ROS) as pleiotropic physiological signalling agents. *Nature Reviews Molecular Cell Biology*, 21(7), 363–383. <https://doi.org/10.1038/s41580-020-0230-3>
- Simon, L., Baldwin, C., Kalea, A. Z., & Slee, A. (2022). Cannabinoid interventions for improving cachexia outcomes in cancer: a systematic review and meta-analysis. *Journal of Cachexia, Sarcopenia and Muscle*, 13(1), 23–41. <https://doi.org/10.1002/jcsm.12861>
- Smiechowska, J., Utech, A., Taffet, G., Hayes, T., Marcelli, M., & Garcia, J. M. (2010). Adipokines in patients with cancer anorexia and cachexia. *Journal of Investigative Medicine*, 58(3), 554–559. <https://doi.org/10.2310/JIM.0b013e3181cf91ca>
- Smith, K. L., & Tisdale, M. J. (1993). Increased protein degradation and decreased protein synthesis in skeletal muscle during cancer cachexia. *British Journal of Cancer*, 67(4), 680–685. <https://doi.org/10.1038/bjc.1993.126>
- Spicarova, D., & Palecek, J. (2010). Tumor necrosis factor α sensitizes spinal cord TRPV1 receptors to the endogenous agonist N-oleoyldopamine. *Journal of Neuroinflammation*, 7, 1–7.

- <https://doi.org/10.1186/1742-2094-7-49>
- Steel, D. M., Rogers, J. T., DeBeer, M. C., DeBeer, F. C., & Whitehead, A. S. (1993). Biosynthesis of human acute-phase serum amyloid A protein (A-SAA) in vitro: the roles of mRNA accumulation, poly(A) tail shortening and translational efficiency. *Biochemical Journal*, 291(3), 701–707. <https://doi.org/10.1042/BJ2910701>
- Stuehr, D. J., Fasehun, O. A., Kwon, N. S., Gross, S. S., Gonzalez, J. A., Levi, R., & Nathan, C. F. (1991). Inhibition of macrophage and endothelial cell nitric oxide synthase by diphenyleneiodonium and its analogs. *The FASEB Journal*, 5(1), 98–103. <https://doi.org/10.1096/FASEBJ.5.1.1703974>
- Sullivan-Gunn, M. J., Campbell-O'Sullivan, S. P., Tisdale, M. J., & Lewandowski, P. A. (2011). Decreased NADPH oxidase expression and antioxidant activity in cachectic skeletal muscle. *Journal of Cachexia, Sarcopenia and Muscle*, 2(3), 181–188. <https://doi.org/10.1007/s13539-011-0037-3>
- Suriben, R., Chen, M., Higbee, J., Oeffinger, J., Ventura, R., Li, B., Mondal, K., Gao, Z., Ayupova, D., Taskar, P., Li, D., Starck, S. R., Chen, H. I. H., McEntee, M., Katewa, S. D., Phung, V., Wang, M., Kekatpure, A., Lakshminarasimhan, D., ... Allan, B. B. (2020). Antibody-mediated inhibition of GDF15–GFRAL activity reverses cancer cachexia in mice. *Nature Medicine*, 26(8), 1264–1270. <https://doi.org/10.1038/s41591-020-0945-x>
- Suzuki, H., Hashimoto, H., Kawasaki, M., Watanabe, M., Otsubo, H., Ishikura, T., Fujihara, H., Ohnishi, H., Onuma, E., Yamada-Okabe, H., Takuwa, Y., Ogata, E., Nakamura, T., & Ueta, Y. (2011). Similar changes of hypothalamic feeding-regulating peptides mRNAs and plasma leptin levels in PTHrP-, LIF-secreting tumors-induced cachectic rats and adjuvant arthritic rats. *International Journal of Cancer*, 128(9), 2215–2223. <https://doi.org/10.1002/ijc.25535>
- Sweeney, G., & Song, J. (2016). *The association between PGC-1 α and Alzheimer's disease*. 1–6.
- Symonds, M. E. (2012). Adipose tissue biology. *Adipose Tissue Biology*, 1–413. <https://doi.org/10.1007/978-1-4614-0965-6>
- T. Todorov, P., M. McDevitt, T., J. Meyer, D., Ueyama, H., Ohkubo, I., & J. Tisdale, M. (1998). Purification and Characterization of a Tumor Lipid-mobilizing Factor. *Cancer Research*, 58(11), 2353–2358. <https://aacrjournals.org/cancerres/article/58/11/2353/504115/Purification-and-Characterization-of-a-Tumor-Lipid>
- Talbert, E. E., Cuitiño, M. C., Ladner, K. J., Rajasekera, P. V., Siebert, M., Shakya, R., Leone, G. W., Ostrowski, M. C., Paleo, B., Weisleder, N., Reiser, P. J., Webb, A., Timmers, C. D., Eiferman, D. S., Evans, D. C., Dillhoff, M. E., Schmidt, C. R., & Guttridge, D. C. (2019). Modeling Human Cancer-induced Cachexia. *Cell Reports*, 28(6), 1612–1622.e4. <https://doi.org/10.1016/j.celrep.2019.07.016>
- Tanaka, Y., Eda, H., Tanaka, T., Udagawa, T., Ishikawa, T., Horii, I., Ishitsuka, H., Kataoka, T., & Taguchi, T. (1990). Experimental Cancer Cachexia Induced by Transplantable Colon 26 Adenocarcinoma in Mice. *Cancer Research*, 50, 2290–2295. <http://aacrjournals.org/cancerres/article-pdf/50/8/2290/2443360/cr0500082290.pdf>
- Temel, J. S., Currow, D. C., Fearon, K., Yan, Y., Friend, J., & Abernethy, A. P. (2015). Anamorelin in patients with advanced non-small cell lung cancer and cachexia: Results from the phase III studies ROMANA 1 and 2. *Journal of Clinical Oncology*, 33(29_suppl), 175. https://doi.org/10.1200/jco.2015.33.29_suppl.175
- Thompson, M. P., Cooper, S. T., Parry, B. R., & Tuckey, J. A. (1993). Increased expression of the mRNA for hormone-sensitive lipase in adipose tissue of cancer patients. *BBA - Molecular Basis of Disease*, 1180(3), 236–242. [https://doi.org/10.1016/0925-4439\(93\)90044-2](https://doi.org/10.1016/0925-4439(93)90044-2)
- Tisdale, M. J. (2009). Mechanisms of cancer cachexia. *Physiological Reviews*, 89(2), 381–410. <https://doi.org/10.1152/physrev.00016.2008>
- Toledo, M., Busquets, S., Penna, F., Zhou, X., Marmonti, E., Betancourt, A., Massa, D., López-Soriano, F. J., Han, H. Q., & Argilés, J. M. (2016). Complete reversal of muscle wasting in experimental cancer cachexia: Additive effects of activin type II receptor inhibition and β -2 agonist. *International Journal*

- of Cancer*, 138(8), 2021–2029. <https://doi.org/10.1002/ijc.29930>
- Toledo, M., Penna, F., Oliva, F., Luque, M., Betancourt, A., Marmonti, E., López-Soriano, F. J., Argilés, J. M., & Busquets, S. (2016). A multifactorial anti-cachectic approach for cancer cachexia in a rat model undergoing chemotherapy. *Journal of Cachexia, Sarcopenia and Muscle*, 7(1), 48–59. <https://doi.org/10.1002/jcsm.12035>
- Trendelenburg, A. U., Meyer, A., Jacobi, C., Feige, J. N., & Glass, D. J. (2012). TAK-1/p38/nNFκB signaling inhibits myoblast differentiation by increasing levels of Activin A. *Skeletal Muscle*, 2(1), 1–14. <https://doi.org/10.1186/2044-5040-2-3>
- Tsoli, M., Schweiger, M., Vanniasinghe, A. S., Painter, A., Zechner, R., Clarke, S., & Robertson, G. (2014). Depletion of white adipose tissue in cancer cachexia syndrome is associated with inflammatory signaling and disrupted circadian regulation. *PLoS ONE*, 9(3). <https://doi.org/10.1371/journal.pone.0092966>
- Vaes, R. D. W., van Dijk, D. P. J., Welbers, T. T. J., Blok, M. J., Aberle, M. R., Heij, L., Boj, S. F., Olde Damink, S. W. M., & Rensen, S. S. (2020). Generation and initial characterization of novel tumour organoid models to study human pancreatic cancer-induced cachexia. *Journal of Cachexia, Sarcopenia and Muscle*, 11(6), 1509–1524. <https://doi.org/10.1002/jcsm.12627>
- van der Ende, M., Grefte, S., Plas, R., Meijerink, J., Witkamp, R. F., Keijer, J., & van Norren, K. (2018). Mitochondrial dynamics in cancer-induced cachexia. *Biochimica et Biophysica Acta - Reviews on Cancer*, 1870(2), 137–150. <https://doi.org/10.1016/j.bbcan.2018.07.008>
- van Herpen, N. A., & Schrauwen-Hinderling, V. B. (2008). Lipid accumulation in non-adipose tissue and lipotoxicity. *Physiology & Behavior*, 94(2), 231–241. <https://doi.org/10.1016/j.physbeh.2007.11.049>
- Vegiopoulos, A., Müller-Decker, K., Strzoda, D., Schmitt, I., Chichelnitskiy, E., Ostertag, A., Diaz, M. B., Rozman, J., Hrabe de Angelis, M., Nüsing, R. M., Meyer, C. W., Wahli, W., Klingenspor, M., & Herzig, S. (2010). Cyclooxygenase-2 Controls Energy Homeostasis in Mice by de Novo Recruitment of Brown Adipocytes. *Science*, 328(5982), 1158–1161. <https://doi.org/10.1126/science.1186034>
- Vegiopoulos, A., Rohm, M., & Herzig, S. (2017). Adipose tissue: between the extremes. *The EMBO Journal*, 36(14), 1999–2017. <https://doi.org/10.15252/emj.201696206>
- Viana, L. R., Canevarolo, R., Luiz, A. C. P., Soares, R. F., Lubaczeuski, C., Zeri, A. C. de M., & Gomes-Marcondes, M. C. C. (2016). Leucine-rich diet alters the 1H-NMR based metabolomic profile without changing the Walker-256 tumour mass in rats. *BMC Cancer*, 16(1), 1–14. <https://doi.org/10.1186/s12885-016-2811-2>
- von Haehling, S., & Anker, S. D. (2010). Cachexia as a major underestimated and unmet medical need: facts and numbers. *Journal of Cachexia, Sarcopenia and Muscle*, 1(1), 1–5. <https://doi.org/10.1007/s13539-010-0002-6>
- von Haehling, S., & Anker, S. D. (2014). Prevalence, incidence and clinical impact of cachexia: facts and numbers—update 2014. In *Journal of Cachexia, Sarcopenia and Muscle*. <https://doi.org/10.1007/s13539-014-0164-8>
- Wakabayashi, H., Arai, H., & Inui, A. (2021). The regulatory approval of anamorelin for treatment of cachexia in patients with non-small cell lung cancer, gastric cancer, pancreatic cancer, and colorectal cancer in Japan: facts and numbers. *Journal of Cachexia, Sarcopenia and Muscle*, 12(1), 14–16. <https://doi.org/10.1002/jcsm.12675>
- Wang, J., Wang, Y., Tong, M., Pan, H., & Li, D. (2019). Medical Cannabinoids for Cancer Cachexia: A Systematic Review and Meta-Analysis. *BioMed Research International*, 2019. <https://doi.org/10.1155/2019/2864384>
- Wang, P., Shi, Q., Deng, W. H., Yu, J., Zuo, T., Mei, F. C., & Wang, W. X. (2015). Relationship between expression of NADPH oxidase 2 and invasion and prognosis of human gastric cancer. *World Journal of Gastroenterology*, 21(20), 6271–6279. <https://doi.org/10.3748/wjg.v21.i20.6271>

- Wang, Y., Lam, K. S. L., Xu, J. Y., Lu, G., Xu, L. Y., Cooper, G. J. S., & Xu, A. (2005). Adiponectin inhibits cell proliferation by interacting with several growth factors in an oligomerization-dependent manner. *Journal of Biological Chemistry*, *280*(18), 18341–18347. <https://doi.org/10.1074/jbc.M501149200>
- Weber, B. Z. C., Arabaci, D. H., & Kir, S. (2022). Metabolic Reprogramming in Adipose Tissue During Cancer Cachexia. *Frontiers in Oncology*, *12*. <https://doi.org/10.3389/FONC.2022.848394>
- Weber, L. V., Al-Refae, K., Wölk, G., Bonatz, G., Altmüller, J., Becker, C., Gisselmann, G., & Hatt, H. (2016). Expression and functionality of TRPV1 in breast cancer cells. *Breast Cancer: Targets and Therapy*, *8*, 243–252. <https://doi.org/10.2147/BCTT.S121610>
- Weryńska, B., Kosacka, M., Gołdecki, M., & Jankowska, R. (2009). Leptin serum levels in cachectic and non-cachectic lung cancer patients. *Pneumonologia i Alergologia Polska*, *77*(6), 500–505. <https://doi.org/10.5603/arm.27762>
- White, J. P., Puppa, M. J., Sato, S., Gao, S., Price, R. L., Baynes, J. W., Kostek, M. C., Matesic, L. E., & Carson, J. A. (2012). IL-6 regulation on skeletal muscle mitochondrial remodeling during cancer cachexia in the ApcMin/+ mouse. *Skeletal Muscle*, *2*(1), 1–16. <https://doi.org/10.1186/2044-5040-2-14>
- Wijaya, Y. T., Setiawan, T., Sari, I. N., Nah, S. Y., & Kwon, H. Y. (2021). Amelioration of muscle wasting by gintonin in cancer cachexia. *Neoplasia (United States)*, *23*(12), 1307–1317. <https://doi.org/10.1016/j.neo.2021.11.008>
- Wilhelm, S. M., Carter, C., Tang, L. Y., Wilkie, D., McNabola, A., Rong, H., Chen, C., Zhang, X., Vincent, P., McHugh, M., Cao, Y., Shujath, J., Gawlak, S., Eveleigh, D., Rowley, B., Liu, L., Adnane, L., Lynch, M., Auclair, D., ... Trail, P. A. (2004). BAY 43-9006 exhibits broad spectrum oral antitumor activity and targets the RAF/MEK/ERK pathway and receptor tyrosine kinases involved in tumor progression and angiogenesis. *Cancer Research*, *64*(19), 7099–7109. <https://doi.org/10.1158/0008-5472.CAN-04-1443>
- Wu, H., Deng, X., Shi, Y., Su, Y., Wei, J., & Duan, H. (2016). PGC-1 α , glucose metabolism and type 2 diabetes mellitus. *Journal of Endocrinology*, *229*(3), R99–R115. <https://doi.org/10.1530/JOE-16-0021>
- Wu, J., Boström, P., Sparks, L. M., Ye, L., Choi, J. H., Giang, A.-H., Khandekar, M., Virtanen, K. A., Nuutila, P., Schaart, G., Huang, K., Tu, H., van Marken Lichtenbelt, W. D., Hoeks, J., Enerbäck, S., Schrauwen, P., & Spiegelman, B. M. (2012). Beige Adipocytes Are a Distinct Type of Thermogenic Fat Cell in Mouse and Human. *Cell*, *150*(2), 366–376. <https://doi.org/10.1016/j.cell.2012.05.016>
- Xie, H., Heier, C., Kien, B., Vesely, P. W., Tang, Z., Sexl, V., Schoiswohl, G., Strießnig-Bina, I., Hoefler, G., Zechner, R., & Schweiger, M. (2020). Adipose triglyceride lipase activity regulates cancer cell proliferation via AMP-kinase and mTOR signaling. *Biochimica et Biophysica Acta - Molecular and Cell Biology of Lipids*, *1865*(9), 158737. <https://doi.org/10.1016/j.bbalip.2020.158737>
- Xie, H., Heier, C., Meng, X., Bakiri, L., Pototschnig, I., Tang, Z., Schauer, S., Baumgartner, V. J., Grabner, G. F., Schabbauer, G., Wolinski, H., Robertson, G. R., Hoefler, G., Zeng, W., Wagner, E. F., Schweiger, M., & Zechner, R. (2022). An immune-sympathetic neuron communication axis guides adipose tissue browning in cancer-associated cachexia. *Proceedings of the National Academy of Sciences of the United States of America*, *119*(9), 1–12. <https://doi.org/10.1073/pnas.2112840119>
- Yamauchi, T., Kamon, J., Waki, H., Terauchi, Y., Kubota, N., Hara, K., Mori, Y., Ide, T., Murakami, K., Tsuboyama-Kasaoka, N., Ezaki, O., Akanuma, Y., Gavrilova, O., Vinson, C., Reitman, M. L., Kagechika, H., Shudo, K., Yoda, M., Nakano, Y., ... Kadowaki, T. (2001). The fat-derived hormone adiponectin reverses insulin resistance associated with both lipoatrophy and obesity. *Nature Medicine*, *7*(8), 941–946. <https://doi.org/10.1038/90984>
- Ye, R., & Scherer, P. E. (2013). Adiponectin, driver or passenger on the road to insulin sensitivity? *Molecular Metabolism*, *2*(3), 133–141. <https://doi.org/10.1016/j.molmet.2013.04.001>
- Zechner, R., Zimmermann, R., Eichmann, T. O., Kohlwein, S. D., Haemmerle, G., Lass, A., & Madeo, F. (2012). FAT SIGNALS - Lipases and lipolysis in lipid metabolism and signaling. *Cell Metabolism*, *15*(3), 279–291. <https://doi.org/10.1016/j.cmet.2011.12.018>

- Zhang, W., Huang, Q., Zeng, Z., Wu, J., Zhang, Y., & Chen, Z. (2017). Sirt1 Inhibits Oxidative Stress in Vascular Endothelial Cells. *Oxidative Medicine and Cellular Longevity*, 2017. <https://doi.org/10.1155/2017/7543973>
- Zhang Y, Proenca R, Maffei M, Barone M, Leopold L, & Friedman JM. (1994). Positional cloning of the mouse obese gene and its human homologue. *Nature*, 372(DECEMBER), 425–432. <https://www.nature.com/articles/372425a0.pdf>
- Zhou, X., Wang, J. L., Lu, J., Song, Y., Kwak, K. S., Jiao, Q., Rosenfeld, R., Chen, Q., Boone, T., Simonet, W. S., Lacey, D. L., Goldberg, A. L., & Han, H. Q. (2010). Reversal of cancer cachexia and muscle wasting by ActRIIB antagonism leads to prolonged survival. *Cell*, 142(4), 531–543. <https://doi.org/10.1016/j.cell.2010.07.011>
- Zimmers, T. A., Davies, M. V., Koniaris, L. G., Haynes, P., Esquela, A. F., Tomkinson, K. N., McPherron, A. C., Wolfman, N. M., & Lee, S. J. (2002). Induction of cachexia in mice by systemically administered myostatin. *Science*, 296(5572), 1486–1488. <https://doi.org/10.1126/science.1069525>